U.S. DEPARTMENT OF COMMERCE
National Technical Information Service

AD-A023 845

VIDEO DATA COMPRESSION STUDY FOR REMOTE SENSORS

OHIO UNIVERSITY

PREPARED FOR
AIR FORCE AVIONICS LABORATORY

FEBRUARY 1976

126111

AFAL-TR-75-173

VIDEO DATA COMPRESSION STUDY FOR REMOTE SENSORS

ADA023845

DEPARTMENT OF ELECTRICAL ENGINEERING
OHIO UNIVERSITY

FEBRUARY 1976

TECHNICAL REPORT AFAL-TR-75-173

Final Report for Period May 1973 to June 1975

DDC
APR 30 1976
B

Approved for public release; distribution unlimited.

AIR FORCE AVIONICS LABORATORY (AFWAL)
Air Force Systems Command
Wright-Patterson AFB, Dayton, Ohio 45433

REPRODUCED BY
NATIONAL TECHNICAL
INFORMATION SERVICE
U.S. DEPARTMENT OF COMMERCE
SPRINGFIELD, VA. 22161

NOTICE

When government drawings, specifications, or other data are used for any purpose other than in connection with a definitely related government procurement operation, the United States Government thereby incurs no responsibility nor any obligation whatsoever; and the fact that the government may have formulated, furnished, or in any way supplied the said drawings, specifications, or other data, is not to be regarded by implication or otherwise as in any manner licensing the holder or any other person or corporation, or conveying any rights or permission to manufacture, use, or sell any patented invention that may in any way be related thereto.

This final report was submitted by Dr. Joseph Essman of the Department of Electrical Engineering, Ohio University, Athens, Ohio, under Contract F33615-73-C-1233, Work Unit 76620702, with the Air Force Avionics Laboratory, System Avionics Division. Capt. Jackson T. Cole was the Project Monitor. This technical report has been reviewed and is approved for publication.

This report has been reviewed by the Information Office (OI) and is releasable to the National Technical Information Service (NTIS). At NTIS, it will be available to the general public, including foreign nations.

JACKSON T. COLE, Capt, USAF
Project Monitor

FOR THE COMMANDER

GEORGE F. CUDA[illegible], Colonel, USAF
[illegible], System Avionics Division
Air Force Avionics Laboratory

[illegible] reproduction [illegible] required by security [illegible]

DISCLAIMER NOTICE

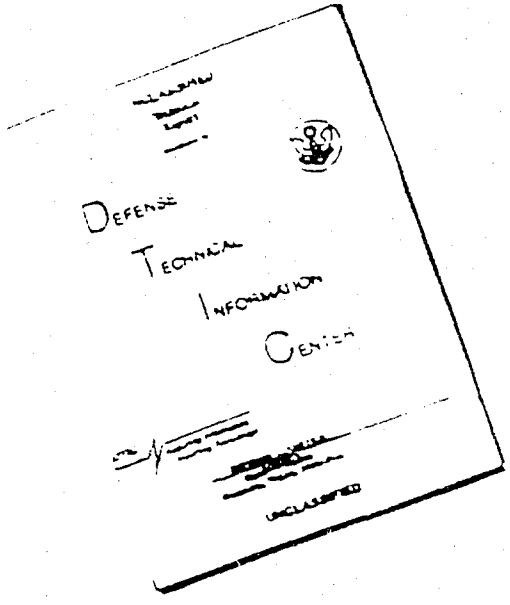

THIS DOCUMENT IS BEST QUALITY AVAILABLE. THE COPY FURNISHED TO DTIC CONTAINED A SIGNIFICANT NUMBER OF PAGES WHICH DO NOT REPRODUCE LEGIBLY.

UNCLASSIFIED

SECURITY CLASSIFICATION OF THIS PAGE (When Data Entered)

REPORT DOCUMENTATION PAGE

READ INSTRUCTIONS BEFORE COMPLETING FORM

1. REPORT NUMBER: AFAL-TR-75-173	2. GOVT ACCESSION NO.
3. RECIPIENT'S CATALOG NUMBER	
4. TITLE (and Subtitle): VIDEO DATA REDUCTION STUDY FOR REMOTE SENSORS	5. TYPE OF REPORT & PERIOD COVERED: Technical - Final, 15 May 73 to 30 Jun 75
	6. PERFORMING ORG. REPORT NUMBER
7. AUTHOR(s): Joseph E. Eseman, Dan Quyen Hua, George Papacostas	8. CONTRACT OR GRANT NUMBER(s): F33615-73-C-1233
9. PERFORMING ORGANIZATION NAME AND ADDRESS: Department of Electrical Engineering, Ohio University, Athens, Ohio 45701	10. PROGRAM ELEMENT, PROJECT, TASK AREA & WORK UNIT NUMBERS: 7662 07 02
11. CONTROLLING OFFICE NAME AND ADDRESS: Air Force Avionics Laboratory (AFAL/AAT-1), Wright-Patterson AFB, Ohio 45433	12. REPORT DATE: February 1976
	13. NUMBER OF PAGES: 347
14. MONITORING AGENCY NAME & ADDRESS (if different from Controlling Office)	15. SECURITY CLASS. (of this report): Unclassified
	15a. DECLASSIFICATION/DOWNGRADING SCHEDULE

16. DISTRIBUTION STATEMENT (of this Report)

Approved for public release; distribution unlimited.

17. DISTRIBUTION STATEMENT (of the abstract entered in Block 20, if different from Report)

18. SUPPLEMENTARY NOTES

19. KEY WORDS (Continue on reverse side if necessary and identify by block number)

Data Reduction
Image Processing
Transform Encoding
Hybrid Techniques
Adaptive Coding
Interframe Coding

20. ABSTRACT (Continue on reverse side if necessary and identify by block number)

This report summarizes a 24 month investigation on video data reduction method applicable to RPV's. Areas investigated included interframe reduction, two-dimensional transform and hybrid coding using Walsh and Fourier transforms and DPCM coding, and adaptive techniques using Hadamard transforms. Included are numerous photographs of low altitude target runs showing the effects of channel errors and coding degradation. A bibliography of up to date references on image processing is also included.

DD FORM 1 JAN 73 1473 EDITION OF 1 NOV 65 IS OBSOLETE

UNCLASSIFIED

SECURITY CLASSIFICATION OF THIS PAGE (When Data Entered)

FOREWORD

This report, AFAL-TR-75-173, was prepared for the Air Force Avionics Laboratory by the Electrical Engineering Department of Ohio University, Athens, Ohio, and summarizes a 24-month (May 1973-June 1975) investigation on video data compression techniques applicable for the RPV mission performed under Contract F33615-73-C-1233, Project 7762. Areas investigated and included in this report are interframe coding methods, two-dimensional transform (adaptive and non-adaptive) and hybrid coding schemes. Numerous photographs are given comparing the techniques using bit rates from 0.25 to 1.5 bits/pel. The effects of noise are considered and both quantitative and qualitative evaluations are given.

The results summarized in this report were obtained by Dr. Joseph E. Essman, principal investigator (Associate Professor and Assistant Chairman, Department of Electrical Engineering, Ohio University), Mr. Dan Quyen Hua, Research Associate, and Mr. George Papacostas, Research Associate. Captain Jack Cole from WPAFB was the Project Monitor.

SUMMARY

This report summarizes the results obtained on data compression techniques applicable for Remote Piloted Vehicles (RPV) under Contract No. F33615-73-C-1233.

During the first year of this contract investigations were conducted on interframe redundancy techniques. Algorithms are developed to account for motion in frame-to-frame aerial photographs resulting in large bit reduction ratios providing that the various parameters of the missions such as altitude, velocity vector, fields of visions of the cameras, etc. are known accurately. Differential encoding is used to further reduce the bandwidth. Sensitivity to the various mission parameters are investigated using computer simulations. Although the interframe techniques require relatively complex instrumentation for RPVs, the techniques can be used for synthetic frame generation at the ground station.

Intraframe techniques suitable for the RPV mission including two-dimensional transform techniques and hybrid coding schemes are investigated and evaluated, both in the mean-squared-error sense and subjectively. It is shown that hybrid scheme using the Hadamard transform in one spatial direction and DPCM in the other performs at least equivalent and most of the time superior to the two-dimensional transform schemes. Due to the simplicity of the hybrid scheme, this may be advantageous for practical implementations.

It is shown that the hybrid scheme is more sensitive to channel noise; however, by optimization and initialization it can be made to perform as well as the transform scheme.

An adaptive scheme is proposed and evaluated which shows increased resolution in regions of high activity within the picture.

Several different error criteria were investigated. Mean-derivative-squared-error tends to be more correlated with subjective evaluations.

Important characteristics and performance indices several data compression techniques applicable for the RPV mission are given in tabular form.

TABLE OF CONTENTS

		PAGE
CHAPTER I	INTRODUCTION	1
CHAPTER II	INTERFRAME REDUCTION FOR RPVs	3
2.1	Introduction	3
2.2	Interframe Technique for RPVs	5
2.3	Geometry of the System	11
	I. Horizontal and Vertical Positions	14
	(1) Steady Straight Flight	17
	(2) Horizontal Circling	22
2.4	Prediction Algorithm	25
2.5	Simulation Results (Interframe-DPCM)	29
2.6	Intraframe-DPCM-Interframe-DPCM System)	37
2.7	Summary of Simulation	44
2.8	Total System Error Including Channel Noise	46
2.9	Summary and Conclusions	50
CHAPTER III	THEORY	52
3.1	Introduction	52
3.2.1	DPCM and Time Predictive Techniques	52
3.2.2	One-Dimensional Transformations	58
3.2.3	The Effects of One-Dimensional Techniques on Two-Dimensional Data	65
3.2.4	Two-Dimensional Transformations	86
3.3	Hybrid Coding Techniques	90
3.3A	Transform-DPCM Coding System	90
3.3B	The DPCM-Transform System	101
3.3C	Comparison of Transform-DPCM and DPCM-Transform Techniques	110
3.4	Hybrid Coding in Noisy Channel	115
CHAPTER IV	SIMULATION RESULTS	119
4.1	Introduction	119
4.2	Picture Statistics	119
4.3	Two-Dimensional Transform Simulation Results (Noiseless Channel)	130
4.4	Hybrid Coding (Noiseless Channel)	150
4.5	The Effects of Channel Noise on The Two-Dimensional Hadamard Transform and Hybrid Coding Schemes	199
4.6	Optimization of The Hybrid Coding Scheme	213

		PAGE
CHAPTER V	2-D TRANSFORM WITH ADAPTIVE QUANTIZATION	255
5.1	Introduction	255
5.2	Two-Dimensional Hadamard Using 32-Coefficients	257
5.3	Adaptive Algorithm Using One Quantizer	259
5.4	DPCM Encoding of the Estimates of the Variances	265
5.5	Variations in Adaptive Scheme and Recommendations for Further Investigations	294
CHAPTER VI	CONCLUSIONS AND RECOMMENDATIONS	296
APPENDIX	Typical Histograms for the Transform Coefficients	303
REFERENCES		312

LIST OF TABLES

Table		Page
2.5.1.	Statistics of the Reference, ZOH and LI Predicted Pictures	31
2.5.2.	Statistics of Difference Signal With ZOH and LI Predicted Images	31
2.5.3.	Number of Difference Signals Exceeding Threshold Levels (Interframe-DPCM)	32
2.5.4.	Interframe-DPCM, Threshold Mean-Squared Error	36
2.5.5.	Interframe-DPCM, Statistics of the Difference Signal at the Input of the Quantizer Using Linear Interpolation	37
2.5.6.	Interframe-DPCM, Total System Mean-Squared Error Using Linear Interpolation	38
2.5.7.	Interframe-DPCM, Total System Mean-Absolute Error Using Linear Interpolation	38
2.6.1.	Statistics of the Intraframe Difference Signal	39
2.6.2.	Intraframe-DPCM-Interframe-DPCM, Statistics of Quantizer Input Signals (Linear Interpolation)	41
2.6.3.	Intraframe-Interframe DPCM, Number of Picture Elements Exceeding a Fixed Threshold Level Using Linear Interpolation Technique	42
2.6.4.	Intraframe-DPCM-Interframe-DPCM, Total System Mean-Squared Error Using Linear Interpolation Technique	43
2.6.5.	Intraframe-DPCM-Interframe-DPCM, Total System Mean-Absolute Error Using Linear Interpolation Technique	43
2.7.1.	Interframe-DPCM, Average of Bits Per Pel Using Linear Interpolation	45
2.7.2.	Intraframe-DPCM-Interframe-DPCM, Average of bits Per Pel Using Linear Interpolation	45
2.7.3.	Interframe-DPCM	47
2.7.4.	Intraframe-Interframe-DPCM	47
2.8.1	Threshold: 8, Probability of Error and Number of Elements Due to Error	49
2.8.2.	Threshold: 16, Probability of Error and Number of Elements Due to Error	49

		Page
4.3.1.	Statistical Properties of Pictures	130
4.3.1a.	Variances of Two-Dimensional Transform Coefficient (Picture Truck) Block Size 8x8 - Discrete Cosine	131
4.3.1b.	Variances of Two-Dimensional Transform Coefficients (Picture Truck) Block Size 8x8 - Walsh Hadamard	131
4.3.1c.	Variances of Two-Dimensional Transform Coefficients (Picture Truck) Block Size 8x8 - Walsh Haar	131
4.3.2a.	Variances of Two-Dimensional Transform Coefficients (Picture Tank) Block Size 8x8 - Discrete Cosine	132
4.3.2b.	Variances of Two-Dimensional Transform Coefficients (Picture Tank) Block Size 8x8 - Walsh Hadamard	132
4.3.2c.	Variances of Two-Dimensional Transform Coefficients (Picture Tank) Block Size 8x8 - Walsh Haar	132
4.3.3a.	Mean-Squared-Error Using Two-Dimensional Transforms	137
4.3.3b.	Normalized-Derivative-Squared-Error Using Two-Dimensional Transforms	138
4.3.3c.	Mean-Absolute-Error (MAE) Using Two-Dimension Transforms	139
4.3.4.	Bit Assignments	141
4.3.5.	Errors Using Modified Bit Assignments	142
4.3.6.	Modified Bit Assignments	142
4.4.1.	Normalized Cumulative Sum of Variance of Hybrid Coding Sample at Input of Quantizer	163
4.4.2.	Bit Assignments for Hybrid Coding Scheme	168
4.4.3.	Variations in Bit Assignments	168
4.4.4.	Bit Assignments for Hybrid Coding	169
4.4.5a.	Mean-Squared-Error Using Hybrid Coding Scheme	169
4.4.5b.	Normalized-Derivative-Squared-Error Using Hybrid Coding Scheme	170
4.4.5c.	Mean-Absolute-Error Using Hybrid Coding Scheme	170
4.4.6.	Correlation of the Transformed Coefficients - Tank (one-element-delay)	172
4.4.7.	Mean-Squared-Error for the Scene of the Tank Using Transform-DPCM and Prediction Coefficients as Given in Table 4.4.5.	172
4.4.8.	Local Mean-Squared-Error	197
4.4.9.	Normalized-Derivative-Squared-Error	197
4.4.10.	Comparison of Six Pictures (Hybrid Coding)	198

		Page
4.5.1.	Mean-Squared-Error for the Scene of the Tank Using Two-Dimensional Hadamard Transform	199
4.5.2.	Mean-Squared-Error for the Scene of the Tank Using Hybrid Coding. The Same Prediction Coefficient is Used for Each Coefficient	206
4.5.3.	Mean-Squared-Error for the Scene of the Tank Using Hybrid Coding. A Different Prediction Coefficient is Used for Each Coefficient	213
4.6.1.	The Effects of Using Optimum Prediction Coefficients in the Transform-DPCM System for the Scene of the Tank	216
4.6.2.	Optimization of the Hybrid Coding Technique	248
5.2.1.	Mean-Squared-Error and Mean-Derivative-Squared-Error for the Scene of the Truck	258
5.2.2.	Bit Assignments Using 32 Total Coefficients	259
5.2.3.	Error Measures for the Scene of the Truck	260
5.3.1.	The Effects of Sample-Size in Estimating the Variance of the Coefficients	261
5.3.2.	Error Measures Using a Common Quantizer for the Coefficients and Different Quantizers for the Estimates of the Standard Deviations	262
5.3.3.	Bit Assignments	262
5.4.1.	Simulation Results Using Adaptive Scheme for the Scene of the Truck	278
5.5.1.	Results Using the Adaptive Scheme on Only the First Few Coefficients	294
6.	Summary of Data Compression Techniques	300-301-302

LIST OF FIGURES

Figure		Page
2.1.1.	Two Consecutive Frames	5
2.2.1.	Philosophy of Data Compression Scheme	6
2.2.2.	Interframe-DPCM Transmitter	7
2.2.3.	Intraframe-DPCM-Interframe-DPCM Transmitter	9
2.2.4.	Receiver	10
2.3.1.	Diagram of the Position Displacement of an Image on the Screen of a Point on the Ground	12
2.3.2.	Geometry of the Scanned Area	12
2.3.3.	Dimensions of the Scanned Area	13
2.3.4.	Image Position of a Point on the Ground	15
2.3.5.	Diagram of the Horizontal Position of Image	16
2.3.6.	Diagram of the Vertical Position Displacement of an Image	19
2.3.7.	Diagram of the Displacement of the Scanned Area on the Ground Due to Straight Flight	20
2.3.8.	Diagram of the Horizontal Position of an Image	21
2.3.9.	Diagram of Horizontal Circling Flight	23
2.4.1.	The Scanned Area on the Ground at Two Consecutive Frame Times	25
2.4.2.	Geometry of a Picture Element on the Screen	26
2.4.3.	Diagram of Zero-Order-Hold Prediction	26
2.4.4.	Diagram of Two-Dimensional Linear Interpolation	27
2.5.1.	The Simulated Interframe-DPCM System	30
2.6.1.	Illustration of Intraframe-Interframe-DPCM Technique	39
3.2.1.	DPCM Coder	55
3.2.2.	2-D DPCM and 1-D DPCM	53
3.2.3.	Interpolative DPCM	53
3.2.4.	Schematic Diagram of One-dimensional Transformation	58
3.2.5.	Variance of Transform Coefficients (ρ=0.9,N=32)	62
3.2.6.	Cumulative Sum of Variances (ρ=0.9)	63
3.2.7.	Schematic Diagram of a One-dimensional Orthogonal Transformation	68

		Page
3.2.8.	Correlation of PCM Signals (Truck)	71
3.2.9.	Correlation of DPCM Signals (ρ=0.91454) (Truck)	73
3.2.10.	Correlation of Aerial Picture	74
3.2.11.	Correlation of Error Picture (Aerial)	75
3.2.12.	One-Dimensional Hadamard (Horizontal) Vertical Correlation of Transform Coefficients (One Element Delay)	76
3.2.13.	Variance of Transform Coefficients of the One-Dimensional Hadamard Transform of PCM Picture	77
3.2.14.	Variance of the One-Dimensional Hadamard Transform Coefficient Differences of the PCM Picture	78
3.2.15.	Variance of the One-Dimensional Hadamard Transform Coefficients of the DPCM Picture (Aerial Photograph)	81
3.2.16.	Variance of the One-Dimensional Hadamard Transform Coefficients of the Difference Picture (Face)	82
3.2.17.	Variances of the Difference of the One-Dimensional Hadamard Transform Coefficients (Face)	83
3.2.18.	Energy of the Transform Coefficients (Picture:Face)	84
3.2.19.	Energy of the Transform Coefficients (Aerial)	85
3.3.1.	Transform-DPCM Hybrid Coding System	91
3.3.2.	The Partitioning of MxM Images Into 1xN Subimages	92
3.3.3.	The j^{th} DPCM Coder	95
3.3.4.	DPCM-Transform Transmitter	99
3.3.4.cont.	DPCM-Transform Receiver	100
3.3.5.	Simplified Block Diagram of the DPCM Coding System	101
3.3.6.	Hybrid Coding System (ρ_x=0.9469, ρ_y=0.8798); N=3. Signal-to-Noise Ratio Vs: Bit Rate	113
3.3.7.	Hybrid Coding (ρ_x=0.9469, ρ_y=0.8798)	114
3.5.	Comparison of Two-Dimensional Coding Schemes (Karhunen Loeve, ρ_x=0.9469, ρ_y=0.8798, N=16)	118
4.2.1.	Histogram of Intensity Levels-Truck	120
4.2.2.	Histogram of Intensity Levels-Tank	121
4.2.3.	Correlation of the Scene of the Truck on the Bridge	122
4.2.4.	Correlation of PCM Signals (Picture:Tank)	123
4.2.5.	Original Picture of Tank	124
4.2.6.	Original Picture of Truck	125
4.2.7.	Original Picture of Trees	126
4.2.8.	Original Picture of Fields	127
4.2.9.	Original Picture of Roads	128
4.2.10.	Original Picture of Coast	129

		Page
4.3.1.	Cumulative Sum of the Variances of the Transform Coefficients, Block Size = 8 x 8. (Truck)	134
4.3.2.	Cumulative Sum of the Variances of the Transform Coefficients, Block Size = 8 x 8. (Tank)	135
4.3.3.	Mean-Squared-Error Using 2-D Transforms	144
4.3.4a.	Two-Dimensional Hadamard Transform Technique of Truck; 0.25 bits/pel	145
4.3.4b.	Two-Dimensional Hadamard Transform Technique of Truck; 0.5 bits/pel	146
4.3.4c.	Two-Dimensional Hadamard Transform Technique of Truck; 1.0 bits/pel	147
4.3.4d.	Two-Dimensional Hadamard Transform Technique of Truck; 1.5 bits/pel	148
4.3.5a.	Two-Dimensional Discrete Cosine Transform Technique of Truck; 0.5 bits/pel	149
4.3.5b	Two-Dimensional Discrete Cosine Transform Technique of Truck; 1.0 bits/pel	150
4.3.5c	Two-Dimensional Discrete Cosine Transform Technique of Truck; 1.5 bits/pel	151
4.3.6a.	Two-Dimensional Hadamard Transform Technique of Tank; 0.25 bits/pel	152
4.3.6b.	Two-Dimensional Hadamard Transform Technique of Tank; 0.5 bits/pel	153
4.3.6c.	Two-Dimensional Hadamard Transform Technique of Tank; 1.0 bits/pel	154
4.3.6d.	Two-Dimensional Hadamard Transform Technique of Tank; 1.5 bits/pel	155
4.3.7a.	Two-Dimensional Discrete Cosine Transform Technique of Tank; 0.5 bits/pel	156
4.3.7b.	Two-Dimensional Discrete Cosine Transform Technique of Tank; 1.0 bits/pel	157
4.3.7c.	Two-Dimensional Discrete Cosine Transform Technique of Tank; 1.5 bits/pel	158
4.4.1.	Variance of Hybrid Coding Signal at the Quantizer Input (6 Pictures), $A=\rho_y$	161
4.4.2.	Cumulative Sum of the Variances of the Hybrid Coding Samples at the Quantizer Input	162
4.4.3a.	Hybrid Coding (Noiseless Channel) Normalized Mean-Squared-Errors	165
4.4.3b.	Hybrid Coding (Noiseless Channel) Normalized Derivative-Squared-Errors	166
4.4.3c.	Normalized Mean-Absolute-Errors (Hybrid Coding)	167

Page

4.4.4a. Hybrid Coding (Transform-DPCM) of the Scene of the Truck; 0.25 bits/pel 173

4.4.4b. Hybrid Coding (Transform-DPCM) of the Scene of the Truck; 0.5 bits/pel 174

4.4.4c. Hybrid Coding (Transform-DPCM) of the Scene of the Truck; 1.0 bits/pel 175

4.4.4d. Hybrid Coding (Transform-DPCM) of the Scene of the Truck; 1.5 bits/pel 176

4.4.5a. Hybrid Coding (Transform-DPCM) of the Scene of the Tank; 0.25 bits/pel 177

4.4.5b. Hybrid Coding (Transform-DPCM) of the Scene of the Tank; 0.5 bits/pel 178

4.4.5c. Hybrid Coding (Transform-DPCM) of the Scene of the Tank; 1.0 bits/pel 179

4.4.5d. Hybrid Coding (Transform-DPCM) of the Scene of the Tank; 1.5 bits/pel 180

4.4.6a. Hybrid Coding (Transform-DPCM) of the Scene of the Trees; 0.25 bits/pel 181

4.4.6b. Hybrid Coding (Transform-DPCM) of the Scene of the Trees; 0.5 bits/pel 182

4.4.6c. Hybrid Coding (Transform-DPCM) of the Scene of the Trees; 1.0 bits/pel 183

4.4.6d. Hybrid Coding (Transform-DPCM) of the Scene of the Trees; 1.5 bits/pel 184

4.4.7a. Hybrid Coding (Transform-DPCM) of the Scene of the Field; 0.25 bits/pel 185

4.4.7b. Hybrid Coding (Transform-DPCM) of the Scene of the Field; 0.5 bits/pel 186

4.4.7c. Hybrid Coding (Transform-DPCM) of the Scene of the Field; 1.0 bits/pel 187

4.4.8a. Hybrid Coding (Transform-DPCM) of the Scene of the Meadow; 0.25 bits/pel 188

4.4.8b Hybrid Coding (Transform-DPCM) of the Scene of the Meadow; 0.5 bits/pel 189

4.4.8c. Hybrid Coding (Transform-DPCM) of the Scene of the Meadow; 1.0 bits/pel 190

4.4.8d. Hybrid Coding (Transform-DPCM) of the Scene of the Meadow; 1.5 bits/pel 191

4.4.9a. Hybrid Coding (Transform-DPCM) of the Scene of the Coast; 0.25 bits/pel 192

4.4.9b. Hybrid Coding (Transform-DPCM) of the Scene of the Coast; 0.5 bits/pel 193

4.4.9c. Hybrid Coding (Transform-DPCM) of the Scene of the Coast; 1.0 bits/pel 194

		Page
4.4.9d.	Hybrid Coding (Transform-DPCM) of the Scene of the Coast; 1.5 bits/pel	195
4.5.1a.	Two-Dimensional Hadamard Transform Technique of the Scene of the Tank; Probability of Bit Error = .001; 0.25 bits/pel	200
4.5.1b.	Two-Dimensional Hadamard Transform Technique of the Scene of the Tank; Probability of Bit Error = .001; 0.5 bits/pel	201
4.5.1c.	Two-Dimensional Hadamard Transform Technique of the Scene of the Tank; Probability of Bit Error = .001; 1.0 bits/pel	202
4.5.2a.	Two-Dimensional Hadamard Transform Technique of the Scene of the Tank; Probability of Bit Error = .01; 0.25 bits/pel	203
4.5.2b.	Two-Dimensional Hadamard Transform Technique of the Scene of the Tank; Probability of Bit Error = .01; 0.5 bits/pel	204
4.5.2c.	Two-Dimensional Hadamard Transform Technique of the Scene of the Tank; Probability of Bit Error = .01; 1.0 bits/pel	205
4.5.3a.	Hybrid Coding (Transform-DPCM) of the Scene of the Tank; Probability of Bit Error = .001; 0.25 bits/pel	207
4.5.3b.	Hybrid Coding (Transform-DPCM) of the Scene of the Tank; Probability of Bit Error = .001; 0.5 bits/pel	208
4.5.3c.	Hybrid Coding (Transform-DPCM) of the Scene of the Tank; Probability of Bit Error = .001; 1.0 bits/pel	209
4.5.4a.	Hybrid Coding (Transform-DPCM) of the Scene of the Tank; Probability of Bit Error = .01; 0.25 bits/pel	210
4.5.4b.	Hybrid Coding (Transform-DPCM) of the Scene of the Tank; Probability of Bit Error = .01; 0.5 bits/pel	211
4.5.4c.	Hybrid Coding (Transform-DPCM) of the Scene of the Tank; Probability of Bit Error = .01; 1.0 bits/pel	212
4.6.1.	Optimum Prediction Coefficient	214
4.6.2.	Mean-Squared-Error Using Optimum Prediction Coefficient	215
4.6.3a.	Hybrid Coding (Transform-DPCM) of the Scene of the Tank Using Optimum Prediction Coefficient; Probability of Bit Error = .001; 0.25 bits/pel	217
4.6.3b.	Hybrid Coding (Transform-DPCM) of the Scene of the Tank Using Optimum Prediction Coefficient; Probability of Bit Error = .001; 0.5 bits/pel	218
4.6.3c	Hybrid Coding (Transform-DPCM) of the Scene of the Tank Using Optimum Prediction Coefficient; Probability of Bit Error = .001; 1.0 bits/pel	219
4.6.4a.	Hybrid Coding (Transform-DPCM) of the Scene of the Tank Using Optimum Prediction Coefficient; Probability of Bit Error = .01; 0.25 bits/pel	220
4.6.4b.	Hybrid Coding (Transform-DPCM) of the Scene of the Tank Using Optimum Prediction Coefficient; Probability of Bit Error = .01; 0.5 bits/pel	221

		Page
4.6.4c.	Hybrid Coding (Transform- PCM) of the Scene of the Tank Using Optimum Prediction Coefficient; Probability of Bit Error = .01; 1.0 bits/pel	222
4.6.5.	Hybrid Coding (Noisy Channel), Mean-Squared-Error	224
4.6.6a.	Hybrid Coding Scheme Using Periodic Resetting; N=16; Probability of Bit Error = .001; 0.25 bits/pel	225
4.6.6b.	Hybrid Coding Scheme Using Periodic Resetting; N=16; Probability of Bit Error = .001; 0.5 bits/pel	226
4.6.6c.	Hybrid Coding Scheme Using Periodic Resetting; N=16; Probability of Bit Error = .001; 1.0 bits/pel	227
4.6.7a.	Hybrid Coding Scheme Using Periodic Resetting; N=16; Probability of Bit Error = .01; 0.25 bits/pel	228
4.6.7b.	Hybrid Coding Scheme Using Periodic Resetting; N=16; Probability of Bit Error = .01; 0.5 bits/pel	229
4.6.7c.	Hybrid Coding Scheme Using Periodic Resetting; N=16; Probability of Bit Error = .01; 1.0 bits/pel	230
4.6.8a.	Hybrid Coding Scheme Using Periodic Resetting; N=32; Probability of Bit Error = .001; 0.25 bits/pel	231
4.6.8b.	Hybrid Coding Scheme Using Periodic Resetting; N=32; Probability of Bit Error = .001; 0.5 bits/pel	232
4.6.9a.	Hybrid Coding Scheme Using Periodic Resetting; N=32; Probability of Bit Error = .01; 0.25 bits/pel	233
4.6.9b.	Hybrid Coding Scheme Using Periodic Resetting; N=32; Probability of Bit Error = .01; 0.5 bits/pel	234
4.6.9c.	Hybrid Coding Scheme Using Periodic Resetting; N=32; Probability of Bit Error = .01; 1.0 bits/pel	235
4.6.10a.	Hybrid Coding Scheme Using Error Correcting Code on First Coefficient; Probability of Error = .001; 0.25 bits/pel	236
4.6.10b.	Hybrid Coding Scheme Using Error Correcting Code on First Coefficient; Probability of Error = .001; 0.5 bits/pel	237
4.6.10c.	Hybrid Coding Scheme Using Error Correcting Code on First Coefficient; Probability of Error = .001; 1.0 bits/pel	238
4.6.11a.	Hybrid Coding Scheme Using Error Correcting Code on First Coefficient; Probability of Error = .01; 0.25 bits/pel	239
4.6.11b.	Hybrid Coding Scheme Using Error Correcting Code on First Coefficient; Probability of Error = .01; 1.0 bits/pel	240

Page

4.6.12a. Hybrid Coding Scheme Using Prediction Coefficients of 0.5 (Non-Optimum); Probability of Error = .001; 0.25 bits/pel 241

4.6.12b. Hybrid Coding Scheme Using Prediction Coefficients of 0.5 (Non-Optimum); Probability of Error = .001; 0.5 bits/pel 242

4.6.12c. Hybrid Coding Scheme Using Prediction Coefficients of 0.5 (Non-Optimum); Probability of Error = .001; 1.0 bits/pel 243

4.6.13a. Hybrid Coding Scheme Using Prediction Coefficients of 0.5 (Non-Optimum); Probability of Error = .01; 0.25 bits/pel 244

4.6.13b. Hybrid Coding Scheme Using Prediction Coefficients of 0.5 (Non-Optimum); Probability of Error = .01; 0.5 bits/pel 245

4.6.13c. Hybrid Coding Scheme Using Prediction Coefficients of 0.5 (Non-Optimum); Probability of Error = .01; 1.0 bits/pel 246

4.6.14a. Hybrid Coding Scheme Using Error Correcting Code on First Coefficient; All $A=\rho_y$; Probability of Error = .001; 0.25 bits/pel 249

4.6.14b. Hybrid Coding Scheme Using Error Correcting Code on First Coefficient; All $A=\rho_y$; Probability of Error = .001; 0.5 bits/pel 250

4.6.14c. Hybrid Coding Scheme Using Error Correcting Code on First Coefficient; All $A=\rho_y$; Probability of Error = .001; 1.0 bits/pel 251

4.6.15a. Hybrid Coding Scheme Using Error Correcting Code on First Coefficient; All $A=\rho_y$; Probability of Error = .01; 0.25 bits/pel 252

4.6.15b. Hybrid Coding Scheme Using Error Correcting Code on First Coefficient; All $A=\rho_y$; Probability of Error = .01; 0.5 bits/pel 253

4.6.15c. Hybrid Coding Scheme Using Error Correcting Code on First Coefficient; All $A=\rho_y$; Probability of Error = .01; 1.0 bits/pel 254

5.1.1. Block Diagram of Adaptive Scheme 256

5.4.1. Autocorrelation of the Estimates of the Variance (Coefficient #1) 264

5.4.2. Estimated Variance for C_1 (N=16) 265

5.4.3. Estimated Variance for C_1 (N=32) 266

5.4.4. Estimated Variance for C_1 (N=64) 267

5.4.5. Estimated Variance for C_1 (N=128) 268

5.4.6. Estimated Variance for C_1 (N=256) 269

5.4.7. Estimated Variance for C_2 (N=32) 270

5.4.8. Estimated Variance for C_3 (N=32) 271

5.4.9. Estimated Variance for C_4 (N=32) 272

5.4.10. Estimated Variance for C_5 (N=32) 273

5.4.11. Histogram of the Differences in the Estimated Variances for Coefficient #1. 274

Page

5.4.12. Histogram of the Differences in the Estimated Variances for Coefficient #2. 275

5.4.13. Histogram of the Differences in the Estimated Variances for Coefficient #4. 276

5.4.14. Histogram of the Differences in the Estimated Variances for Coefficient #5. 277

5.4.15. Histogram of the Estimates of the variance for Coefficient #1. 279

5.4.16. Two-dimensional Hadamard transform with zonal filtering using the exponential quantizer. 4 bits/pel. 32 retained coefficients. 281

5.4.17. Two-dimensional Hadamard transform with zonal filtering and PCM encoding. Different bit assignments from chapter 4. 32 retained coefficients. 1.5 bits/pel. 282

5.4.18. Two-dimensional Hadamard transform with zonal filtering and PCM encoding. Different bit assignments from chapter 4. 32 retained coefficients. 1.0 bits/pel. 283

5.4.19. Two-dimensional Hadamard transform with zonal filtering and PCM encoding. Different bit assignments from chapter 4. 20 retained coefficients. 0.5 bits/pel. 284

5.4.20. Two-dimensional Hadamard transform with zonal filtering and differential encoding. 2.0 bits/pel. Adaptive algorithm on 32 retained coefficients. 285

5.4.21. Two-dimensional Hadamard transform with zonal filtering and differential encoding. 1.5 bits/pel. Adaptive algorithm on 32 retained coefficients. 286

5.4.22. Two-dimensional Hadamard transform with zonal filtering and DPCM encoding. 1.0 bits/pel. Adaptive algorithm on 20 retained coefficients. 287

5.4.23. Two-dimensional Hadamard transform with zonal filtering and adaptive differential encoding on c_1 only. 20 coefficients retained. 0.5156 bits/pel. 288

5.4.24. Two-dimensional Hadamard transform with zonal filtering and adaptive differential encoding on c_1 and c_2 only. 20 coefficients retained. 0.53125 bits/pel. 289

5.4.25. Two-dimensional Hadamard transform with zonal filtering and adaptive differential encoding on c_1, c_2 and c_3 only. 20 coefficients retained. 0.55469 bits/pel. 290

5.4.26. Two-dimensional Hadamard transform with zonal filtering and adaptive differential encoding on 8 coefficients. 12 retained coefficients. 0.5 bits/pel. 291

5.4.27. Two-dimensional transform with zonal filtering, and adaptive DPCM. 24 retained coefficients. 8 adaptive coefficients. 1.0 bits/pel. 292

5.4.28. Two-dimensional Hadamard transform with zonal filtering and differential encoding. 11 retained coefficients. 11 adaptive coefficients. 2 bits/diff. Average bit assignment: 1.0625 bits/pel. 293

Page

APPENDIX

Fig. A-1 Histogram of Transform Coefficient #1 Using One-Dimensional Hadamard Transform (Block Size 1x32), Variance = 3473.328. 304

A-2 Histogram of Transform Coefficient #4 Using One-Dimensional Hadamard Transform (Block Size 1x32), Variance = 47.0241. 305

A-3 Histogram of Transform Coefficient #7 Using One-Dimensional Hadamard Transform (Block Size 1x32), Variance = 31.8469. 306

A-4 Histogram of Transform Coefficient #10 Using One-Dimensional Hadamard Transform (Block Size 1x32), Variance = 7.7750. 307

A-5 Histogram of the Difference of the One-Dimensional Hadamard Transform Coefficient #1 (Block Size 1x32), Variance = 127.214. 308

A-6 Histogram of the Difference of the One-Dimensional Hadamard Transform Coefficient #4 (Block Size 1x32), Variance = 17.6124. 309

A-7 Histogram of the Difference of the One-Dimensional Hadamard Transform Coefficient #7 (Block Size 1x32), Variance = 10.5453. 310

A-8 Histogram of the Difference of the One-Dimensional Hadamard Transform Coefficient #10 (Block Size 1x32), Variance = 5.8997. 311

CHAPTER I

INTRODUCTION

The report covers work performed over a 24-month period on Contract F 33 615-73-C-1233. Although the emphasis on the work tasks listed under the above contract were changed somewhat by the Project Monitor as outlined in the Monthly Progress Reports, all the tasks listed were completed during the contract. The main deviations include rather complete investigations of methods of data compressions applicable to Remote-Piloted-Vehicles (RPV).

Chapter II summarizes the work performed during the first year on interframe (Frame-to-frame) techniques. The important concepts and investigations of this work are included in this report; however, detailed descriptions of the theoretical and simulation results are given in the Interim Technical Report on Contract F 33 615-73-C-1233, June, 1974.

Chapter III gives theoretical results using two-dimensional transform and Hybrid coding techniques of data compression. Detailed results are given for the two-dimensional Hadamard, Discrete Cosine, and Haar transform techniques. The Hybrid coding schemes using transform-DPCM or DPCM-transform techniques, which are shown to be equivalent in performance, are analyzed using the one-dimensional Hadamard transform to remove the correlation in one spatial directions. The above techniques were investigated due to their applicability in the RPV. The effects of channel errors are also investigated theoretically. Investigations concerning the suitability of the Markov model for aerial type photographs are included.

Chapter IV contains the simulation results using aerial photographs supplied by WPAFB. Numerous photographs are presented that have been processed using the

Reproduced from best available copy.

techniques described in Chapter III. Bit rates from 0.25 to 1.5 bits/pel are considered, using various encoding procedures. The effects of channel noise on the different processing schemes and optimization techniques for noisy channels are presented. In addition several techniques of periodic resetting and error correcting coding are considered.

In Chapter V an adaptive scheme is investigated using the two-dimensional Hadamard transform. In this scheme the quantizer is adjusted by estimating the standard deviation and using this estimate to normalize the coefficients before quantization. The standard deviation is transmitted using DPCM techniques. Several variations, using the adaptation algorithm on only the first few coefficients are considered. Simulation results are given for the scene of the "Truck". In Chapter VI a brief summary of the important results are given. Table 6 gives in tabular form the characteristics of several methods of data compression which may be useful for RPV.

An extensive selection of the most important references on data compression techniques applicable to the RPV mission is given. These references are grouped according to Transform techniques, differential techniques, frame-to-frame techniques, etc.

CHAPTER II

INTERFRAME REDUCTION FOR RPV'S

2.1 Introduction

During the first year of this contract it was decided that emphasis should be placed on possible interframe data compression techniques applicable to Remote Piloted Vehicles (RPVs), assuming one frame of storage available on the RPV.

Due to the nature of the RPV mission the use of frame-to-frame techniques should allow for large bandwidth reductions, with of course increased complexity due to the storage requirements. Fig. 2.1.1. illustrates the areas scanned on the ground by a television camera located on the vehicle for two consecutive frames. For this illustration we have assumed a constant velocity vector in a horizontal plane at an

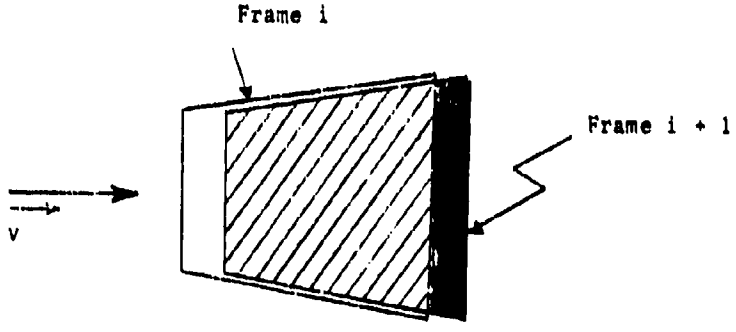

Fig. 2.1.1. Two Consecutive Frames

altitude h above the ground. The cross-hatched area shown in Fig. 2.1.1. represents the redundant information in frame i + 1 given from i. The non-redundant information is indicated by the shaded area. Applying this technique to the RPV video system should result in large bit reductions. Recently, some real time experiments that take advantage of the frame-to-frame correlation in picture-phone applications have been conducted at Bell System Laboratories. Early experiments using frame repeating

techniques [114, 115] show that simple frame repeating reduces the rate of transmission, avoiding flicker by displaying each frame several times before replacing it with a new frame. To improve the efficiency of transmission, the frame-to-frame differential PCM has been used, this is similar to DPCM except that the signal value of the previously reconstructed frame is used as the predicted value rather than the previous sample of the same frame. It has been observed that only those elements that change between frames are encoded for transmission, accompanied by their respective position location codes. This method of coding is referred to as conditional replenishment [116]. A different coder has been described by Candy, et. al. [120] in which clusters of significant frame differences are transmitted using a double-length code (4-bit and 6-bit) for the frame differences and 8-bit addresses for the clusters. For signals containing differential quantizing noise, improved methods are described by Connor, et. al. [123] in which the noisy picture is segmented into moving areas and background areas. References [119, 121] describe other methods that have been experimented with to fully exploit the high spatial and temporal (frame-to-frame) correlation. The use of a frame memory capable of storing the entire frame image is practical with the present state of art. Manasse [111] has presented a method which involves the use of high directional correlation inherent in successive samples along a scanning line, corresponding samples of two successive lines of the same frame, and the corresponding samples of two successive frames. Rocca [112] has studied a bandwidth compression method utilizing interframe correlation in which the effects of movements of the camera and of the objects are compensated. Rocca and Zanoletti [113] have presented a simple movement compensation procedure which can be obtained by dividing the image into zones and then transmitting for each zone a displacement vector relating the zone in a particular frame to

a zone in the previous frame that is maximally correlated with it. A frame-to-frame coding technique using two-dimensional Fourier transforms has been described by Haskell [128].

Since the television pictures from an RPV mission contains high frame-to-frame correlation, the use of interframe techniques would seem to be advantageous. The remainder of this chapter describes an interframe technique that utilizes measured data, such as velocity, altitude, horizontal and vertical field of vision, depression angle, etc., to exploit the high correlation between successive frames. A prediction algorithm is found whereby frame i is predicted from frame i - 1 using the measured parameters of the vehicle. The performance of the system is studied subject to the mean-squared-error criterion of goodness.

In this chapter we summarize the work performed during the first year of interframe techniques and its application to RVPs. For a detailed description of the study the reader is referred to the Interim Technical Report for Contract F 33 615-73-C-1233, Video Data Compression Study For Remote Sensors, June 1974.

2.2 Interframe Technique for RPVs.

Fig. 2.2.1 illustrates the basic philosophy of the technique. Initially we assume one frame stored in memory, using this frame as a reference the next frame is predicted using a predetermined "prediction algorithm". The pels of the predicted frame are then compared with the new frame and if no significant difference exists, no picture element is transmitted. This technique is repeated so as to continuously store the predicted reference picture and update only those pels that differ significantly from the new frame. Only those pels required to update the reference picture, along with positional information, are transmitted. At receiver, which is located on the ground, the received information is used

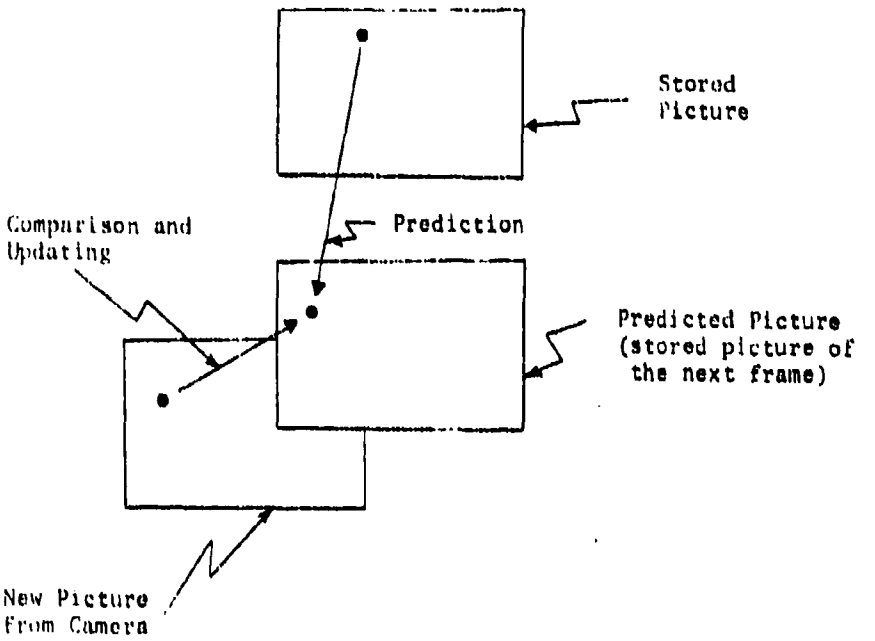

Fig. 2.2.1. Philosophy of Data Compression Scheme.

to update a similar predicted reference frame which tracks the one at the transmitter. The information transmitted contains positional and intensity information which enables the reference frame to be correctly updated.

Fig. 2.2.2 shows a block diagram of one possible implementation of the transmitter portion of the system. There are of course other variations which can be made, for example one could omit the 8-bit analog-to-digital converter and insert a digital-to-analog converter just before the subtractor. Depending upon which way the system is implemented the differential quantizer would have a different implementation. For illustration of the system operation we will assume the configuration shown in Fig. 2.2.2.

In operation the transmitter is assumed to have a reference frame in memory.

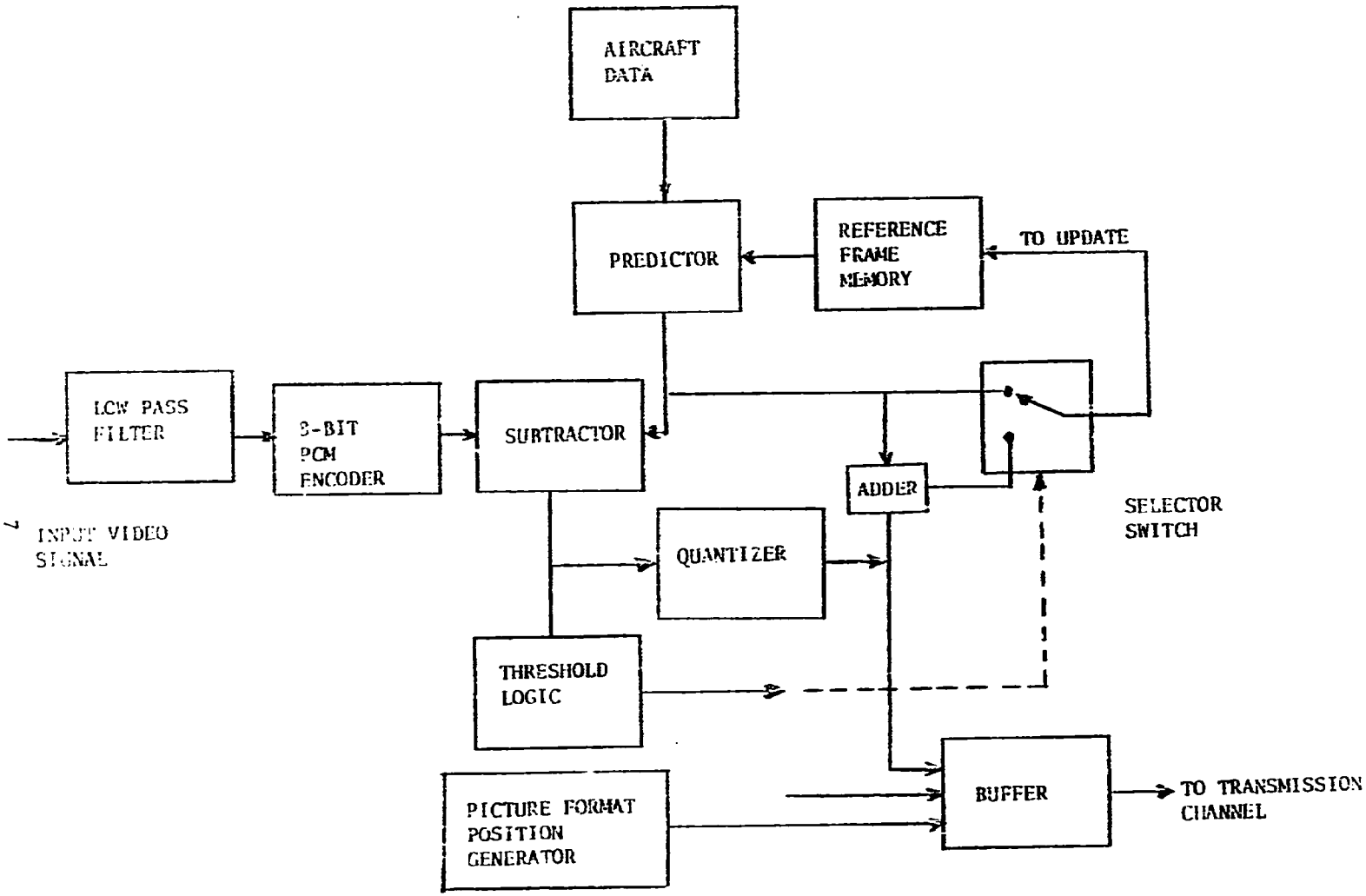

Fig. 2.2.2. Interframe-DPCM Transmitter.

Using this reference frame the predictor is programmed so as to predict the location and intensity value of an incoming pel. This intensity value of the predicted pel and its location in the new frame is determined by a predetermined prediction algorithm using measured vehicle data such as velocity, altitude, etc. This predicted value is compared with the new information in the subtractor circuit which yields an intensity difference signal. The difference signal is quantized using a differential quantizer. During each sample period, the threshold control logic makes a decision depending upon the absolute magnitude of the difference signal. If the difference signal magnitude is considered to be insignificant, the predicted value is used to update the reference frame memory. If a significant difference between the predicted and the actual picture element occurs, the output of the control logic operates a selector switch which strobes the output of the adder into the memory. In addition to updating the memory the control logic also causes the quantized difference signal, accompanied by its corresponding address, to be stored in a buffer. The buffer store is used to match the random updating rate to the constant bit rate of the transmission channel.

The system shown in Fig. 2.2.2 can easily be modified so as to exploit both intraframe and interframe correlation. Such a system is shown in Fig. 2.2.3. The operation is basically the same as the interframe DPCM system with the exceptions that the inputs to the subtractor are the differences of two successive samples of the input signal and the predicted signal respectively.

Delay lines A and B delay the incoming signal sample and the reference sample respectively. The subtractors A and B compute the actual sample-delayed and the predicted sample-delayed difference respectively. These delayed difference signals are compared using the differential subtractor.

In both systems, the inputs to the adder are the predicted signal value and

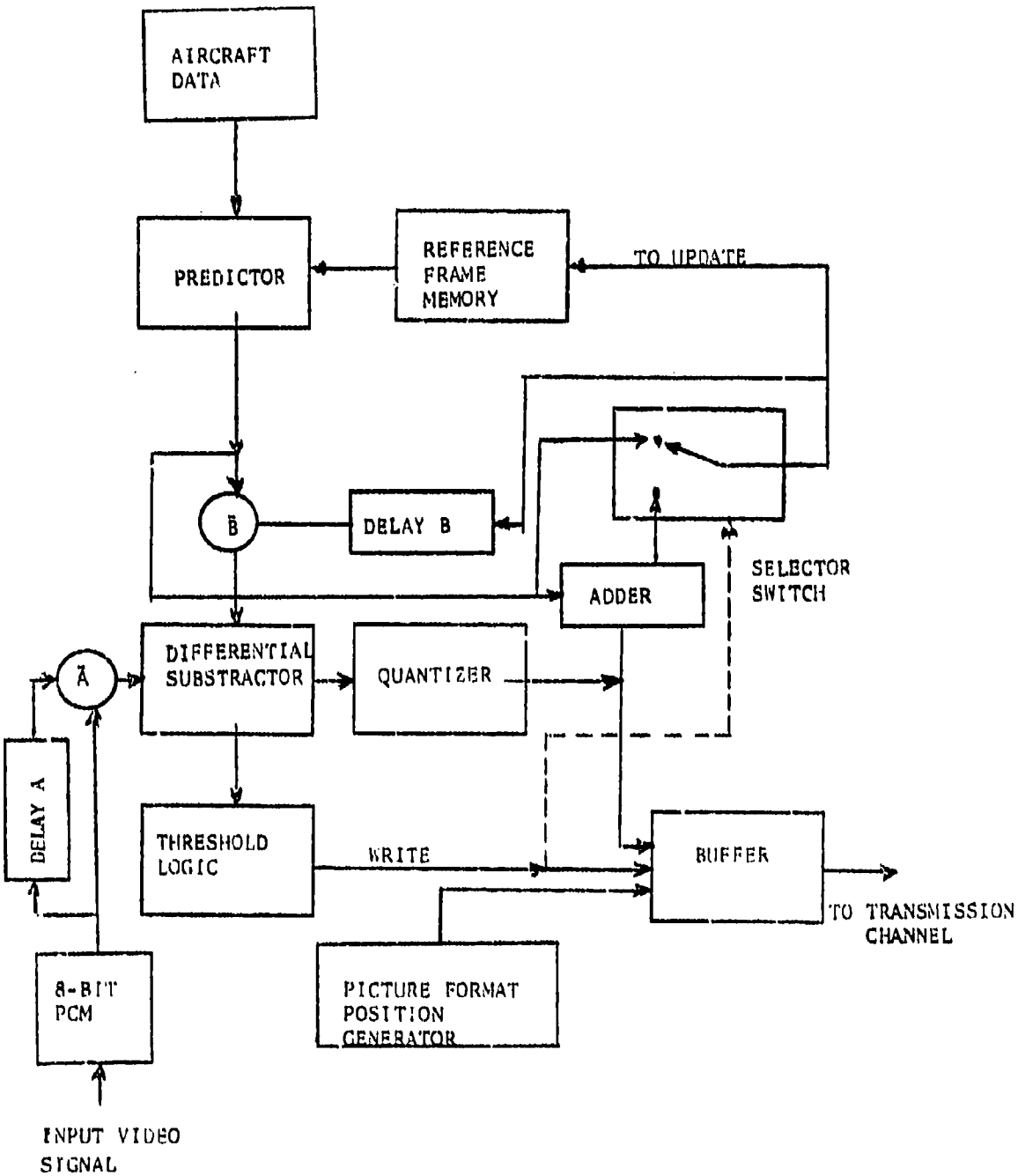

Fig. 2.2.3. Intraframe-DPCM-Interframe-DPCM Transmitter.

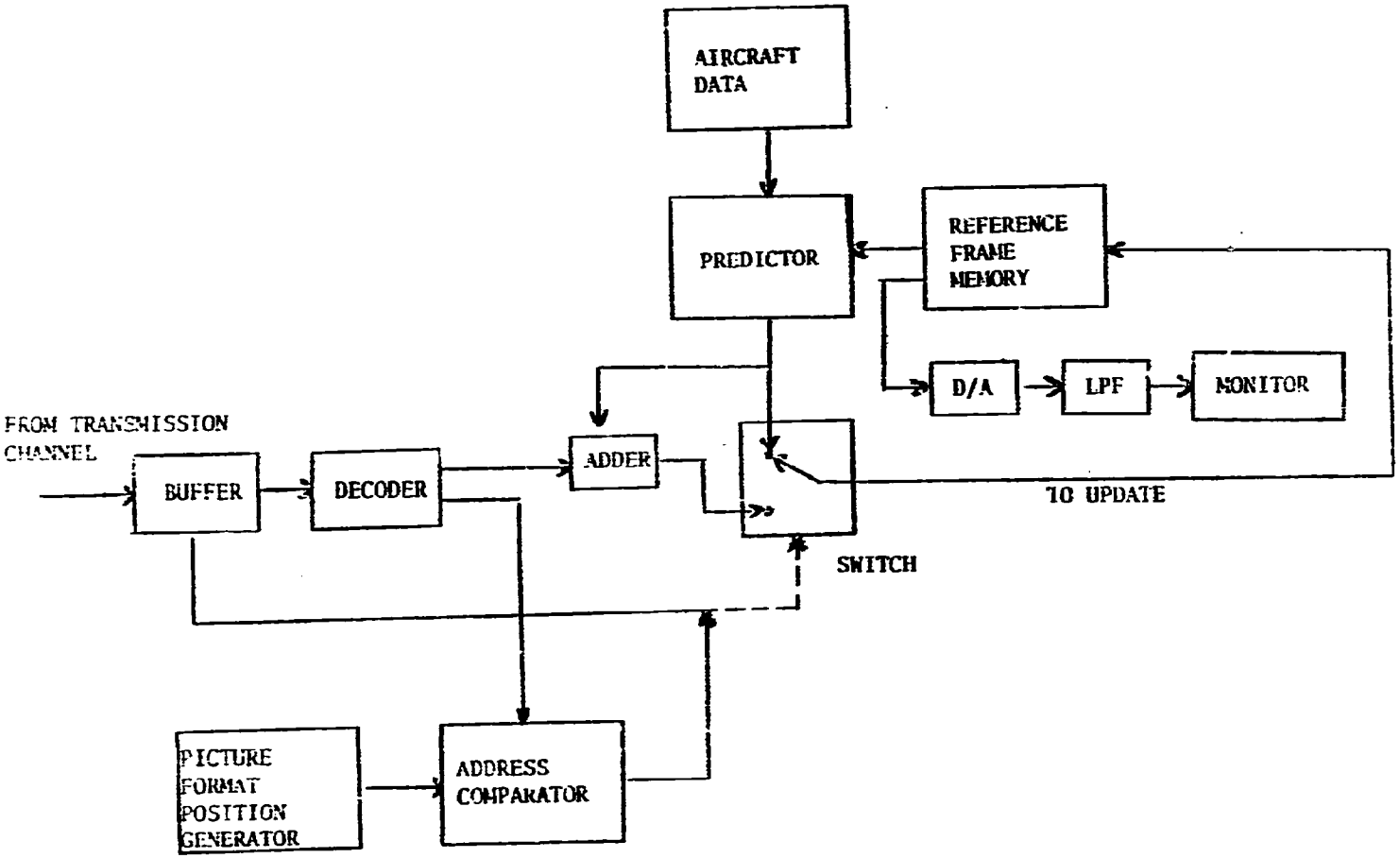

Fig. 2.2.4. Receiver.

the output of the differential quantizer.

A buffer may be employed at the receiver as shown in Fig. 2.2.4 to store the received picture information until it can be strobed in proper time sequence into the receiver's adder circuit. A transfer of new information from the buffer to the adder is accomplished whenever the output of the picture format address generator is in agreement with the address information of the picture element to be read from the buffer. This agreement is determined by the address comparison circuit which operates a selector switch enabling the new information to update the receiver's frame memory. When the addresses do not coincide the predicted value is used to update the receiver's frame memory. After this occurs, the buffer read out then advances to the next element. After each frame time, the picture information stored in the receiver's memory is matched to the transmitter's stored reference picture.

The information stored in the frame memory is decoded to recover the video information for visual display.

2.3 Geometry of the System

In order for the predictor to accurately predict the intensity level of a pel in frame i + 1, from frame i, it is necessary to account for the movement of each pel from one frame to another. This is illustrated in Fig. 2.3.1 where we illustrate the typical movement of a point $P'(x_1,y_1)$ on the screen of the camera, which is the image of poing P(x,y) on the ground. The point P'(x,y) in frame i moves to $P''(x_2,y_2)$ in frame i + 1 due to motion of the vehicle. Based on the coordinates (x_1,y_1), the new coordinates (x_2,y_2) can be estimated using measurements of the vehicle dynamics and known characteristics of the optical system. It should be realized that some points will move out of the new frame and become distorted, while others will appear that cannot be predicted from the previous frame.

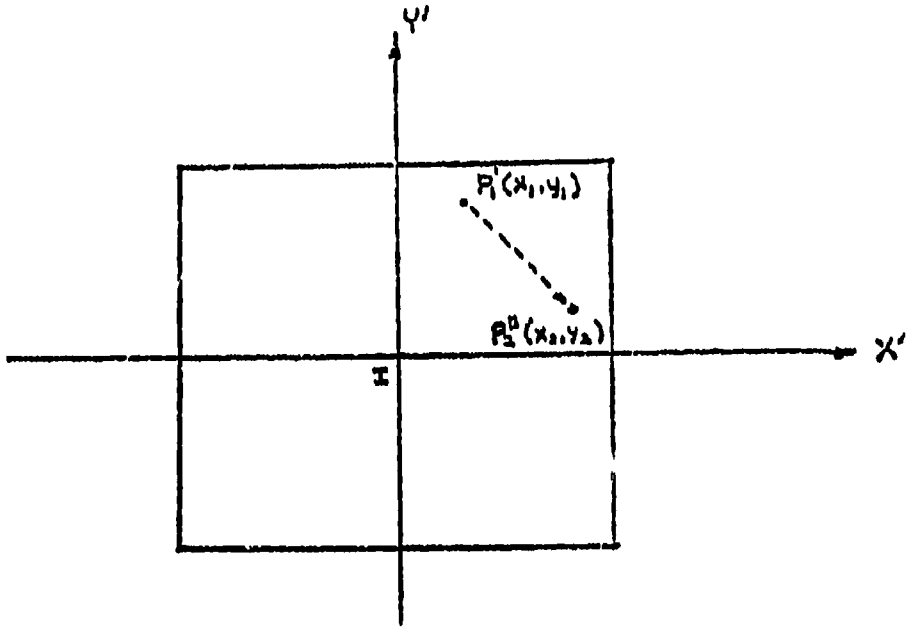

Fig. 2.3.1. Diagram of the Position Displacement of an Image on the Screen of a Point on the Ground.

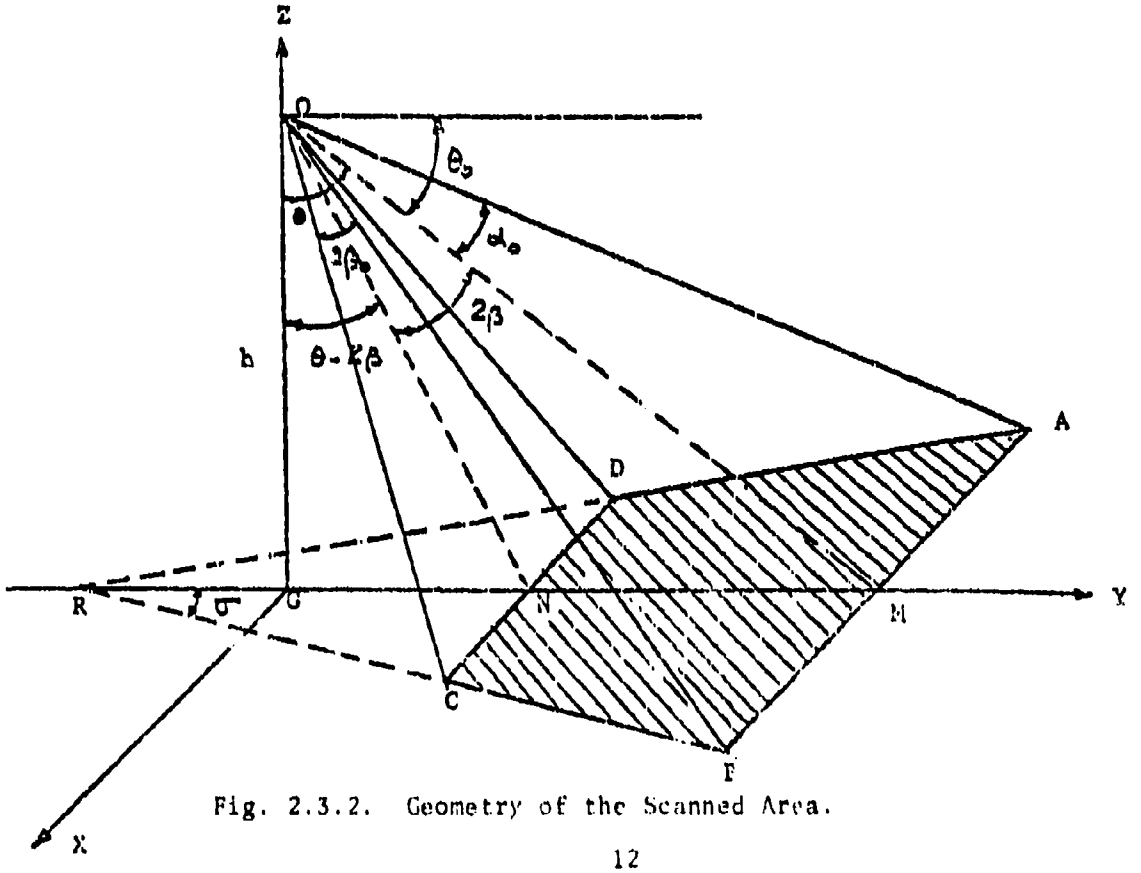

Fig. 2.3.2. Geometry of the Scanned Area.

In order to determine the prediction algorithm, the geometry of the system must be investigated. Assuming the vehicle at point O at some instant of time, the area scanned on the ground is an isolete trapezoid whose dimensions depend on the altitude h of the vehicle, the horizontal and vertical fields of vision of the camera, $2\alpha_o$ and $2\beta_o$ respectively and the depression angle θ_o of the camera position. This is illustrated in Fig. 2.3.2.

The dimensions of the trapezoid shown in Fig. 2.3.3 can be calculated in terms of h, α_o, β_o and θ where θ is a new angle defined by

$$\theta = 90^o - \theta_o$$

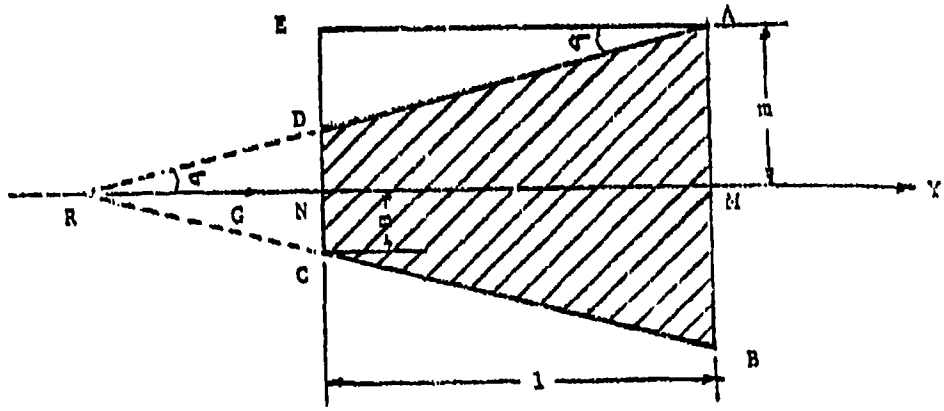

Fig. 2.3.3. Dimensions of the Scanned Area.

From geometrical considerations the following can be determined (see Interim Technical Report, June 1974 for details):

$$2\beta = \tan^{-1}\left[\sin\beta_o\left(2/(\cos 2\alpha_o + 2\beta_o)\right)^{\frac{1}{2}}\right] \qquad (2.3.1)$$

$$m = OM \tan \alpha_o = h \sec \theta \tan \alpha_o \qquad (2.3.2)$$

$$n = ON \tan \alpha_o = h \sec (\theta - 2\beta) \tan \alpha_o \qquad (2.3.3)$$

and

$$\tan \sigma = \frac{(\tan \alpha_o)\ (\ \sin (\theta - \beta)\ )}{\cos \beta} \qquad (2.3.4)$$

It is seen in Fig. 2.3.4 that the scanned trapezoidal area ABCD on the ground is projected on the screen of the camera system as the rectangle A'B'C'D'. We can observe that within the scanned area, any line parallel to line AB will be projected as a horizontal line on the screen; and any line that passes through point R will appear as a vertical line on the screen.

These observations are used to derive a relation between the coordinates (b_1,b_2) of a point P located within the scanned area on the ground and its projected image coordinates (x,y) on the screen.

I. Horizontal and Vertical Positions

Referring to Fig. 2.3.4, it is seen that the projected images of points $P(b_1,b_2)$ and $P_1(MP_1,GM)$ have the same horizontal coordinate x_1 on the screen, since the three points R,P and P_1 are colinear. The relation between x_1 and b_1 and b_2 is obtained considering the plane which contains lines AB and OM as shown in Fig. 2.3.5.

It is seen from Fig. 2.3.5 that the algebraic length $M'P_1'$ is the horizontal coordinate of the projected image of point P_1 or P on the ground, namely x_1.

Using geometric relationships it is shown that the relation between the horizontal coordinate x_1 of the projected image P' on the screen corresponding to coordinate b_1 and b_2 of a point on the ground is

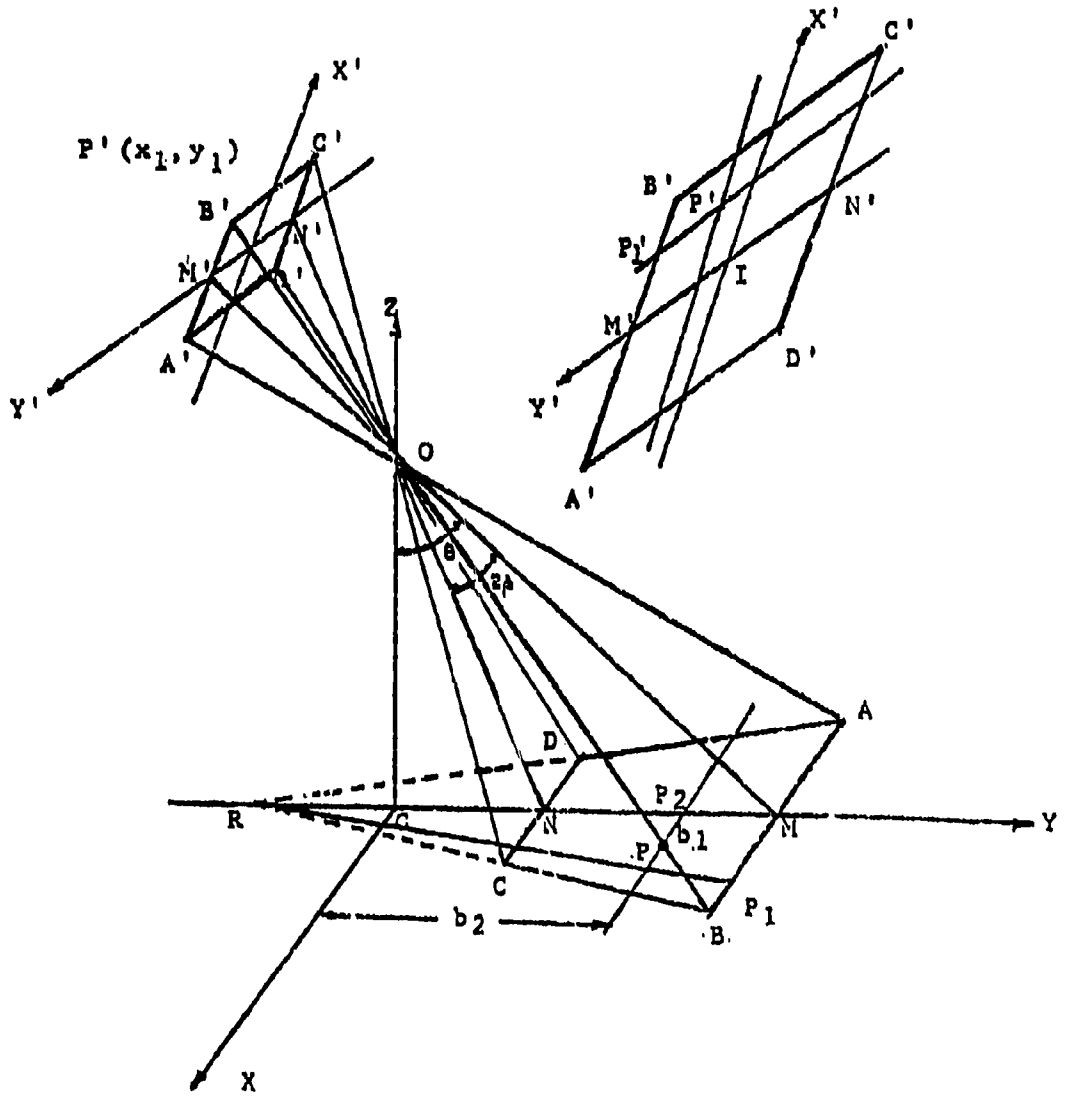

Fig. 2.3.4. Image Position of a Point on the Ground.

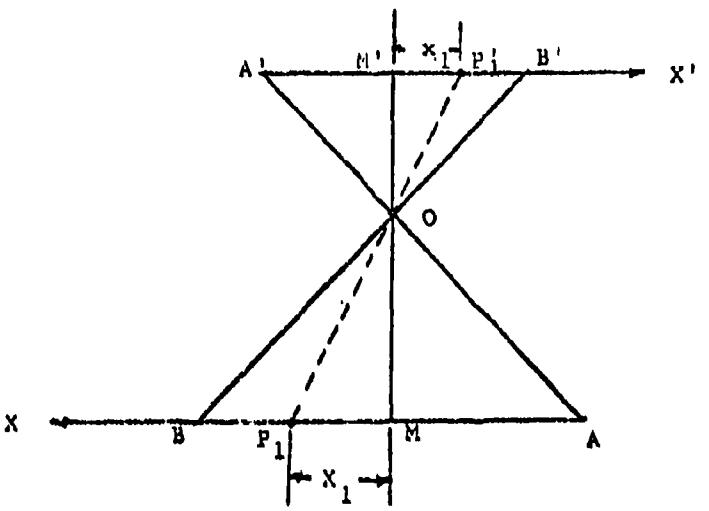

Fig. 2.3.5. Diagram of the Horizontal Position of an Image.

$$x_1 = \frac{a - b_1}{h \cos(\theta - \beta) + b_2 \sin(\theta - \beta)} \qquad (2.3.5a)$$

where a is defined as the distance from the screen to the lense.

In similar manner using a plane in the zy directions, it can be shown that the relation between the vertical position y_1 on the screen and the coordinates b_1 and b_2 is

$$y_1 = \frac{a[b_2 - h \tan(\theta - \beta)]}{h + b_2 \tan(\theta - \beta)} \qquad (2.3.5b)$$

Having obtained the position coordinates (x_1, y_1) of a point P' in terms of its corresponding point on the ground, with coordinates (b_1, b_2) and assuming knowledge of

the present position of the vehicle's camera, i.e. the altitude of the aircraft, the horizontal and vertical fields of vision, the depression angle of the camera and the perpendicular distance from the camera's lense position to the screen; the next step is to derive an analytical expression of the displacement in position of a point $P'(x_1,y_1)$ due to the motion of the aircraft.

Consider a point $P(b_1,b_2)$ within the scanned area on the ground with its image $P'(x_1,y_1)$ on the screen, due to the motion of the aircraft the point P', after some frame time T_f, will move to $P''(x_2,y_2)$. The new position (x_2,y_2) is related to the original position (x_1,y_1) which depends on the attitude of the flight and other parameters such as altitude, aircraft velocity, depression angle of the camera, etc.

This investigation will include two modes of flight (1) Steady Straight Flight, and (2) Horizontal Circling Flight.

In either case it is assumed that the camera attached to the aircraft has been stabilized vertically as well as horizontally and the depression angle is kept unchanged regardless of the aircraft flight attitudes.

(1) Steady Straight Flight

A straight flight is defined as the motion of an aircraft in direction parallel to its plane of symmetry. Generally, the direction of motion is inclined upwards or downwards by an angle of inclination.

The horizontal and vertical position displacement of an image will be investigated and the new projected position coordinates (x_2,y_2) on the screen of a point P on the ground in the new frame will be derived as functions of points $P'(x_1,y_1)$ in the previous frame. These expressions will be used in the prediction algorithm to determine the positions.

We assume that the aircraft is at position 0 originally and it moves to position 0_2, as seen in Fig. 2.3.6 after some frame time T_f. The velocity vector V of the aircraft at any instance is:

$$\hat{V} = v_y\hat{y} + v_z\hat{z}$$

where $\hat{y}$ and $\hat{z}$ are unit vectors in the Y- and Z-coordinate of the ground reference coordination system, respectively.

Referring to Fig. 2.3.4, when the aircraft was at 0, the image of a point $P(b_1,b_2)$ projected on the screen was $P'(x_1,y_1)$ and the relation between the vertical coordinate y_1 and (b_1,b_2) is expressed using (2.3.5b) which is presented below for convenience.

$$\frac{b_2}{h} = \frac{y_1 + a.\tan(\theta - \beta)}{a - y_1.\tan(\theta - \beta)}$$

After some time interval T_f, the aircraft moves forward a distance $y = v_y.T_f$ and upward or downward a distance $z = v_z.T_f$ depending upon the direction of inclination. Fig. 2.3.6 shows an upward distance z. The aircraft is now at the altitude of (h + z) and is closer to point P_2 by a distance y. The new reference coordinate system Z_2Y_2 on the ground can be considered as a result of translating the original reference coordinate system ZY a distance y in the Y-direction.

With respect to the new reference coordinate system whose origin is now at 0_2, the Y_2-coordinate of point P_2 now becomes b_2' where:

$$b_2' = b_2 - y \qquad (2.3.6)$$

Since the vertical coordinate of the new image P'' of point P_2 becomes y_2, due to the motion of the aircraft from point 0 to point 0_2, the translation of the ground reference coordinate system origin to 0_2 the relation between the vertical coordinate of the image on the screen and the coordinate b_2' of point P with respect to the new reference coordinate system now becomes

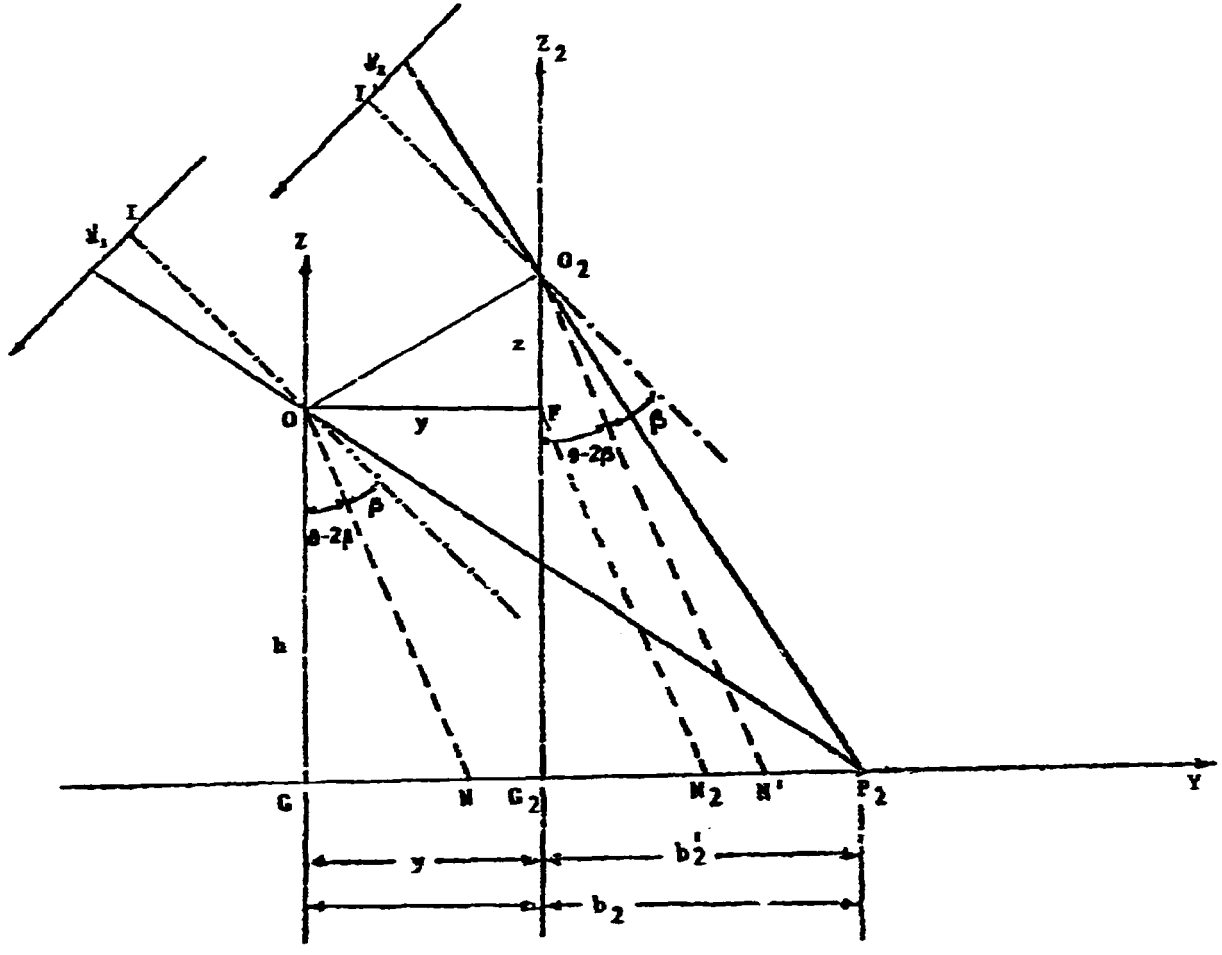

Fig. 2.3.6. Diagram of the Vertical Position Displacement of an Image.

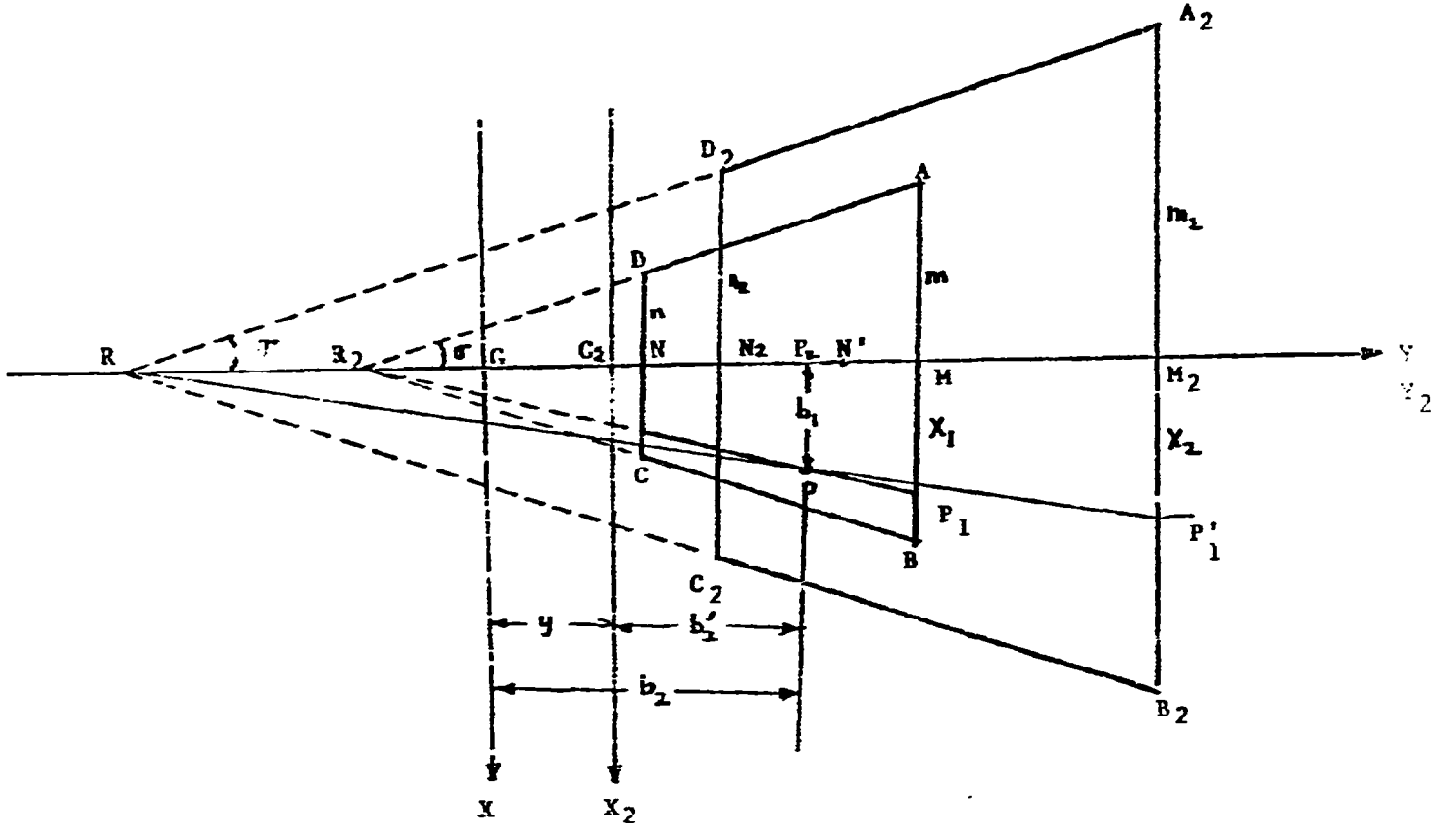

Fig. 2.3.7. Diagram of the Displacement of the Scanned Area on the Ground Due to Straight Flight.

$$\overline{R_2N_2} = \frac{(h + z).\sec\theta.\cos\beta}{\sin(\theta-\beta)} \qquad (2.3.5)$$

The relation between X_2 and the coordinates b_1, b_2 is expressed by

$$\frac{X_2}{b_1} = \frac{(h + z).\sec\theta.\cos\beta}{(h+z).\cos(\theta-\beta) + (b_2-y).\sin(\theta-\beta)} \qquad (2.3.6)$$

The relation between the coordinate $\overline{M_2P_1}$ which is X_2 and its image on the screen, namely $\overline{M_2'P_2'}$ which is x_2, is obtained with the aid of Fig. 2.3.8.

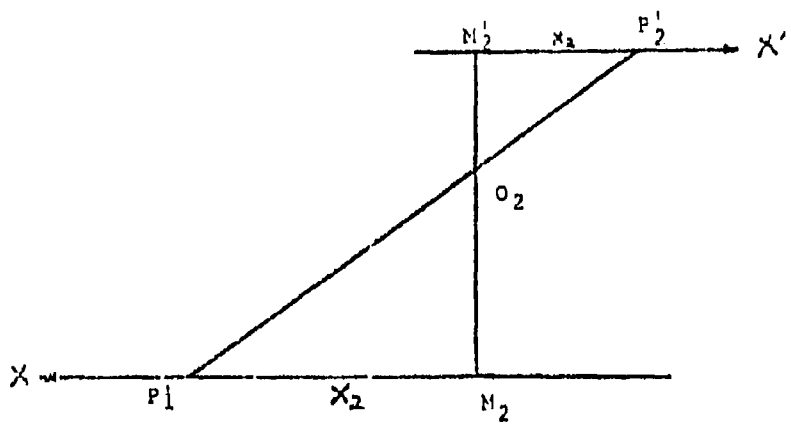

Fig. 2.3.8. Diagram of the Horizontal Position of an Image.

$$\frac{b'_2}{h+z} = \frac{y_2 + a.\tan(\theta-\beta)}{a - y_2.\tan(\theta-\beta)} \qquad (2.3.7)$$

Using (2.3.5b and (2.3.6), (2.3.7) the new vertical coordinate y_2 can be obtained as an explicit function of its original vertical position y_1 and the velocity components in the previous frame, (for mathematical details, see Interim Technical Report, June 1974).

$$y_2 = \frac{a\{h.y_1.\sec^2(\theta-\beta) - T_f[v_y + v_z.\tan(\theta-\beta)][a - y_1.\tan(\theta-\beta)]\}}{h.a.\sec^2(\theta-\beta) - T_f[v_y.\tan(\theta-\beta) - v_z][a - y_1.\tan(\theta-\beta)]} \qquad (2.3.8)$$

In a similar manner using Figs. 2.3.7 and 2.3.8 it can be shown that the new horizontal coordinate is given by (for details see ITR, June, 1974)

$$x_2 = \frac{x_1 ha}{ha + T_f[v_z.\cos(\theta-\beta) - v_y.\sin(\theta-\beta)][a.\cos(\theta-\beta) - y_1.\sin(\theta-\beta)]} \qquad (2.3.9)$$

(2) Horizontal Circling Flight

A second case of interest is when the aircraft's flight path is a true-bank turn as shown in Fig. 2.3.9. We assume that the camera is inertially stabilized as previously mentioned.

The velocity vectors $\hat{V}$ and $\hat{V}_2$ are tangential to the curve path at point 0 and 0_2 respectively. With the knowledge of magnitudes and directions of the velocity vectors as measured by the aircraft's instruments, the distance traveled by the aircraft with respect to its starting position can be calculated with the aid of an air-data computer system installed in the aircraft. A detailed explanation of these computations is given in Reference [121]. For simplicity, we assume that after some

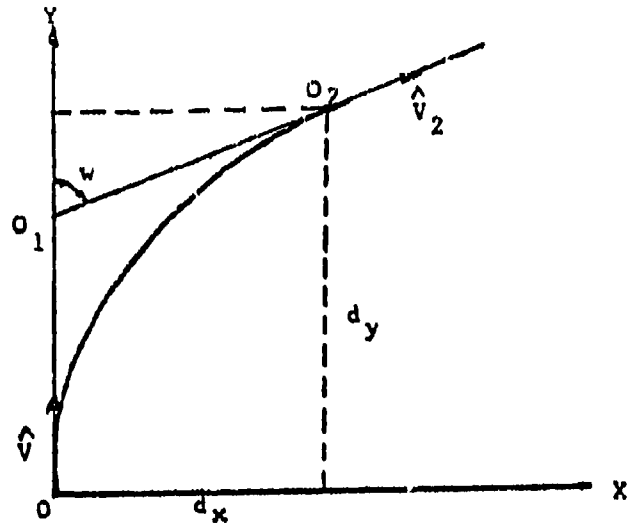

Fig. 2.3.9. Diagram of Horizontal Circling Flight.

time T_f the horizontal and vertical distances traveled, noted as d_x and d_y respectively, and the defined angle w are known. These quantities are used for computation of position displacements. A point $P(b_1,b_2)$ on the ground has its projected image point $P_1(x_1,y_1)$ on the screen which moves to $P_2(x_2,y_2)$ some time T_f later due to the motion of the aircraft. In the case of horizontal circling flight, the new position coordinates (x_2,y_2) can be calculated in terms of its initial position coordinates (x_1,y_1) and the flight dynamics by considering the motion of the camera in three separate phases:

(i) First, the aircraft hypothetically moves from point 0 to O_1, referring to Fig. 2.3.9, following a straight flight path which covers the distance $00_1 = d_y - \cot w$. With respect to its initial position coordinates (x_1,y_1), the new position coordinates of the intermediate point image P_2', namely x_2' and y_2', can be calculated using the straight flight vertical and horizontal displacement equations obtained in the previous part.

(ii) At point O_1 the aircraft rotates by an angle w in zero time.

An expression accounting for this hypothetical situation will be derived to calculate the new position coordinates (x_2'', y_2'') of a point P_2'' on the screen, as the result of the rotation of the aircraft, with respect to its previous position coordinates, namely x_2' and y_2'.

(iii) Finally, the aircraft is again following another straight flight puth from point O_1 to O_2 which covers a distance of $O_1O_2 = d_x.\csc w$. The final position coordinates (x_2, y_2) are obtained by using the equations in the previous part.

We now investigate the position displacement of a point $P_1(x_1, y_1)$ on the screen which is the image of a point $P(b_1, b_2)$ on the ground when the aircraft is moving in a curve path such that the camera makes an angle w with respect to the original flight path.

It is shown in the Interim Technical Report (F 33 615-73-C-1233) that the relations between the coordinates in the two frames for the case is given by

$$y_2 = \frac{a[y_1[\cos w+\tan^2(\theta-\beta)]+x_1.\sin w.\sec(\theta-\beta)+a.\tan(\theta-\beta)(\cos w-1)]}{y_1\tan(\theta-\beta)(\cos w-1)+x_1\sin w\ \sec(\theta-\beta)\tan(\theta-\beta)+ a[1+\cos w.\tan^2(\theta-\beta)]} \qquad (2.3.10)$$

$$x_2 = \frac{a[x_1.\cos w -[y_1.\cos(\theta-\beta) + a.\sin(\theta-\beta)]]}{x_1.\sin w.\sin(\theta-\beta) + y_1.\sin(\theta-\beta).\cos(\theta-\beta).(\cos w-1)+ a[\sin^2(\theta-\beta).\cos w + \cos^2(\theta-\beta)]} \qquad (2.3.11)$$

2.4 Prediction Algorithm

With the results of the positional relations for pels one can predict the movement of redundant pels in frame i + 1 from those in frame i (redundant pel are shown by the cross-hatched area in Fig. 2.4.1). Due to the trapezoidal nature of the area scanned on by the camera there will be some distortion due to the fact that a pel in frame i represents more area than that in frame i + 1. The prediction algorithm must account for this distortion in addition to determining the positional information.

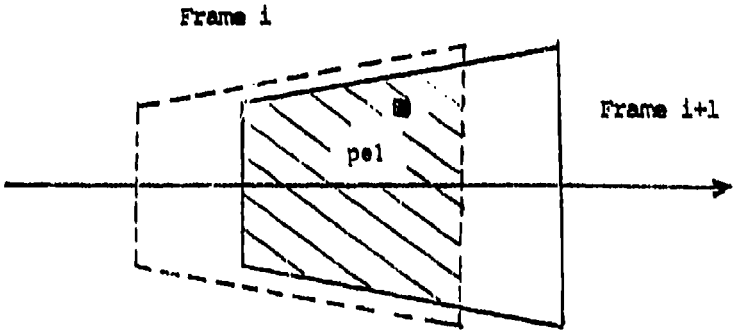

Fig. 2.4.1. The Scanned Area on the Ground at Two Consecutive Frame Time

The frame image is assumed to be spatially sampled and represented by a square array of NxN intensity samples as illustrated in Fig. 2.4.2. Each picture element is represented by a discrete function f(i,j), where f( ) is the intensity level and i,j are the coordinates of the picture element.

The entire area covered by an image is divided into NxN rectangular elements which are labeled accordingly. Thus, the ij^{th} picture element whose intensity value is f(i,j) is assumed to be at the center of the ij^{th} sub-area as shown in Fig. 2.4.2.

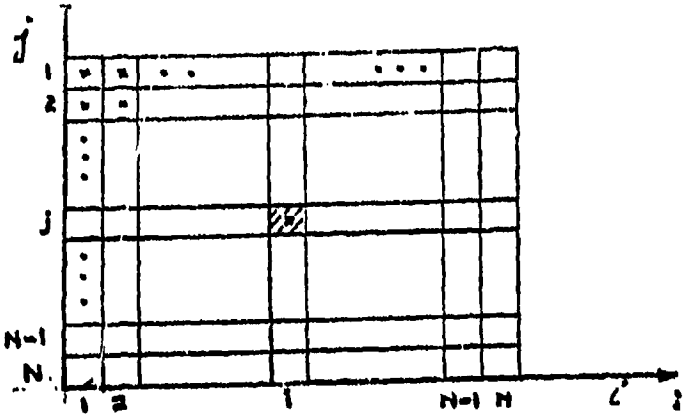

Fig. 2.4.2. Geometry of a Picture Element on the Screen.

For every redundant picture element in frame i with coordinates (8,j), there is a pel with coordinates (x_1,y_1) on the previous frame which can be calculated using the frame-to-frame positional relation given in the previous section.

The ij^{th} predicted intensity value $\hat{f}_2(i,j)$ of the pel is obtained from the intensity value $f_1(x_1,y_1)$ of the pel in the previous frame.

To account for the spatial distortion from frame-to-frame, two techniques are used to specify the predicted value $\hat{f}_2(i,j)$.

One type of algorithm is to assign the intensity value of the nearest position (i',j') in the previous frame to be the predicted value $\hat{f}_2(i,j)$, as illustrated in Fig. 2.4.3, i.e., the predicted value $\hat{f}_2(i,j)$ of the pel is the intensity value of the pel whose sub-area covers the position (x_1,y_1). We designate this as the zero-order-hold (ZOH) technique.

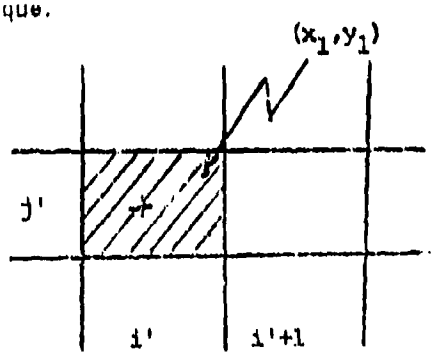

Fig. 2.4.3. Diagram of Zero-Order-Hold Prediction.

The predicted value of the pel will be

$$\hat{f}_2(i,j) = f_1(i' j') \tag{2.4.1}$$

Another method that could be used is to linearly interpolate from the four samples surrounding the position (x_1,y_1). This is illustrated in Fig. 2.4.4, and is designated as the linear interpolator technique (LI).

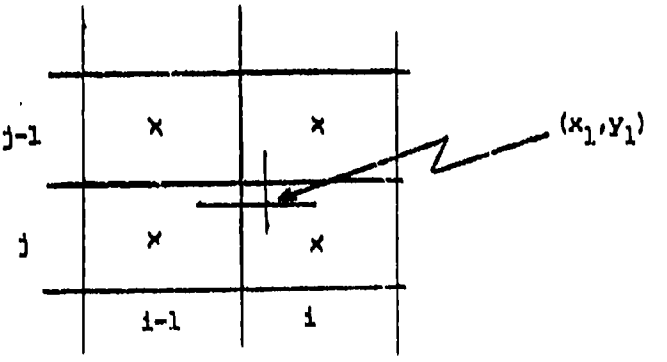

Fig. 2.4.4. Diagram of Two-Dimensional Linear Interpolation.

The predicted value $f_2(i,j)$ is calculated by linearly interpolating in the j-direction.

$$\hat{f}_2(i,j) = g_2(j-1) + [g_2(j')-g_2(j'-1)]\ [y_1-(j'-1)] \tag{2.4.2}$$

The error $e(i,j)$ due to predicting the ij^{th} picture element is the difference between the incoming signal value $f_2(i,j)$ and its corresponding predicted value $f_2(i,j)$

$$e(i,j) = f_2(i,j) - \hat{f}_2(i,j)$$

It is seen from Fig. 2.4.1 that some picture elements in frame i + 1 on a particularly line will not correspond to a particular picture element in frame i.

To account for this situation, the predicted values of these picture elements are assumed to be the values of the nearest picture elements that have correspondents in the previous frame.

In summary, the prediction algorithm must perform the following functions:

(1) Compute the position of the pels using (2.3.8) and (2.3.9).

(2) Predict the intensity level.

Since the prediction algorithm requires the use of measurements of velocity, altitude, heading, etc., there will be errors introduced which will limit the accuracy of the prediction; thus, the amount of compression that can be achieved.

A theoretical analysis relating to the sensitivity of the prediction is given in the Interim Technical Report for Contract F 33-615-73-C-1233, June 1974. In the simulations described in the next section we introduce random noise to account for the errors in the measurements.

2.5 Simulation Results (Interframe-DPCM)

Several frames of a typical RPV mission containing some fuel tanks were supplied by WPAFB. However, upon investigation it was found the movement of fuel tanks followed no predictable path. This could have been the result of several things, such as movement of the camera during the mission, etc. Along with this behavior, several parameters such as velocity, altitude, depression angle, horizontal and vertical fields of vision were unknown. The best data that could be obtained regarding the parameters that were needed was:

(1) Velocity of 200 knots.
(2) An altitude of 1500 feet.
(3) Depression angle of 15°.
(4) Horizontal field of vision 18°.
(5) Vertical field of vision 13°.
(6) A frame rate of 5 per second.
(7) Dimensions of the frame is .631" x .872".

Due to the fact that most of the above parameters were, at best, a good guess and that the camera was apparently continuously moved in an unpredictable manner, as evidenced by the erratic movement of the targets from one frame to another, the pictures were found unusable. In order to test the system a 256 by 256 portion of one of the pictures containing the fuel tanks was used as a frame (frame i) and the input picture (frame i+1) was generated using the prediction algorithm described in Section 2.4. The effect of a real system was simulated by making the velocity, altitude, etc., random variables. This was done by adding predetermined amounts of noise to the parameters. The mean values of the parameters were assumed to be those specified above.

Fig. 2.5.1 shows a block diagram of the interframe DPCM simulation. For this simulation a 256 x 256 portion of the aerial photograph, containing the fuel tanks, was used as the reference picture. The new frame input was simulated by using the reference frame to predict the new frame and adding noise to the assumed velocity.

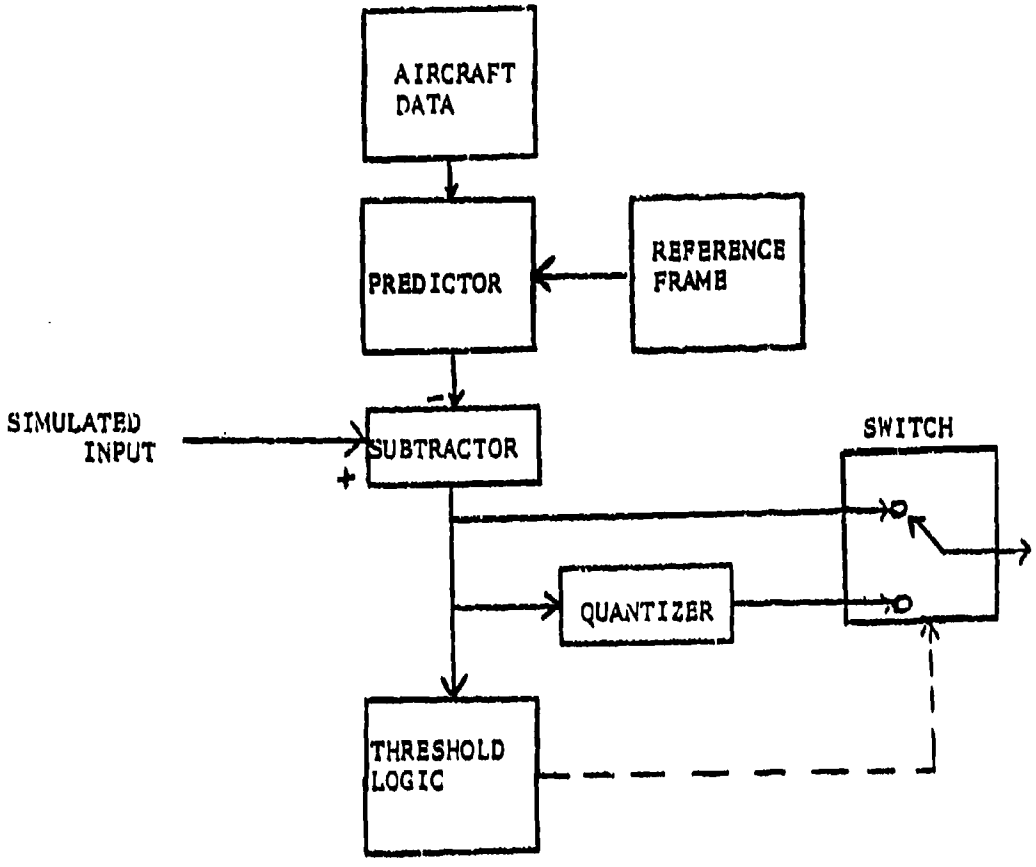

Fig. 2.5.1. The Simulated Interframe-DPCM System.

The velocity was assumed to be a gaussian random variable with a mean equal to the true velocity and variance σ_v^2. This in effect implies noise in the measurement of the velocity.

Histograms of the grey levels of a portion of the aerial photograph containing the fuel tanks, the simulated pictures and the difference signals between the input signal and its predicted value for various predetermined values of standard deviation assumed for the aircraft speed are given in the Interim Technical Report. These statistical characteristics are summarized in Tables 2.5.1 and 2.5.2.

	Average	Variance
Reference picture	112.5972	2448.504
ZOH predicted picture	114.9017	2113.270
LI predicted picture	114.6425	2121.805

Table 2.5.1. Statistics of the Reference, ZOH and LI Predicted Pictures.

	Z.O.H.		L.I.	
STD	Average	Variance	Average	Variance
5	-0.34207	196.1564	-0.14900	7.60037
10	-0.30305	189.8243	-0.13400	26.37233
15	-0.28219	185.2324	-0.12480	49.72946
20	-0.27388	185.0328	-0.12226	72.39265

Table 2.5.2. Statistics of Difference Signal With ZOH and LI Predicted Images.

As shown in Fig. 2.5.1, the difference signal passes through a threshold logic network, and those difference signals which are greater than a preset threshold (T) are quantized and transmitted.

The number of difference signal samples of an entire picture which exceed some preset threshold levels are shown in Table 2.5.3 for various aircraft speed standard deviations.

	STD : 5		STD : 10		STD : 15		STD : 20	
T	ZOH	L.I	ZOH	L.I	ZOH	L.I	ZOH	L.I
1	60336	29769	59873	40959	59308	46152	58860	49319
2	57416	20213	56717	32364	55851	38777	55053	42852
4	51728	10006	50690	21310	49289	28282	48043	33216
8	40853	3068	39514	10155	37844	16048	36645	20761
16	23465	351	22491	2924	21399	5766	20710	8581

Table 2.5.3. Number of Difference Signals Exceeding Threshold Levels (Interframe-DPCM).

The difference signal is assumed to be normally distributed with zero mean and variance proportional to the standard deviation of the aircraft speed measurement. This assumption is an approximation of the actual statistical characteristics of the difference signal as obtained in Table 2.5.2.

With this simplified approximation, a 16-level non-uniform quantizer for minimum distortion as described by Max [137] is used to quantized those difference signals that exceed a preset threshold level.

The total error of the system is defined as the difference between the input

signal to the system and the reconstructed signal. The transmission system is indicated in the following diagram

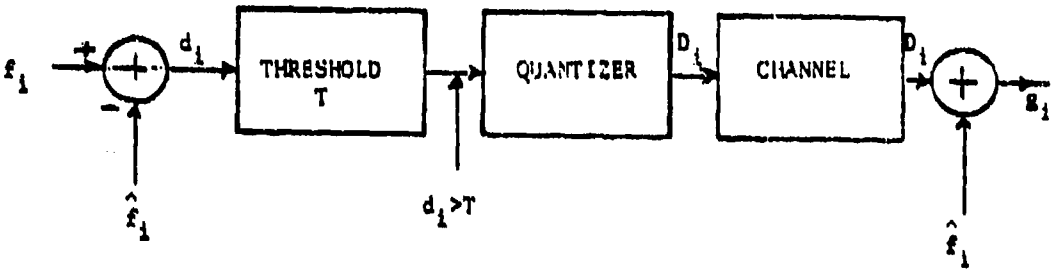

Assuming noiseless channel, the total system error specifications are calculated as follows:

(1) Mean-squared error (MSE) is $\frac{1}{N} \sum_{i=1}^{N} (f_i - g_i)^2$

$$MSE = \frac{1}{N} \sum_{i=1}^{N} (f_i - D_i - \hat{f}_i)^2 = \frac{1}{N} \sum_{i=1}^{N} (d_i - D_i)^2 \tag{2.5.1}$$

$$= \frac{1}{N} \left[\sum_{\substack{i=1 \\ d_i \le T}}^{N-M} (d_i - D_i)^2 + \sum_{\substack{i=1 \\ d_i > T}}^{M} (d_i - D_i)^2 \right]$$

where M is the number of difference signals that exceed the preset threshold level T. When the difference signal is considered to be insignificant, the quantizer output D_i is assumed to be zero, thus the total system mean-squared error can be rewritten as

$$MSE = \frac{1}{N} \left[\sum_{\substack{i=1 \\ d_i \le T}}^{N-M} d_i^2 + \sum_{\substack{i=1 \\ d_i > T}}^{M} (d_i - D_i)^2 \right] \tag{2.5.2}$$

(2) Normalized mean-squared error (MSE_n) is

$$MSE_n = \frac{\sum_{i=1}^{N-M} d_i^2 + \sum_{i=1}^{M} (d_i - D_i)^2}{\sum_{i=1}^{N} f_i^2} \qquad (2.5.3)$$

(3) Mean-absolute error (MAE) is

$$MAE = \frac{1}{N} \sum_{i=1}^{N} |d_i - D_i| \qquad (2.5.4)$$

In addition to the above error specifications, we define the following error specifications that will be calculated and observed throughout the experiment.

(4) Threshold mean-squared error (MSE_T) is

$$MSE_T = \frac{1}{N-M} \sum_{i=1}^{N-M} d_i^2 \quad , \quad (d_i \leq T) \qquad (2.5.5)$$

(5) Quantization mean-squared error (MSE_Q) is

$$MSE_Q = \frac{1}{M} \sum_{i=1}^{M} (d_i - D_i)^2 \quad , \quad (d_i > T) \qquad (2.5.6)$$

(6) Threshold mean-absolute error (MAE_T) is

$$MAE_T = \frac{1}{N-M} \sum_{i=1}^{N-M} | d_i | , \quad (d_i \leq T) \tag{2.5.7}$$

(7) Quantization mean-absolute error (MAE_Q) is

$$MAE_Q = \frac{1}{M} \sum_{i=1}^{M} | d_i - D_i | , \quad (d_i > T) \tag{2.5.8}$$

The results in Table 2.5.3 indicate that a large bit savings can be obtained provided that velocity is known accurately. These results also indicate that linear interpolator technique gives superior results over the zero-order-hold technique. This is to be expected since the input frame was simulated using the LI technique. The results also indicate that the number of difference signals which must be transmitted increases as the velocity standard deviation increases and decreases as the threshold increases; however, increasing the threshold results in more error. Table 2.5.4 shows the corresponding threshold mean-squared error. The relative large amount of error using the ZOH technique is to be expected.

Since it is the difference signal at the output of the threshold logic that is quantized and transmitted, the statistical characteristics of this signal are of importance and are given in Table 2.5.5, with threshold levels of 8 and 16.

Comparing the statistics given in Table 2.5.5 with those in Table 2.5.2 it is seen that the difference signal at the output of the threshold logic has somewhat higher variances, as is to be expected. It is the values given in Table 2.5.5 that are useful for design purposes.

	STD : 5		STD : 10		STD : 15		STD : 2	
T	Z.O.H.	L.I.	Z.O.H.	L.I.	Z.O.H.	L.I.	Z.O.H.	L.I.
1	0.57885	0.50915	0.58980	0.53770	0.60323	0.54585	0.61578	0.54769
2	1.80911	1.24517	1.81018	1.43477	1.81568	1.49783	1.84479	1.53190
4	6.18313	3.17695	6.15531	4.08586	6.11370	4.51622	6.07706	4.70495
8	22.34930	7.11892	21.85526	11.32363	21.15172	13.52356	20.40690	14.83867
16	77.39830	12.09982	74.24700	26.13490	70.73786	35.73230	67.64717	42.80522

Table 2.5.4. Interframe - DPCM. Threshold Mean-Squared Error.

	Threshold : 8		Threshold : 16	
STD	Average	Variance	Average	Variance
5	0.878070	149.0368	1.939582	416.0647
10	0.692972	246.3818	1.721252	547.2219
15	0.640642	325.3997	1.535428	676.3428

Table 2.5.5. Interframe - DPCM. Statistics of Difference Signal at the Input of the Quantizer Using Linear Interpolation.

Tables 2.5.6 and 2.5.7 show the total mean-squared error and mean absolute error assuming a noiseless channel for threshold levels of 8 and 16.

2.6 Intraframe-DPCM-Interframe-DPCM System

An Intraframe-DPCM-Interframe-DPCM system described in Chapter II was simulated on the IBM/360 computer and is investigated for the possibility of more bit savings as compared with the Interframe-DPCM version. Fig. 2.6.1 illustrates the simulation procedure.

Histograms of the intraframe difference signals between two successive picture elements along a scan line of the memory-stored reference picture and the predicted images of the reference picture using both the ZOH and LI techniques are given with Interim Technical Report. Table 2.6.1 summarizes the statistical characteristics of the intraframe difference signals.

In this system it is the significant frame-to-frame difference of the corresponding intraframe differences between two successive picture elements that is quantized and transmitted.

	THRESHOLD : 8				THRESHOLD : 16			
STD	MSE_T	MSE_Q	MSE	MSE_n	MSE_T	MSE_Q	MSE	MSE_n
5	7.11892	1.30164	6.24578	0.439257	12.09982	3.67399	11.69813	0.822714
10	11.32363	2.40259	8.92886	0.178303	26.13490	4.72302	24.15799	0.482419
15	13.52356	3.83486	9.98816	0.106102	35.73230	4.98115	31.35423	0.333079

Table 2.5.6. Interframe - DPCM. Total System Mean-Squared Error Using Linear Interpolation.

	THRESHOLD : 8			THRESHOLD : 16		
STD	MAE_T	MAE_Q	MAE	MAE_T	MAE_Q	MAE
5	1.775666	0.923405	1.729903	2.192957	1.683049	2.189869
10	2.382424	1.261615	2.193051	3.483616	1.920409	3.409077
15	2.669774	1.514608	2.367058	4.250789	1.830568	4.024779

Table 2.5.7. Interframe - DPCM. Total System Mean-Absolute Error Using Linear Interpolation.

	Average	Variance
Reference picture	-0.223514	1030.840
ZOH-predicted picture	-0.201945	357.5129
LI-predicted picture	-0.202053	354.3640

Table 2.6.1. Statistics of the Intraframe Difference Signal

Fig. 2.6.1 illustrates the operation of the intraframe-interframe DPCM technique.

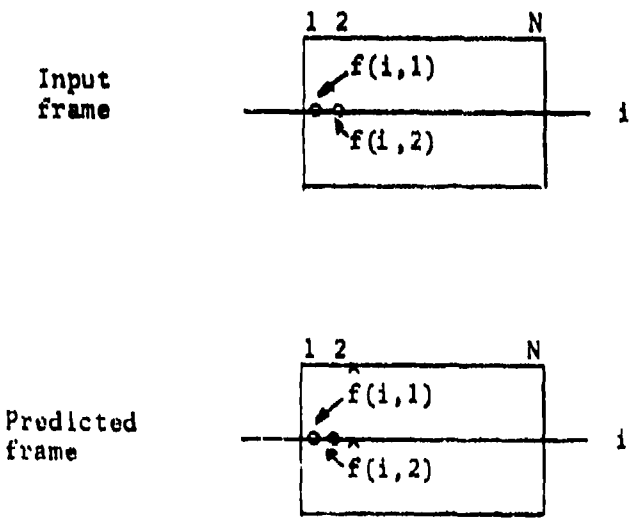

Fig. 2.6.1. Illustration of Intraframe-Interframe-DPCM Technique.

For an ijth picture element of intensity value f(i,j), a predicted intensity value $\hat{f}(i,j)$ is obtained using the predictive techniques as described previously. Assuming that the input picture is scanned from left to right and considering a line i in the input picture, the first intraframe difference obtained is

$$s(i,1) = f(i,2) - f(i,1) \qquad (2.6.1)$$

The intraframe difference of the predicted picture elements corresponding to f(i,1) and f(i,2), i.e., $\hat{f}(i,1)$ and $\hat{f}(i,2)$ respectively, is similarly obtained

$$\hat{s}(i,1) = \hat{f}(i,2) - \hat{f}(i,1) \qquad (2.6.2)$$

The interframe-intraframe difference d(i,1) is thus the difference between s(i,1) and $\hat{s}(i,1)$, i.e.,

$$d(i,1) = s(i,1) - \hat{s}(i,1) \qquad (2.6.3)$$

Substituting (2.6.1) and (2.6.2) into (2.6.3), we have

$$d(i,1) = [f(i,2) - \hat{f}(i,2)] - [f(i,1) - \hat{f}(i,1)]$$

$$d(i,1) = d_{FP}(i,2) - d_{FP}(i,1) \qquad (2.6.4)$$

where $d_{FP}(i,1)$ and dFF(i,2) are the interframe (frame-to-frame) differences of the 1st and 2nd picture elements, respectively.

The procedure to predict the difference signal is described as follows:

First, we obtain the difference between the first input picture element on line i and its predicted value, i.e., $d_{FP}(i,1)$. As the second element is scanned, the difference $d_{FF}(i,2)$ between the new picture element and its predicted value is obtained and compared with $d_{FP}(i,1)$. If their difference is considered significant then the 2nd picture element is transmitted and we proceed to the next element. If this difference is insignificant, we let d(i,1) be zero and from (2.6.4) it is seen that $d_{FF}(i,2)$ can be assigned the value of $d_{FP}(i,1)$. No picture element is transmitted since the present picture element intensity value is not significantly

	STD : 5		STD : 10		STD : 15	
T	Average	Variance	Average	Variance	Average	Variance
1	-0.034613	47.51811	-0.242429	138.3335	-0.108097	235.4219
2	0.200627	62.16763	0.141359	167.1270	0.116615	279.6116
4	0.025263	93.77348	-0.305930	234.1079	1.407681	351.6843
8	1.433904	209.69441	1.767702	383.6450	1.322620	548.5386
16	0.342162	532.02172	2.254504	791.0749	1.655807	929.1135

Table 2.6.2. Intraframe DPCM-Interframe-DPCM. Statistics of Quantizer Input Signals (Linear Interpolation).

different from its predicted value. After this step has been done, we proceed to the next element and compute the corresponding interframe difference $d_{FF}(i,3)$ which in turn is compared with $d_{FF}(i,2)$ and so on, until the last picture element of line i is reached. This procedure is applied repeatedly for every line of the input picture.

Since it is the interframe-intraframe difference which exceeds the threshold that is quantized and transmitted, the statistics of this difference signal with respect to the preset threshold level are of importance and are shown in Table 2.6.2.

Histograms of the interframe-interframe difference signals are given in the Interim Technical Report.

Tables 2.6.3, 2.6.4 and 2.6.5 show the results obtained using the intraframe-interframe DPCM technique. It is interesting to compare these results with those of the interframe DPCM. Comparing the results of Tables 2.5.3 and 2.6.3, we see that the number of nonredundant pels for the intraframe-interframe DPCM technique is somewhat higher than that of the interframe technique. Similarily the results

	STD		
T	5	10	15
1	41549	49771	53743
2	29385	41320	46434
4	16527	29012	35993
8	5848	16083	22853
16	961	5313	9673

Table 2.6.3. Intraframe-Interframe DPCM. Number of Picture Elements Exceeding a Fixed Threshold Level Using Linear Interpolation Technique.

	THRESHOLD : 8				THRESHOLD : 16			
STD	MSE_T	MSE_Q	MSE	MSE_n	MSE_T	MSE_Q	MSE	MSE_n
5	7.17369	1.81335	6.69349	0.263265	14.26320	4.73581	14.12296	0.646877
10	10.59299	4.41127	9.07691	0.087991	27.92874	6.10296	26.15239	0.289540
15	12.36913	7.01809	10.49594	0.052355	36.79207	7.69500	32.48055	0.191850

Table 2.6.4. Intraframe-DPCM-Interframe-DPCM. Total System Mean-Squared Error Using Linear Interpolation Technique.

	THRESHOLD : 8			THRESHOLD : 16		
STD	MAE_T	MAEQ	MAE	MAE_T	MAE_Q	MAE
5	1.878663	1.068798	1.806112	2.436672	1.950784	2.429520
10	2.427824	1.588326	2.220997	3.711013	2.006469	3.572283
15	2.694620	1.790348	2.378175	4.436924	2.346384	4.127153

Table 2.6.5. Intraframe-DPCM-Interframe-DPCM. Total System Mean-Absolute Error Using Linear Interpolation Technique.

of Tables 2.5.6, 2.5.7, 2.6.4 and 2.6.5 show that there is essentially no gain in using intraframe-interframe DPCM over simply interframe-DPCM. Such a result tends to indicate that the use of two dimensional schemes may not have much advantage over simple one-dimensional schemes for some pictures.

2.7 Summary of Simulation

From the results of the system simulation, it is seen that a large bit saving factor can be realized. Referring to Tables 2.5.3 and 2.5.4, a substantial amount of bits can be saved when the threshold logic in either system is set at levels as high as 8 or 16.

Using a 4-bit quantizer to encode the transmitted difference signal and a 16-bit address generator to specify its position (assuming a 256 x 256 array) each element is transmitted using a total of 20 bits. The average number of bits required for each transmitted element is calculated as follows:

$$\text{Bits/pel} = \frac{20 \times M}{256 \times 256} \qquad (2.7.1)$$

where M is the number of picture elements which is transmitted over the channel.

Using the data given in Tables 2.5.3 and 2.6.3, the average bits per picture element for the Interframe-DPCM and the Intraframe-DPCM-Interframe-DPCM systems are obtained using (2.7.1) for various speed standard deviations. This data is shown in Tables 2.7.1 and 2.7.2, together with their corresponding total normalized mean-squared errors and mean-absolute errors.

It is seen from Tables 2.7.1 and 2.7.2 that the Intraframe-DPCM-Interframe-DPCM system does not have any significant advantage over the Interframe-DPCM system. In both systems there is a trade-off between the total system normalized mean-squared

	THRESHOLD : 8			THRESHOLD : 16		
STD	Bit/pel	MSE_n	MAE	Bit/pel	MSE_n	MAE
5	0.93628	0.439257	1.729903	0.10712	0.822714	2.189869
10	3.09906	0.178303	2.193051	0.89233	0.482419	3.409077
15	4.89746	0.106102	2.367058	1.76069	0.333070	4.024779

Table 2.7.1. Interframe-DPCM Average of Bits Per Pel Using Linear Interpolation.

	THRESHOLD : 8			THRESHOLD : 16		
STD	Bit/pel	MSE_n	MAE	Bit/pel	MSE_n	MAE
5	1.78467	0.263265	1.806112	0.29327	0.646877	2.429520
10	4.90815	0.087991	2.220997	1.62140	0.289540	3.572283
15	6.97386	0.052355	2.378175	2.95200	0.191650	4.127153

Table 2.7.2. Intraframe-DPCM-Interframe-DPCM. Average of Bits Per Pel Using Linear Interpolation.

error and the amount of bit savings as compared with the standard 8-bit PCM system.

In view of the fact that each nonredundant element requires 8-bits to specify the horizontal position, 8-bits to specify the vertical position and 4-bits to specify the intensity value of the difference signal, it is possible that increased bit savings could be obtained by forcing the first pel of each line to be transmitted. Using this technique would require only 8-bits for the horizontal position and 4-bits for the intensity of the difference signal. Although more pels would be transmitted the net savings in the number of bits required might be substantial. Simulations were performed to evaluate this type system and the results are shown in Tables 2.7.3 and 2.7.4. Also shown for comparison purposes in parenthesis are the results obtained using 16-bits to specify the position. The latter technique would have essentially the same or slightly better error performance due to the fact that the first element of every line is assumed nonredundant. Some special coding technique would be required so that the receiver could properly identify the first pel of each line.

2.8 Total System Error Including Channel Noise

In this section we include the effect of channel noise on the transmission system and investigate the performance of the Interframe-DPCM system using Linear Interpolation technique for the simulated input picture and the predicted picture. The total system error calculations are based on the hypothesis that the system transmission is coherent phase-shift keying (PSK). A 20-bit word is transmitted over the noisy channel for each non-redundant picture element. The 16 most significant bits carry the information of the element position and the 4 least significant bits are the coded intensity value of the transmitting signal. Due to transmission channel noise, the received word may be different from the one that was transmitted. The error can occur in the position information part of the intensity value part or both.

Threshold	Velocity Standard Deviation	Bits Per Picture Element
8	5	.608 (1.074)
8	10	1.906 (3.38)
8	15	2.985 (5.24)
16	5	.111 (.123)
16	10	.582 (.954)
16	15	1.103 (1.895)

Table 2.7.3. Interframe-DPCM.

Threshold	Velocity Standard Deviation	Bits Per Picture Element
8	5	1.12 (1.785)
8	10	2.99 (4.91)
8	15	4.23 (6.97)
16	5	.223 (.293)
16	10	1.02 (1.62)
16	15	1.82 (2.95)

Table 2.7.4. Intraframe-Interframe-DPCM.

The probability of error using coherent-PSK transmission is well known to be

$$PE = \tfrac{1}{2}\left[1 - \operatorname{erf}\left(\sqrt{\frac{E}{R}}\right)\right] \qquad (2.8.1)$$

where E is the energy of the transmitted signal and R is the rate of transmission of the system.

The rate of transmission R is expressed as the total number of bits transmitted over the channel for each picture, i.e.,

$$R = 20 \text{ bits/pel} \times M \qquad (2.8.2)$$

where M is the number of picture elements transmitted for each frame.

Using (2.8.2) the probability of error in (2.8.1) can be rewritten as follows:

$$PE = \tfrac{1}{2}\left[1 - \operatorname{erf}\left(\sqrt{\frac{E}{20 \cdot M}}\right)\right] \qquad (2.8.3)$$

A threshold of detection is defined as follows:

$$TH = 1 - PE \qquad (2.8.4)$$

The coherent-PSK transmission channel was simulated on the IBM/360 computer.

Tables 2.8.1 and 2.8.2 show the probability of error and the number of picture elements in error (E is the total energy for a picture). The number of picture elements which are transmitted for each frame is derived from the results of Table 2.5.3.

The total system mean squared errors including channel noise are shown in Tables 2.8.3 and 2.8.4 using threshold levels of 8 and 16 respectively together with their corresponding noiseless channel total system mean-squared errors for comparison.

		E : 128K		E : 256K		E : 640K	
STD	M	PE	M_E	PE	M_E	PE	M_E
5	3519	0.028247	1534	0.003496	237	0.000010	0
10	11073	0.141152	10565	0.064192	8188	0.008106	1694
15	17174	0.193892	16959	0.111060	15606	0.020777	7213

Table 2.3.1. Threshold : 8.
Probability of Error and Number of Elements Due to Error.

		E : 128K		E : 256K		E : 640K	
STD	M	PE	M_E	PE	M_E	PE	M_E
5	397	0.000000	0	0.000000	0	0.000000	0
10	3125	0.021492	1106	0.002104	127	0.000003	0
15	6120	0.074060	4887	0.020416	2081	0.000611	73

Table 2.8.2. Threshold : 16.
Probability of Error and Number of Elements Due to Error.

2.9 Summary and Conclusions

The results of the simulations have shown that the interframe bandwidth reduction scheme can be utilized to achieve a low average number of bits required for each picture transmitted to the receiver. A trade-off between the amount of bandwidth reduction and the system error is an important consideration. The effectiveness of the system depends largely upon the degree of accuracy of the instrumental measurements of the vehicle dynamics.

In this experiment, a 20-bit word is transmitted to represent each nonredundant picture element, in which a total of 16-bits are used to carry the address information of the transmitted signal. This position bit requirement may be further reduced by forcing the first pel of each line to be a nonredundant sample. Using this technique only 8-bits are required for the horizontal positional information and 4-bits for the grey level information. A higher reduction in bit requirement may be realized with a total of 12-bits being used for each picture element transmitted to the receiver.

The complexity of the system implementation is in the realization of the predictor to faithfully predict the next picture and the storage required to store one frame. The system implementation is further complicated when the problem of optimizing the capacity of the buffers employed at both the transmitter and the receiver is considered in order to avoid the problems of buffer overloading or underloading, which can result in a loss of information needed or a waste in necessary bandwidth requirement for picture reconstruction.

Although the interframe techniques described in this report requires rather complex hardware and software, the scheme can be used at the ground station for synthetic frame generation or frame replenishment. This would allow for relative low frame rates without detrimental visual effects on the observer. The predictor algorithms can easily be generalized to include roll and simulation. It is the

conclusion of the authors that the practicability of such a scheme as described in this chapter would require excessive complexity for use in the vehicle; however, would be of value and easily implemented for synthetic frame generation at the ground station. This would allow for relative slow frame rates without serious disadvantages of flicker, etc.

There are several other possibilities using frame-to-frame techniques which might be considered, such as using intraframe transform techniques to first process the picture and then use differential techniques frame-to-frame. Such techniques would have an advantage in that intraframe techniques would have already compressed the data; therefore, relieving, somewhat, the memory requirements. In addition the use of differential techniques on transform coefficients may be less sensitive to parameters such as the velocity, altitude, etc.

Due to the relative complex instrumentation required to implement these frame-to frame techniques, the project monitor requested we terminate the emphasis on frame-to-frame methods in favor of the more practical intraframe techniques described in the next chapter.

CHAPTER III

THEORY

3.1 Introduction

Recently there has been increased interest in a combination of the orthogonal transformation techniques and DPCM [83-93]. A brief theoretical analysis of the DPCM and the transformation techniques and their combinations, the Hybrid Coding Techniques, are presented in the following sections. Relevant to television and video data transmission, the processed data are assumed to be real random variables generated from a separately-multidirectional first order Markov process.

Without loss of generality, these random variables are assumed to have zero mean and unity variance.

For analytical purpose, the performances of the coding systems are measured using the normalized mean-square error criterion which is mathematically tractable.

3.2.1 DPCM and Time Predictive Techniques

Among the many intraframe data compression techniques that have been investigated in recent years, one- and two-dimensional differential Pulse Code Modulation (DPCM) systems have received a considerable amount of attention. This is probably due to its simplicity. Fig. 3.2.1 illustrates by block diagram the operation of a DPCM encoder. In DPCM systems a differential signal e_{ij} is obtained by taking the difference between the sample value u_{ij} and its predicted value $\hat{u}_{ij}$. The predicted value is generally obtained by taking a linear combination of the previously scanned picture elements. The weighting coefficients in this linear combination are normally determined by assuming known stationary statistics for the image. This process is illustrated for the general case in Fig. 3.2.2.

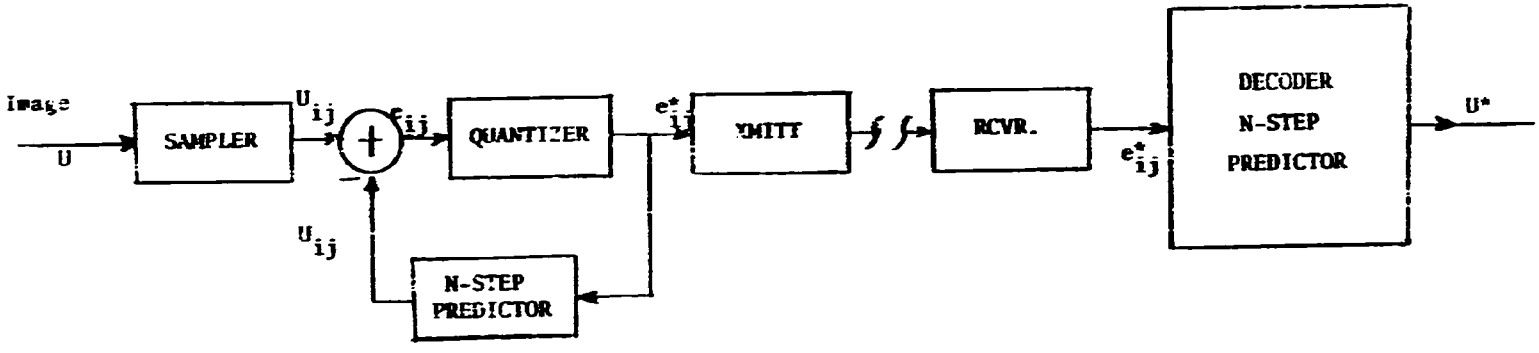

Fig. 3.2.1 DPCM Coder

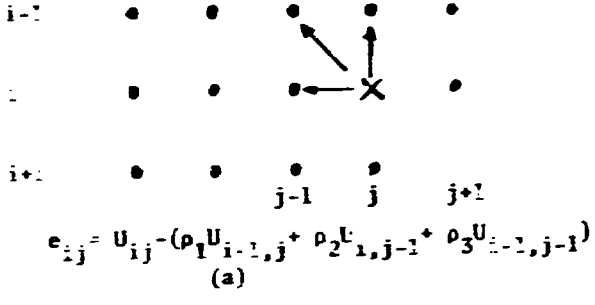

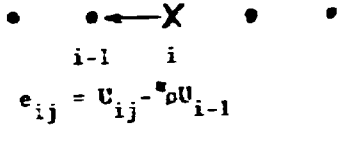

Fig.3.2.2 (a) 2-D DPCM; (b) 1-D DPCM

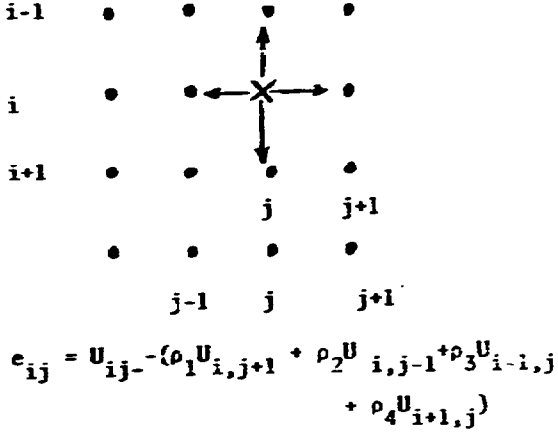

Fig. 3.2.3. Interpolative DPCM.

The difference samples e_{ij} are uncorrelated for cases of stationary statistics and these difference samples are quantized and coded for transmission over the channel. The receiver then reconstructs the waveform by a similar procedure as shown in Fig. 3.2.1.

The efficiency of the coder not only depends on the difference samples being uncorrelated but also on the variances of the e_{ij}'s. The variances of these difference signals are related to the number of samples used in predicting $\hat{u}_{ij}$ and to the relative locations of these samples with respect to the point (i,j). Either 1-, 2- or n-dimensional, causal and noncausal DPCM systems may be used.

The one-dimensional DPCM encoder is frequently preferred because of its extreme simplicity. An analysis of DPCM encoders using total mean-squared error (including the effects of channel errors) as a measure of fidelity is given by Kassman and Wintz [158]. Results of this study indicate that the one-dimensional DPCM encoder gives good results using three bits per picture element (pel). Abbort [178] designed a DPCM codec (coder-decoder) which gives minimal subjective impairment using four bits/pixel. Habibi [74] evaluated the performance of an N^{th} order DPCM systems for N ranging from 1 to 22 and compared it to the performance of unitary transform techniques. His results indicate that a DPCM system using a third or higher order predictor performs superior to all transform techniques when the system is optimized for a particular picture; however, the transform technique is much less sensitive to variations in picture statistics than are DPCM systems. More recently Habibi [6,7,89] has shown the relationship between the DPCM and transform coding. A considerable number of earlier works on DPCM have been reported. O'Neal [153,159,165] gives both theoretical and computer simulation results of processing still pictures. The use of one bit DPCM

or delta modulation has been studied by O'Neal [179]. More recently adaptive data modulation schemes have been investigated. In adaptive delta modulation the step size is either increased or decreased depending on whether the modulator is in the slope overload region or the granular region. Many algorithms for increasing or decreasing the step have been investigated. Step size alteration schemes can be either analog or digital. Analog or continuous schemes measure some property of the input signal, such as the average slope, and adjust the step size accordingly. The digital methods adjust the step size only at certain sampling instants using some type of algorithm based on previous digits. Several studies using adaptive delta modulation schemes to transmit speech have been reported. References [180,195] give results for both analog and digital companding. Since the clock rate required for these techniques is relatively high, their usefulness for the RPV application is questionable. It is possible that a combination adaptive delta modulation with other schemes such as DPCM might be of importance. In this case the adaptive delta modulator would be used essentially as an analog-to-digital converter and the output bit stream would be encoded in some other method such as DPCM before transmission. There has been little reported in the literature on such schemes as applied to image processing. Oliver [196] describes an adaptive delta modulator for pictorial data using overshoot compensation which operates satisfactorily using less than 3 bits/pixel. Several other authors have investigated the use of DPCM and delta modulation [197-212].

Recently Jain [91] and Jain and Angel [171] has considered DPCM encoders which are interpolative in nature and indicate the relationship between this type of coding and transform coding. The computational requirements are shown to be considerably less for this coding scheme than for transform coding and performance

almost equivalent. However, in differential systems a major concern is the sensitivity to noise, which has not been exploited for these types of systems. Chang and Donaldson [173,174] investigate non-adaptive DPCM coders over noisy channels with and without error correcting coding using arbitrary linear predictors. The signal-to-noise ratio over previous sample feedback coders is shown to increase approximately 2.6 dB for noiseless channels and 4 dB for noisy channels. Optimization of the predictive coefficient for noisy channels is shown to reduce the sensitivity of SNR to both variation in the input signal and channel parameters without much degradation of the SNR below its optimum value for error free channels.

O'Neal [177] has shown that DPCM followed by entropy encoding performs within 1.5 dB of Shannon's rate distortion function, which bounds the performance of any encoding system using minimum mean-square-error criterion. In this study uniform quantization is used with entropy encoding which increases the complexity somewhat. Jayant [169] gives a tutorial type paper on PCM, DPCM and DM (delta modulation) for speech type signals.

DPCM coders are still of considerable interest due to their relative simplicity. The primary disadvantage of differential coders is their sensitivity to signal statistics and to channel noise. I believe that investigations of methods to reduce this sensitivity is still needed and once solved, would make DPCM systems attractive for use in the RPV vehicle. The hardware simplicities would probably make it a strong contender for these types of applications.

Time predictive techniques generally operate on data in such a way that the outputs of the data compressor are actual sample values of the input signal or actual values within a specified tolerance. These techniques employ algorithms using simple averaging techniques, polynomial predictors, etc. A rather

complete listing of these techniques is given in the Interim Technical Report for Contract F33615-73-C-1233, June, 1974. These schemes rely on conventional sampling and the use of a predetermined compression algorithm and generally require that synchronization information or "sample tagging" be inserted before transmission, thus reducing the overall efficiency of the data compression system. Systems relying on these techniques generally require a large buffer storage and due to the rather minimal reduction ratios obtained (2 to 4 in most cases) do not seem to be contenders for applications in the RPV.

3.2.2 One-dimensional Transformations

The techniques of unitary (orthogonal) transformations have been developed primarily from the point of view of redundancy reduction [12]. The objectives of such a technique are to map the original image into another domain such that the redundant information is readily evident and is arranged in order of decreasing information content.

A one-dimensional unitary transformation can be presented by the block diagram in Fig. 3.2.4.

Fig. 3.2.4. Schematic Diagram of One-dimensional Transformation.

The coding system shown in Fig. 3.2.4 will be analyzed using matrix methods. The N image sample values can be represented by a column vector $u = [u_1 \ldots u_N]^T$ in vector space S consisting of column vectors of dimension N. A linear orthogonal operation L on S which transforms u into an Nx1 column vector $v = [v_1 v_2 \ldots v_N]^T$ in S can be represented by the matrix multiplication:

$$v = Tu \tag{3.2.1}$$

where the NxN matrix T is the matrix representation of the linear operation L. For orthogonal transformation, T is an orthogonal matrix, i.e. $T^{-1} = T^T$ (for convenience, T is assumed to be real) and the elements of the transform vector v give the values of transform coefficients. The inverse operation to retrieve u is accomplished by the inverse transformation

$$u = T^T v \tag{3.2.2}$$

where T^T is the transpose matrix of T

The best invertible transformation for random data, linear or otherwise, for efficient coding would be one which results in independent coefficients. Since the problem of determining such a transformation remains unsolved in general the closest we can get with linear transformations is one which produces uncorrelated coefficients, which in the case of gaussian signals, produces independent samples. It has been shown that the transformation matrix T which produces uncorrelated coefficients is associated with the autocovariance matrix C_u of the image vector:

$$C_u = E(uu^T) \tag{3.2.3}$$

Without loss of generality, we assume that the real random variable u_i has zero mean and unity variance. Since C_u is a real symmetric matrix it possesses a complete orthonormal set of eigenvectors corresponding to real eigenvalues. These eigenvectors can be chosen to be real. A matrix T whose rows are the eigenvectors of C_u diagonizes the covariance matrix C_u. The autocovariance matrix C_v of the transform coefficients is given by

$$C_v = TC_uT^T = \text{diag}[\lambda_1\ \lambda_2\ \ldots\ \lambda_N]$$

where $\lambda_1 \geq \lambda_2 \geq \ldots \geq \lambda_N$ are eigenvalues of the matrix characteristic equation

$$C_u\phi = \lambda\phi \tag{3.2.4}$$

This transformation has been known by several different names such as the eigenvector transformation [27], the Hotelling transformation [3], the Karhunen-Loève transformation [7], or basis-restricted transformation [10]. Henceforth, it will be referred to as the Karhunen-Loève transformation.

Other non-basis restricted linear transformations (non-optimum) other than the optimum eigenvector transformations have been investigated for use in image coding. These include the Fourier transformation [23-30], the Hadamard transformations [33] (Walsh (sequency-ordering) Hadamard, Kronecker (natural) Hadamard, Paley (dyadic-ordering) Hadamard [55], etc.), the Walsh-Haar transformation [35, 72], the Discrete Cosine transformation [79,80], the Slant transformation [75-78], the Discrete Linear Basis transformation [88] etc.

These non-optimum transformations produce only approximately uncorrelated coefficients, however, their computational difficulties are greatly reduced with the advent of fast transform algorithms [94-108]. Furthermore, these transformations systems can be more economically implemented than the theoretically optimum Karhunen-Loeve transformations.

Theoretically, it has been shown that for data with autocorrelation matrix having cyclic-translational symmetry, the autocovariance matrix of the transform coefficients is diagonized using Fourier transformation. Furthermore, the Walsh-Hadamard transformation uncorrelates data with dyadic-Markov covariance matrix [40].

If the transformation is chosen properly, the information bearing transform coefficients are many orders of magnitude larger than those reflecting redundancy. A common practice with Fourier analysis is to assume that the low-frequencies are important while the high frequencies represent only noise. The high frequencies may then be deleted in order to compress the data.

The process of deleting high-frequency[1] terms may be represented by a proper matrix operation:

[1] The more popular term "sequency" has been coined by Harmuth [54] as a generalized frequency. Yuen [42] has introduced the term "frequency" to account for the number of zero-crossings.

$$v^{(n)} = W_n v \quad ; \tag{3.2.5}$$

where $n \geq N$ is the number of coefficients to be retained.

The NxN truncating matrix W_n[2] is defined as

$$W_n = \begin{bmatrix} I_n & 0 \\ 0 & 0 \end{bmatrix} \tag{3.2.6}$$

where the partitioned matrix I_n is the identity matrix of order n.

The compliment matrix W_n^c of W_n can also be defined as

$$W_n^c = I_N - W_n = \begin{bmatrix} 0 & 0 \\ 0 & I_{N-n} \end{bmatrix} \tag{3.2.7}$$

where I_N and I_{N-n} are identity matrices of orders N and N-n, respectively. The series truncation process described by (3.2.5) where the truncating matrix W_n is defined in (3.2.6) is a non-adaptive technique for retaining those coefficients that on the average have the largest variance (energy). This procedure is some times referred to as "zonal sampling" [27] or "geometrical sampling". Another alternative would be to retain those coefficients whose variances exceed a preset threshold. This adaptive technique is sometimes referred to as "threshold sampling" [66]. When threshold sampling is used certain "bookkeeping information" that specifies which coefficients have been retained (or discarded) must also be coded for transmission.

The sample variances of the coefficients, presented in Fig. 3.2.5 can be interpreted as generalized power spectra of the original data. Note from Fig. 3.2.6 that all five linear transformations are approximately equally efficient in packing the variances into lower order coefficients. Figs. 3.2.5 and 3.2.6 are

[2] the definition of the truncating matrix W_n in 3.2.6) has implied that the transform coefficients had been properly arranged in order of decreasing variance.

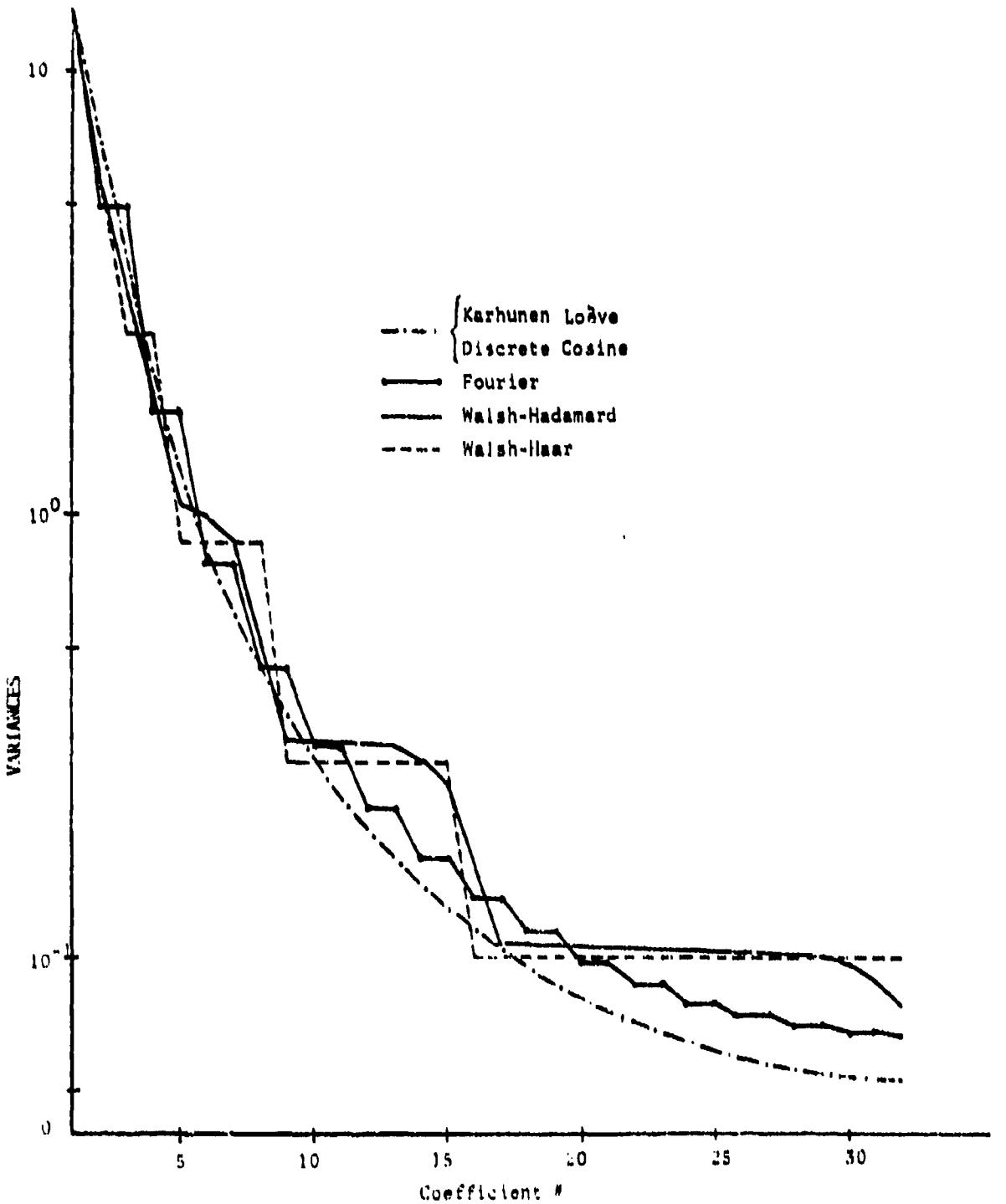

Fig. 3.2.5. Variance of Transform Coefficients (ρ=0.9, N=32).

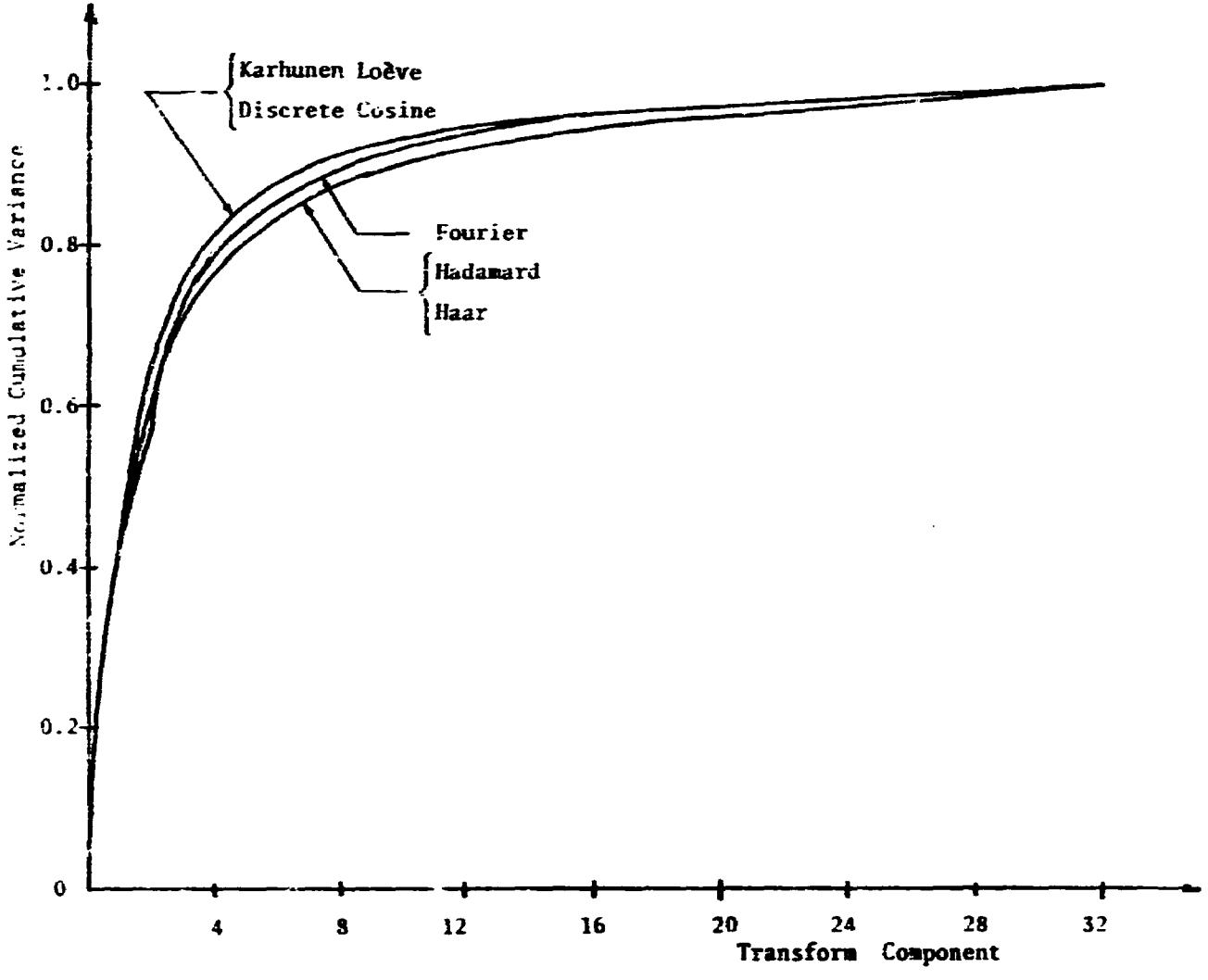

Fig.3.2.6. Cumulative Sum of Variances(ρ=0.9).

obtained for one-dimensional unitary transformation with N = 32, assuming first-order Markov data, i.e., the covariance matrix is a Toëplitz matrix of the form

$$C_u = [\rho^{|i-j|}]_{N\times N} \tag{3.2.8}$$

Theoretical researches have shown that when compared with other linear transformations mentioned above, the Karhunen-Loève [4] transformation

a) produces uncorrelated coefficients;

b) packs the maximum amount of cumulative variance into the first n coefficients (for any n);

and c) minimizes the mean-squared sampling error due to the truncation process.

Referring to Fig. 3.2.4 the mean-square truncation error is given by:

$$\varepsilon_t^2 = E\{\| u-v \|^2\} \tag{3.2.9.a}$$

In terms of the variances of the retained coefficients σ_{vi}^2 i = 1, 2, ... n, the error is expressed by

$$\varepsilon_t^2 = 1 - \frac{1}{S}\sum_{i=1}^{n} \sigma_{vi}^2 \tag{3.2.9.b}$$

The total system mean square coding error, assuming noiseless transmission channel, is the sum of the truncation error and the quantization error associated with the transmitting coefficients, i.e.

$$\varepsilon^2 = 1 - \frac{1}{S}\sum_{i=1}^{n} \sigma_{vi}^2 + \frac{1}{N}\sum_{i=1}^{n} \sigma_{qi}^2 \tag{3.2.10}$$

3.2.3 The Effects of One-Dimensional Techniques on Two-Dimensional Data

The band-limited analog signal is sampled in both the horizontal and the vertical directions. The input pictorial data may be represented by an MxN matrix U of discrete intensity levels u(i,j), i = 1,2 ... M; j = 1,2 ... N. In subsequent analysis the sampling error will be ignored.

Theoretically relevant to television and facsimile transmission, the image may be assumed as a two-dimensional first-order Markov process. Let u(i,j) be a real, stationary random variable with zero mean, unity variance and autocorrelation

$$R_u(i,j,k,l) = E\{u(i,j)u(k,l)\} = \rho_y^{|i-k|}\,\rho_x^{|j-l|}$$

$$\text{where} \quad 0 \le \rho_x, \rho_y \le 1 \quad \text{and} \quad \begin{matrix} i,k = 1, 2, \ldots M \\ j,l = 1, 2, \ldots N \end{matrix} \qquad (3.2.11)$$

The input data is thus separately correlated in all directions. The implication of this basic assumption of correlation separateness applied to systems utilizing one-dimensional DPCM or unitary transformation techniques is considered in the following sections. Without loss of generality, we assume that the one-dimensional DPCM or transformation is performed in the horizontal direction.

A One-Dimensional Differential PCM

In a one-dimensional DPCM (or 1st order DPCM) system, the difference (error) value between an input sample value and its estimate is quantized, coded and transmitted to the receiver.

It has been shown that for 1st order Markov process, the best causal linear estimate $\hat{u}(i,j)$, in the mean-squared error sense, of the next sample value u(i,j) based on the most recent sample value available on the same line u(i,j-1) is:

$$\hat{u}(i,j) = \rho_x\, u(i,j-1) \qquad (3.2.12)$$

where ρ_x is the correlation coefficient of horizontally adjacent sample values as defined in (3.2.11).

A linear predictive encoder forms this estimate $\hat{u}(i,j)$ and transmitted the difference or error

$$e(i,j) = u(i,j) - \rho_x u(i,j-1) \qquad (3.2.13)$$

$$i = 1, 2, \ldots M$$
$$j = 2, 3, \ldots N$$

where $e(i,j) \triangleq 0$, for $j = 1$

This process is continued along the entire line of the input picture and is vertically reset at the beginning of the next line. The two-dimensional sequence of error samples $e(i,j)$ forms an NxN matrix E representing the error picture.

The two-dimensional autocorrelation function of the error samples is

$$R_e(i,j,k,l) = E\{e(i,j)e(k,l)\} \qquad (3.2.14)$$

It can be shown that

$$R_e(i,j,k,l) = R_e(i-k,j-l) = \rho_y^{|i-k|}(1-\rho_x^2)\delta_{jl} \qquad (3.2.15)$$

where δ_{jl} is the Kronecker delta function.

If a prediction coefficient A other than the optimum (ρ_x) is used, where $0 \le A \le 1$, it can be shown that

$$R_e(i-k,j-l) = \rho_y^{|i-k|}\left[(1+A^2)\rho_x^{|j-l|} - A\left(\rho_x^{|j-l+1|} + \rho_x^{|j-l-1|}\right)\right] \qquad (3.2.16)$$

The horizontal and the vertical correlation functions of the error samples can be obtained separately by setting $i-k = 0$ and $j-l = 0$, respectively. The horizontal correlation function of the difference sample using both the optimum and the

non-optimum prediction coefficients are, respectively

$$R_e(0,j-1) = (1-\rho_x^2)\,\delta_{j1} \tag{3.2.17}$$

and $$R_e(0,j-1) = (1+A^2)\,\rho_x^{|j-1|} - A\,[\rho_x^{|j-1+1|} + \rho_x^{|j-1-1|}] \tag{3.2.18}$$

We can observe that the one-dimensional DPCM performed along the x-direction forms a sequence of error samples whose horizontal correlation is reduced or, in case of optimum prediction, is zero.

The vertical correlation functions are

$$R_e(i-k,0) = (1-\rho_x^2)\,\rho_y^{|i-k|} \tag{3.2.19}$$

and $$R_e(i-k,0) = [1-\rho_x^2 + (A-\rho_x)^2]\,\rho_y^{|i-k|} \tag{3.2.20}$$

Equations (3.2.19) and (3.2.20) indicate that the vertical correlation function of the error samples retains the original functional form, $\rho_y^{|i-k|}$. Thus, a one-dimensional DPCM performing on one-direction reduces the correlation in that direction but does not affect the correlation in the other direction.

The above observation is conformed with the theoretical results of optimum-DPCM techniques where a two-dimensional (or 3rd order) DPCM must be used to reduce the correlation in both directions, assuming a two-dimensional 1st order Markov process.

B One-Dimensional Orthogonal Transformations

The objectives of orthogonal transformations are to represent the original image in another form such that the redundant information is readily evident and is arranged in order of decreasing information content.

In this section, an analysis using matrix approach will be rendered.

The input image matrix U of dimension MxN is seen to be composed of M (1xN) row-vectors u_i, i = 1, ... M. The autocovariance matrix C_u of u_i is:

$$C_u = E\,(u_i^T u_i) \tag{3.2.21}$$

From (3.2.21), we have

$$C_u = \begin{bmatrix} 1 & \rho_x & \rho_x^2 & \cdots & \rho_x^{N-1} \\ \rho_x & 1 & \rho_x & & \rho_x^{N-2} \\ \vdots & & & & \vdots \\ \rho_x^{N-1} & \rho_x^{N-2} & \cdots & & 1 \end{bmatrix} \tag{3.2.22}$$

which is a Toëplitz matrix [18].

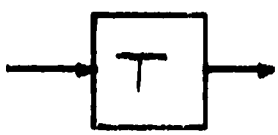

Fig. 3.2.7. Schematic Diagram of a One-dimension Orthogonal Transformation.

Referring to Fig. 3.2.7, the linear transformation of the original image can be represented by a matrix multiplication:

$$V_i^T = T u_i^T \tag{3.2.23}$$

where T is the matrix representation of an orthogonal transformation which may be real or complex, i.e., $T^T = T^{-1}$. In the transform domain, the transformed sample vector v_i has autocovariance matrix

$$C_v = E\,(v_i^T v_i)$$

or

$$C_v = T C_u T^{-1} \tag{3.2.24}$$

It has been shown that the optimum (Karhunen-Loève) transformation diagonizes the autocovariance matrix C_v. The diagonal elements of the diagonal matrix C_v are real eigenvalues of the Toëplitz matrix C_u, i.e.

$$C_v = \text{diag}\,(\lambda_1, \lambda_2 \ldots \lambda_N) \tag{3.2.25}$$

where $\lambda_1 > \lambda_2 > \ldots > \lambda_N$.

When non-basis-restricted transformations are used, such as Walsh-Hadamard, Walsh-Haar, Fourier, Discrete Cosine, Slant, etc., the off-diagonal elements of C_v have non-zero values but the correlation of adjacent transformed coefficients is also reduced compared to the original image.

The vertical correlation of adjacent blocks of transformed coefficients can be obtained as follows.

From (3.2.23), a transform coefficient $v(i,j)$ of transform vector v_j can be expressed by

$$v(i,j) = \sum_{r=1}^{N} \phi(j,r)u(i,r) \tag{3.2.26}$$

where $\phi(i,j)$ is the i,j^{th} element of the transformation matrix Φ.

For the j^{th} coefficient, the vertical correlation is:

$$R_v(i,j,k,j) = E\{v(i,j)v(k,j)\}$$

$$\text{or} \qquad R_v(i,j,k,j) = \rho_y^{|i-k|} \sum_{r=1}^{N}\sum_{r'=1}^{N} \rho_x^{|r-r'|}\, \phi(j,r)\phi(j,r')$$

$$= \sigma_{vj}^2\, \rho_y^{|i-k|} \tag{3.2.27}$$

where $\sigma_{vj}^2 = \sum_{r=1}^{N}\sum_{r'=1}^{N} \rho_x^{|r-r'|}\, \phi(j,r)\phi(j,r')$ is the variance of the j^{th} transform coefficient; if optimum transformation is used, the j^{th} variance σ_{vj}^2 is identical with the j^{th} eigenvalue λ_j of the autocovariance matrix C_u.

From (3.2.27) it can be seen that the transform coefficients have different magnitudes of information content. However, the correlations of coefficients of the same order normalized to their respective variances retain the functional form $\rho_y^{|1-k|}$ of the vertical correlation of the original image in the spatial domain. Thus, as in the previous case of one-dimensional DPCM, the one-dimensional orthogonal transformation, either optimum or non-optimum, performed on horizontal blocks of data decorrelates the resulting transform coefficient in that direction but does not affect the vertical correlation.

Summarily, with the basic assumption of representing the input image by a separate, two-dimensional first-order Markov process, one-dimensional techniques (DPCM or transformation) can only decorrelate the mapped image in the direction of operation. The redundancy inherent in the other direction remains intact and another operation should be done in that direction, either by DPCM or orthogonal transformation, in order that all redundancy is to be efficiently removed. A two-dimensional operation can be obtained by a combination of one-dimensional DPCM and unitary transformation. This combination results in

(1) Two-dimensional DPCM or 3rd order (3-point) DPCM;

(2) Two dimensional unitary transformation or block quantization;

(3) Transform-DPCM;

and (4) DPCM-transform.

The last two techniques mentioned above comprise the Hybrid Coding methods which are distinct by their respective order of operations.

The above discussion resulting from the basic assumption of directional separateness, seems to be in contrast with results obtained from data of real interest. Considering the correlation of the original image of the Truck (in Fig. 3.2.8) and of the error picture obtained by one dimensional DPCM in the

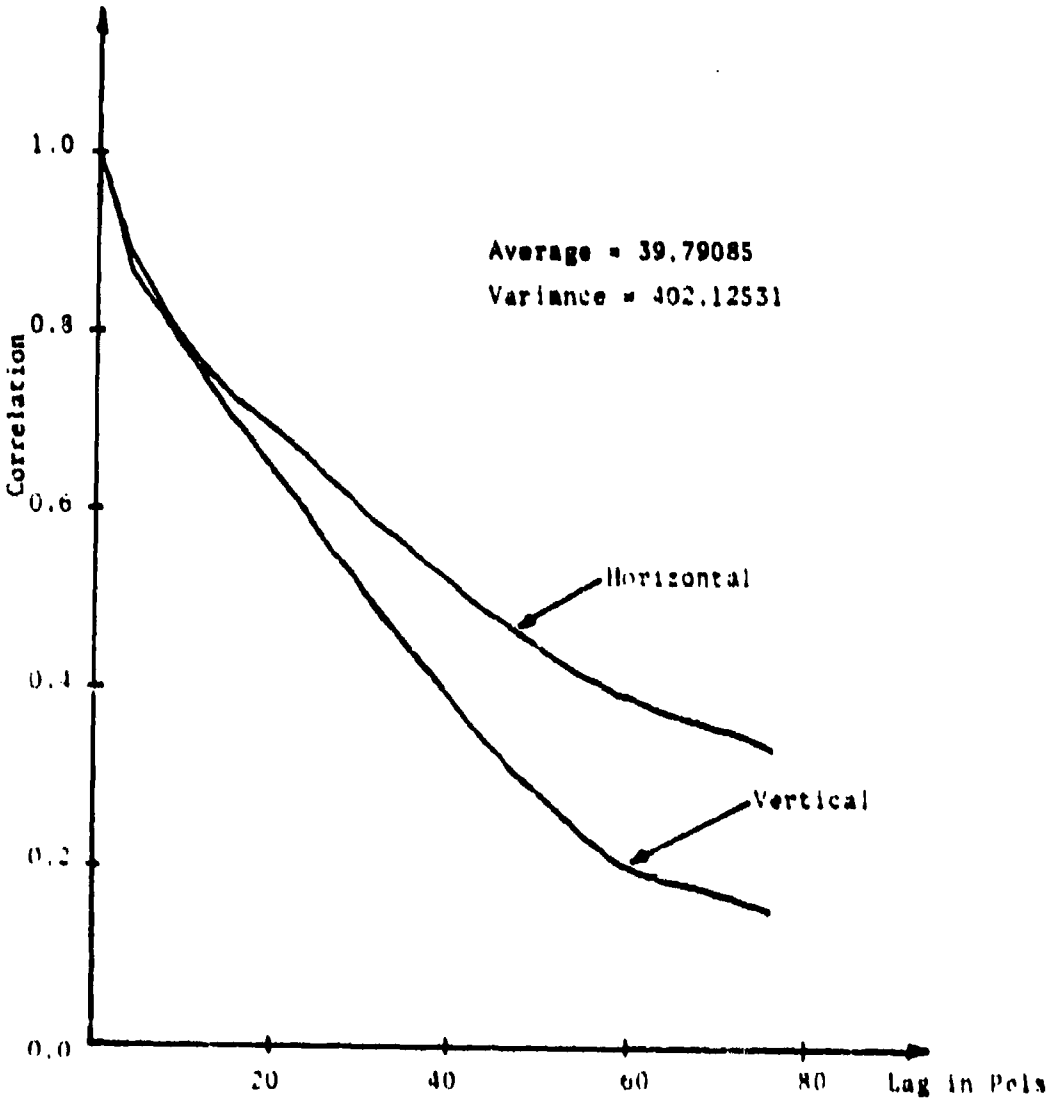

Fig.3.2.8 Correlation of PCM Signals (Truck)

vertical direction (in Fig. 3.2.9) It can be seen that the vertical correlation of the error picture is significantly smaller than that of the original image, but so also is the horizontal correlation. This deviation from the theoretical analysis witnesses a questionable problem on the relative validity of the basic assumption of directionally-separate correlation. Thus in reality there exists a certain degree of operational dependence contradicting with the directional-independence implicit in the afore-mentioned theoretical analysis.

A DPCM operation performed in one direction does affect the correlation in the remaining direction. In a particular picture of interest, the "Aerial photograph", a DPCM operation in the horizontal direction reduces the vertical correlation to such an extent that any two-dimensional technique introduced above does not appear to have significant advantages over the one-dimensional scheme. These results are shown in Figs. 3.2.10 and 3.2.11. The "Aerial photo--raph" used in obtaining these results contained several storage tanks located in fields.

A similar phenomenon also exists in reality using one-dimensional orthogonal transformation. In the foregoing discussions in relation with equation (3.2.27) it has been shown theoretically that a one-dimensional transformation performed in one direction does not affect the correlation pattern in the remaining direction Referring to Fig. 3.2.12 which presents the vertical one-element delay correlation of the 16 transform coefficients resulting from a one-dimensional Walsh-Hadamard transformation in the horizontal direction of the pictures of the Tank and the Truck, it can be seen that the correlation between adjacent-transform coefficients varies unpredictably with sequencies.

Fig. 3.2.13 shows the variances of the transform coefficients using a one-dimensional Hadamard transformation and block sizes of 16 and 32. Fig. 3.2.14 shows the variance of the difference between the transform coefficients of the

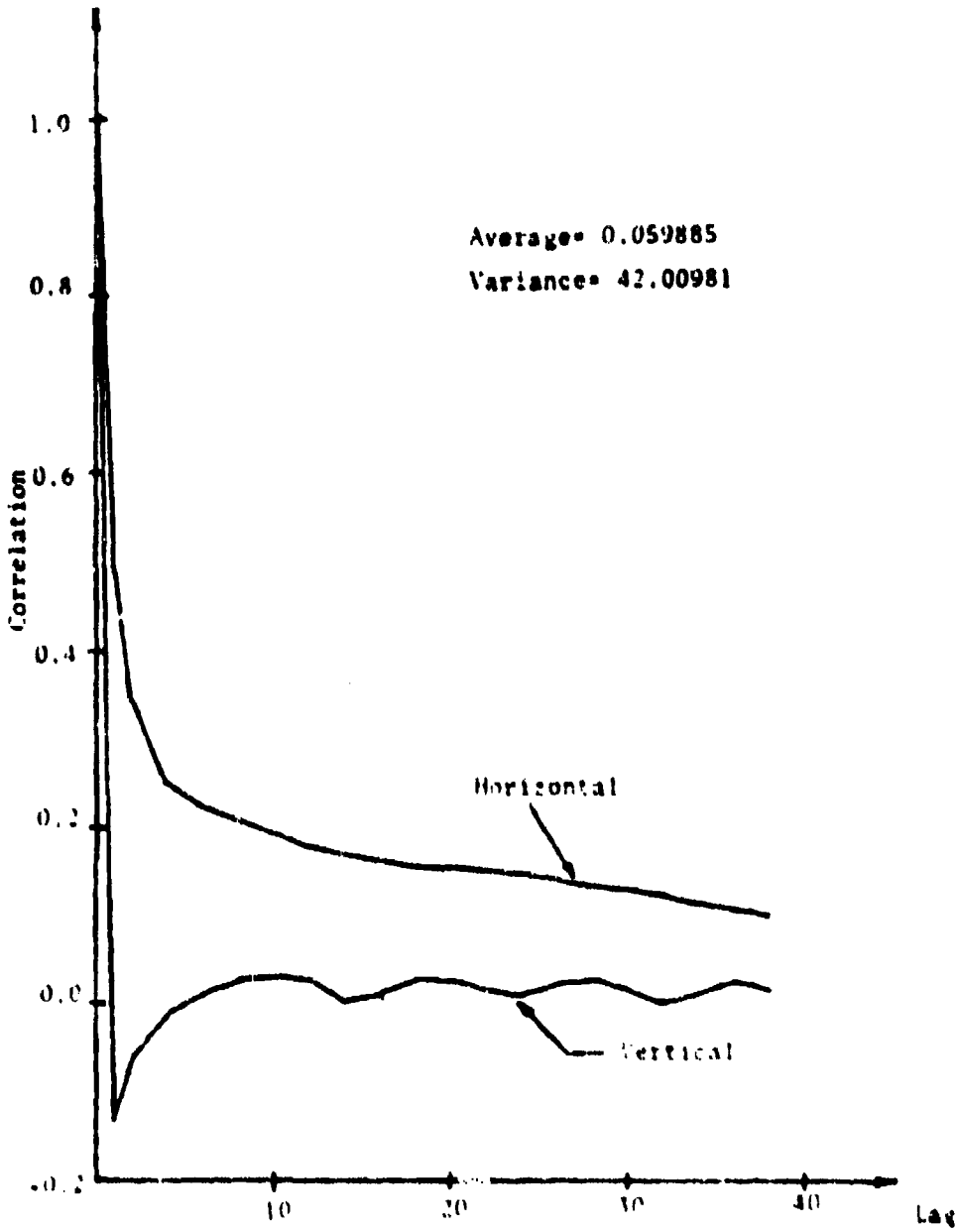

Fig. 3.2.9 Correlation of DPCM Signals (no.044341--Truck

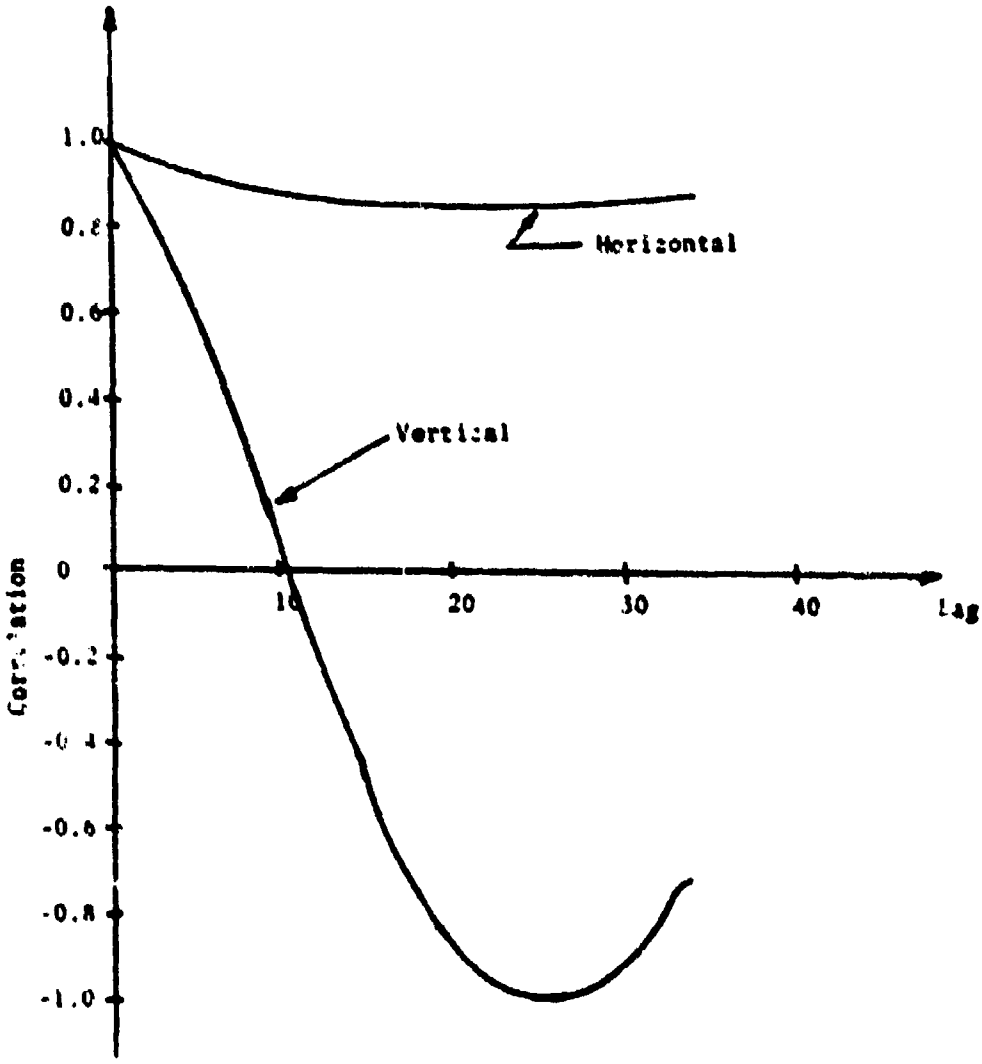

Fig.3.2.10. Correlation of the Aerial Picture.

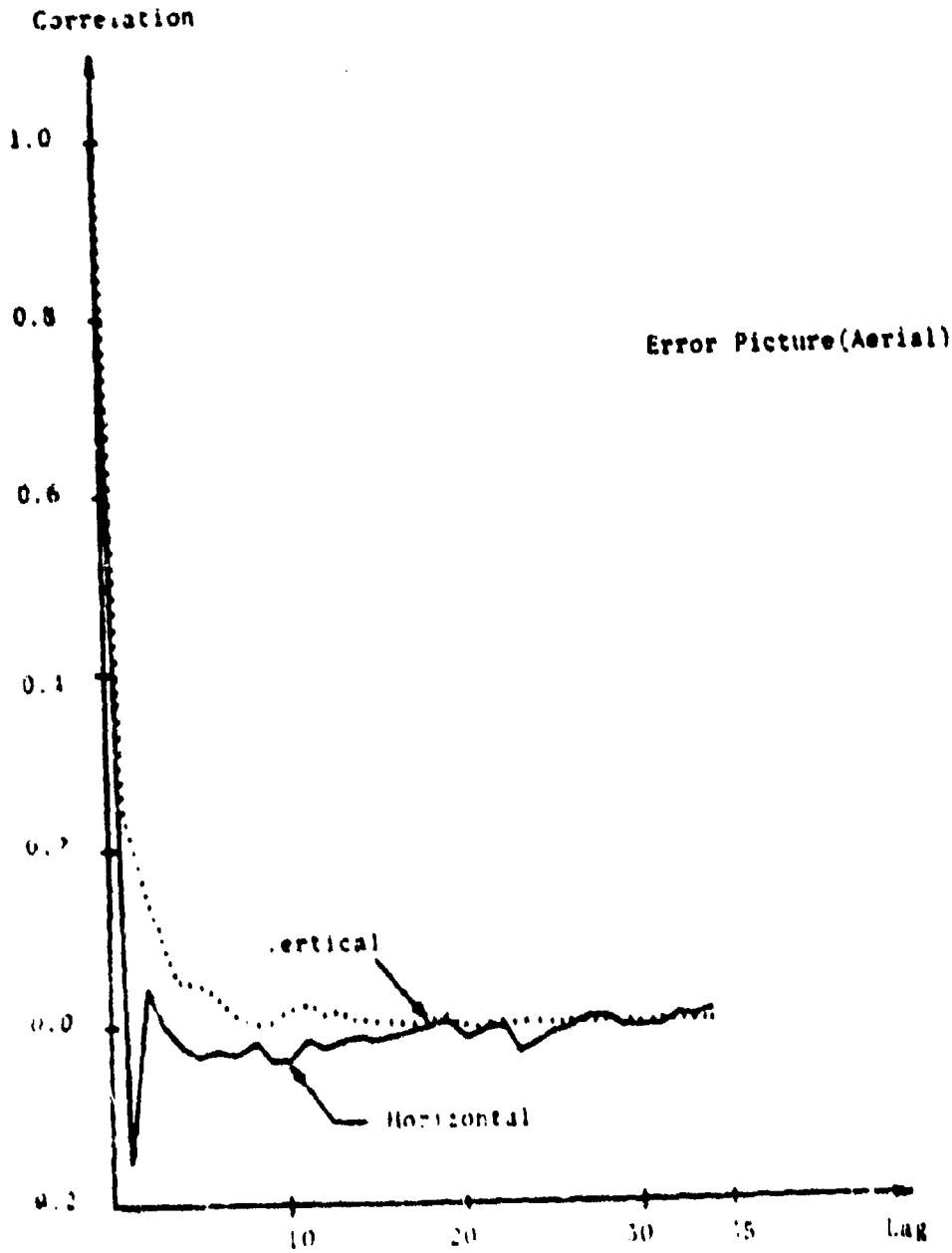

Fig. V.21 Correlation of Error Picture(Aerial)

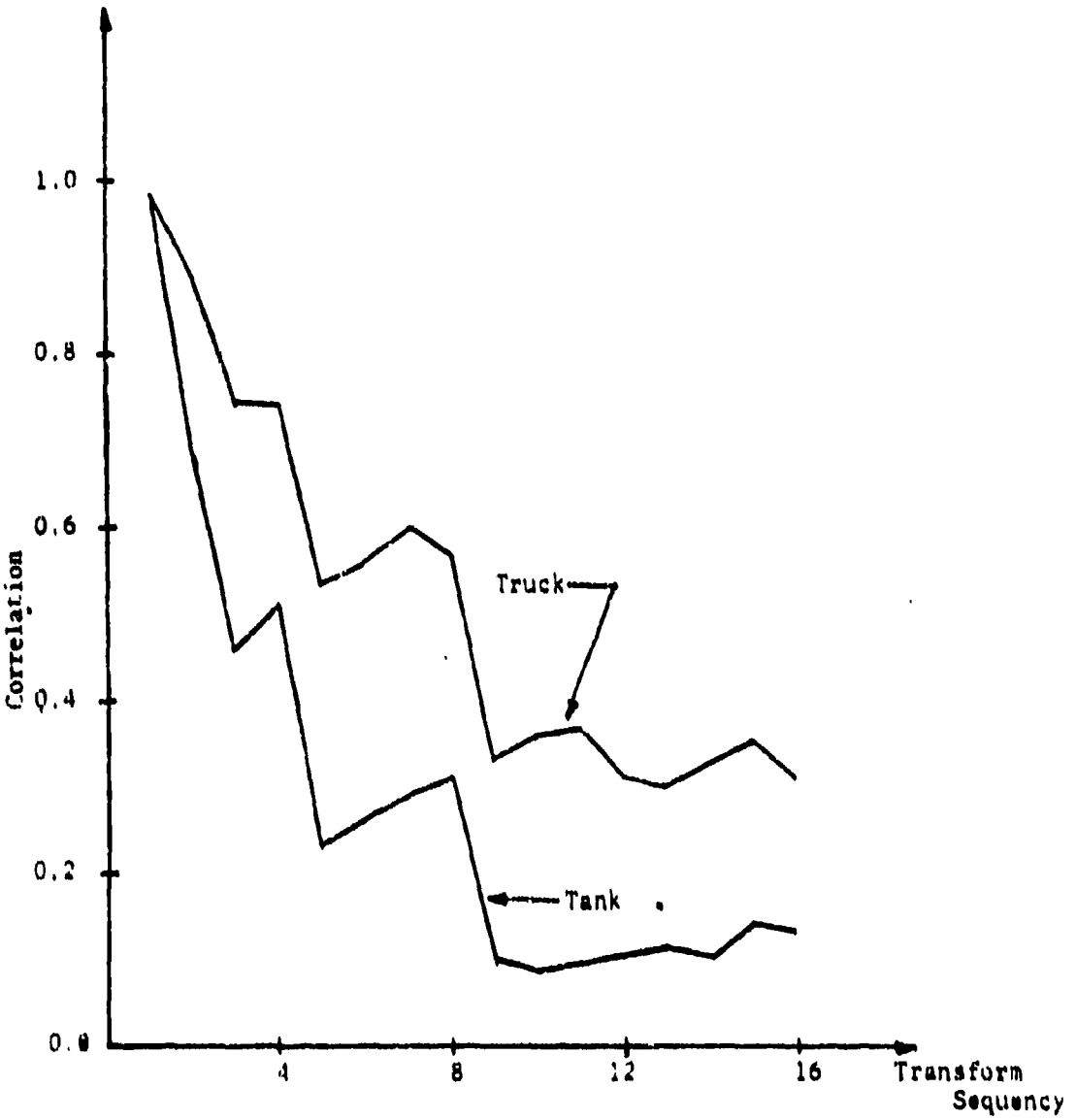

Fig. 3.2.12 One-Dimensional Hadamard(Horizontal) Vertical Correlation of Transform Coefficients(One Element Delay).

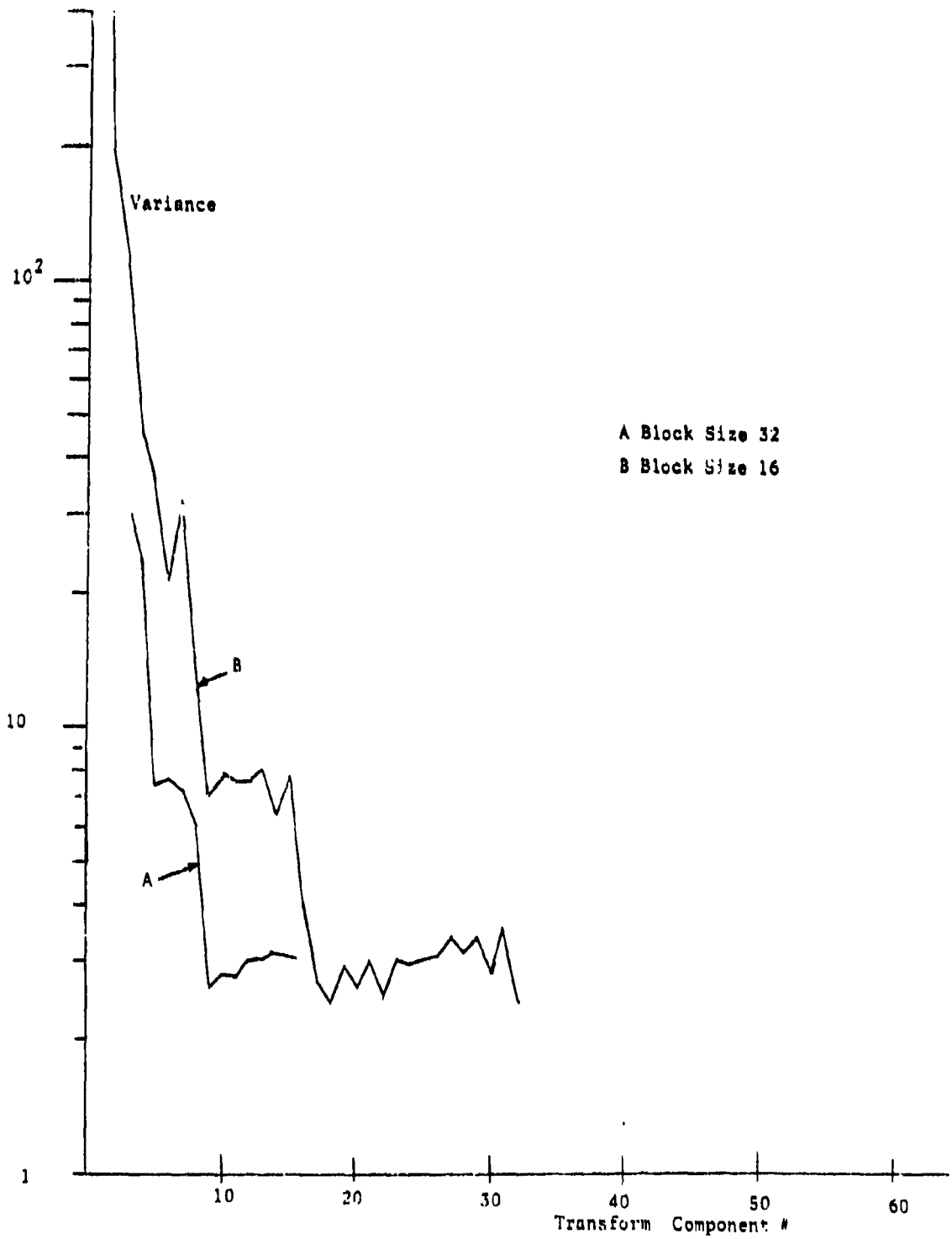

Fig.3.2.13. Variance of Transform Coefficients of the One-Dimensional Hadamard Transform of PCM Picture.

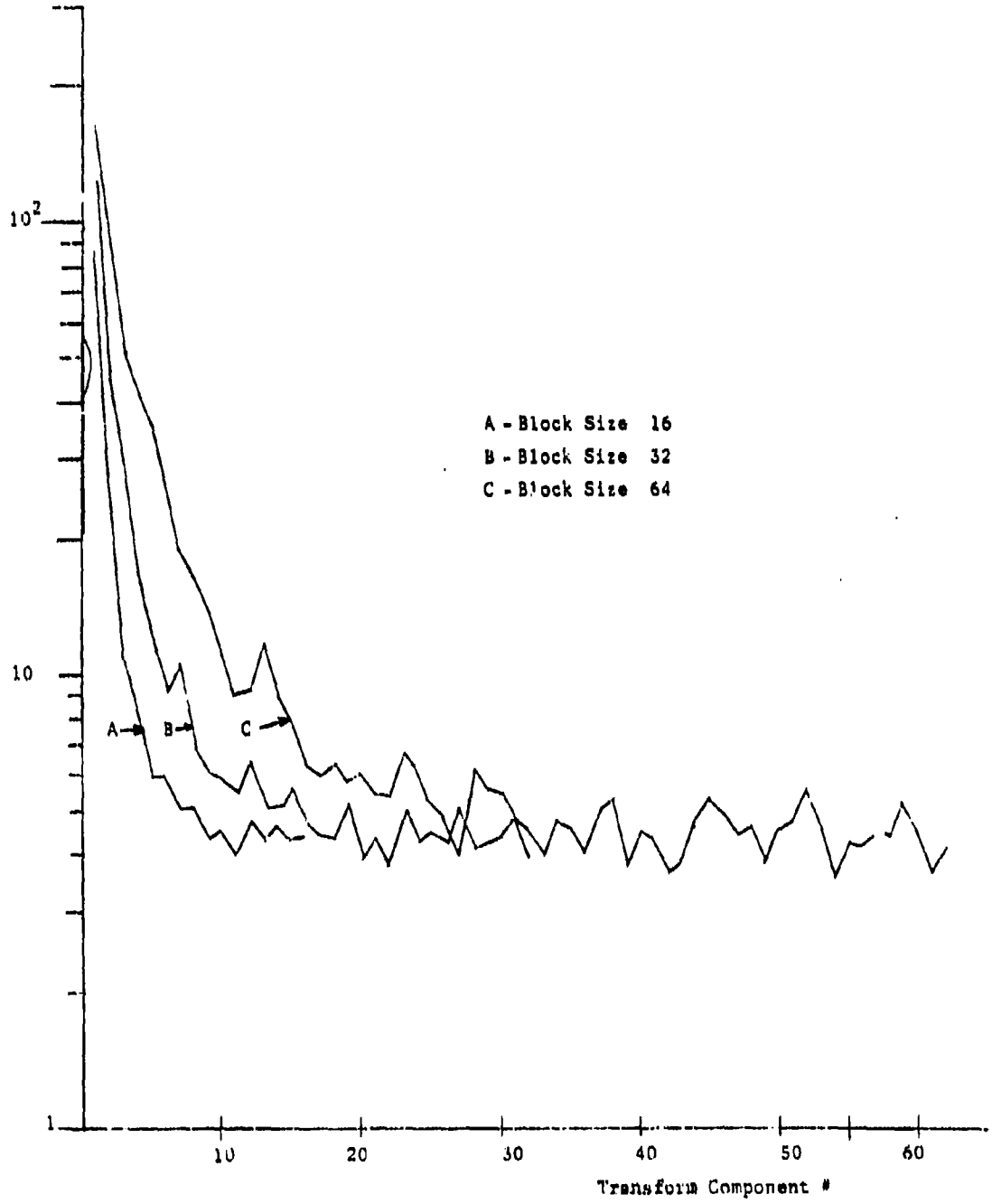

Fig. 3.2.14. Variance of the One-Dimensional Hadamard Transform Coefficient Differences of the PCM Picture.

same sequency. These are the results obtained in making a one-dimensional transform in the horizontal direction and taking the difference in the vertical direction. These results indicate that there appears to be little advantage in performing DPCM in the vertical direction. It should also be noticed that the variances of the difference signals tend to level off at a relative high level, indicating that all coefficients of order higher than 20 are of equal importance. Fig. 3.3.15 shows the variances of the one-dimensional Hadamard transform coefficients of the difference picture. To obtain these results DPCM techniques are used in the horizontal direction and transform techniques in the vertical direction using the "Aerial photograph". Again no significant improvement is seen in using this two-dimensional Hybrid technique over the one-dimensional scheme. It is again apparent that coefficients after order 15 are of equal importance. These results tend to indicate that little is gained from the two-dimensional Hybrid schemes for this type of picture.

Fig. 3.2.16 shows the variances of the one-dimensional Hadamard transform coefficients of the difference picture. Note that in this case the use of the two-dimensional Hybrid scheme gives good results. The variances of the higher order coefficients decrease continuously, with the higher order terms becoming insignificant. Similar results are shown in Fig. 3.2.17 using the Transform-DPCM technique. These results, using the picture of a "Face" (a still picture of a face of a woman), are in direct contrast with those obtained using the "Aerial photograph" and indicate that unless the correlation is high in both spatial directions little is gained in using a two-dimensional scheme.

Figs. 3.2.18 and 3.2.19 show the percentage of energy contained in the coefficients for the one-dimensional Hadamard transformation, the difference of transform coefficients and the transform of difference samples for the scenes of the "Face" and the "Aerial photograph". When only a portion of the

coefficients are retained for further processing, the performance of a hybrid coding scheme would give better results for the scene of the "Face" than for the "Aerial photograph" as far as truncation errors are concerned.

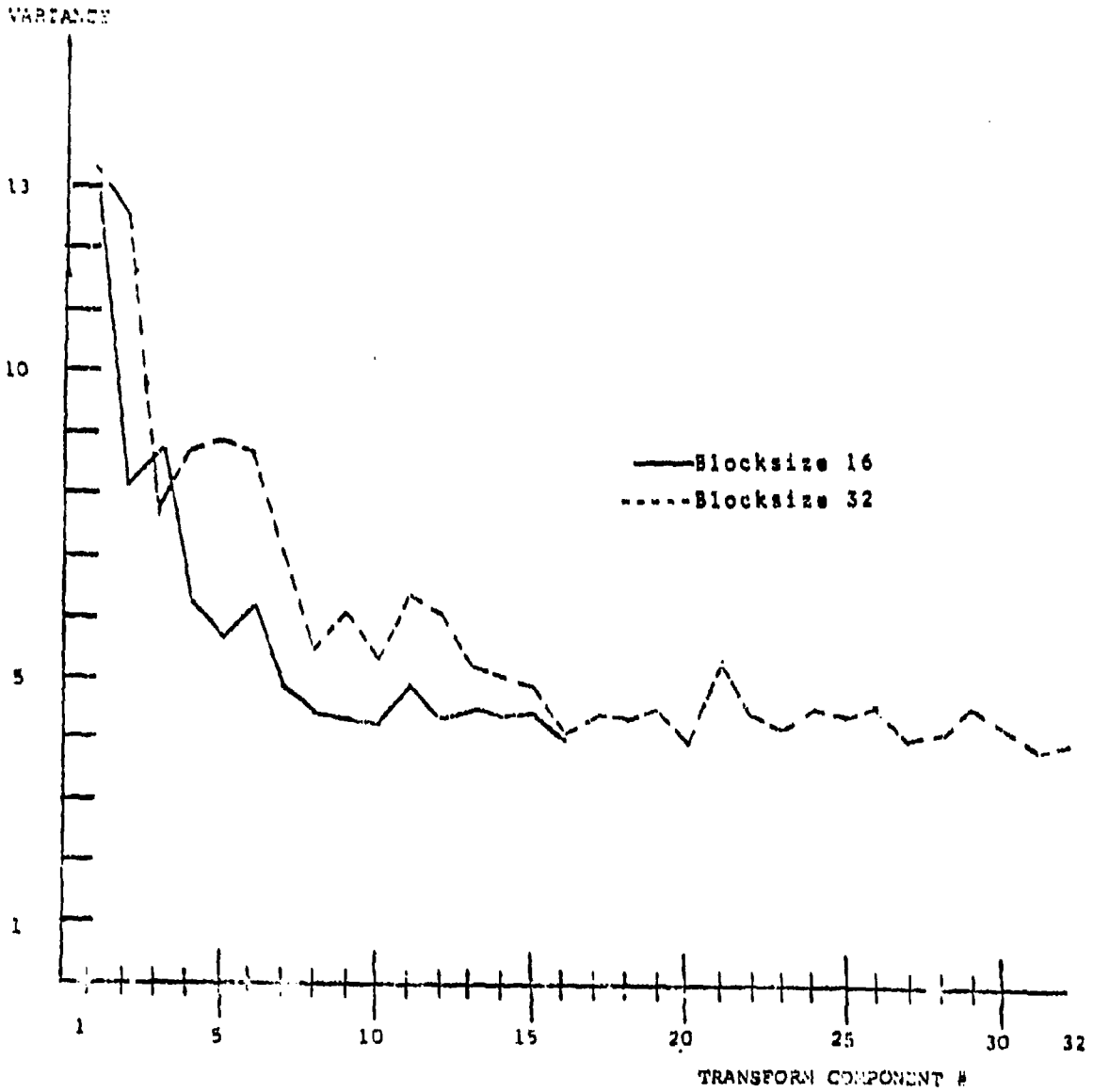

Fig. 3.2.15 Variance of One-Dimensional Hadamard Transform Coefficients of the DPCM Picture (Aerial Photograph)

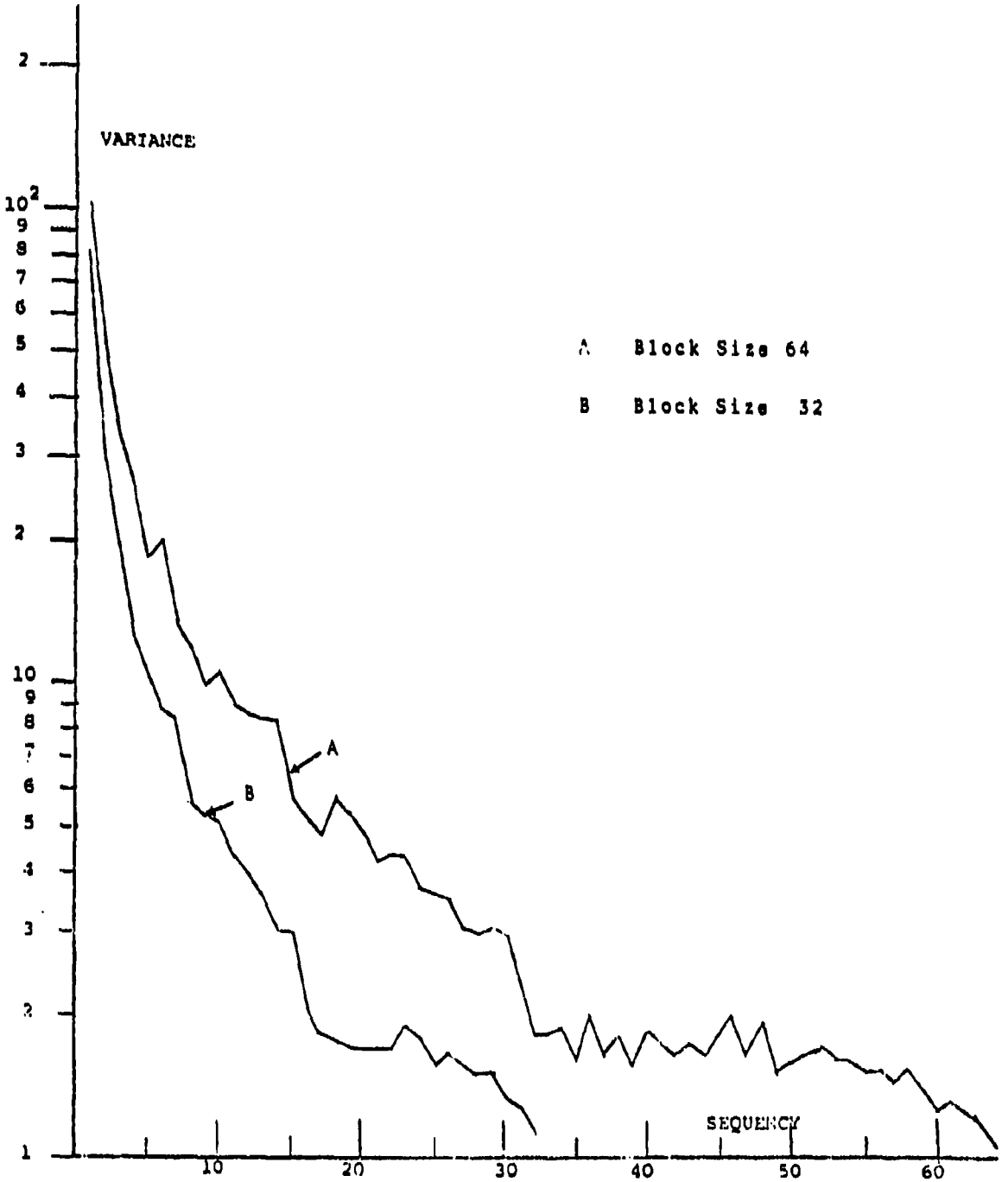

Fig. 3.2.16. Variances of One-Dimensional Hadamard Transform Coefficients of the Difference Picture(Face).

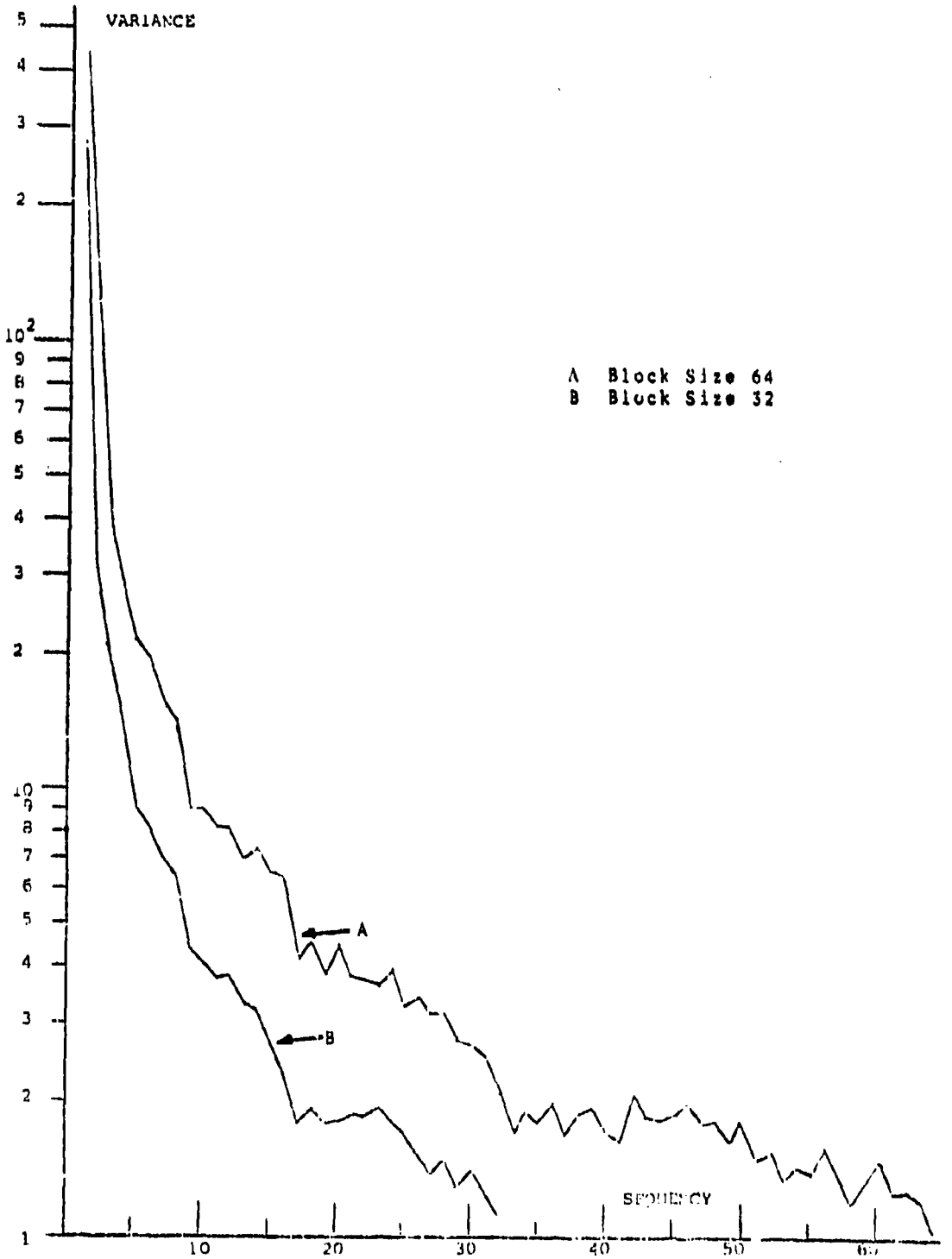

Fig.3.2.17. Variances of the Difference of the One-Dimensional Hadamard Transform Coefficients(Face).

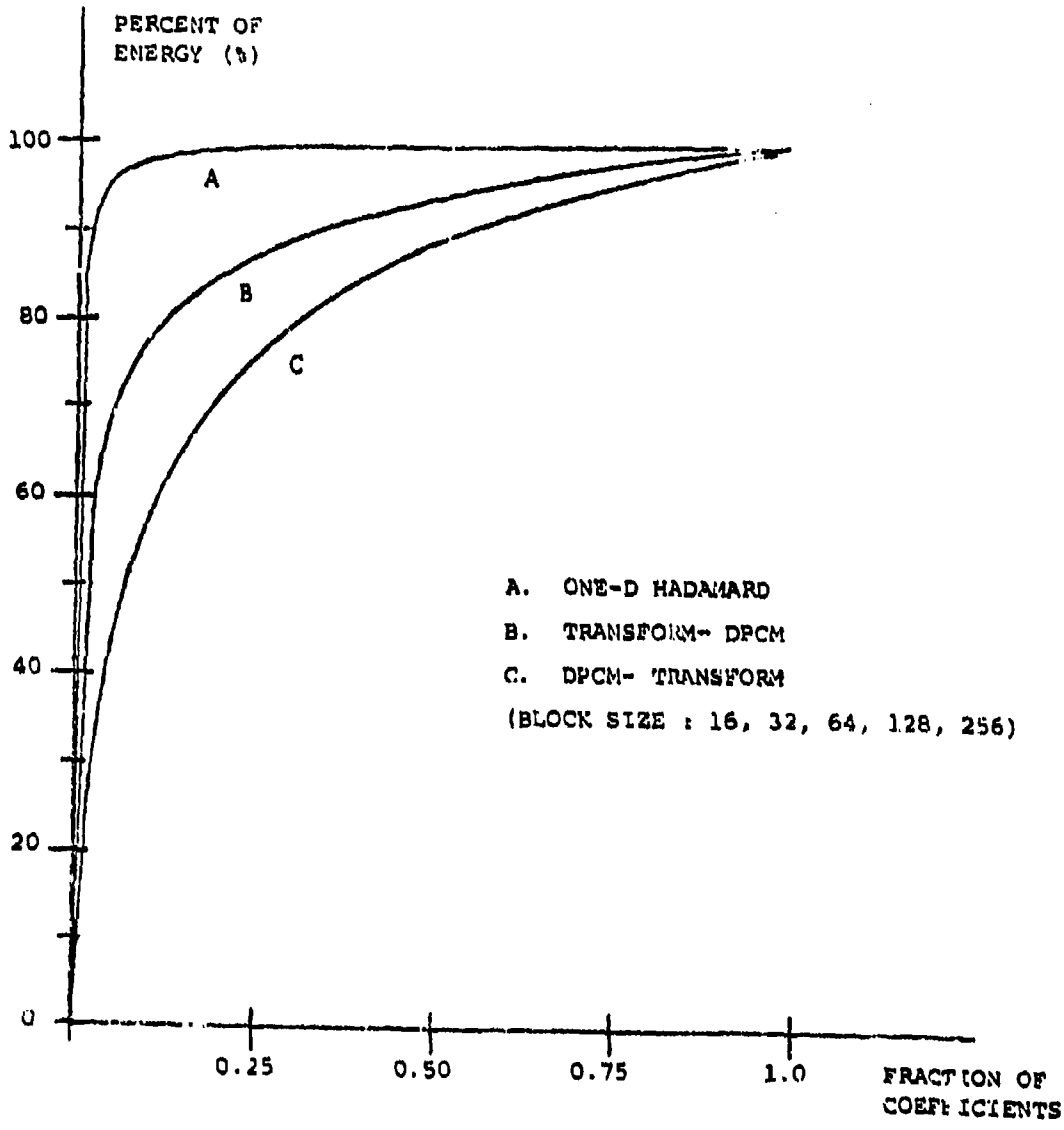

Fig.3.2.18. Energy of Transform Coefficients (Picture : Face).

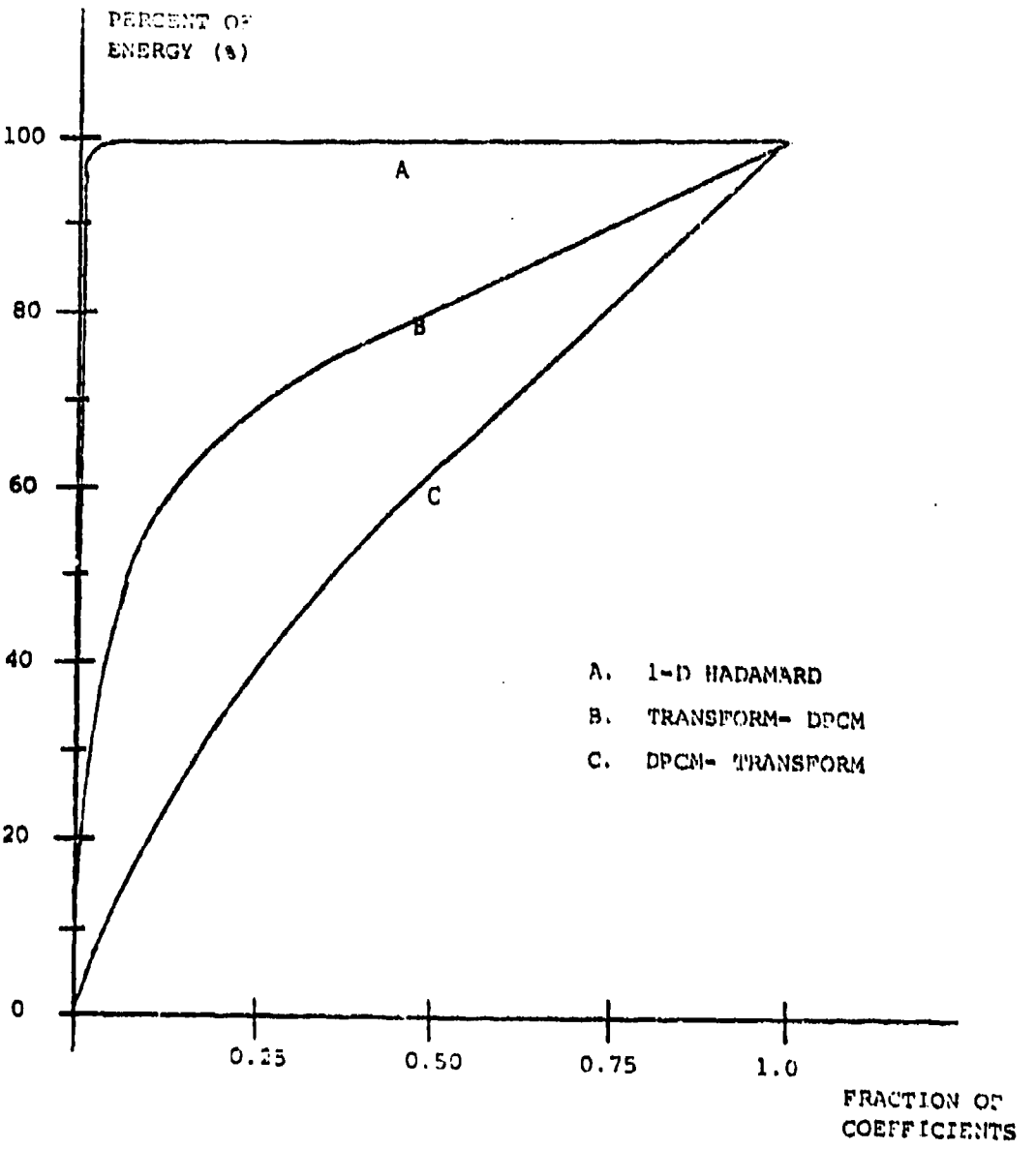

Fig. 3.2.19. Energy of Transform Coefficients (aerial photograph).

3.2.4 Two-Dimensional Transformations

If the original image is arranged into an NxN matrix U with sample elements u(i,j), i,j = 1, 2, ... N, a two-dimensional orthogonal transformation T operates on U and produces a matrix V of transform coefficients v(i,j), i,j = 1, 2, ... N is given by

$$V = TUT^T \tag{3.2.28}$$

The inverse operation on V to retrieve U is accomplished by

$$U = T^T VT \tag{3.2.29}$$

A generalized two-dimensional transformation and its inverse may be defined as

$$V = T_1 U T_2^T \tag{3.2.30}$$

and

$$U = T_1^T V T_2 \tag{3.2.31}$$

where T_1 and T_2 are orthogonal matrices and, in general, $T_1 \neq T_2$. Equations (3.2.30) and (3.2.31) will be identical to (3.2.28) and (3.2.29), respectively, when $T_1 = T_2$.

The generalized two-dimensional transformation defined by (3.2.30) may be considered as an extension of one-dimensional scheme by separating the former into two independent procedures as follows:

(1) A one-dimensional transformation T_1 operates on the columns of U to produce an intermediate matrix V', i.e. $V' = T_1 U$ (3.2.32)

(2) The coefficient matrix V is obtained by a second one-dimensional transformation T_2 operating on V', i.e. $V = V' T_2^T$ (3.2.33)

Clearly, both the one-dimensional transformation (3.2.2) and the two-dimensional transformation (3.2.30) result in a set of coefficients each of which is a linear combination of the data sample values.

The characteristics of one-dimensional transformations discussed in preceding sections can be similarly applied to the two-dimensional case. From (3.2.32), a column $c_{v'j}$ of the intermediate matrix V' is expressed by:

$$c_{v'j} = T_1 c_{uj} \tag{3.2.34}$$

where c_{uj} is the j^{th} column of the image matrix U.

The input sample u(i,j) is modelled as a real random variable of a two-dimensional Markov process whose correlation function is defined in (3.2.35), i.e.

$$E\{u(i,j)u(k,l)\} = \rho_y^{|i-k|} \rho_x^{|j-l|} \tag{3.2.35}$$

The column covariance matrix C_{yu} of any data column c_{uj} j = 1, 2, ... N is obtained from (3.2.35) to be

$$C_{yu} = E(c_{uj} c_{uj}^T) = \begin{bmatrix} 1 & \rho_y & \cdots & \rho_y^{N-1} \\ \rho_y & 1 & & \rho_y^{N-2} \\ \vdots & & & \vdots \\ \rho_y^{N-1} & \cdots & & 1 \end{bmatrix} \tag{3.2.36}$$

From results of the preceding section, if the rows of the transformation matrix T_1 are eigenvectors associated with eigenvalues λ_{yk} k = 1, 2, ... N of the column covariance matrix C_{yu} then the elements of column vector $c_{v'j}$ are uncorrelated. The Karhunen-Loève transformation T_1 operating on all columns of U produces an intermediate matrix V' which is composed of uncorrelated columns, i.e. the covariance matrix of each column $c_{v'j}$ is diagonal:

$$C_{yv'_j} = \text{diag}(\lambda_{y1}, \lambda_{y2}, \ldots \lambda_{yN}) \tag{3.2.37}$$

with $\lambda_{y1} > \lambda_{y2} > \ldots > \lambda_{yN}$, for all $j = 1, 2, \ldots N$.

From results of the theoretical analysis of one-dimensional transformations, it can be seen that the row correlation of the transform values of V' is affected by the decorrelation process using one-dimensional eigenvector transformation T_1. The row-correlation of element $v'(i,j)$ of row $r_{v'i}$ can be written as

$$E\{v'(i,j)v'(i,k)\} = \lambda_{yi}\, \rho_x^{|j-k|} \tag{3.2.38}$$

The row covariance matrix of $r_{v'i}$ is

$$C_{xv'_i} = E\{r_{v'i}^T\, r_{v'i}\} = \lambda_{yi} \begin{matrix} 1 & \rho_x & \ldots & \rho_x^{N-1} \\ \rho_x & 1 & & \rho_x^{N-2} \\ \vdots & & & \vdots \\ \rho_x^{N-1} & & \ldots & 1 \end{matrix} \tag{3.2.39}$$

From (3.2.2) a row r_{vi} of the transform matrix V is expressed by

$$r_{vi} = r_{v'i}\, T_2^T$$

or
$$r_{vi}^T = T_2 r_{v'i}^T \tag{3.2.40}$$

Then if the rows of T_2 are eigenvectors associated with eigenvalues λ_{xk}, $k = 1, 2, \ldots N$ of the row covariance matrix $C_{xv'_i}$ the elements of the row vector r_{vi} are uncorrelated. The row covariance matrix of row r_{vi} is:

$$C_{xv_i} = \lambda_{yi}\, \mathrm{diag}\,[\lambda_{x1}\, \lambda_{x2} \ldots \lambda_{xN}] \tag{3.2.41}$$

$$i = 1, 2, \ldots N.$$

To conclude, the two-dimensional transformation in (3.2.30) with individual Karhunen-Loeve transformations T_1 and T_2 properly chosen, produces a transform coefficient matrix whose elements are uncorrelated in all directions. The variances of transform coefficients are different in magnitude. Thus the information contents of each coefficient is different.

In such a case, the variance of a transform coefficient v(i,j) is given by

$$\sigma_v^2 (i,j) = E (v^2(i,j)) = \lambda_{xi} \lambda_{yj} \qquad (3.2.42)$$

The transform matrices T_1 and T_2 are associated with the vertical correlation coefficient ρ_y and the horizontal correlation coefficient ρ_x, respectively. In general $\rho_x \neq \rho_y$, hence $T_1 \neq T_2$.

The non basis-restricted transformations, as their names implies, are independent of the statistical characteristics of the image.

Therefore, two-dimensional orthogonal transformations and their inverses using Discrete Fourier, Hadamard, Haar matrices, etc. are defined using (3.2.28) and (3.2.29) respectively.

Retaining the n coefficients with the largest variances by a series transaction process can be viewed as a "zonal filtering" or "masking" in the transform domain [27].

Similar to the one-dimensional case, the mean-square-approximation error due to the truncation process in reconstructing the original image by an inverse transformation is given by the variances of the retained coefficients, i.e.

$$\varepsilon_t^2 = 1 - \frac{1}{N^2} \sum_{i,j} \sigma_v^2 (i,j) \qquad (3.2.43.a)$$

When Karhunen-Loève transformation is used, $\sigma_v^2 (i,j)$ is given by (3.2.42).

And the total system mean-square coding error including the quantization error encountered in quantizing the retained coefficients for transmission is similarly obtained as:

$$\varepsilon^2 = 1 - \frac{1}{N^2} \sum_{i,j} \sigma_v^2 (i,j) + \frac{1}{N^2} \sum_{i,j} \sigma_q^2 (i,j) \qquad (3.2.43.b)$$

assuming a noiseless transmission channel.

3.3 Hybrid Coding Techniques

One of the most important objectives of an efficient coding system is to produce uncorrelated sample values even if they are not necessarily independent.

For images whose picture-elements (pels) are correlated in all directions, one-dimensional techniques are not sufficient in removing all redundancy which is inherently embodied in the image.

At present we are concerned with the techniques of DPCM and orthogonal transformations. A two-dimensional scheme can be introduced by any possible combination of one-dimensional DPCM and one-dimensional transformations:

(1) DPCM-DPCM,

(2) Transform-Transform,

(3) Transform-DPCM,

and (4) DPCM-Transform.

The first two combinations are identically equivalent to the third-order (3-point) DPCM and the two-dimensional transformation, respectively. The last two combinations constitute the Hybrid Coding Technique which is the subject of this section.

3.3A Transform-DPCM Coding System

As implied by its name, the Transform-DPCM technique results in a coding system in which the transform coefficients produced by a one-dimensional orthogonal transformation in the horizontal (vertical direction) are subjected to a predictive quantizing system operating along the vertical (horizontal) direction.

Without loss of generality, we assume that a one-dimensional transformation of individual rows of the image matrix, i.e., in the horizontal direction, produces a transform coefficient matrix whose individual columns are subjected to DPCM coding. The block diagram of the proposed hybrid system is shown in Fig. 3.3.1.

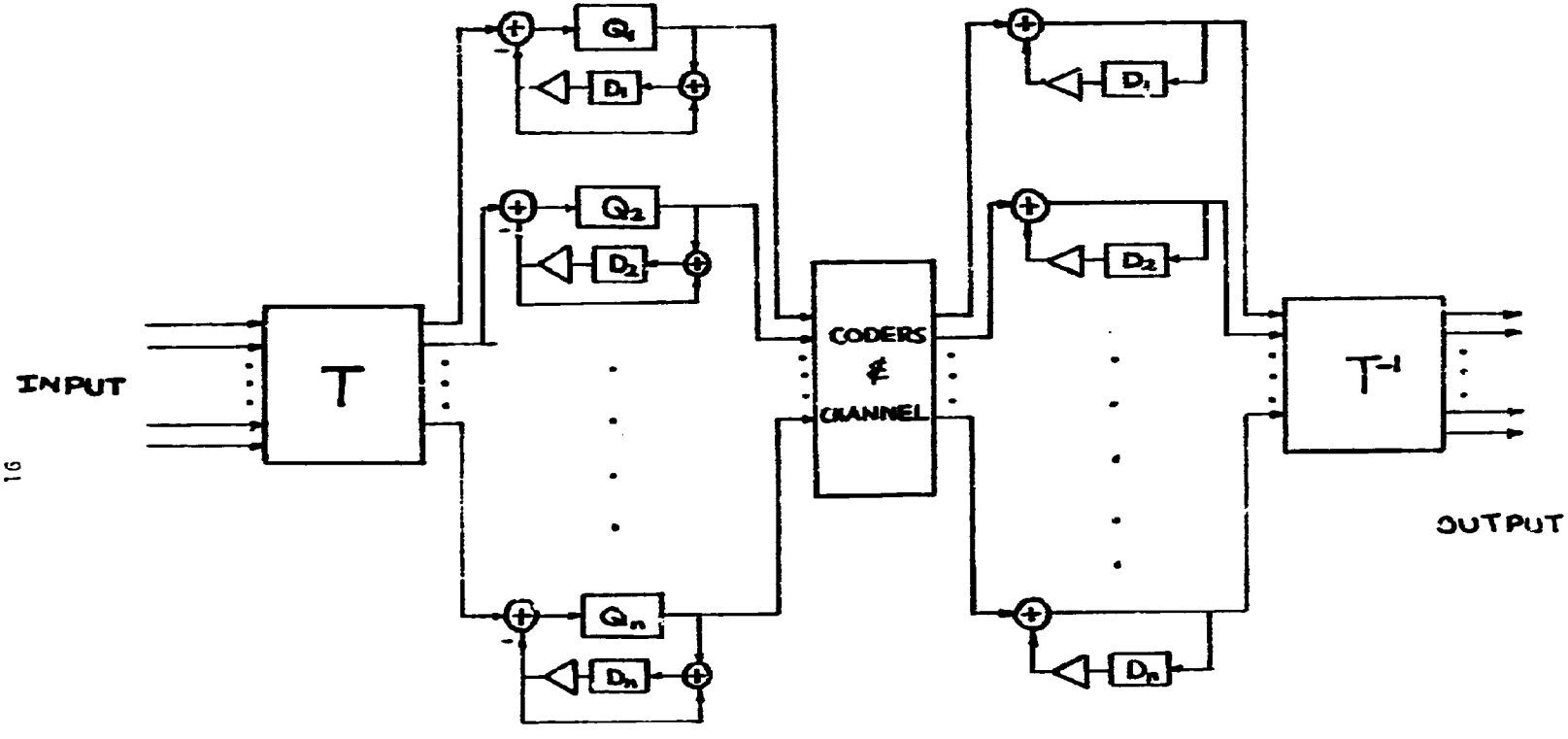

Fig. 3.3.1. Transform-DPCM Hybrid Coding System

The first step in implementing a Transform-DPCM system is to divide the MxM image matrix into a set of nonoverlapping rows of N pels where $N = 2^k$ is an integer multiple of N, as illustrated in Fig. 3.3.2.

The image is thus a collection of L, $L = \frac{M^2}{N}$, vectors of dimension N. For simplicity we will consider only the first vertical subset of M vectors and let $u_1, u_2 \ldots u_M$ denote the collection of M data row vectors, i.e., $u_i = [u(i,1)\ u(i,2) \ldots\ u(i,N)]$

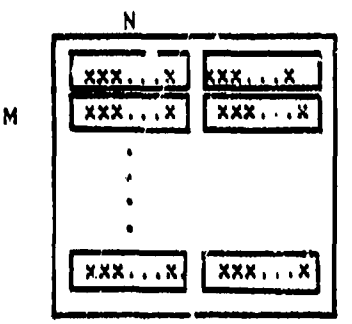

Fig. 3.3.2. The Partitioning of MxM Image Into 1xN Subimages.

Each data vector u_i, i = 1, 2, .. M is projected into an N-dimensional coefficient vector $V_{xi} = [v(i,1)\ v(i,2) \ldots\ V(i,N)]$ using a one-dimensional orthogonal transformation represented by a NxN matrix T whose rows form a complete orthonormal set of basis vectors $T_1, T_2, \ldots T_N$. The i^{th} coefficient row is given by

$$v_{xi}^T = T\, u_i^T \tag{3.3.1}$$

where the i,j^{th} element is:

$$v(i,j) = T_j\, u_i^T \quad ; \quad \begin{matrix} i = 1,2, \ldots M \\ j = 1,2, \ldots N \end{matrix} \tag{3.3.2}$$

Since the data vectors u_k are vertically adjacent in the spatial domain, their corresponding transform coefficient vectors v_k will also be vertically correlated.

The column correlation of the j^{th} transform coefficient v(i,j) is given by

$$E\{v(i,j)\ v(k,j)\} = \sigma_{vj}^2\ \rho_y^{|i-k|} \tag{3.3.3}$$

where σ_{vj}^2 is variance of the j^{th} transform coefficient. In the particular case of Karhunen-Loève transformation, $\sigma_{vj}^2 = \lambda_{xj}$, the j^{th} eigervalue of the Toëplitz covariance matrix

$$C_{xu} = \begin{bmatrix} 1 & \rho_x & \cdots & \rho_x^{N-1} \\ \vdots & & & \vdots \\ \rho_x^{N-1} & \cdots & & 1 \end{bmatrix} \tag{3.3.4}$$

Equation (3.3.3) indicates that the correlation functions of transform coefficients normalized to their corresponding variances in various columns of the transformed array are identical to the correlation of image samples in the vertical direction. This functional relationship is invariant to the different types of transformation employed - basis-restricted or non basis-restricted.

A number of different DPCM coders are subsequently used to encode the individual columns of the retained transform coefficients. Note that in all the DPCM orders the same feedback coefficient is employed resulting from the identical normalized correlation of coefficients of all sequencies.

Studies of linear prediction theory have shown that for first-order Markov process, the optimum linear estimate, in the least mean-square prediction error sense, of a transform coefficient v(i,j) can be obtained from the previous coefficient in the j^{th} transform column, i.e.

$$\hat{v}(i,j) = \rho_y\ v(i-1,j) \qquad i = 2, 3, \ldots, N \tag{3.3.5}$$

In the following discussion, we will analyze the performance of the Transform-DPCM Hybrid coding system using a prediction coefficient which can either be

optimum or non-optimum. To extend our generalization further, we will assume that it is possible to use different prediction coefficients A_1, A_2 ... A_n for different DPCM coders, i.e.

$$\hat{v}(i,j) = A_j\, v(i-1,j) \quad . \tag{3.3.6}$$

The coefficient difference or error

$$d(i,j) = v(i,j) - A_j\, v(i-1,j) \tag{3.3.7}$$

is quantized and coded for transmission.

At the receiver end, the channel-corrupted sample value $e_o(i,j)$ is added to the predicted sample $\hat{v}_o(i,j)$ to reconstruct the coefficient $v_o(i,j)$ which is a corrupted version of transform coefficient $v(i,j)$, i e.

$$v_o(i,j) = e_o(i,j) + A_j\, v_o(i-1,j) \tag{3.3.8}$$

Finally, an inverse transformation operating on each row of $v_o(i,j)$ reconstructs the image.

The output sample vector $u_{oi} = [uo(1,1)\ u_o(i,2) \ldots u_o(i,N)]$ resulting from the hybrid coding of input image vector u_i within some degree of error. For mathematical tractability, the objective performance of the proposed coding system are measured by the total mean-square coding error

$$\epsilon^2_{TD} = \frac{1}{NM} \sum_{j=1}^{N} E\,(u_i - u_{oi})\,(u_i - u_{oi})^T) \tag{3.3.9}$$

The total system mean-square-error defined in (3.3.9) will be evaluated in the following analysis. For clarity, the j^{th} DPCM coder is shown here for further reference (Fig. 3.3.3)

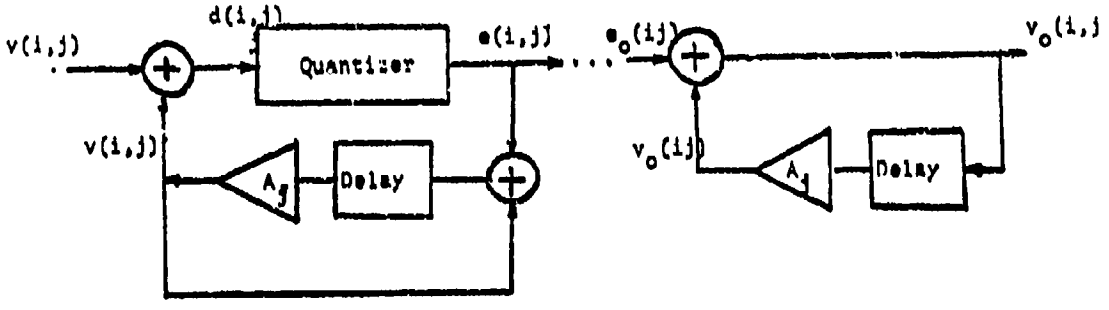

Fig. 3.3.3. The j^{th} DPCM Coder.

Referring to Fig. 3.3.3, the predicted coefficient $\hat{v}(i,j)$ the transmitter can be expressed by

$$\hat{v}(i,j) = A_j [e(i-1,j) + \hat{v}(i-1,j)] \tag{3.3.10}$$

The sequence of predicted transform coefficients can be derived from (3.3.10) as

$$\begin{aligned} \hat{v}(i-1,j) &= A_j [e(i-2,j) + \hat{v}(i-2,j)] \\ &\vdots \\ \hat{v}(i-k,j) &= A_j [e(i-k-1,j) + \hat{v}(i-k-1,j)] \end{aligned} \tag{3.3.11}$$

or:
$$\hat{v}(i,j) = \sum_{k=1}^{M} A_j^k \, e(i-k,j) \tag{3.3.12}$$

At the receiver, the predicted coefficient $\hat{v}_o(i,j)$ can be similarly expressed by considering

$$\hat{v}_o(i,j) = A_j \, v_o(i-1,j) \tag{3.3.13}$$

Since $v_o(i-1,j) = e_o(i-1,j) + \hat{v}_o(i-1,j)$, (3.3.13) can be rewritten as

$$\hat{v}_o(i,j) = A_j [e_o(i-1,j) + \hat{v}_o(i-1,j) \tag{3.3.14}$$

The sequence of predicted coefficient reconstructed at the receiver is derived from (3.3.14):

$$\hat{v}_o(i-1,j) = A_j\,[e_o(i-2,j) + \hat{v}_o(i-2,j)]$$

$$\hat{v}_o(i-k,j) = A_j\,[e_o(i-k-1,j) + \hat{v}_o(i-k-1,j)] \qquad (3.3.14)$$

Hence, $\hat{v}_o(i,j)$ can be approximated as

$$\hat{v}_o(i,j) = \sum_{k=1}^{M} A_j^k\, e_o(i-k,j) \qquad (3.3.15)$$

From (3.3.12) and (3.3.15) the transform coefficient $v(i,j)$ and its corrupted version $v_o(i,j)$ are obtained referring to Fig. 3.3.3.

$$v(i,j) = \sum_{k=0}^{M} A_j^k\, e(i-k,j) - q(i,j) \qquad (3.3.16)$$

and

$$v_o(i,j) = \sum_{k=0}^{M} A_j^k\, e_o(i-k,j) \qquad (3.3.17)$$

where $q(i,j) = e(i,j)-d(i,j)$ is the quantizing noise associated with transform difference $d(i,j)$.

The reconstructed image sample $u_o(i,j)$ is obtained by the inverse orthogonal transformation T^{-1}, where $T^{-1} = [\phi(i,j)]^T$, of the noise-affected coefficients $v_o(i,1)$, $v_o(i,2)$, ... $v_o(i,n)$ and can be expressed as:

$$u_o(i,j) = \sum_{r=1}^{n} \phi(r,j)\, v_o(i,r) \qquad (3.3.18)$$

Similarly, the image sample $u(i,j)$ can be considered as resulting from the inverse transformation T^{-1} of coefficients $v(i,1)$, $v(i,2)$, ... $v(i,N)$, i.e.

$$u(i,j) = \sum_{r=1}^{N} \phi(r,j)\, v(i,r) \qquad (3.3.19)$$

The reconstruction error $\epsilon(i,j) \triangleq u(i,j)-u_o(i,j)$ is calculated using (3.3.16), (3.3.17), (3.3.18) and (3.3.19) to yield

$$\epsilon(i,j) = \sum_{r=n+1}^{N} \phi(r,j)\, v(i,r) - \sum_{r=1}^{n} \phi(r,j) q(i,r)$$

$$- \sum_{r=1}^{n} \sum_{k=0}^{M} A^k \phi(r,j)\, c(i-k,j) \qquad (3.3.20)$$

where $c(i,j) = \hat{v}_Q(i,j) - e(i,j)$ is the channel error resulting from transmitting data over a noisy channel. The total system mean-squared error ϵ^2_{TD} defined in (3.3.9) is rewritten as:

$$\epsilon^2_{TD} = \frac{1}{MN} \sum_{i=1}^{M} \sum_{j=1}^{N} E\{\epsilon^2(i,j)\} \qquad (3.3.21)$$

Totty and Clark [138] have shown that if the quantization process is done in an optimum manner, the channel error and the quantization error are independent. It has also been shown that when the quantization is done finely, we can assume the quantization noise and the quantized sample independent. Furthermore, since $d(i,j) = v(i,j) - A_j\, v(i-1,j)$ is a finite linear combination of transform coefficients the assumption of uncorrelatedness between the transform coefficient and the quantization noise follows. Restricting ourselves to the above approximation, the total system coding error ϵ^2_{TD} in (3.3.21) can be formulated as:

$$\epsilon^2_{TD} = \frac{1}{N} \sum_{j=n+1}^{N} \sigma^2_{vj} + \frac{1}{N} \sum_{j=1}^{n} \sigma^2_{qj}$$

$$+ \frac{1}{MN} \sum_{i=1}^{M} \sum_{j=1}^{n} \sum_{k=0}^{M} A_j^{2k}\, E\{c^2(i-k,j)\} \qquad (3.3.22)$$

where σ^2_{vj} is the variance of the j^{th} transform coefficient and σ^2_{qj} the variance of quantization noise in the j^{th} DPCM systems. Recalling that the horizontal covariance matrix of transform coefficient C_{xv} is the orthogonal transformation of the horizontal covariance matrix of the original image C_{xu}, i.e. $C_{xv} = TC_{xu}T^T$ and that orthogonal transformation preserves the trace of the transformed matrix, i.e.

$$\text{Trace } [C_{xv}] = \text{Trace } [C_{xu}]$$

or
$$\sum_{j=1}^{N} \sigma_{vj}^2 = N \qquad (3.3.23)$$

The above relationship can be applied to (3.3.22) and the total system mean-square error can then be expressed in relation with the n retained transform coefficients.

$$\epsilon_{TD}^2 = 1 - \frac{1}{N} \sum_{j=1}^{n} \sigma_{vj}^2 + \frac{1}{N} \sum_{j=1}^{n} \sigma_{qj}^2$$

$$+ \frac{1}{NN} \sum_{i=1}^{N} \sum_{j=1}^{n} \sum_{k=0}^{M} A_j^{2k} E\{\epsilon^2(i-k,j)\} \qquad (3.3.24)$$

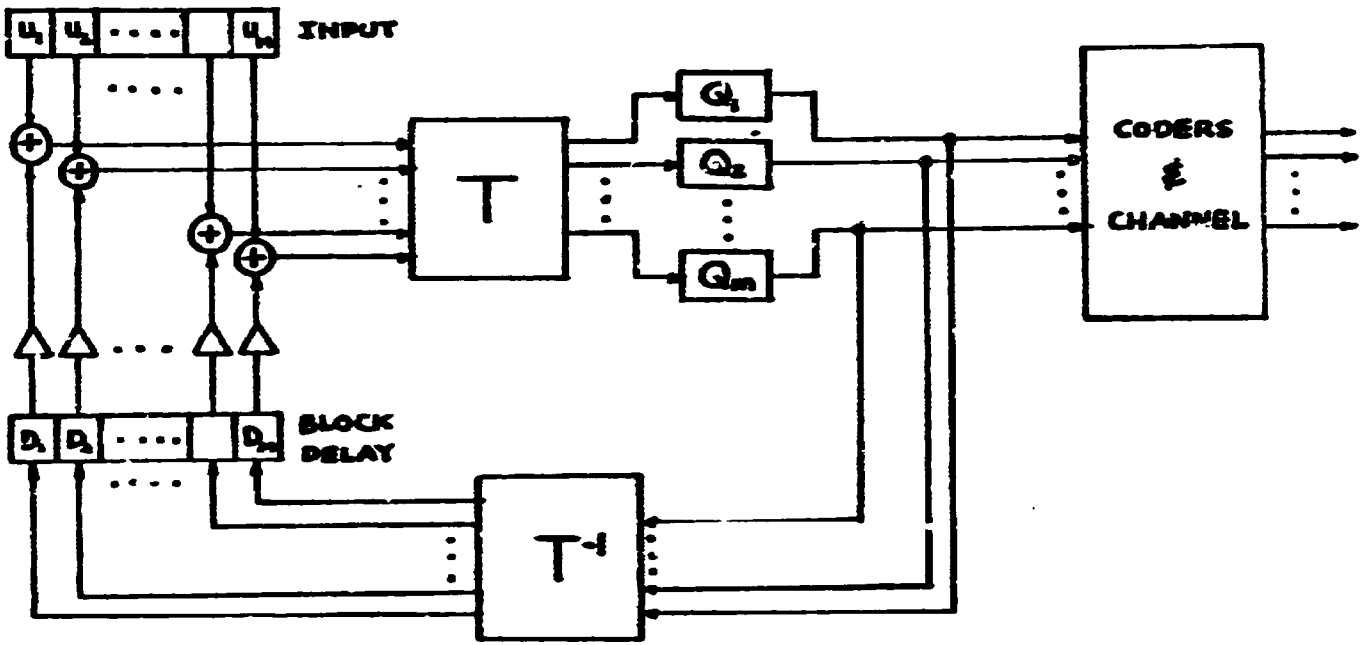

Fig. 3.3.4. DPCM-Transform Transmitter.

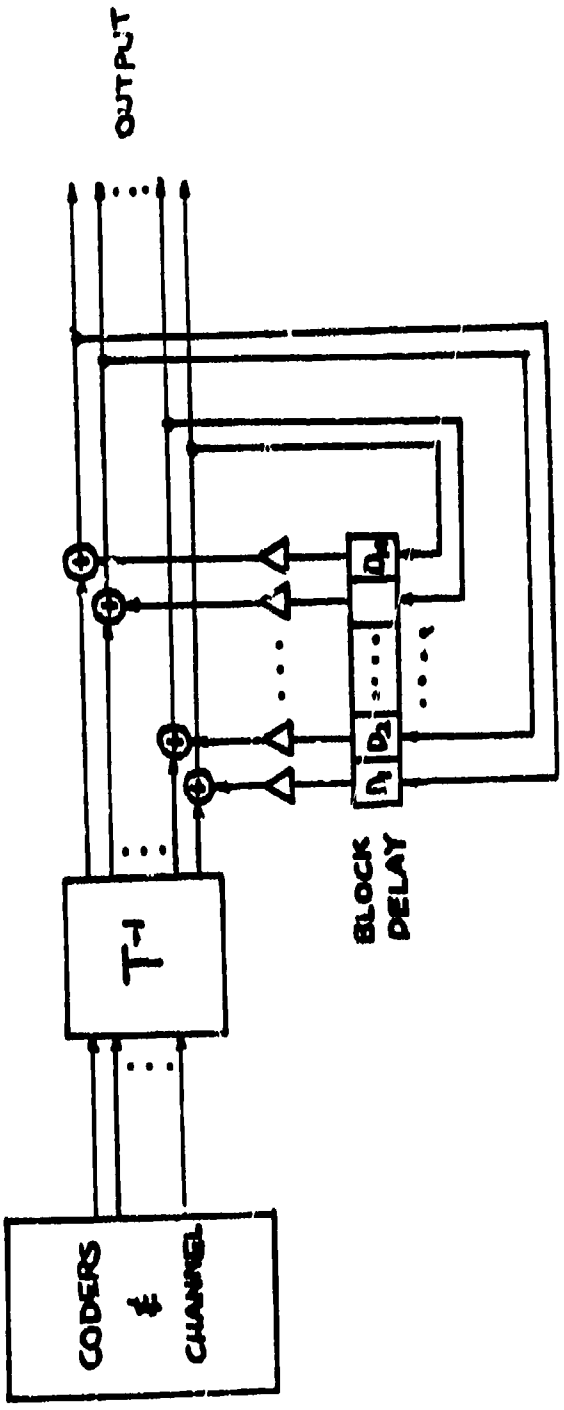

Fig. 3.3.4 cont. DPCM-Transform Receiver

3.3.8 The DPCM-Transform System

To complete the last of all possible combinations of one-dimensional techniques emphasizing on the decorrelating of multidimensionally-correlated data, we propose the DPCM-Transform hybrid coding system as illustrated in Fig. 3.3.4.

As the designation implies, the DPCM-Transform system employs at the transmitter and the receiver, one-dimensional orthogonal transformation of the differences or errors between the image sample values and their corresponding estimates. The transformed differences are then quantized and coded for transmission. A reverse process at the receiver end reconstructs the image samples within an acceptable limit of degradation. A simplified block diagram of the DPCM-Transform coding system is shown in Fig. 3.3.5.

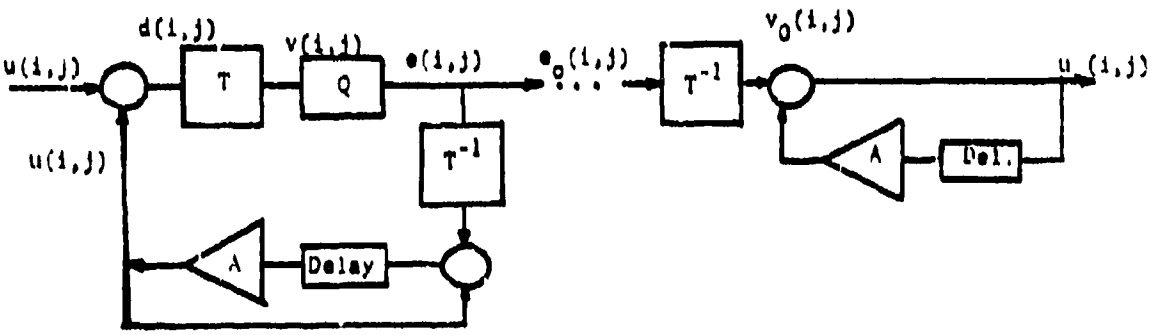

Fig. 3.3.5. Simplified Block Diagram of the DPCM-Transform Coding System.

The DPCM-Transform system is basically a modified one-dimensional DPCM coder in which one-dimensional orthogonal transformation processes are incorporated to further exploit the directional correlation of input image which cannot be completely removed by the one-dimensional DPCM process alone.

In the following discussion, the system operation is briefly outlined assuming that, without loss of generality, the DPCM process operates on columns of image matrix (i.e. in the vertical direction) and the orthogonal transformation

on rows of the resulting DPCM-difference samples. Referring to Fig. 3.3.4 an N-dimensioned image row vector $u_i = [u(i,1)...u(i,N)]$ is subtracted from its estimate given by $\hat{u}_i = [\hat{u}(i,1)...\hat{u}(i,N)]$ using N identical systems of delays, attenuators and comparators. The resulting image difference row vector $d_i = [d(i,1)...d(i,N)]$ is subjected to a one-dimensional orthogonal transformation process to produce a transform coefficient row $v_i = [v(i,1)...v(i,N)]$ whose elements of less significant information-content are discarded and those retained are quantized and coded for transmission. These coded coefficients which will be subsequently transmitted are also fed back through an inverse transformation process to produce an approximated version of the image vector u_i whose delayed values are attenuated to furnish the estimate row vector in the next DPCM-operation. The process is continued in this fashion along the vertical direction for all rows of the image sample matrix. In addition to the truncation error and the quantization error encountered at the transmitter, the coded transform coefficients which are transmitted to the receiver, in general, would be contaminated by noise in the transmission channel and their noisy versions are inversely transformed to reproduce an approximated difference vector $do_i = [d_o(i,1)...d_o(i,N)]$. The output row vector $u_{oi} = [u_o(i,1)...u_o(i,N)]$ which is the reconstructed version of the image data vector u_i is obtained by adding its estimate, which is also affected by noisy channel, to the difference vector d_o. Referring to Fig. 3.3.5, the transform coefficient of the difference sample can be expressed as

$$v(i,j) = \sum_{r=1}^{N} a(j,r)d(i,r) \qquad (3.3.25.a)$$

or inversely,

$$d(i,j) = \sum_{r=1}^{N} a(r,j)v(i,r) \qquad (3.3.25.b)$$

At the receiver the estimate $\hat{u}(i,j)$ can be expressed as

$$\hat{u}(i,j) = A\,[d'(i-1,j) + \hat{u}(i-1,j)] \qquad (3.3.26.a)$$

The sequence of estimated values are obtained from (3.3.26.a), i.e.

$$\hat{u}(i-1,j) = A\,[d'(i-2,j) + \hat{u}(i-2,j)]$$

$$\hat{u}(i-k,j) = A\,[d'(i-k-1,j) + \hat{u}(i-k-1,j)] \qquad (3.3.26.b)$$

or
$$\hat{u}(i,j) = \sum_{k=1}^{M} A^k\, d'(i-k,j) \qquad (3.3.27.a)$$

At the receiver the sequence of estimate values $\hat{u}_o(i,j)$ which are the approximate versions of $\hat{u}(i,j)$ can be similarly written as:

$$\hat{u}_o(i,j) = \sum_{k=1}^{M} A^k\, d_o(i-k,j) \qquad (3.3.27.b)$$

The approximations of the difference sample - $d'(i,j)$ and $d_o(i,j)$ - are one-dimensional transform coefficients of the transmitted signal sequence and the received signal sequence, respectively, i.e.

$$d'(i,j) = \sum_{r=1}^{n} \phi(r,j)\,[v(i,r) + q(i,r)] \qquad (3.3.28.a)$$

and
$$d_o(i,j) = \sum_{r=1}^{n} \phi(r,j)\,[v(i,r) + q(i,r) + c(i,r)] \qquad (3.3.28.b)$$

Using (3.3.25.b)

$$d'(i,j) = d(i,j) - \sum_{r'=1}^{N} \sum_{r=n+1}^{N} \phi(r,j)\phi(r,r')d(i,r') + \sum_{r=1}^{n} \phi(r,j)q(i,r) \qquad (3.3.28.c)$$

and
$$d_o(i,j) = d'(i,j) + \sum_{r=1}^{n} \phi(r,j)c(i,r) \qquad (3.3.28.d)$$

$q(i,j)$ and $c(i,j)$ being the quantization noise and the channel noise associated with the transmitted coefficient.

The coding error between the input image sample and its reconstructed version at the output, namely $\varepsilon(i,j)$, can be expressed in terms of the difference sample and its approximates using (3.3.27.a) and (3.3.27.b) as

$$\varepsilon(i,j) = u(i,j) - u_o(i,j)$$

$$\text{or} \qquad \varepsilon(i,j) = d(i,j) + \sum_{k=1}^{M} A^k d'(i-k,j) - \sum_{k=0}^{M} A^k d_o(i-k,j) \qquad (3.3.29)$$

From (3.3.28.a), (3.3.28.c) and (3.3.25.b) we have

$$\varepsilon(i,j) = \sum_{r=n+1}^{N} \phi(r,j)v(i,r) - \sum_{r=1}^{n} \phi(r,j)q(i,r) - \sum_{r=1}^{n}\sum_{k=0}^{M} A^k\phi(r,j)c(i-k,j) \qquad (3.3.20)$$

And the total system mean-square coding error is

$$\varepsilon_{DT}^2 = \frac{1}{MN} \sum_{i=1}^{M}\sum_{j=1}^{N} E\{\varepsilon^2(i,j)\} \qquad (3.3.31)$$

Restricting ourselves to the approximations of uncorrelatedness discussed in the preceding section, the system mean-square error can now be readily obtained using (3.3.30)

$$\varepsilon_{DT}^2 = \frac{1}{MN} \sum_{i=1}^{M}\sum_{j=1}^{N}\sum_{r=n+1}^{N}\sum_{r'=n+1}^{N} \phi(r,j)\phi(r',j)\, E\{v(i,r)v(i,r')\}$$

$$+ \frac{1}{MN} \sum_{i=1}^{M}\sum_{j=1}^{N}\sum_{r=1}^{n}\sum_{r'=1}^{n} \phi(r,j)\phi(r',j)\, E\{q(i,r)q(i,r')\}$$

$$+ \frac{1}{MN} \sum_{i=1}^{M}\sum_{j=1}^{N}\sum_{r=1}^{n}\sum_{r'=1}^{n}\sum_{k=0}^{M} A^{2k}\, \phi(r,j)\phi(r',j)\, E\{c(i-k,r)c(i-k,r')\} \qquad (3.3.32)$$

For orthogonal transformation, the basis vectors are orthonormal, i.e.

$$\sum_{j=1}^{N} \phi(r,j)\phi(r',j) = \delta_{rr'} \qquad (3.3.33)$$

$\delta_{rr'}$ being the Kronecker delta function.

Using (3.3.33), ϵ_{DT}^2 can be further simplified as:

$$\epsilon_{DT}^2 = \frac{1}{MN} \sum_{i=1}^{M} \sum_{j=n+1}^{N} E\{v^2(i,j)\} + \frac{1}{MN} \sum_{i=1}^{M} \sum_{j=1}^{n} E\{q^2(i,j)\}$$

$$+ \frac{1}{MN} \sum_{i=1}^{N} \sum_{j=1}^{n} \sum_{k=0}^{M} A^{2k} E\{e^2(i-k,j)\} \qquad (3.3.34)$$

The first term in (3.3.34) is the error incurred due to the truncating operation in which only n lower-sequency coefficients are retained for further processing.

In the analysis that follows, we attempt to derive an analytical expression for the truncation error, designated by ϵ_t^2, in terms of the image correlation functions. For convenience, the matrix notation will be used.

The difference sample vector $d_i = u_i - \hat{u}_i$ can be written as:

$$d_i = u_i - Au_{i-1} + A(d_{i-1} - d'_{i-1}) \qquad (3.3.35)$$

Since $\hat{u}_i = A(\hat{u}_{i-1} + d'_{i-1})$

and $$\hat{u}_{i-1} = u_{i-1} - d_{i-1} \qquad (3.3.36)$$

Rewriting equation (3.3.28.c) in matrix form, we have

$$d'^T_i = d_i^T - T^{-1} W_n^c T d_i^T + T^{-1} q_i^T \qquad (3.3.37)$$

where q_i is the quantization noise vector associated with the truncated coefficient vector of v_i, elements of q_i corresponding to the discarded coefficients having zero-values, i.e. $q(i,j) = 0$ for $j = n+1, \ldots N$. The matrix W_n represents the truncation process as defined in section 3.2.

Using (3.3.37) in (3.3.35) we have

$$d_i = u_i - Au_{i-1} + A(d_{i-1}T^{-1}W_n^cT - q_{i-1}{}^T) \qquad (3.3.38.a)$$

Since $T^{-1} = T^T$ and $(T^{-1}W_n^cT)^T = T^{-1}W_n^cT$.

The sequence of difference vectors d_i can be obtained from (3.3.38.a) as

$$d_{i-1} = u_{i-1} - Au_{i-2} + A(d_{i-2}T^{-1}W_n^cT - q_{i-2}{}^T) \qquad (3.3.38.b)$$

$$d_{i-k} = u_{i-k} - Au_{i-k-1} + A(d_{i-k-1}T^{-1}W_n^cT - q_{i-k-1}{}^T) \qquad (3.3.38.c)$$

or:

$$d_i = \sum_{k=0}^{M} A^k (u_{i-k} - Au_{i-k-1} - Aq_{i-k-1}{}^T)(T^{-1}W_n^cT)^k \qquad (3.3.39)$$

Note that $T^{-1}W_n^cT$ is an idempotent matrix, i.e.

$$(T^{-1}W_n^cT)^k = T^{-1}W_n^cT \quad , \qquad k > 0 \qquad (3.3.40)$$

In matrix form, the truncation error in (3.3.34) can be rewritten as:

$$\epsilon_t^2 = \frac{1}{MN} \sum_{i=1}^{M} \sum_{j=n+1}^{N} [E\,(v_i{}^T v_i)]_{jj} \qquad (3.3.41)$$

where $[F]_{jj}$ denotes the j^{th} diagonal element of matrix F.

The accumulative sum of variances of the discarded coefficients which constitutes the truncation error described by the summation $\sum_{j=n+1}^{N} [E\,(v_i{}^T v_i)]_{jj}$ can also be equivalently expressed by $\sum_{j=1}^{N} [W_n^c\, E\,(v^T v_i)\, W_n^c]_{jj}$ which is the trace of matrix $W_n^c\, E\,(v_i{}^T v_i)\, W_n^c$ since the first n lower-order diagonal elements of the matrix $W_n^c\, E\,(v_i{}^T v_i)\, W_n^c$ are, the result of the truncating process, identically zero.

Furthermore, since orthogonal transformations preserve the trace of the transformed matrix, the truncation error ϵ_t^2 can be equally obtained by

$$\epsilon_t^2 = \frac{1}{MN} \sum_{i=1}^{M} \sum_{j=1}^{N} [T^{-1}W_n^cT\, E\,(d_i{}^T d_i)\, T^{-1}W_n^cT]_{jj} \qquad (3.3.42)$$

Since $v_i^T = Td_i^T$ and $T^T = T^{-1}$,

$$\text{Let} \qquad Q = (T^{-1}W_n^c T)\, E\,(d_i^T d_i)\, (T^{-1}W_n^c T) \tag{3.3.43}$$

Substituting (3.3.39) into (3.3.43) we have

$$Q = \sum_{k=0}^{M}\sum_{k'=0}^{M} A^{k+k'}\,(T^{-1}W_n^c T)\,E\,\{(u_{i-k}-Au_{i-k-1})^T(u_{i-k'}-Au_{i-k'-1})\}\,(T^{-1}W_n^c T)$$

$$+ \sum_{k=0}^{M}\sum_{k'=0}^{M} A^{k+k'+2}\,(T^{-1}W_n^c T)\,T^T E\,(q_{i-k'-1}^T q_{i-k'-1})\,T\,(T^{-1}W_n^c T) \tag{3.3.44}$$

Note that $TT^T = TT^{-1} = I$ and $W_n^c E\,(q_{i-k-1}^T q_{i-k'-1})\,W_n^c = 0$ resulting from the characteristic of quantization noise vector q_i previously defined. The second term in (3.3.44) can be eliminated.

Recall that, for real stationary random variable u(i,j) generated from a directionally-seperable first-order Markov process

$$E\,\{u(i,j)u(i',j')\} = \rho_y^{|i-i'|}\,\rho_x^{|j-j'|} \tag{3.3.45.a}$$

as in matrix form

$$E\,(u_i^T u_i) = \rho_y^{|i-i'|}\,C_{xu} \tag{3.3.45.b}$$

where C_{xu} is the Toëplitz matrix of row correlation coefficient ρ_x, i.e.

$$C_{xu} = \begin{bmatrix} 1 & \rho_x & \cdots & \rho_x^{N-1} \\ \vdots & & & \vdots \\ \rho_x^{N-1} & & \cdots & 1 \end{bmatrix} \tag{3.3.45.c}$$

Using (3.3.45.b) we have:

$$E\,\{(u_{i-k} - Au_{i-k-1})^T (u_{i-k'} - Au_{i-k'-1})\} = a_{kk'}(A,\rho_y)\,C_{xu}$$

where $a_{kk'}(A,\rho_y) = (1 + A^2)\,\rho_y^{|k-k'|} - A(\rho_y^{|k-k'-1|} + \rho_y^{|k-k'+1|})$ (3.3.46.a)

In the particular case when optimum prediction coefficient is used, i.e. $A = \rho_y$, the coefficient $a_{kk'}(A,\rho_y)$ becomes

$$a_{kk'}(A,\rho_y) = a_{kk'}(\rho_y,\rho_y) = (1-\rho_y^2)\,\delta_{kk'} \qquad (3.3.46.b)$$

Substituting (3.3.46.a) into (3.3.44) we have, in the general case:

$$Q = \sum_{k=0}^{M}\sum_{k'=0}^{M} A^{k+k'}\, a_{kk'}(A,\rho_y)\, T^{-1}W_n^c T C_{xu} T^{-1} W_n^c T \qquad (3.3.47)$$

let $C_{xz} \triangleq [r(i,j)] = TC_{xu}T^{-1}$ be the transformed covariance matrix. The truncation error in (3.3.42) can then be expressed in terms of image correlations ρ_x and ρ_y:

$$\varepsilon_t^2 = \left[\sum_{k=0}^{M}\sum_{k'=0}^{M} a_{kk'}(A,\rho_y)A^{k+k}\right]\left[1 - \frac{1}{N}\sum_{j=1}^{n} z_x(j,j)\right] \qquad (3.3.48)$$

let: $$\beta(A,\rho_y) \equiv \sum_{k=0}^{M}\sum_{k'=0}^{M} a_{kk'}(A,\rho_y)\, A^{k+k'} \qquad (3.3.49)$$

When optimum prediction is used, i.e. $A = \rho_y$, (3.3.46.b) applies and the truncation error coefficient $\beta(A,\rho_y)$ becomes

$$\beta(\rho_y,\rho_y) = (1-\rho_y^2)\sum_{k=0}^{M}\rho_y^{2k} \qquad (3.3.50.a)$$

When M is sufficiently large, $\beta(\rho_y,\rho_y)$ approaches unity.

Since $$\sum_{k=0}^{M}\rho_y^{2k} = \frac{1}{1-\rho_y^2} \text{ for } M \to \infty \qquad (3.3.50.b)$$

and the truncation error would be

$$\varepsilon_{t\,opt}^2 = 1 - \frac{1}{N}\sum_{i=1}^{n} z_x(j,j) \qquad (3.3.51)$$

which would be the error experienced if the image sample, instead of the difference sample, were to be directly transformed. In this sense, it is compatible and

numerically equivalent to its counterpart in the Transform-DPCM system as expressed in (3.3.19). Thus the coefficient $\beta(A,\rho_y)$ as defined in (3.3.49) could be interpreted as a measurement of inferiority resulting from deviating from the optimum condition, in the least mean-square prediction error sense.

The coefficient $\beta(A,\rho_y)$ can be expressed in closed form in what follows. Recall from (3.3.46.a) that

$$a_{kk'}(A,\rho_y) = a_{kk'}(A,\rho_y) = (1+A^2)\rho_y^{|k-k'|} - A(\rho_y^{|k-k'+1|}+\rho_y^{|k-k'-1|})$$

$$\text{or} \qquad a_{k-k'}(A,\rho_y) = \begin{cases} 1+A^2-2A\rho_y & , \ k=k' \\ (\rho_y-A)\rho_y^{|k-k'|-1} & , \ k\neq k' \end{cases} \qquad (3.3.52)$$

$$\text{let} \qquad S(A,\rho_y) = \sum_{k=0}^{\infty}\sum_{k'=0}^{\infty} a_{k-k'}(A,\rho_y)A^{k+k'} \qquad (3.3.53.a)$$

$$\text{then for sufficiently large } N \quad \beta(A,\rho_y) \simeq S(A,\rho_y) \qquad (3.3.53.b)$$

$S(A,\rho_y)$ can be written as:

$$S(A,\rho_y) = \underbrace{\sum_{k=0}^{\infty}(1+A^2-2A\rho_y)A^{2k}}_{\text{for } k=k'} + \underbrace{2\sum_{k=0}^{\infty}\sum_{k'=k+1}^{\infty}(\rho_y-A)\rho_y^{|k-k'|-1}A^{k+k'}}_{\text{for } k\neq k'} \qquad (3.3.54)$$

Using (3.3.50.b) and let $w = k'-k$, we have

$$S(A,\rho_y) = \frac{1+A^2-2A\rho_y}{1-A^2} + 2(\rho_y-A)\sum_{k=0}^{\infty}\sum_{w=1}^{\infty}\rho_y^{w-1}A^{2k+w} \qquad (3.3.55)$$

We can observe that in the second term of (3.3.55)

$$\sum_{k=0}^{\infty}\sum_{w=1}^{\infty}\rho_y^{w-1}A^{2k+w} = \sum_{k=0}^{\infty}A^{2k}\ A\sum_{w=0}^{\infty}A^w\rho^w$$

hence:

$$\beta(A,\rho_y) = S(A,\rho_y) = \frac{1+A^2-2A\rho_x}{1-A^2} + \frac{2A(\rho_x-A)}{(1-A^2)(1-A\rho_y)} \qquad (3.3.56)$$

and when A is closed to ρ_y, the first term in (3.3.56) approaches unity while the second term vanishes.

To conclude, the system total mean-square error ϵ^2_{DT} in (3.3.34) can also be generally expressed as

$$\epsilon^2_{DT} = \beta(A,\rho_y)\left(1 - \frac{1}{N}\sum_{j=1}^{n} z_x(j,j)\right) + \frac{1}{N}\sum_{j=1}^{n}\sigma^2_{qj}$$

$$+ \frac{1}{NN}\sum_{i=1}^{M}\sum_{j=1}^{n}\sum_{k=0}^{M} A^{2k}\, R\,(\epsilon^2(i-k,j)) \qquad (3.3.57)$$

C Comparison of the Transform-DPCM and the DPCM-Transform Techniques

For simplicity, we consider the optimum case in which the one-dimensional transformation process is done using Karhunen-Loève transformation and the optimum feedback coefficient is used in the DPCM system. When the transmission channel is noiseless, the total system mean-square errors for both hybrid coding systems are given by

$$\epsilon^2_{TD} = \epsilon^2_{DT} = 1 - \frac{1}{N}\sum_{j=1}^{n}\lambda_{xj} + \frac{1}{N}\sum_{j=1}^{n}\sigma^2_{qj} \qquad (3.3.58)$$

where λ_{xj} is the j^{th} eigenvalue of the Toeplitz covariance matrix of the original image in the horizontal direction, and σ^2_{qj} the variance of the quantization noise associated with the j^{th} transmitted coefficient which is the difference of transform coefficients in the Transform-DPCM system or the transformed of difference of input sample in the DPCM-Transform system. It can be shown that the input sample to the quantizer which is transmitted to the receiver for both hybrid systems are identical regardless of the order in which the DPCM and the

transformation are done. Thus the error encountered would be identical, assuming optimum conditions, for both systems and they could be considered equivalent in the mean-square error sense.

The complexities involved in implementing the hybrid systems would be less favorable for the DPCM-Transform system since it employs an additional inverse transform process in the feedback loop of the transmitter. However, the prediction coefficients A used in the DPCM-Transform system are identical, theoretically or practically, since it is the correlation of the input sample while in the other system, these coefficients are generally different since in reality, correlations for transform coefficients of different-sequency would not be exactly alike due to the effect of the preceding one-dimensional transformation process as discussed in previous sections. Let s(i,j) be the input sample to the j^{th} quantizer in both systems, the optimum DPCM process in the vertical direction yields

$$\sigma_s^2 = (1-\rho_y^2)\,\lambda_{xj} \tag{3.3.59}$$

assuming that the Karhunen-Loève (optimum) transformation is also employed.

Studies of quantization noise have shown that

$$\sigma_q^2 = K(B_j)\,\sigma_s^2 \tag{3.3.60}$$

where $K(B_j)$ is the quantization error of a variate with a unity variance in a quantizer with 2^{Bj} levels.

When the quantization process is finely done, i.e. $B_j > 1$, $K(B_j)$ may be closely approximated by [60]

$$K(B_j) = b \exp(-aB_j) \tag{3.3.61}$$

where $b = 20$

and $a = 0.5 \ln 10$

The bit assignment B_j is obtained by:

$$B_j = \frac{M_b}{n} + \frac{1}{a}\left[\ln \sigma_s^2 - \frac{1}{n}\sum_{i=1}^{n} \ln \sigma_s^2\right] \qquad (3.3.62.a)$$

with the constraint

$$\sum_{j=1}^{n} B_j = M_b \qquad (3.3.62.b)$$

M_b being the total number of bits assigned to one block of transmitted coefficients.

Thus, the total system mean-square error of both hybrid coding systems, designated by ϵ^2_{Hybrid}, can now be expressed by

$$\epsilon^2_{Hybrid} = 1 - \frac{1}{N}\sum_{j=1}^{n} \left(1-b(1-\rho_y^2)\exp(-aB_j)\right)\lambda_{xj} \qquad (3.3.63)$$

The total system signal-to-noise ratios, which is defined as SNR = $10 \log_{10}(1/\epsilon^2_{Hybrid})$, in the particular case of noiseless channel given by (3.3.63) is presented in Fig. 3.3.6 for various bit rates. The graph was obtained using $\rho_x = 0.9469$ and $\rho_y = 0.8798$ for various transformation processes on blocks of size 32.

Fig. 3.3.7 shows the effect on system performance using different block sizes. It can be seen that the improvement is negligible using larger block size which involves more computational complexity.

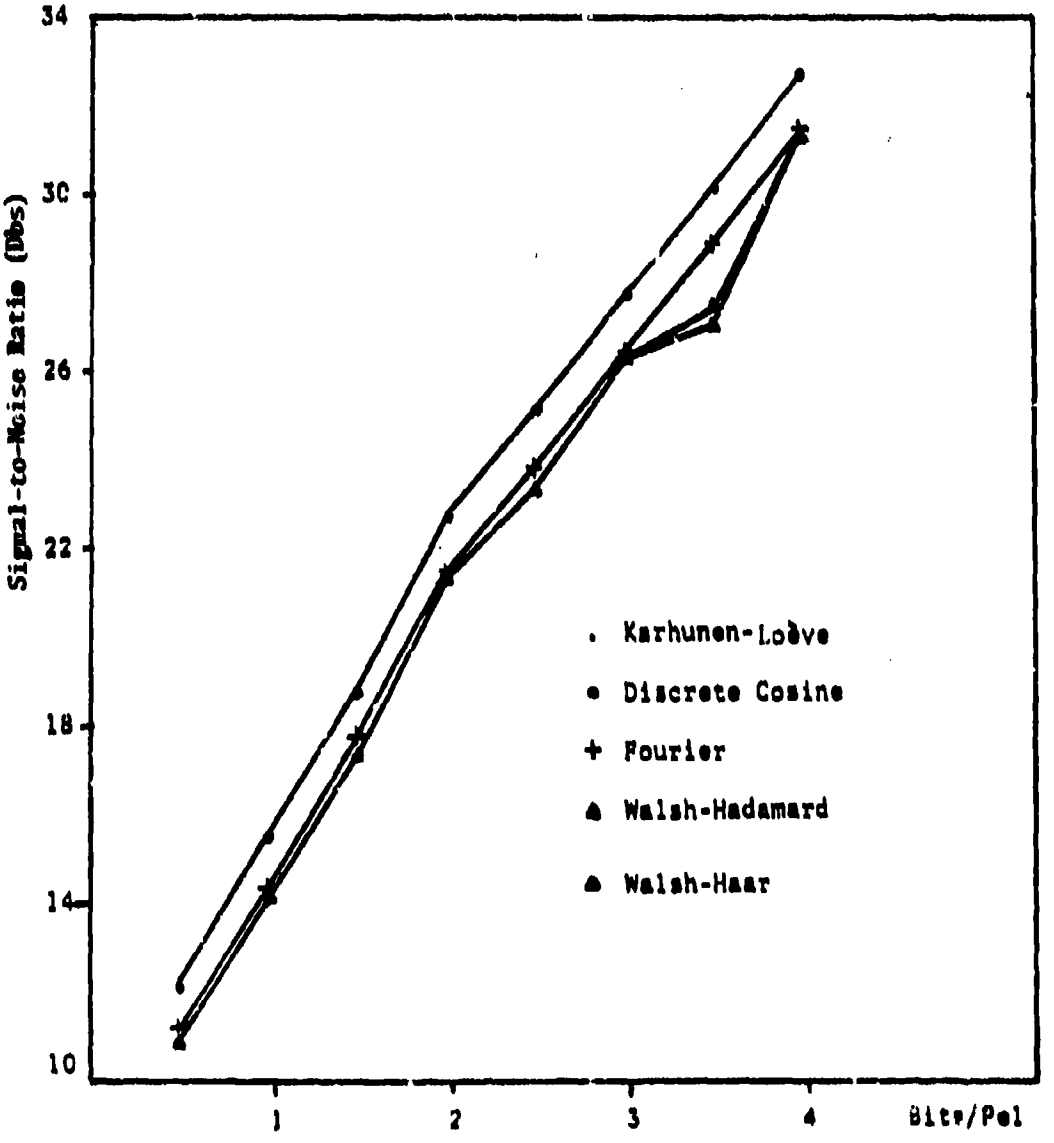

Fig. 3.3.6 Hybrid Coding System(ρ_x=0.9469, ρ_y= 0.8798) ; N=32, Signal-to-Noise Ratio Vs: Bit Rate.

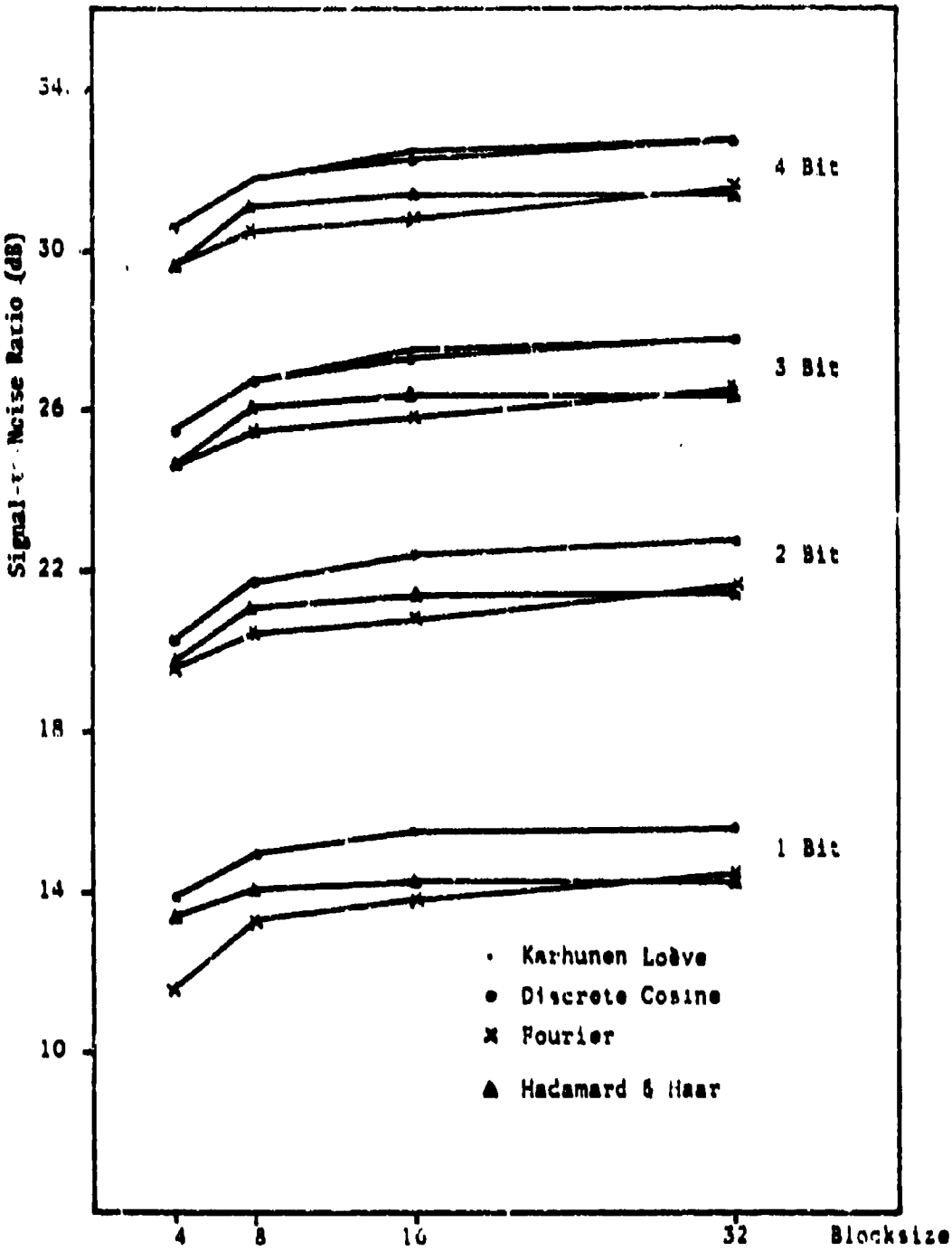

Fig. 3.3.7. Hybrid Coding(ρ_x=0.9409, ρ_y=0.8798)

3.4 Hybrid Coding in Noisy Channel

The theoretical analysis of the Hybrid Coding system performances in previous sections indicates that the total mean-square-error measure can be expressed as the sum of the truncation, the quantization and the channel errors, i.e.

$$\varepsilon_{Hybrid} = \varepsilon_t^2 + \varepsilon_q^2 + \varepsilon_c^2 \tag{3.4.1}$$

where

a) The truncation error

$$\varepsilon_t^2 = 1 - \frac{1}{N}\sum_{j=1}^{n}\sigma_{v_j}^2 \tag{3.4.2}$$

is a function the horizontal correlation ρ_x and the type of transformation chosen.

b) The quantization error

$$\varepsilon_q^2 = \frac{1}{N}\sum_{j=1}^{n}\sigma_{q_j}^2 \tag{3.4.3}$$

is obtained in the preceding section and can be expressed, in general, as

$$\varepsilon_q^2 = \frac{1}{N}\sum_{j=1}^{n} b(1-A_j^2 - 2A_j\rho_y)\exp(-aB_j)\sigma_{v_j}^2 \tag{3.4.4}$$

where in the Transform-DPCM system, the prediction coefficients A_j's are, in general, different due to the statistical difference of individual coefficient.

c) And the channel error

$$\varepsilon_c^2 = \frac{1}{N}\sum_{i=1}^{M}\sum_{j=1}^{n}\sum_{k=1}^{M} A_j^{2k} E\ c^2(i-k,j) \tag{3.4.5}$$

It has been shown that

$$\varepsilon_c^2 = \frac{1}{N}\sum_{j=1}^{n}\frac{1}{1-A_j^2}\Psi_{ch}(B_j, V_j) \tag{3.4.6}$$

where V_j is the jth quantizer level.

Essman and Wintz [158] have shown that if more than 3 bits are assigned and if each level V_j is sufficiently greater than the standard deviation of the quantizer input $\Psi_{ch}(B_j, v_j)$ is independent of B_j and V_j and can be approximated by

$$\Psi_{ch}(B_j, v_j) = \frac{21PE}{2}\sigma_{s_j}^2 \qquad (3.4.7)$$

where PE is the probability of channel error and $\sigma_{s_j}^2$ the variance of the jth quantizer input.

Thus, from (3.4.2), (3.4.4), (3.4.6) and (3.4.7) the total system mean-squared-error using transform-DPCM system can be expressed as

$$\epsilon_{TD}^2 = 1 - \frac{1}{N}\sum_{j=1}^{n}(1 - b(1 + A_j^2 - 2A_j\rho_y)\exp(-aB_j) + \frac{21PE}{2}(1 + A_j^2 - 2A_j\rho_y)/(1 - A_j^2))\sigma_{V_j}^2 \qquad (3.4.8)$$

Our optimization scheme is to minimize the total system mean-squared-error in (3.4.8) with respect to the employed predictor coefficients.

These optimum prediction coefficients are obtained by solving n 5th-order polynomials.

$$K_1(j)A_j^5 - \rho_y K_1(j)A_j^4 - 2K_1(j)A_j^3 + \rho_y(2K_1(j) - K_2)A_j^2 + (K_1(j) + 2K_2)A_j - \rho_y(K_1(j) + K_2) = 0; \quad \text{for } j = 1, 2, \cdots, n \qquad (3.4.9)$$

where $K_1(j) = b\exp(-aB_j)$

$K_2 = 21PE/2$

The optimum prediction coefficients thus obtained for each DPCM encoder is a function of B_j, the number of bits assigned to the transformed difference.

Fig. 3.6.1 shows the optimum prediction coefficients as functions of the bit

assignments for probabilities of channel errors of 0.001, 0.005 and 0.01.

To conclude, a theoretical comparison of various two-dimensional techniques described in this chapter is shown in Fig. 3.5.

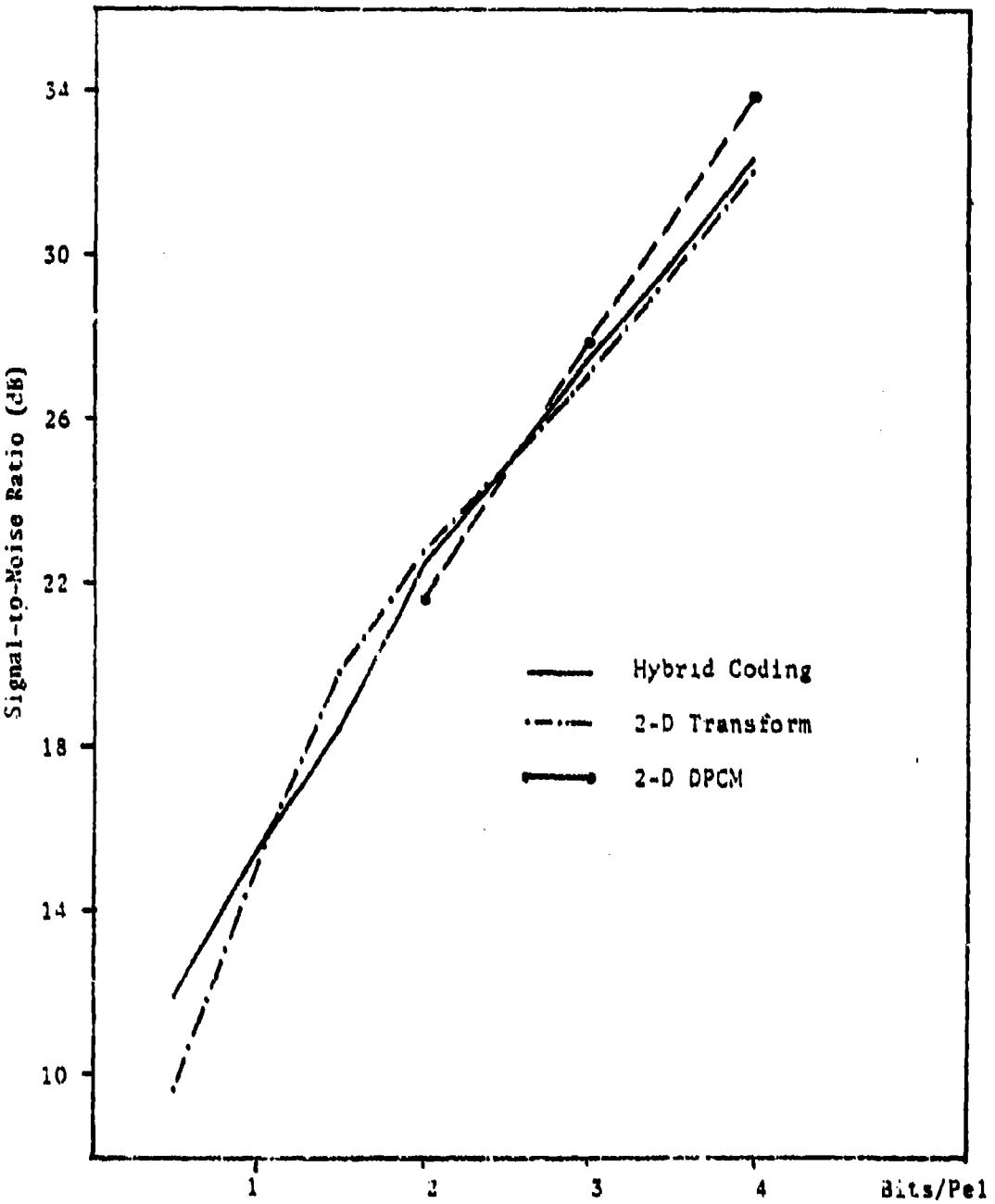

Fig. 3.5. Comparison of Two-Dimensional Coding Schemes, (Karhunen Loève ρ_x=0.9469, ρ_y=0.8798), N=16.

CHAPTER IV

SIMULATION RESULTS

4.1 Introduction

In this chapter simulation results using aerial photographs of the methods, except DPCM, described in Chapter III are given. Section 4.2 describes the pictures to be used in the investigations. Sections 4.3 and 4.4 give results using two-dimensional transform techniques (Hadamard, Discrete Cosine and Haar) and the Hybrid methods (Transform-DPCM and DPCM-Transform) respectively. In section 4.5 the effects of channel noise on the two-dimensional transform and the Hybrid coding schemes are investigated.

Processing of the pictures were performed using the IBM 360-44 Ohio University Computer.

One of the main disadvantages of differential encoding is its sensitivity to noise. Results of optimizing the Hybrid coding scheme in the presence of channel noise are given in Section 4.6.

4.2 Picture Statistics

The pictures used in the simulations consisted of six aerial reconnaissance type photographs supplied by WPAFB. Each picture consists of 512 picture elements per line and 512 lines. The intensity levels are represented by an integer number between 0 and 63, which is equivalent to six bits. Except for a limited number of experiments using all six pictures, the majority of the simulations were performed using the scenes of the Tank and the Truck shown in Figs. 4.2.5 and 4.2.6. Figs. 4.2.7-4.2.10 show original pictures of the remaining four pictures.

Histograms of the gray levels of the scenes of the Truck and the Tank are given in Figs. 4.2.1 and 4.2.2, respectively. Figs. 4.2.3 and 4.2.4 show the horizontal and

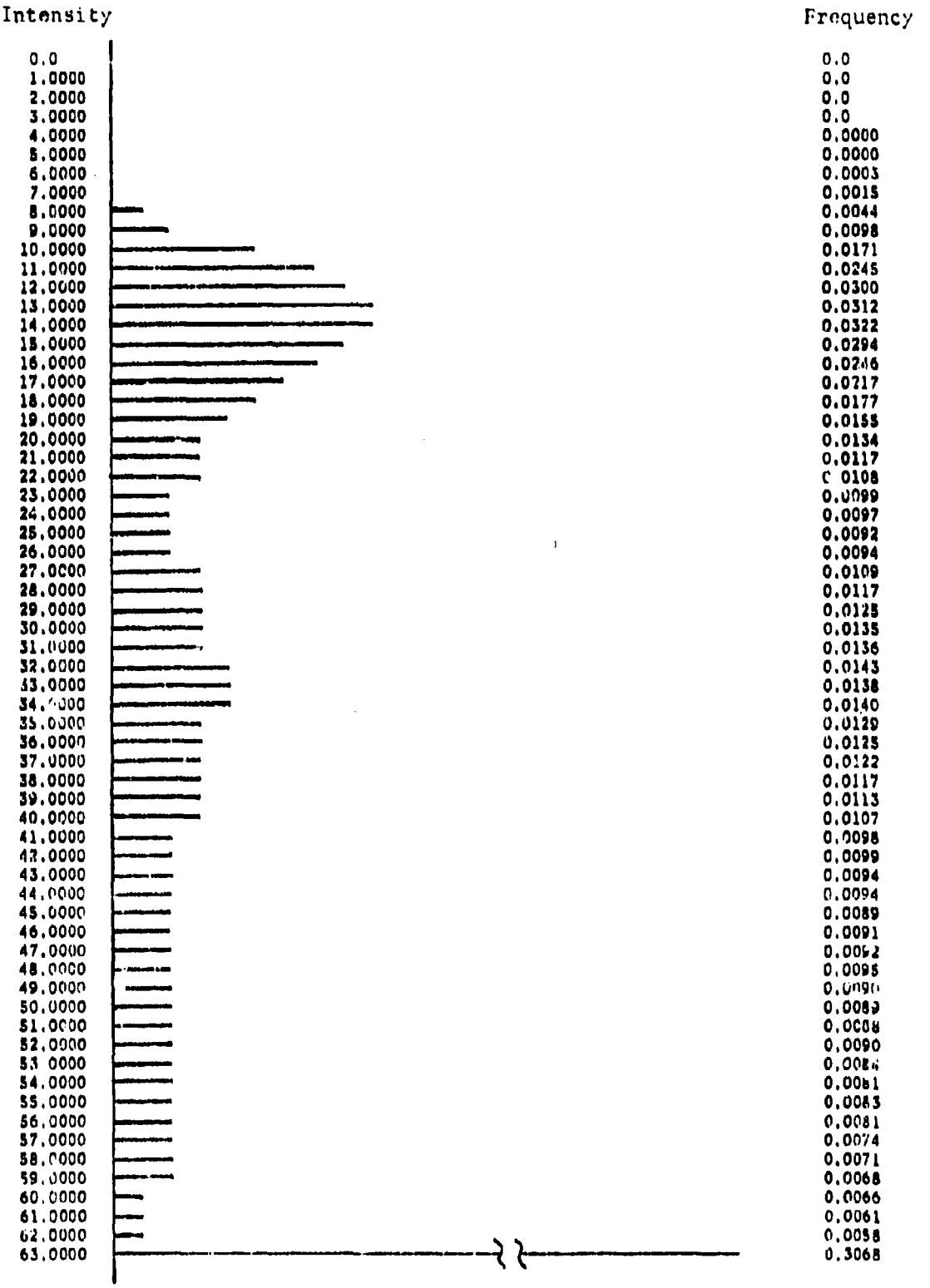

Fig. 4.2.1. Histogram of Intensity Levels - Truck

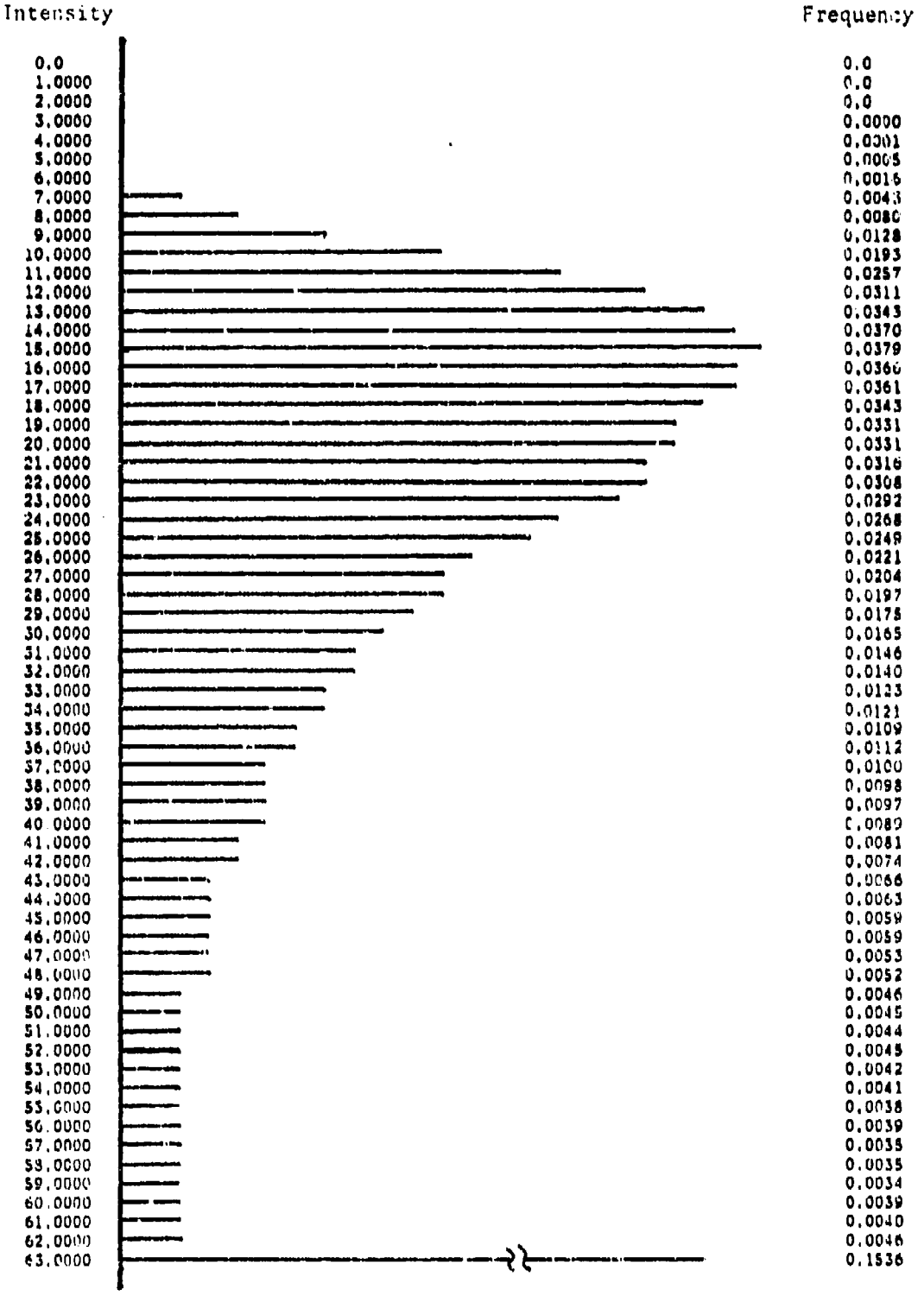

Fig. 4.2.2. Histogram of Intensity Levels - Tank

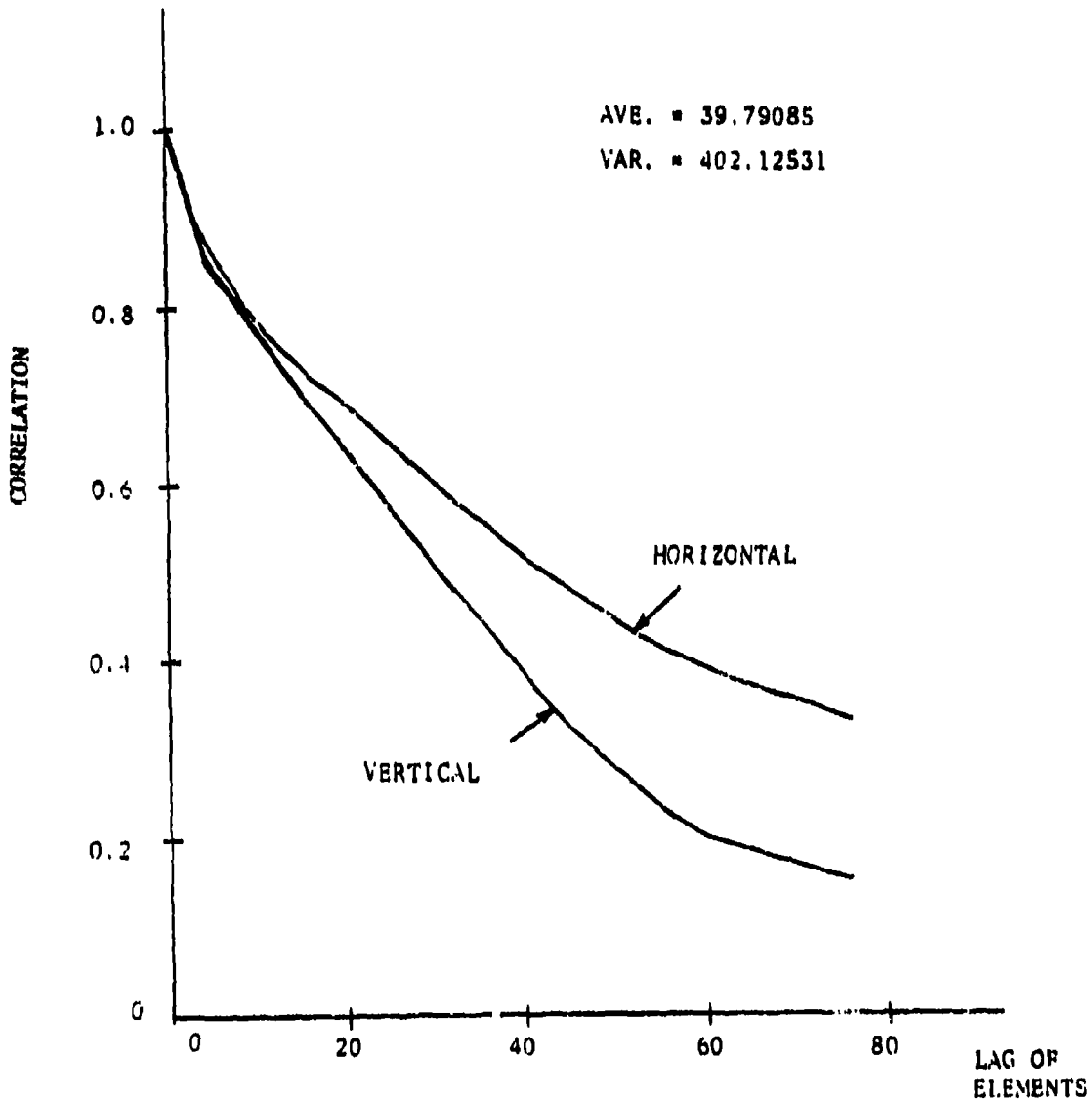

Fig. 4.2.3. Correlation of the Scene of the Truck on the Bridge.

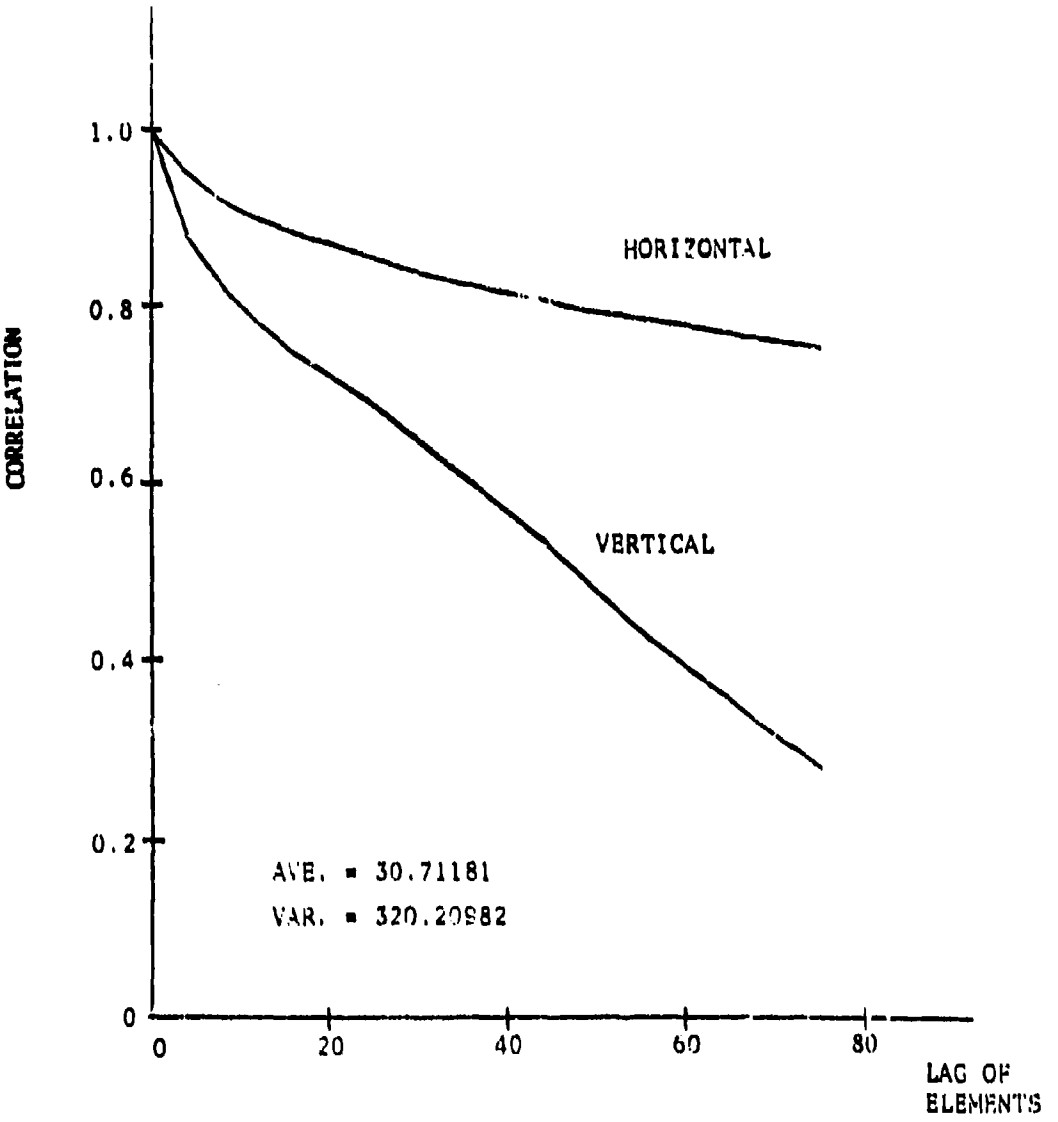

Fig. 4.2.4. Correlation of PCA Signals
(Picture: "Tank")

4.2.5 Original Picture of Tank

4.2.6 Original Picture of Truck

4.4.7 Original Picture of Trees

4.2.8 Original Picture of Fields

4.2.9 Original Picture of Roads

4.2.10 Original Picture of Coast

vertical correlations for the scenes of the Truck and the Tank . These figures indicate that the horizontal correlation is much higher than the vertical correlation. Such characteristics will be useful in designing the Hybrid coding systems described in Section 4.4. The important statistical characteristics are given in Table 4.2.1.

Picture #	Scene	Average	Variance	Vertical Correlation
1	Tank	30.71181	320.20982	0.95531
2	Truck	39.79085	402.12531	0.94434
3	Trees	20.22319	408.4589	0.96897
4	Fields	22.85955	204.5677	0.90949
5	Roads	20.04826	352.5544	0.96470
6	Coast	33.86632	372.5037	0.94476

Table 4.2.1. Statistical Properties of the Pictures.

4.3 Two-Dimensional Transform Simulation Results (Noiseless Channel)

Several two-dimensional transform techniques were investigated. Simulation results have been obtained for the Hadamard, the Discrete Cosine and the Haar transformation. Tables 4.3.1a, 4.3.1b and 4.3.1c give the variances of the two-dimensional transform coefficients using the Discrete Cosine, Walsh Hadamard and Walsh Haar transforms respectively for the scene of the Truck. Similar results are given in Table 4.3.2a, 4.3.2b and 4.3.2c for the scene of the Tank. The results given in these tables clearly indicate the redistribution of the information into the lower ordered

a

22272.75	559.24	161.36	95.23	48.49	31.78	21.83	19.86
845.68	126.06	54.69	31.66	21.07	15.81	13.37	11.16
344.18	69.58	44.29	26.71	17.79	14.41	12.38	9.97
127.40	43.67	33.49	22.85	16.50	13.81	11.19	10.20
78.80	32.69	24.56	19.07	13.78	12.73	10.95	10.15
48.09	23.12	18.02	15.80	12.95	10.95	10.00	9.28
34.54	18.68	16.14	13.09	11.16	9.85	9.85	8.96
33.85	15.69	14.38	10.99	10.21	9.03	9.14	8.34

b

22272.75	467.60	144.31	152.29	48.49	45.59	38.88	40.63
709.97	101.96	46.80	35.29	20.88	19.54	18.50	14.90
293.79	57.95	37.34	23.98	17.45	17.23	15.88	11.42
109.61	42.13	28.78	21.97	16.20	15.84	13.40	11.15
78.80	31.17	22.35	18.38	13.78	14.25	13.15	10.85
75.65	26.56	19.96	17.35	13.04	12.44	11.82	10.81
84.93	22.95	18.57	14.51	11.50	11.64	10.86	9.56
69.79	17.88	15.12	12.12	10.60	10.09	9.90	8.39

c

22272.75	467.60	125.62	170.98	41.10	39.69	52.28	40.53
709.97	101.96	40.65	41.44	19.10	18.18	18.09	18.45
245.05	47.89	29.18	27.73	14.69	14.89	14.08	14.57
248.35	52.19	27.84	29.31	15.25	15.27	15.59	14.21
92.20	24.48	16.96	17.22	11.73	10.96	10.23	11.92
80.07	24.03	17.70	17.17	11.45	11.96	10.94	11.14
74.08	25.05	17.37	16.83	11.99	12.40	11.40	11.81
62.82	24.98	17.44	17.67	10.79	10.71	11.23	12.01

Table 4.3.1a,b and c - Variances of Two-Dimensional Transform Coefficients (Picture "Truck") Blocksize 8 x 8"

a - Discrete Cosine
b - Walsh Hadamard
c - Walsh Haar

a

[illegible]	66.88	24.45	12.29	8.48	6.72	6.01	5.97
551.08	68.05	22.80	12.45	8.58	7.06	6.01	5.88
206.78	52.84	22.08	11.38	8.16	6.90	6.30	5.55
88.98	34.59	18.84	11.58	8.08	6.90	6.16	5.93
49.40	26.18	14.85	10.06	7.94	6.60	5.97	5.38
27.98	18.18	12.82	8.55	6.84	6.12	5.73	5.37
18.88	13.50	10.90	7.60	6.38	6.04	5.37	5.39
13.19	11.09	9.14	7.32	6.17	5.45	5.38	5.13

b

18793.47	80.11	22.04	23.16	8.48	8.34	8.42	9.26
481.84	55.24	20.76	17.22	8.57	8.90	8.44	8.12
179.48	41.68	19.31	15.14	8.02	7.98	8.01	6.80
123.94	31.49	16.14	13.05	7.92	7.97	7.50	6.62
49.40	23.68	13.70	11.01	7.84	7.45	7.12	6.08
45.15	18.44	12.26	9.29	7.10	6.60	6.64	5.89
46.18	16.50	11.14	8.78	6.52	6.52	6.20	5.80
30.30	12.03	8.99	7.33	5.07	6.12	6.16	5.33

c

18793.47	80.11	21.34	23.87	8.00	8.81	9.12	8.56
481.84	55.24	18.68	19.29	8.47	8.25	8.38	8.93
149.70	36.35	15.80	16.01	7.59	7.68	7.65	7.15
153.73	36.83	15.79	16.03	7.66	7.63	7.48	8.00
41.50	17.00	10.36	10.24	6.30	6.32	6.69	6.22
42.08	17.87	10.66	10.07	6.62	6.77	6.29	6.56
42.76	17.89	10.36	10.09	6.66	6.28	6.39	6.70
44.69	17.88	9.94	10.76	6.61	6.47	6.22	6.35

Table 4.3.2a,b and c. Variances of Two-Dimensional Transform Coefficients (Picture "Tank")
Blocksize 8 x 8

a - Discrete Cosine
b - Walsh Hadamard
c - Walsh Haar

coefficients which is necessary for data compression.

Clearly the most important coefficient is C_{11} which is the D-C level of the picture. Because of its importance, techniques for error-correcting coding for this coefficient will be discussed in Section 4.6.

Figs. 4.3.1 and 4.3.2 show the cumulative sum of variances for each of the pictures. In both cases a block size of 8 x 8 was used. Using these results one can determine amount of energy lost in truncating the coefficients.

Although it is known that mean-squared-error is not a satisfactory measure of the "goodness" of a picture in the subjective sense, it can be used as a rough quantitative measure for pictures processed using the same techniques. Its usefulness as a measure of "goodness" when comparing two different techniques of data compression is questionable. For these cases one would have to revert to subjective evaluations. In an effort to determine a useful quantitative error measure which agrees with subjective evaluations, several different error criteria which are listed below were calculated and used in some of the simulation results.

1) Normalized Mean-Squared-Error (MSE)

$$\bar{\varepsilon}_1^2 = \sum_{i=1}^{N} (f_i - g_i)^2 \; / \; \sum_{i=1}^{N} f_i^2$$

2) Normalized Mean-Derivative-Squared-Error (NDSE)

$$\bar{\varepsilon}_2^2 = \sum_{i=1}^{N} [(f_{i+1} - f_i) - (g_{i+1} - g_i)]^2 \; / \; \sum_{i=1}^{N} (f_{i+1} - f_i)^2$$

3) Normalized Mean-Absolute-Error (MAE)

$$\bar{\varepsilon}_3 = \sum_{i=1}^{N} |f_i - g_i| \; / \; \sum_{i=1}^{N} |f_i|$$

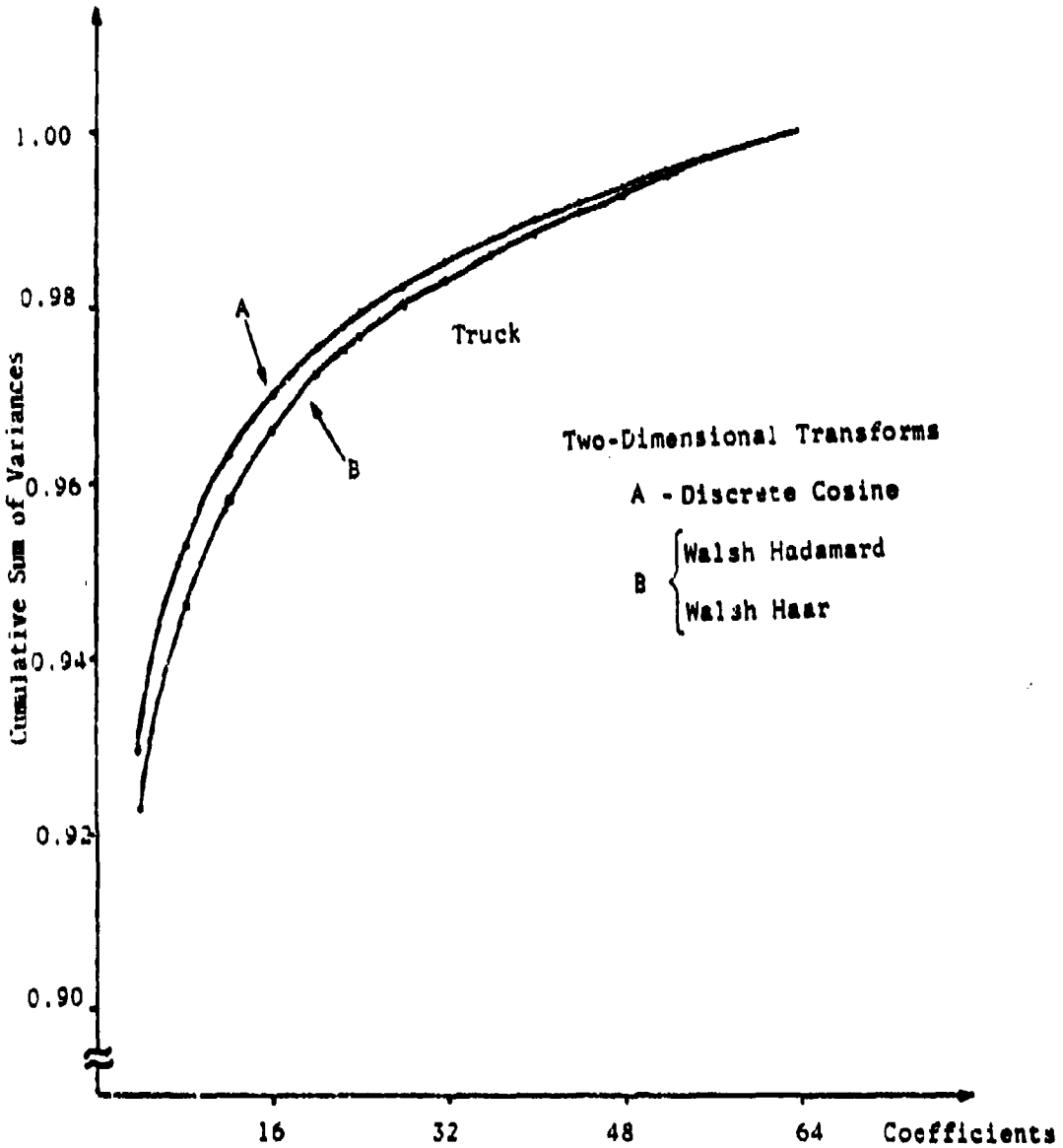

Fig. 4.3.1. Cumulative Sum of the Variances of the Transform Coefficients, Block Size = 8 x 8. (Truck)

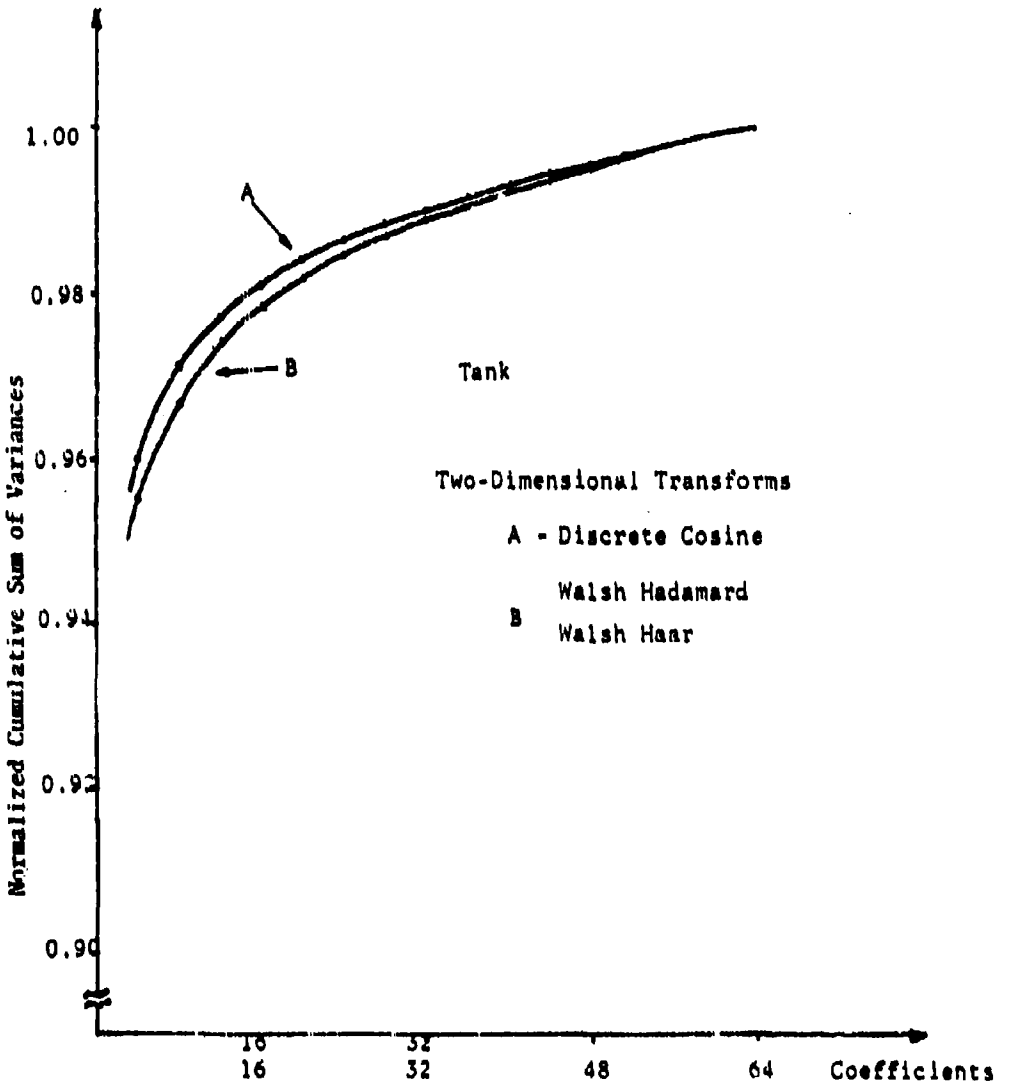

Fig.4.3.2. Cumulative Sum of the Variances of the Transform Coefficients, Block Size-8x8. (Tank)

where

f_i = original signal value.

g_i = approximate signal value.

The results obtained during the investigations indicated that perhaps the normalized-mean-derivative-squared-error (NDSE) would be more correlated with subjective evaluations rather than the MSE criterion. The premise behind this hypothesis is that the overall MSE measure does not indicate local distortions in regions where sharp contours exist; however, the NDSE would tend to emphasize distortions in regions containing sharp contours and high resolution.

The results using two-dimensional Hadamard, Haar and Discrete Cosine Transform for bit rates of 0.25, 0.5, 1.0 and 1.5 bits/pel are given in Table 4.3.3a,b,c for both the scene of the Truck and the Tank. These results indicate that the Discrete Cosine Transform performs superior to either the Haar or the Hadamard. Using MSE criterion one may order the transforms in the following order with respect to performance:

(1) Discrete Cosine

(2) Hadamard

(3) Haar,

the Hadamard and Haar being essentially equal in performance.

Results were obtained using several different bit assignments. Initially the bit assignment procedure described by Wintz and Kurtenbach [51] was used to assign bits. The algorithm specified by the authors is based on the log of the variance of the coefficients and is shown to be near optimum. In this procedure a total number of bits M_b is assumed such that

$$M_b = \sum_{j=1}^{n} B_j \qquad (4.3.1)$$

		Average Bit/Picture Element			
		0.25	0.50	1.0	1.50
"Truck"	Hadamard	0.103280	0.083081	0.043831	0.033530
	Haar	0.121353	0.076094	0.051375	0.040179
	Discrete Cosine		0.074704	0.039031	0.031982
"Tank"	Hadamard	0.059022	0.046464	0.023510	0.018536
	Haar	0.060894	0.047577	0.024624	0.020147
	Discrete Cosine		0.035128	0.020663	0.016661

Table 4.3.3a. Mean-Squared-Error Using Two-Dimensional Transforms.

		Average Bit/Picture Element			
		0.25	0.50	1.0	1.50
"Truck"	Hadamard	1.12427	1.03858	0.78083	0.50030
	Haar				
	Discrete Cosine		0.98963	0.69503	0.51607
"Tank"	Hadamard	1.20331	1.13386	0.86938	0.60979
	Haar				
	Discrete Cosine		1.02675	0.80725	0.56446

Table 4.3.3b Normalized-Derivative-Squared-Error Using Two-Dimensional Transforms.

		Average Bit/Picture Element			
		0.25	0.50	1.0	1.50
"Truck"	Hadamard	0.119495	0.109960	0.076998	0.063380
	Haar	0.132335	0.105232	0.086227	0.075051
	Discrete Cosine		0.104725	0.075518	0.067853
"Tank"	Hadamard	0.108461	0.093573	0.066251	0.056647
	Haar	0.111450	0.098104	0.069985	0.062761
	Discrete Cosine		0.083479	0.063816	0.057035

Table 4.3.3c Mean-Absolute-Error (MAE) Using Two-Dimensional Transforms.

where B_j is the bits assigned to coefficient c_j. Using Lagrange multipliers an equation for the bits for each coefficients is obtained, i.e.

$$B_j = \frac{M_b}{n} + \frac{2}{\ln 10} \left(\ln\sigma_j^2 - \frac{1}{n} \sum_{j=1}^{n} \ln\sigma_j^2\right). \qquad (4.3.2)$$

The values for B_j ($j = 1,2,3...n$) determined by (4.3.2) are next rounded to the nearest integer. It can be shown that $B_1 \geq B_2 \geq \ldots \geq B_n$ and should the assignment dictated by (4.3.2) not satisfy (4.3.1), some of the B_j are adjusted according to the following rules:

(1) If $M_b < \sum_{j=1}^{n} B_j$, take that B_j corresponding to the largest j such that $B_j > 1$ and replace it by $B_j + 1$.

(2) If $M_b < \sum_{j=1}^{n} B_j$, take that B_j corresponding to the smallest j such that $B_j = B_n$ and replace it by $B_1 + 1$.

The above procedures constitute a suboptimum algorithm which provides an unequal assignment of M_b bits to the n samples.

Table 4.3.4 indicates the bit assignments on the 64 transform coefficients using this procedure. Using this procedure, truncations of the transform coefficients are obtained by not assigning any bits to them. On real data such as the pictures used in this study, bit assignments giving better results than those shown in Table 4.3.3 are obtained. One such variation is to arbitrarily truncate the number of coefficients to 32 and then use the Wintz and Kurtenbach algorithm on these 32 coefficients. The MSE obtained using this modified scheme are given in Table 4.3.5 and the bit assignments for this case are given in Table 4.3.6. It is noted that a reduction by an order of magnitude in the MSE is obtained using this procedure. This is due

2-DIM HADAMARD-HAAR

6	3	1	1	1	1	1	1
3	1	1	1				
2	1	1					
1	1						
1	1						
1							
1							
1							

0.5 bits/pel

7	3	3	3	1	1	1	1
4	2	2	2	1	1	1	
3	2	1	1	1	1		
3	1	1	1				
2	1	1	1				
2	1	1	1				
2	1	1					
2	1						

1.0 bits/pel

7	4	3	3	2	2	2	2
4	3	2	2	1	1	1	1
3	2	1	1	1	1	1	1
3	2	1	1	1	1	1	1
2	1	1	1	1	1	1	1
2	1	1	1	1	1	1	1
2	1	1	1	1	1	1	1
2	1	1	1	1	1	1	

1.5 bits/pel

2-DIM DISCRETE COSINE

6	2	1	1	1	1		
4	1	1	1				
2	1	1	1				
2	1	1					
1	1						
1							
1							
1							

0.5 bits/pel

7	4	3	3	2	1	1	1
4	3	2	1	1	1		
3	2	1	1	1			
3	1	1	1	1			
2	1	1	1				
2	1	1	1				
1	1	1					
1	1						

1.0 bits/pel

7	4	3	3	2	1	1	1
5	3	2	2	1	1	1	1
4	2	2	1	1	1	1	1
3	2	1	1	1	1	1	1
2	1	1	1	1	1	1	1
2	1	1	1	1	1	1	1
1	1	1	1	1	1	1	1
1	1	1	1	1	1	1	1

1.5 bits/pel

Table 4.3.4. Bit Assignments

Bit Assignments	MSE	NDSE	MSE Using Wintz Kurtenbach Algorithm on 64 Coefficients
0.5 b/p	0.011993	0.017753	0.1
1.0 b/p	0.0057216	0.0085961	0.08
1.5 b/p	0.0032147	0.0048886	0.04

Table 4.3.5. Errors Using Modified Bit Assignments

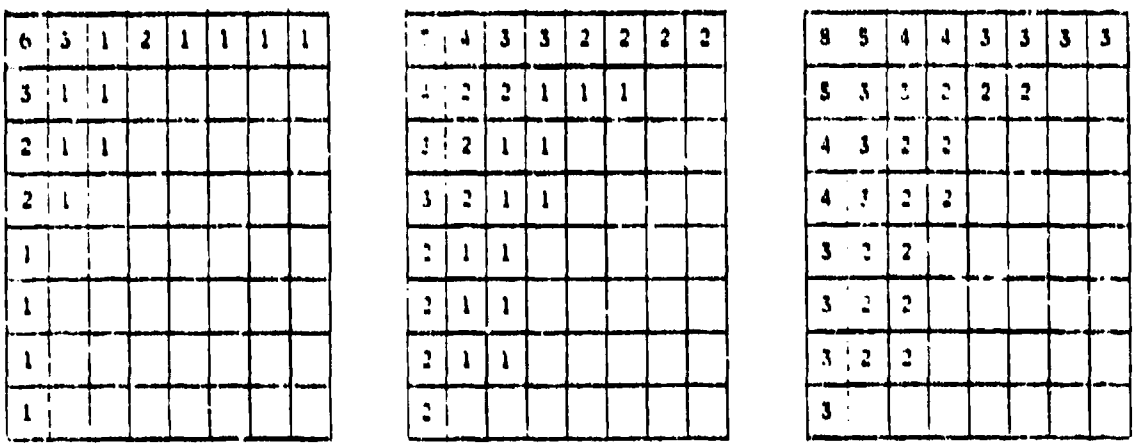

Table 4.3.6. Modified Bit Assignments

to the fact that using the algorithm on 64 samples (using an 8 x 8 block) a significant number of coefficients are kept and assigned only one bit which probably does little to improve the performance. On the other hand, when one first truncates the 64 coefficients to the 32 containing the highest information and then applies the bit assignment procedure, more bits are assigned to the coefficients containing the most information.

Figs. 4.3.4a,b,c,d and 4.3.5a,b,c show the results obtained using the two-dimensional Hadamard and the Discrete Cosine Transformations for the scene of the Truck. Results are shown for 0.25, 0.5, 1.0 and 1.5 bits/pel. Similar results for the scene of the Tank are given in Figs. 4.3.6a,b,c,d and 4.3.7a,b,c. Results are not given using the Haar Transform since the performance using this technique is essentially equivalent to the Hadamard. In all cases the qualities of the pictures obtained using the Discrete Cosine are superior to those obtained using the Hadamard; however, the computational requirements of the Discrete Cosine are more complicated than those of the Hadamard. The number of computations (additions) required for a two-dimensional Hadamard are $2N \log_2 N$, while for the two-dimensional Discrete Cosine the number of computations required are ($4N \log_2 N + 4 N$) multiplications and approximately the same number of additions as for the Hadamard transformation. Due to the complexity of the Discrete Cosine algorithm, the Hadamard transformation is preferred.

One may draw several other conclusions from the pictures shown in Figs. 4.3.4a,b,c,d; 4.3.5a,b,c; 4.3.6a,b,c,d and 4.3.7a,b,c. First, it is observed that even at extremely low bit rates (0.25 and 0.5 bits/pel) reasonable results are obtained. There is some loss of details; however, the results of 0.25 bits/pel are not significantly poorer than those obtained using 0.5 bits/pel. If one can withstand the amount of degradation shown in these figures using 0.25 or 0.5

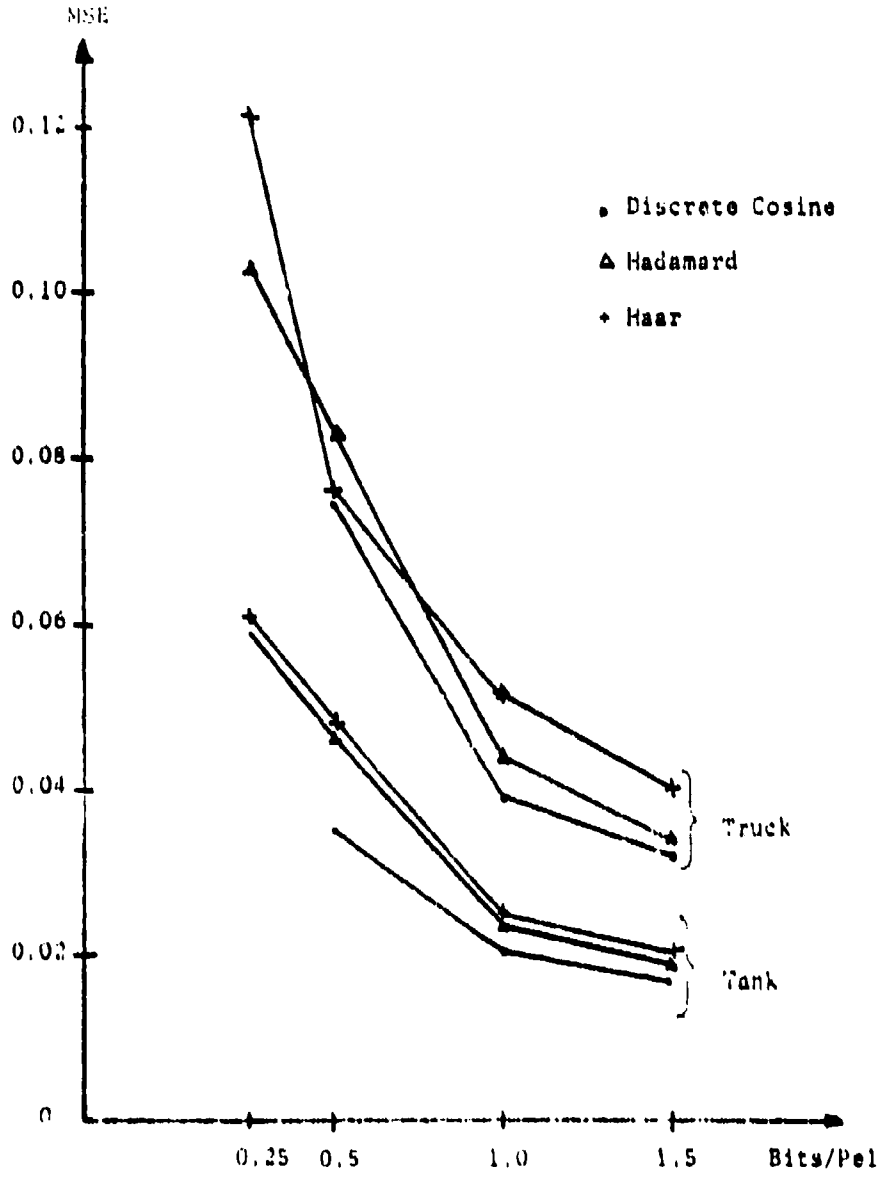

Fig. 4.3.3 Mean-Squared-Error Using 2-D Transform.

4.3.4a Two-Dimensional Hadamard Transform Technique of Truck; 0.25 bits/pel.

4.3.4b Two-Dimensional Hadamard Transform Technique of Truck; 0.5 bits/pel.

4.3.4c Two-Dimensional Hadamard Transform Technique of Truck: 1.0 bits/pel.

4.3.4d Two-Dimensional Hadamard Transform
Technique of Truck; 1.5 bits/pel.

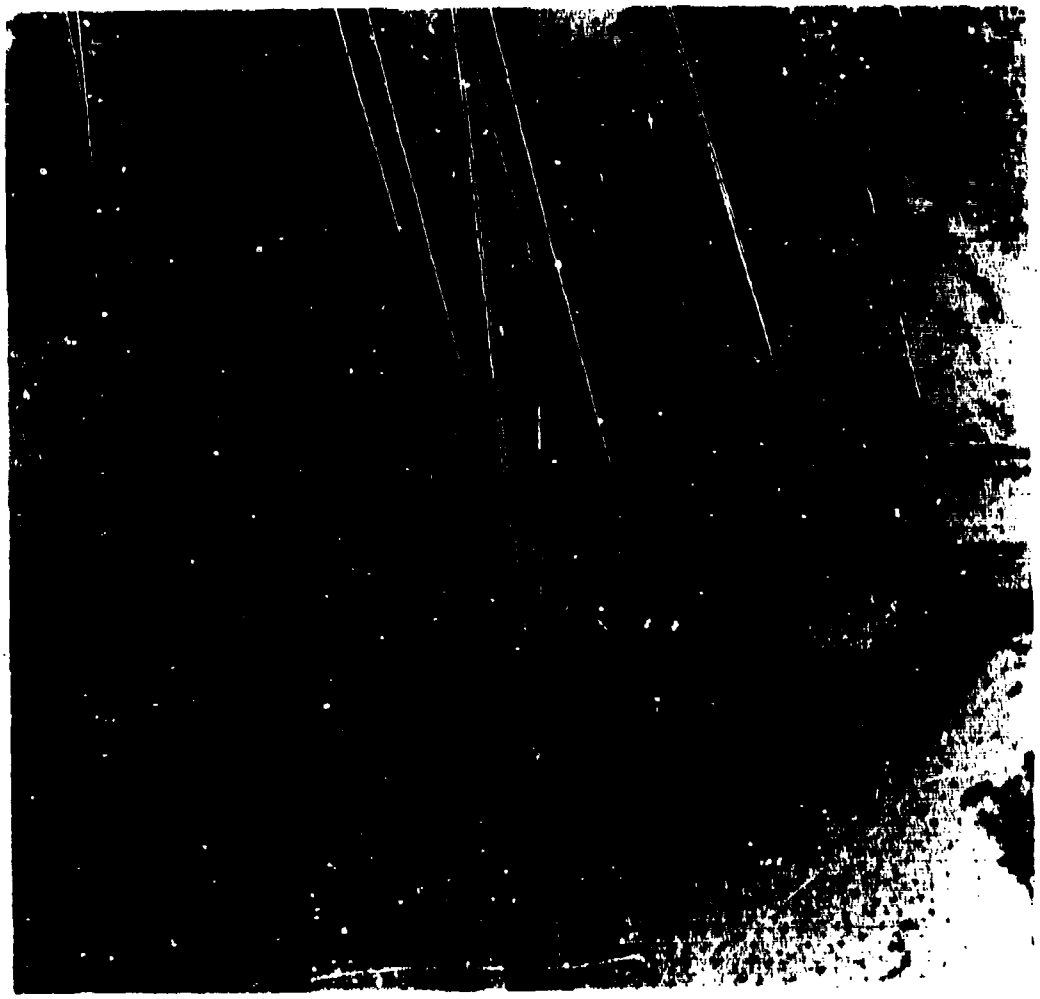

4.3.5a Two-Dimensional Discrete Cosine Transform Technique of Truck; 0.5 bits/pel.

4.3.5b Two-Dimensional Discrete Cosine Transform Technique of Truck; 1.0 bits/pel.

4.3.5c Two-Dimensional Discrete Cosine Transform Technique of Truck; 1.5 bits/pel.

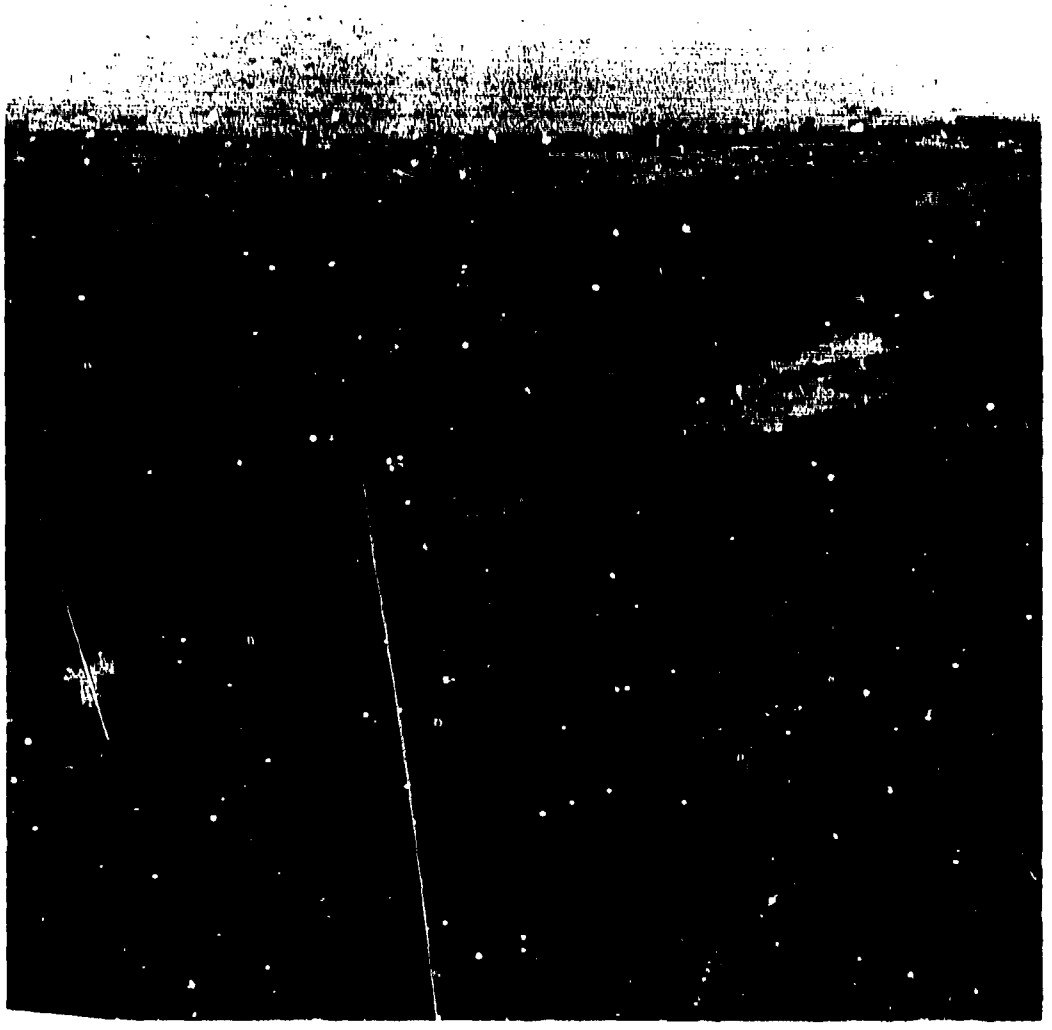

4.3.6a Two-Dimensional Hadamard Transform Technique of Tank; 0.25 bits/pel.

4.3.6b Two-Dimensional Hadamard Transform Technique of Tank: 0.5 bits/pel.

4.3.6c Two-Dimensional Hadamard Transform Technique of Tank; 1.0 bits/pel.

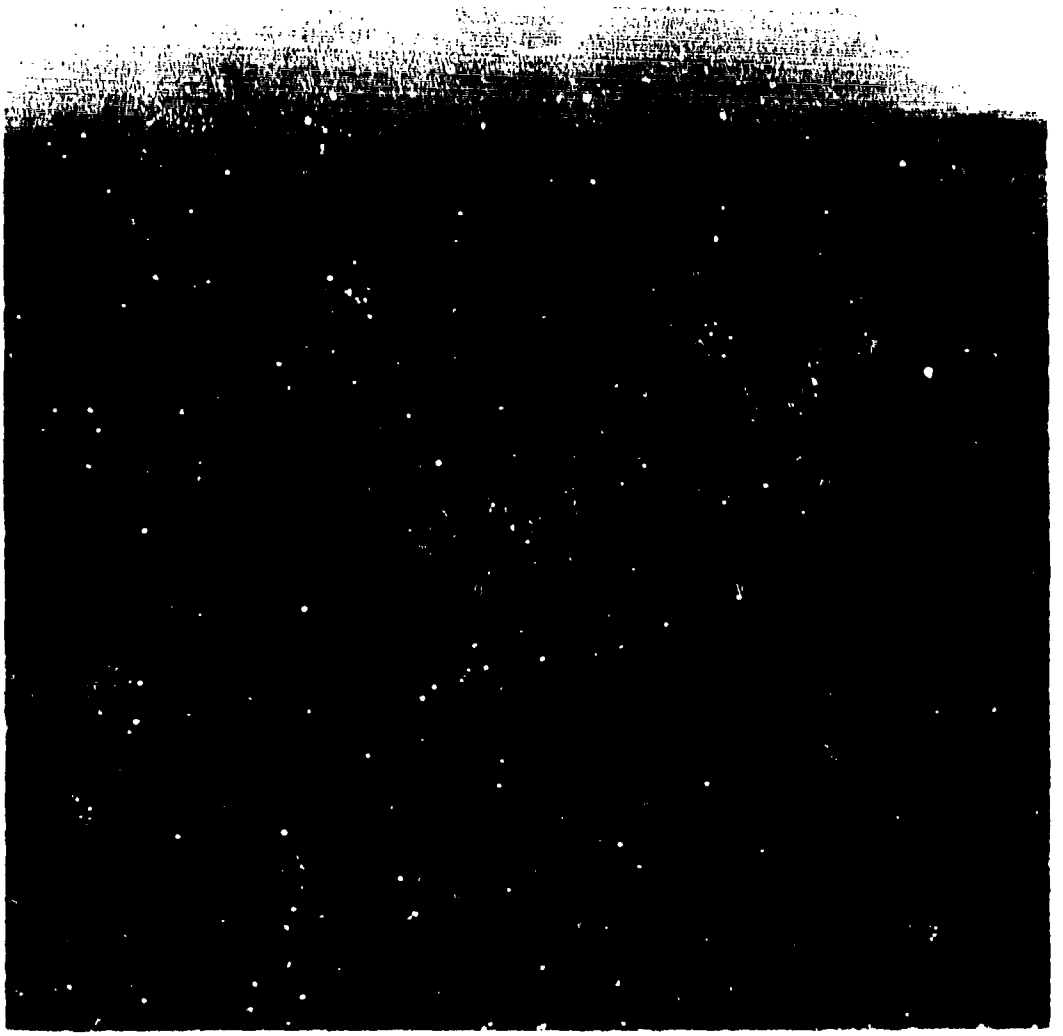

4.3.6d Two-Dimensional Hadamard Transform Technique of Tank, 1.5 bits/pel.

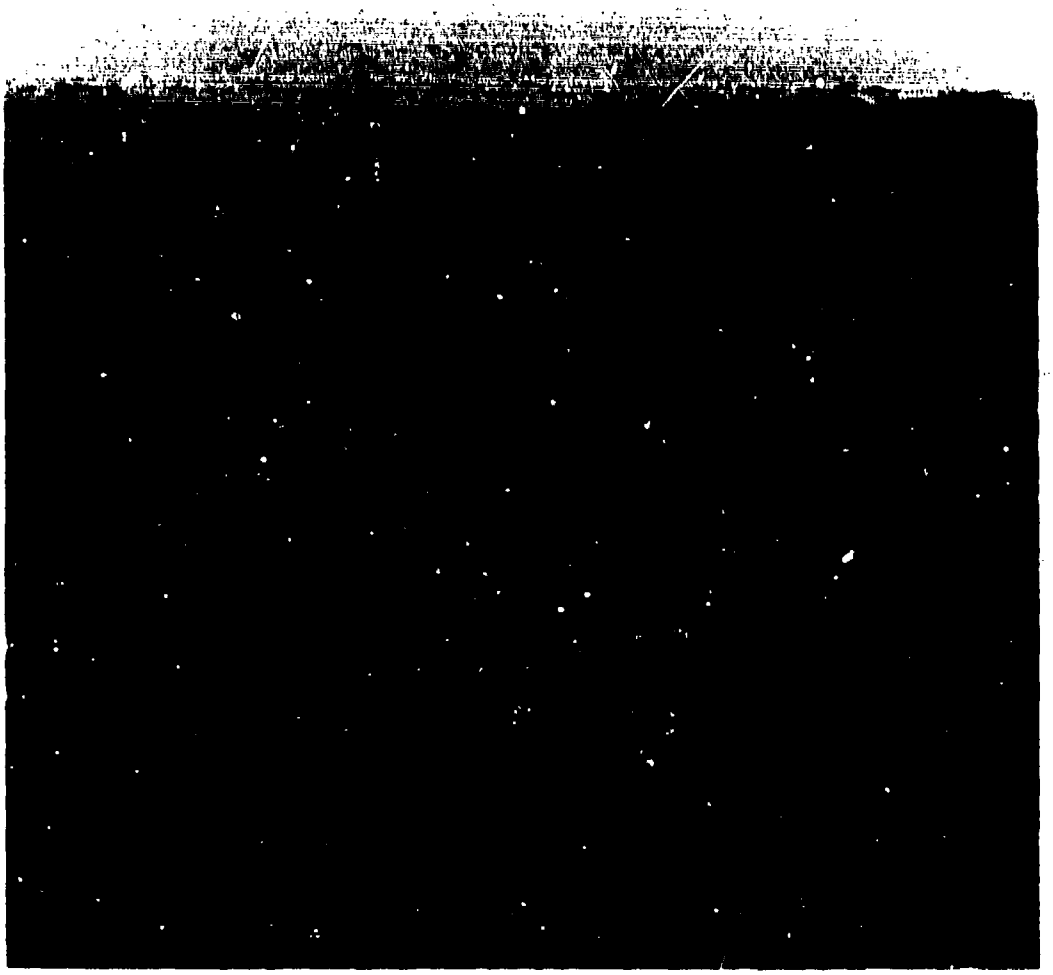

4.3.7a Two-Dimensional Discrete Cosine Transform Technique of Tank; 0.5 bits/pel.

4.3.7b Two-Dimensional Discrete Cosine Transform Technique of Tank; 1.0 bits/pel.

4.3.7c Two-Dimensional Discrete Cosine Transform Technique of Tank; 1.5 bits/pel.

bits/pel, then a substantial reduction in bandwidth can be obtained. Whether an RPV can accept this amount of degradation depends on the resolution required which depends upon the many parameters of the mission. To my knowledge, no predetermined resolution or mission parameters have been specified which would make a "yes" or "no" answer possible. It is suggested that suitable guidelines or limits be determined in order to make these judgements.

Comparing the results, which are almost equivalent, of 0.25 or 0.5 bits/pel with those obtained using 1.0 and 1.5 bits for these pictures indicate that the pictures processed using 1.0 and 1.5 bits/pel are of significantly better quality than those using 0.25 and 0.5 bits/pel. Subjectively it appears that there is a threshold type effect whereby the improvement due to doubling the bit rate is considerably better in going from 0.5 to 1.0 bits/pel than they are in going either from 0.25 to 0.5 or 1.0 to 1.5 bits/pel. Although this threshold type effect seems true from the subjective point of view, it is not noticeable in the MSE measures given in Tables 4.3.3 and 4.3.5. The MSE measures given in Table 4.3.3a indicate that in general the scene of the "Tank" gives significantly superior results than the scene of the "Truck". This improvement is not apparent subjectively when looking for specific objects within the pictures. In particular when we specify objects within each picture, for example, the tank in one picture and a wheel on the truck in the other, considerable degradation is seen in both pictures for 0.25 bits/pel. The overall MSE measure does not indicate these results due to the fact that relatively high MSE for a small area does not contribute significantly to the overall MSE. In order to determine an error measure which would tend to indicate the degradations in areas of high resolution without resorting to a calculation of MSE for some selected area in a picture, the normalized-derivative-squared-error (NDSE) was calculated for these pictures and the results are given in Table 4.3.3b. Using this error criterion should enhance the

error at sharp contours or regions of high activity within the picture. Although the numerical values of these errors are relatively high, they do tend to indicate the same trend as do subjective evaluations in that they do indicate the threshold effect somewhat between 0.5 and 1.0 bits/pel.

4.4 Hybrid Coding (Noiseless Channel)

In this section we evaluate the performance of the Hybrid coding schemes described in Chapter III. Since it has been shown that the Transform-DPCM and DPCM-Transform techniques are equivalent in performance, all results given are for the Transform-DPCM scheme. Results have also been obtained using DPCM-Transform technique; however, they are identical to the Transform-DPCM technique. One can interpret the same results for either system. In this scheme a one-dimensional Hadamard transform, using a block size of 16, was used to remove the correlation in the horizontal direction and DPCM techniques are used in the vertical direction. Several variations in the DPCM structures were investigated.

Fig. 4.4.1 gives the variances of the Hybrid coding signal at the input to the quantizer for the six pictures. In these simulations the prediction coefficients in the DPCM coders are equal to the vertical correlation coefficient of the picture. In this case all of the DPCM coders use the same prediction coefficient, but each has a different number of quantization levels. In reality for real data the vertical correlations for each coefficient will be different and different prediction coefficients should be used for an optimum system. However, the simplicity gained by using only one prediction coefficient is probably worth the slight increase in error. Fig. 4.4.2 and Table 4.4.1 show the normalized cumulative sum of the variances of signals at the input to the quantizer.

Histograms of the difference of the transform coefficients have been obtained and are given in Appendix A of this report. Histograms of difference of the

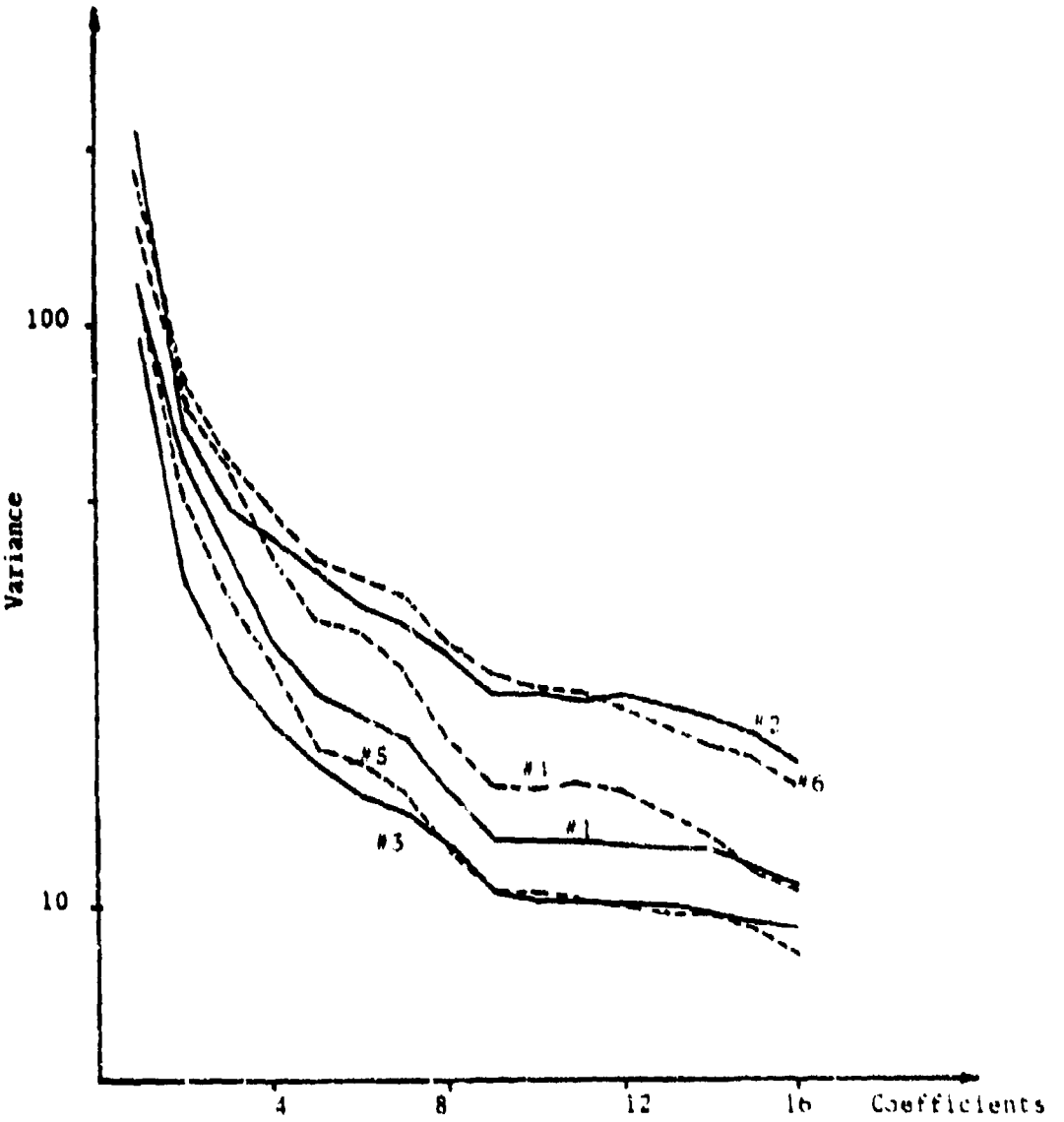

Fig. 4.4.1. Variances of the Hybrid Coding Signal at the Quantizer Input (6 pictures), ρ_y.

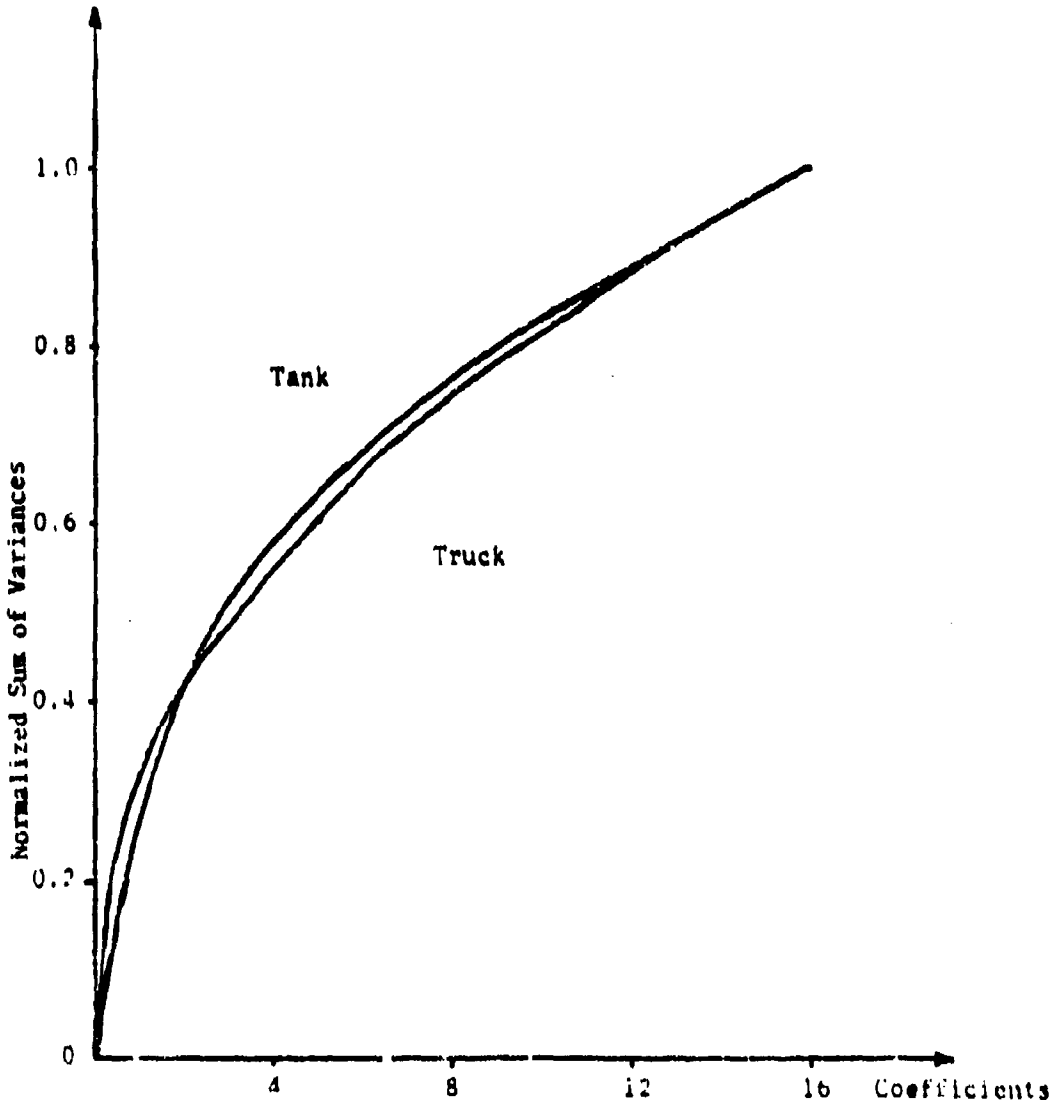

Fig. 4.4.2. Cumulative Sum of the Variances of the Hybrid Coding Samples at the Quantizer Input.

Coefficients	#1	#2	#3	#4	#5	#6
1	0.27425	0.31885	0.30585	0.27246	0.31753	0.27207
2	0.41278	0.41785	0.41894	0.40766	0.45469	0.38979
3	0.50864	0.49047	0.49958	0.51277	0.54742	0.47746
4	0.57679	0.55460	0.56529	0.58675	0.61769	0.54928
5	0.63206	0.61071	0.62043	0.64436	0.66824	0.60783
6	0.68255	0.65999	0.66957	0.69928	0.71576	0.66228
7	0.72858	0.70574	0.71569	0.74662	0.75780	0.71312
8	0.76565	0.74571	0.75521	0.78246	0.79125	0.75508
9	0.79679	0.78027	0.78873	0.81216	0.81953	0.79205
10	0.82764	0.81476	0.82188	0.84139	0.84738	0.82655
11	0.85848	0.84815	0.85443	0.87141	0.87479	0.86066
12	0.88850	0.88217	0.88616	0.90014	0.90159	0.89263
13	0.91814	0.91451	0.91757	0.92822	0.92754	0.92230
14	0.94744	0.94542	0.94709	0.95468	0.95548	0.94988
15	0.97465	0.97418	0.97447	0.97899	0.97790	0.97616
16	1.00000	1.00000	1.00000	1.00000	1.00000	1.00000

Table 4.4.1. Normalized Cumulative Sum of Variances of Hybrid Coding Sample at Input of Quantizer.

transform coefficients appear bell shaped for all coefficients except the first. The histogram for the first coefficient appears to be completely random, almost uniform in nature. Such characteristics indicate the majority of the information is contained in the differences of the first coefficients.

Table 4.4.2 shows the bit assignments obtained using the Wintz-Kurtenbach algorithm. It has been pointed out before that this bit assignment procedure for real data appears to be rather poor due to the fact that many unimportant coefficients are assigned only one bit, thus leaving fewer bits for the high information-carrying coefficients. A computer search routine was used to modify the bit assignment procedure in order to minimize the MSE. Table 4.4.3 shows results for several variations in the bit assignment procedure. Table 4.4.4 shows the actual bit assignments, determined from this study, which were used in the simulations.

Tables 4.4.5a,b and c show error measures for the scenes of the Truck and the Tank. The prediction coefficients used in the DPCM coder were set equal to ρ_y, the vertical correlations of the pictures. The MSE and NDSE are shown graphically in Figs. 4.4.3a,b and c. Comparing the results of Table 4.4.5 with those given in Table 4.3.3 for the two-dimensional transforms, it is observed that the hybrid coding scheme performs almost equivalent to the Discrete Cosine, which is superior to the performances of both the two-dimensional Hadamard and Haar transform techniques.

It has been pointed out in Chapter III that using one-dimensional techniques to remove the correlation in the horizontal (vertical) direction does not leave the correlation in the vertical (horizontal) direction intact as theory would suggest. This is illustrated in Table 4.4.6 where we show the vertical correlation of the transform coefficients. These results indicate that a different prediction coefficient in the DPCM coder should be used for each coefficient.

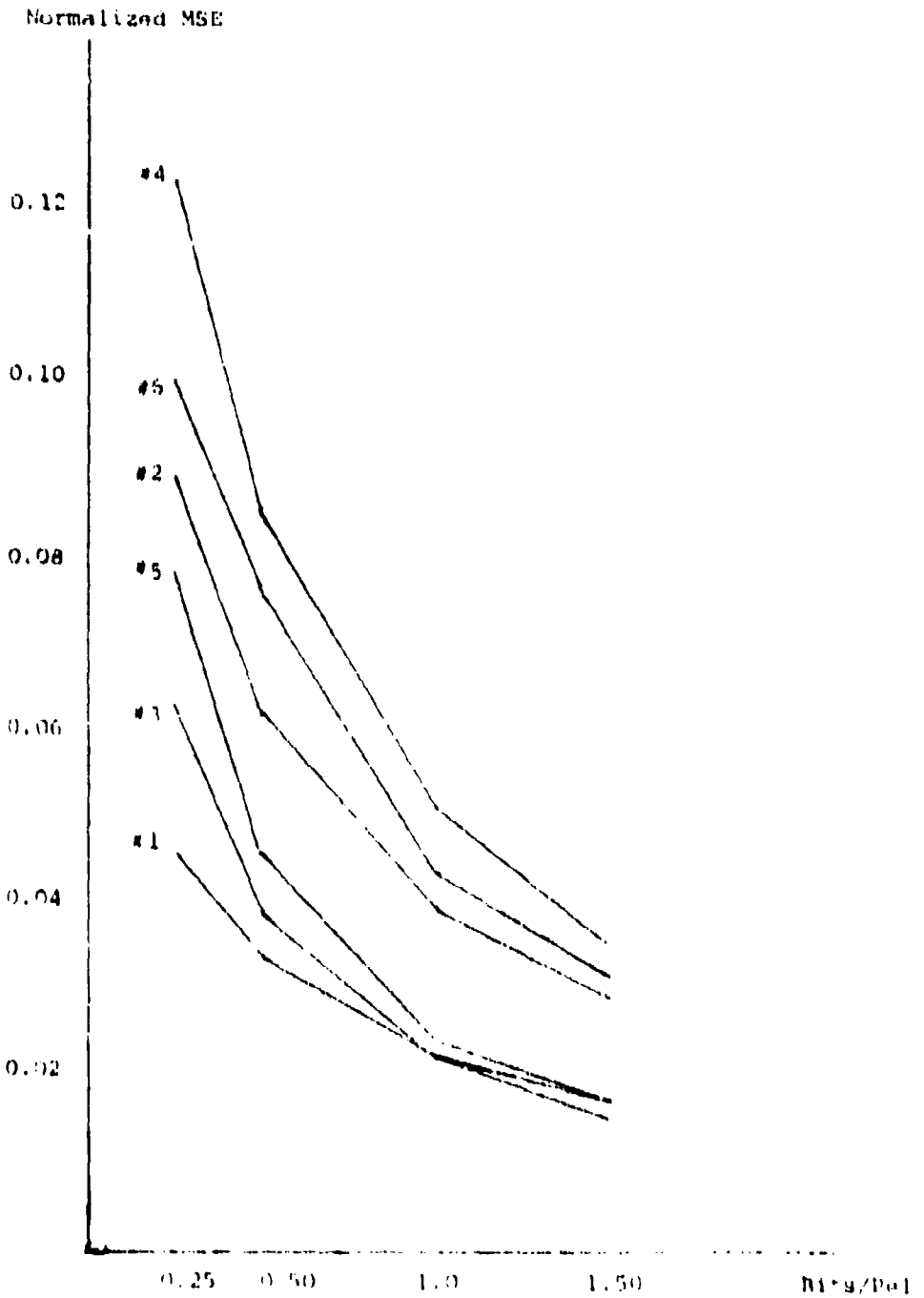

Fig. 4.3.3a Hybrid coding (Rayleigh channel)
Normalized Mean-squared error

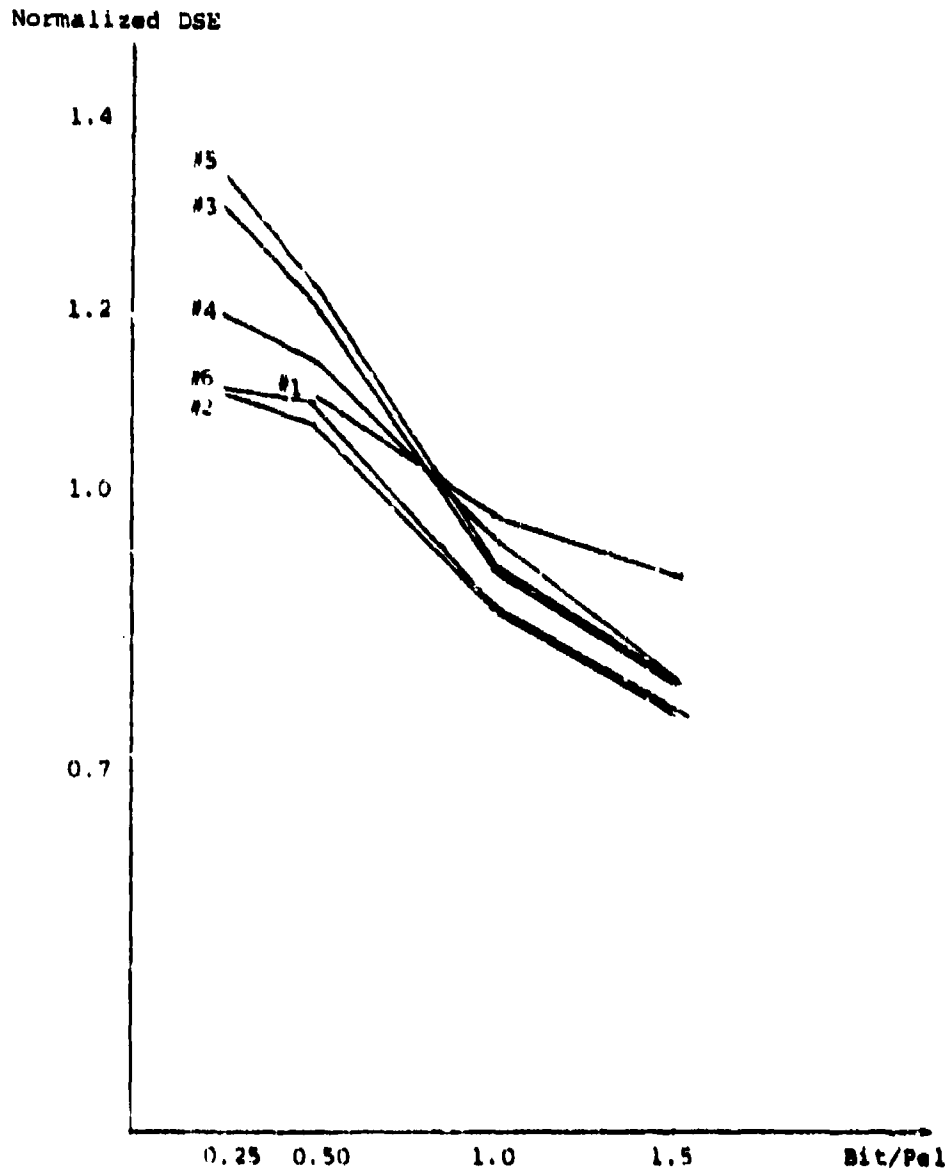

Fig. 4.4.1b. Hybrid Coding (Noiseless Channel) Normalized Derivative-Square-Errors.

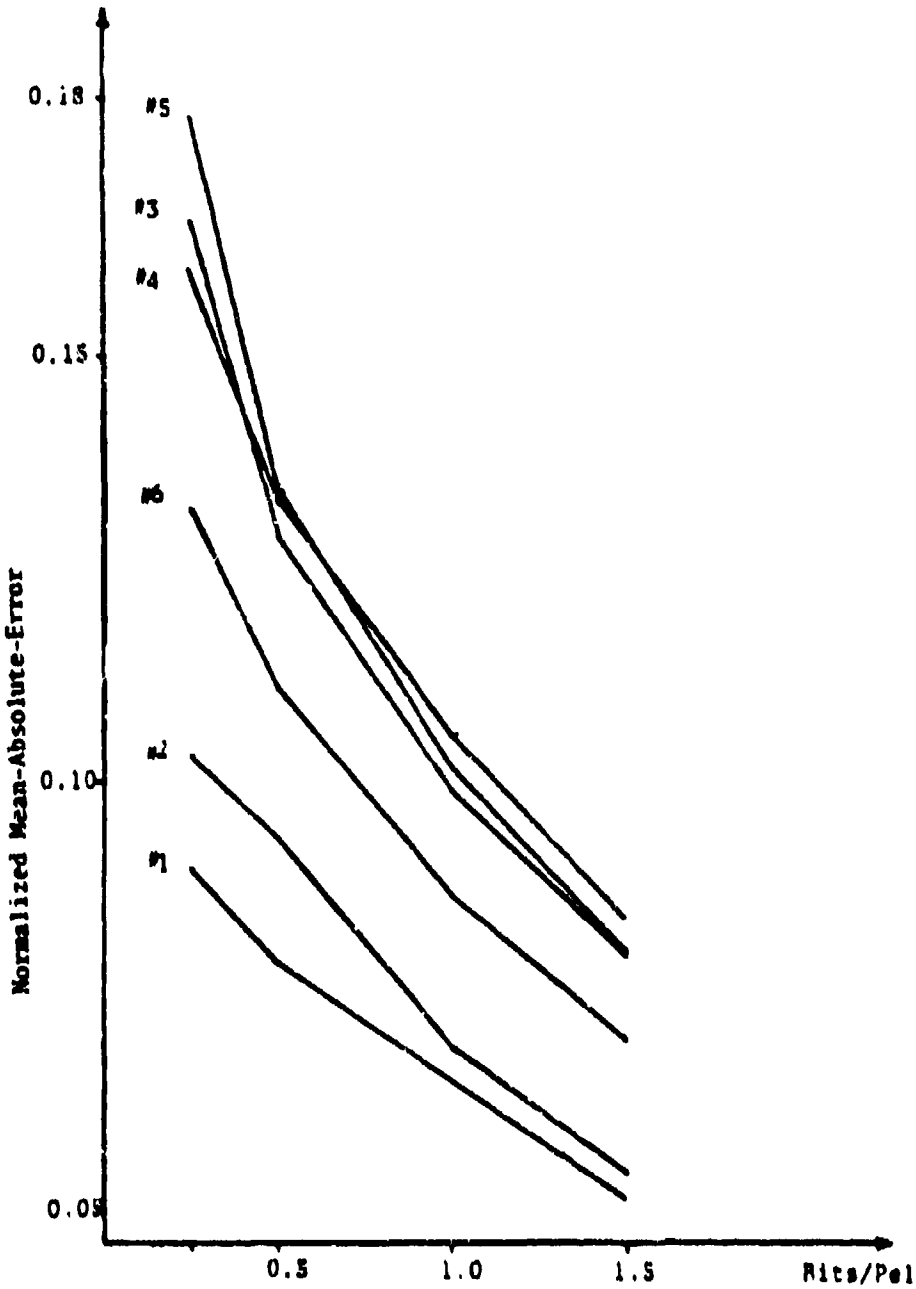

Fig. 4.4.3c. Normalized Mean-Absolute-Error (Hybrid Coding)

0.5 bits/pel		2	1	1	1	2												
1.0 bits/pel	2	1	1	1	1	1	1	1	1	1	1	1	1	1	1	1	1	
1.5 bits/pel	3	2	2	2	2	2	2	1	1	1	1	1	1	1	1	1	1	1

Transform/DPCM (Hadamard, A = 1.5, R = 0.94434)

Table 3.4.2 Bit Assignments for Hybrid Coding Scheme

PSF	Average Cumulative Sum Of Hybrid Signal	Bit Assignments (Bit/Pel = 1.0)															
		1	2	3	4	5	6	7	8	9	10	11	12	13	14	15	16
1	37.03357	4	3	2	2	2	1	1	1								
2	39.[illegible]	4	2	2	2	2	1	1	1	1							
3	40.[illegible]21	3	2	2	2	2	2	1	1	1							
4	39.[illegible]36	4	3	2	2	1	1	1	1	1							
5	42.[illegible]71	3	2	2	2	2	1	1	1	1	1						
6	45.[illegible]75	3	2	2	2	1	1	1	1	1	1	1					
7	47.[illegible]217	3	2	2	1	2	1	1	1	1	1	1	1				
8	50.[illegible]76	3	2	1	1	1	1	1	1	1	1	2	1	1			
9	56.[illegible]3	2	1	1	1	1	1	1	1	1	2	1	1	1	1	1	

*Multi-threshold technique

Table 3.4.3 Variations of Bit Assignments

Bits/Pixel	Bit Assignment							
	C_1	C_2	C_3	C_4	C_5	C_6	C_7	C_8
0.25	2	1	1					
0.5	4	2	1	1				
1.0	4	3	2	2	2	1	1	1
1.5	5	4	3	3	3	2	2	2

Table 4.3.4. Bit Assignments for Hybrid Coding

		Average Bit/Picture Element			
		0.25	0.50	1.0	1.50
Truck	$\rho = 1$	--	0.071488	0.067997	0.036743
	$\rho = \rho_x = \rho_y = 0.94434$	0.099508	0.062092	0.038979	0.028699
Tank	$\rho = \rho_x = \rho_y = 0.95631$	0.045915	0.034021	0.022545	0.015122

Table 4.4.5. Mean-Squared-Error Using Hybrid Coding Scheme.

		Average Bit/Picture Element			
		0.25	0.5	1.0	1.5
Frame	$\lambda = 1$	--	1.05223	0.77999	0.58759
	$\lambda = \lambda_y = 0.8333$	--	1.05845	0.86826	0.76431
Line	$\lambda = \lambda_y = 0.5556$	--	1.11637	0.97795	0.81101

Table 4.4.(5) Normalized-Derivative-Squared-Error Using Hybrid Coding Scheme

		Average Bit/Picture Element			
		0.25	0.5	1.0	1.5
Frame	$\lambda = 1$	--	0.093176	--	0.069747
	$\lambda = \lambda_y = 0.8333$	0.103671	0.085785	0.069058	0.054252
Line	$\lambda = \lambda_y = 0.5556$	0.089595	0.078931	0.065048	0.051427

Table 4.4.(6) Mean-Absolute-Error Using Hybrid Coding Scheme

This would require a different prediction coefficient for each DPCM coder. Table 4.4.7 shows the results obtained using the scene of the Tank when different prediction coefficients, equal to the correlation coefficients given in Table 4.4.6, are used in the DPCM coders. Comparing these results with those given in Table 4.4.5a where the same prediction coefficient ($A_j = \rho_y$) is used for all coefficients, there appears to be little differences. This is due to the fact that the performance of the DPCM coder is insensitive to the prediction coefficient for noiseless channels. This statement is not true if noisy channels are assumed.

Figs. 4.4.4a,b,c,d; 4.4.5a,b,c,d; 4.4.6a,b,c,d; 4.4.7a,b,c; 4.4.8a,b,c,d and 4.4.9a,b,c,d show the results obtained using Hybrid techniques on the six pictures for bit rates of 0.25, 0.5, 1.0 and 1.5 bits/pel. In all cases the prediction coefficient in the DPCM coders was equal to the vertical correlation coefficient of the picture. Comparing the pictures obtained using the Hybrid coding scheme with those obtained using the two-dimensional transforms given in the previous section, it appears subjectively that the Hybrid coding technique gives superior results to the transform techniques except at extremely low bit rates of 0.25 bits/pel. At this low bit rate there appears to be noticeably more "blocking effect" in the Hybrid scheme than in the two-dimensional transform techniques, which was unexpected. The overall quality of the pictures obtained using the Hybrid technique appears to be somewhat better than that of the two-dimensional transforms, which agrees with the MSE results given previously. One noticeable point which is different in the pictures processed using the Hybrid coding scheme is that the subjective quality of the pictures appears to improve in a linear sense as the bits/pel are increased. This was not true for the pictures obtained using two-dimensional transform techniques.

Coefficient	Correlation
1	0.98603
2	0.68408
3	0.46013
4	0.50872
5	0.22920
6	0.26723
7	0.29189
8	0.31042
9	0.10161
10	0.08560
11	0.09810
12	0.10369
13	0.11658
14	0.10069
15	0.14176
16	0.1330

Table 4.4.6. Correlation of the Transformed Coefficients - Tank (one-element delay)

Bits Per Pel	MSE	MSE (using all feedback factors = .95531
0.25	0.045522	0.045915
0.50	0.032644	0.034021
1.0	0.020409	0.022545

Table 4.4.7. Mean-Squared-Error for the Scene of the Tank Using Transform-DPCM and Prediction Coefficients as given in Table 4.4.5.

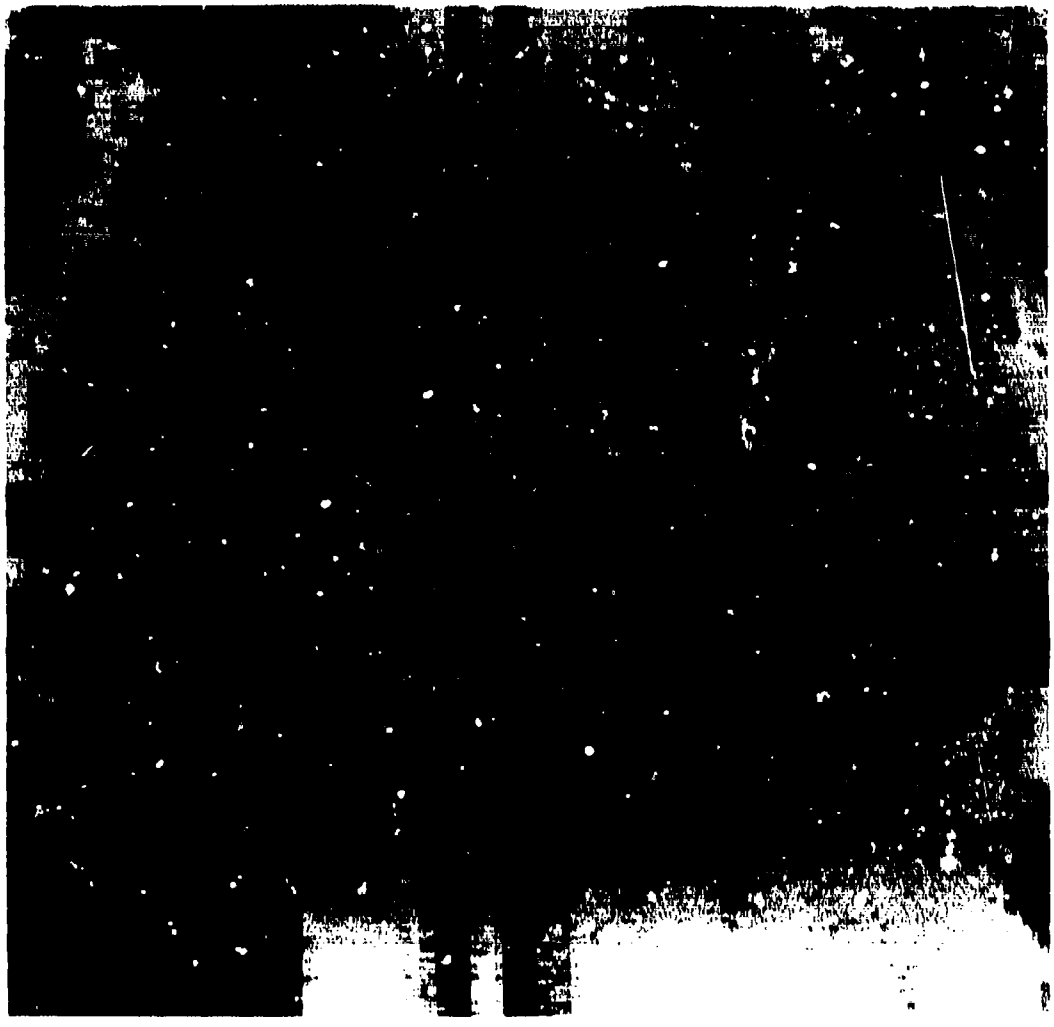

4.4.4a Hybrid Coding (Transform-DPCM) of the Scene of the Truck; 0.25 bits/pel.

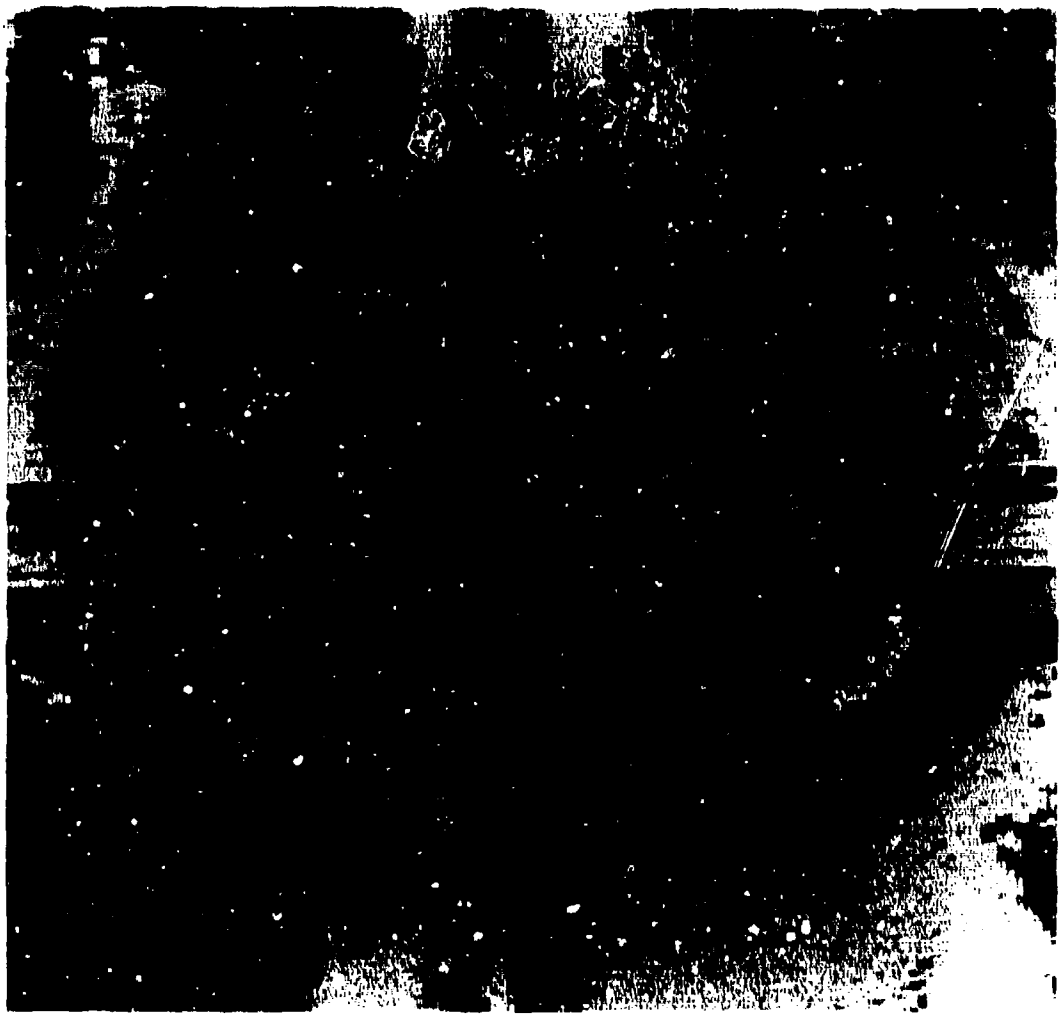

4.4.4b Hybrid Coding (Transform-DPCM)
of the Scene of the Truck;
0.5 bits/pel.

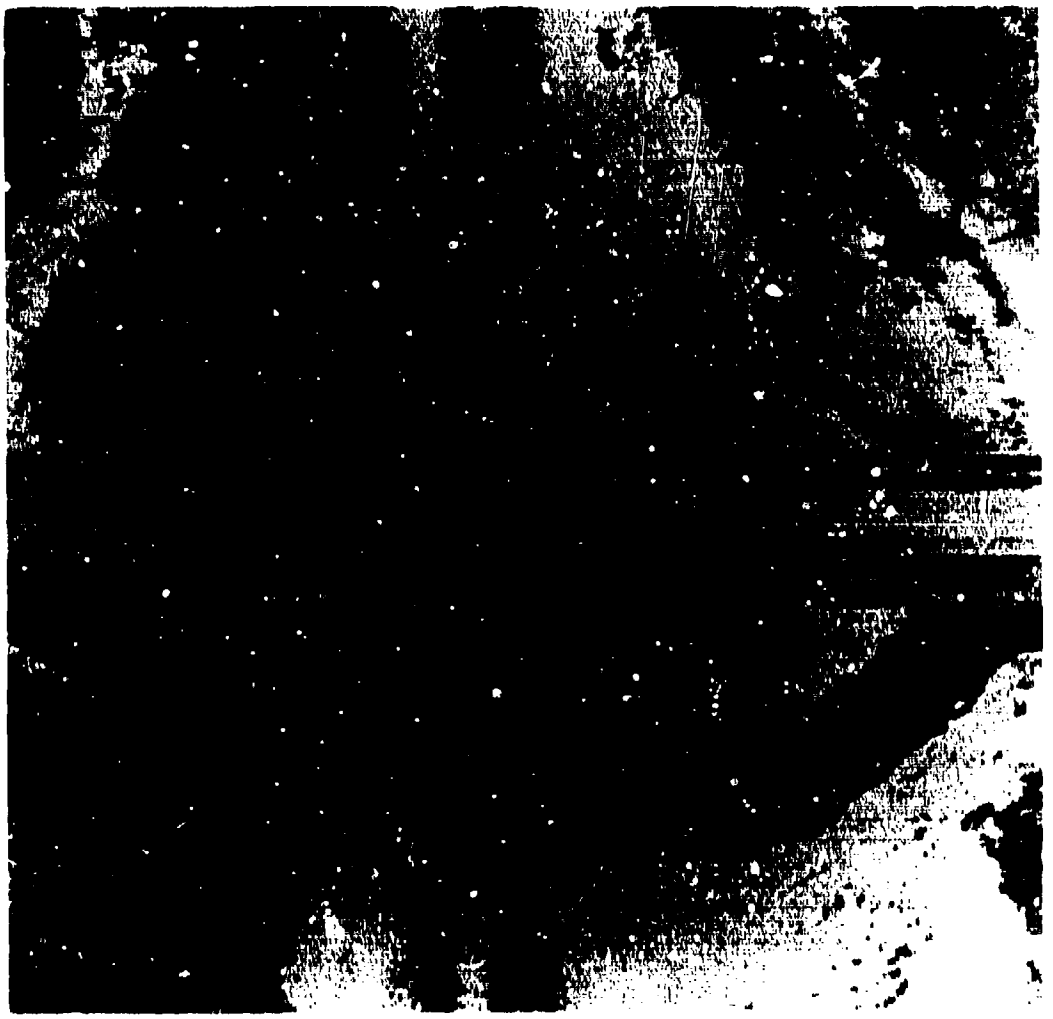

4.4.4c Hybrid Coding (Transform-DPCM) of the Scene of the Truck; 1.0 bits/pel.

4.4.4d Hybrid Coding (Transform-DPCM) of the Scene of the Truck; 1.5 bits/pel.

4.4.5a Hybrid Coding (Transform-DPCM)
of the Scene of the Tank;
0.25 bits/pel.

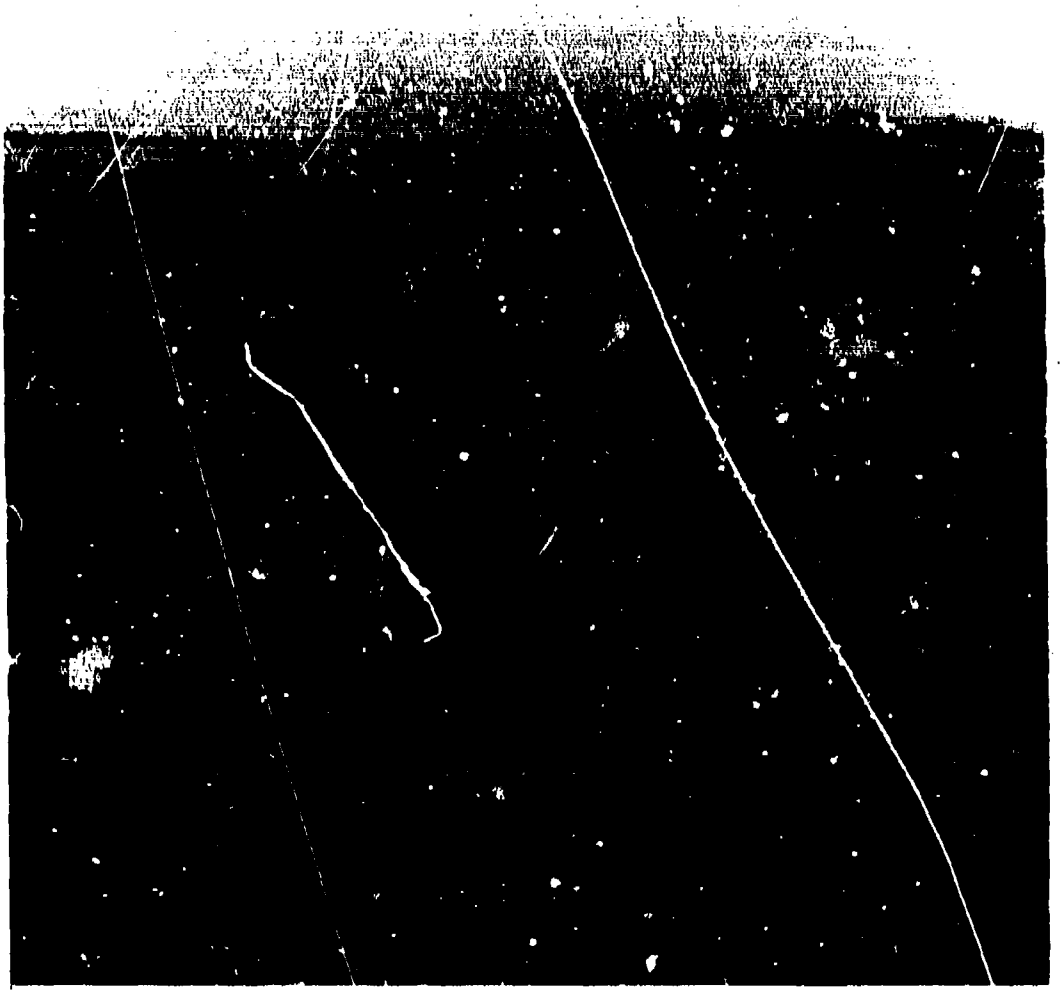

4.4.5b Hybrid Coding (Transform-DPCM) of the Scene of the Tank; 0.5 bits/pel.

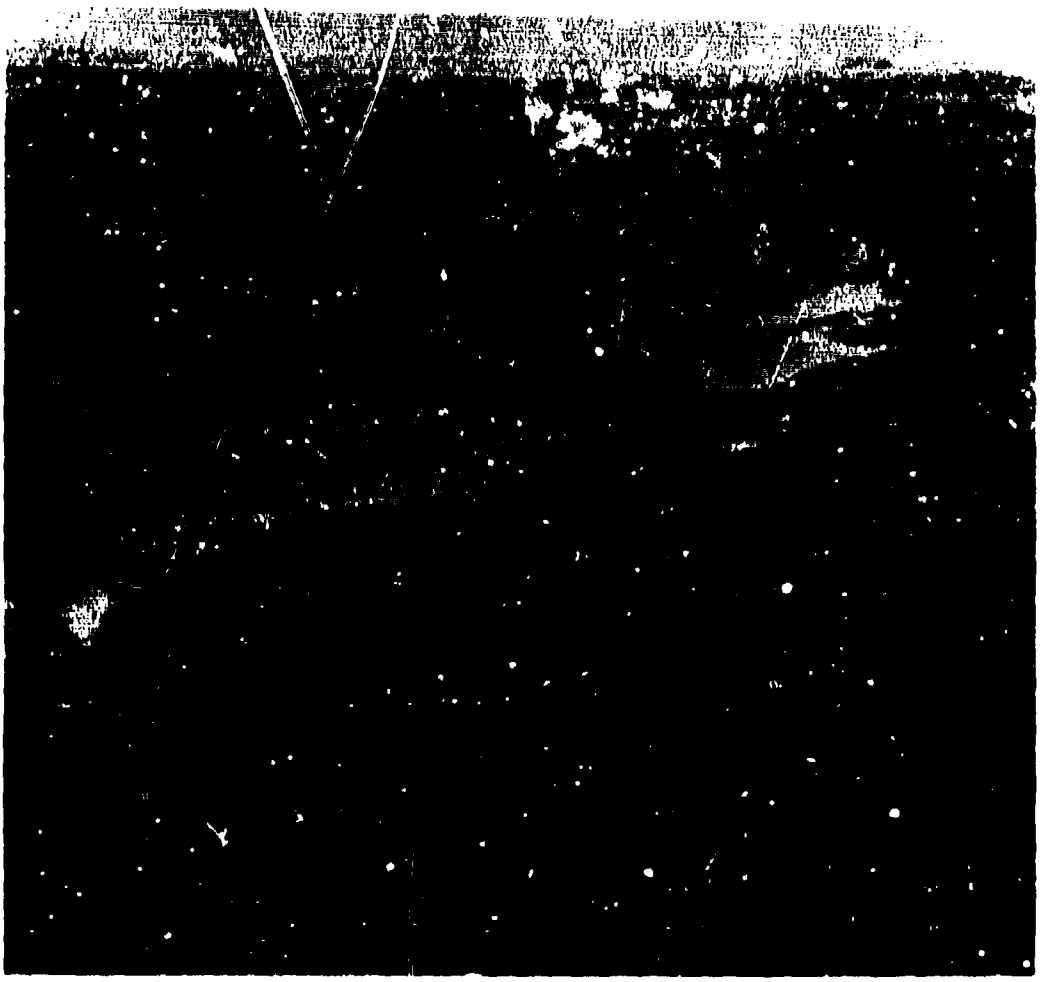

4.4.5c Hybrid Coding (Transform-DPCM) of the Scene of the Tank; 1.0 bits/pel.

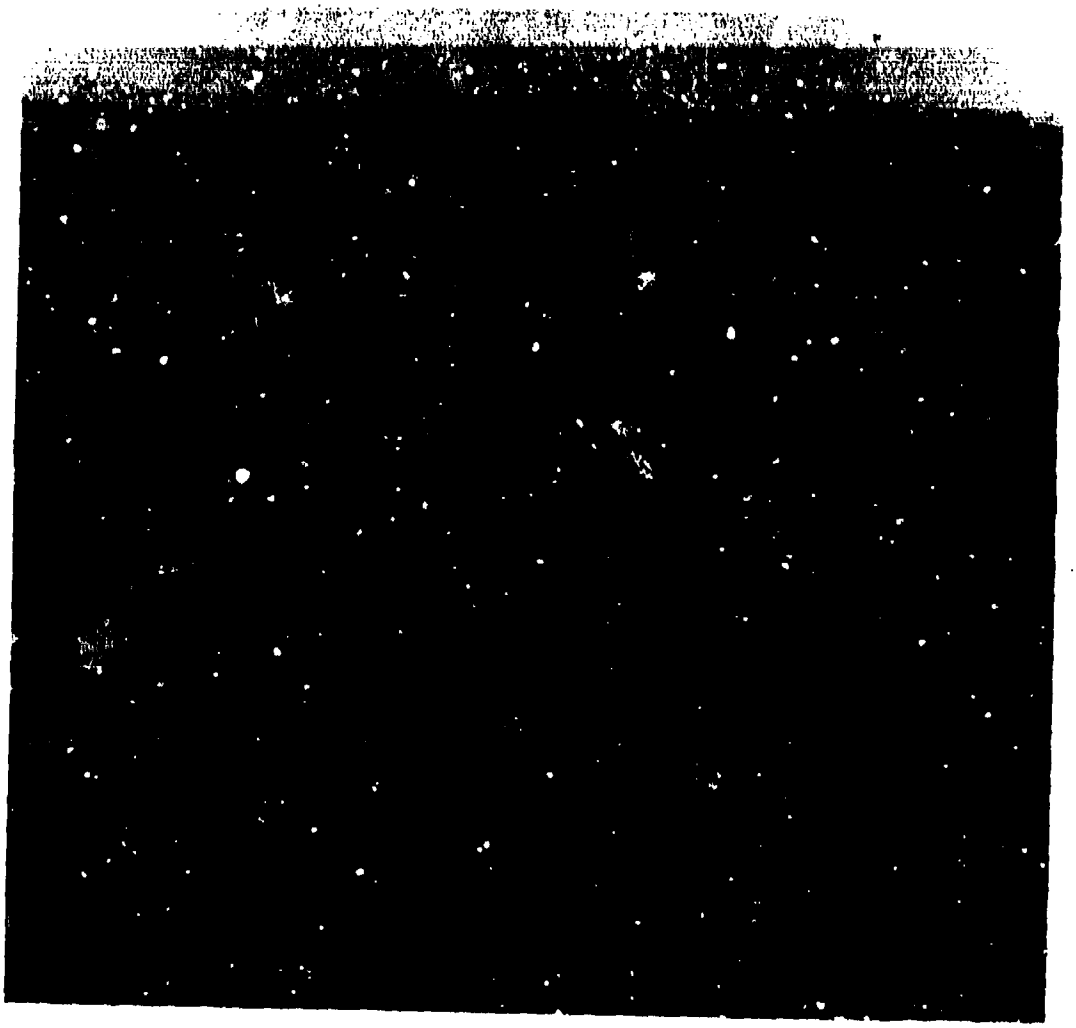

4.4.5d Hybrid Coding (Transform-DPCM) of the Scene of tho Tank; 1.5 bits/pel.

4.4.6a Hybrid Coding (Transform-DPCM)
of the Scene of the Trees;
0.25 bits/pel.

4.4.6b Hybrid Coding (Transform-DPCM) of the Scene of the Trees; 0.5 bits/pel.

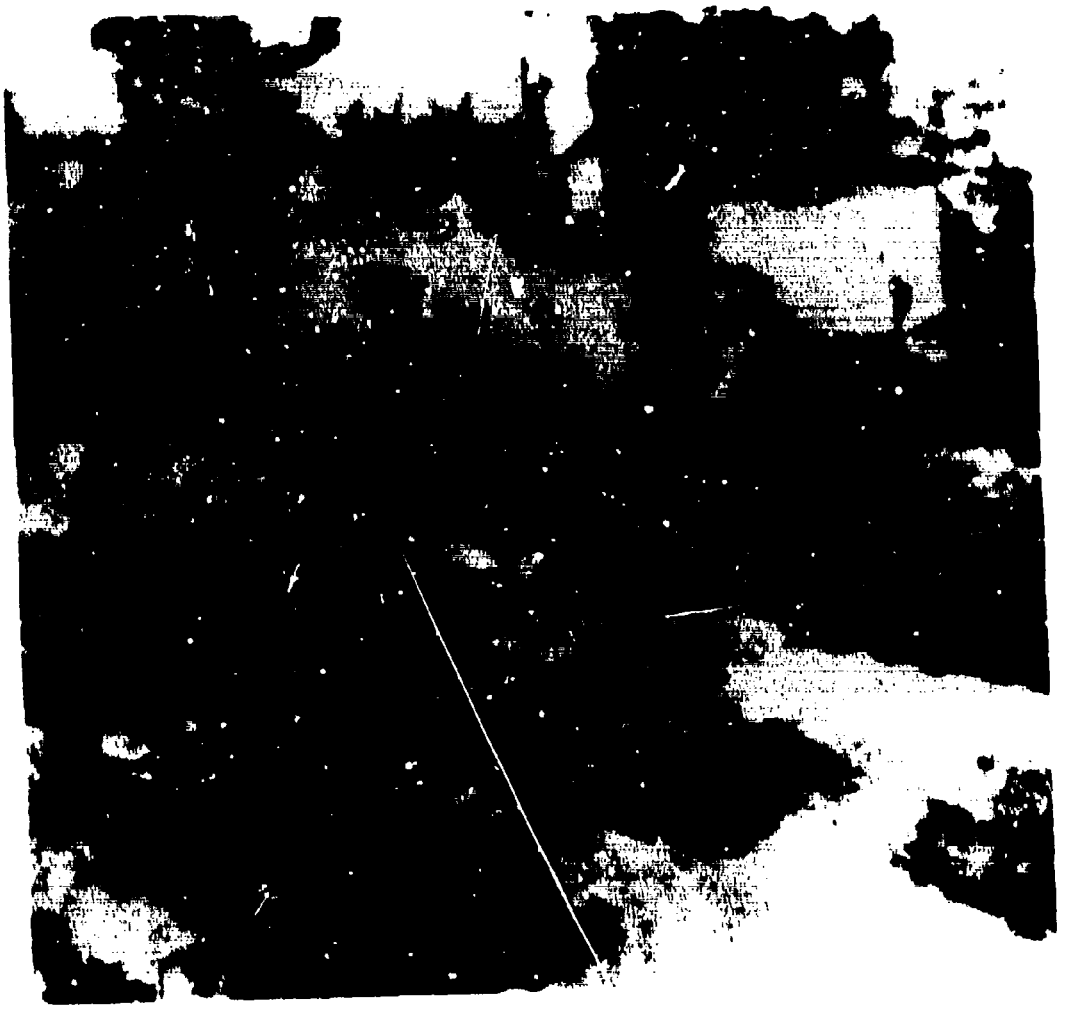

4.4.6c Hybrid Coding (Transform-DPCM) of the Scene of the Trees; 1.0 bits/pel.

Reproduced from
best available copy.

4.4.6d Hybrid Coding (Transform-DPCM)
of the Scene of the Trees;
1.5 bits/pel.

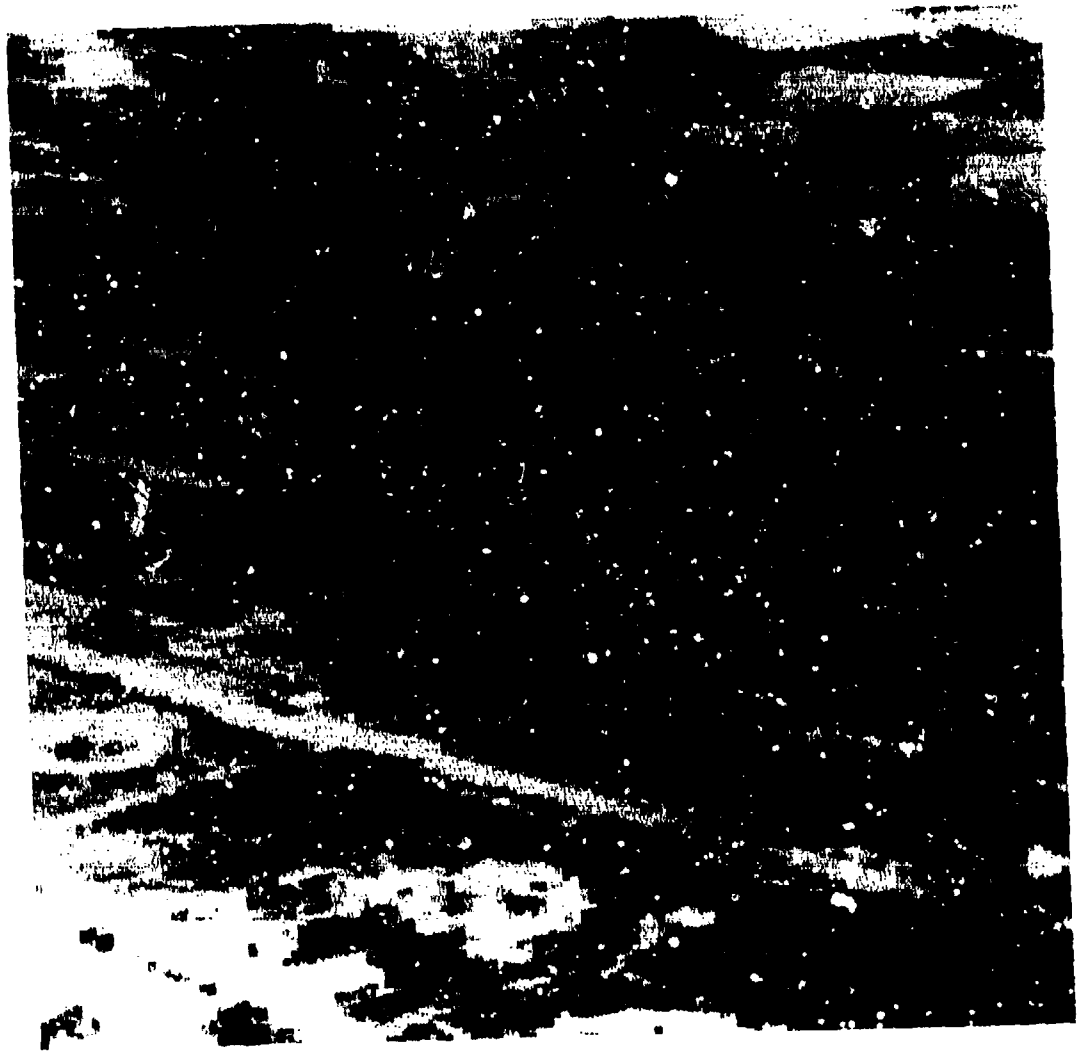

4.4.7a Hybrid Coding (Transform-DPCM)
of the Scene of the Field;
0.25 bits/pel.

4.4.7b Hybrid Coding (Transform-DPCM)
of the Scene of the Field;
0.5 bits/pel.

4.4.7c Hybrid Coding (Transform-DPCM)
of the Scene of the Field;
1.0 bits/pel

4.4.8a Hybrid Coding (Transform-DPCM) of the Scene of the Meadow; 0.25 bits/pel.

4.4.8b Hybrid Coding (Transform-DPCM) of the Scene of the Meadow; 0.5 bits/pel.

4.4.8c Hybrid Coding (Transform-DPCM) of the Scene of the Meadow; 1.0 bits/pel.

4.4.8d Hybrid Coding (Transform-DPCM) of the Scene of the Meadow; 1.5 bits/pel.

4.4.9a Hybrid Coding (Transform-DPCM)
of the Scene of the Coast;
0.25 bits/pel.

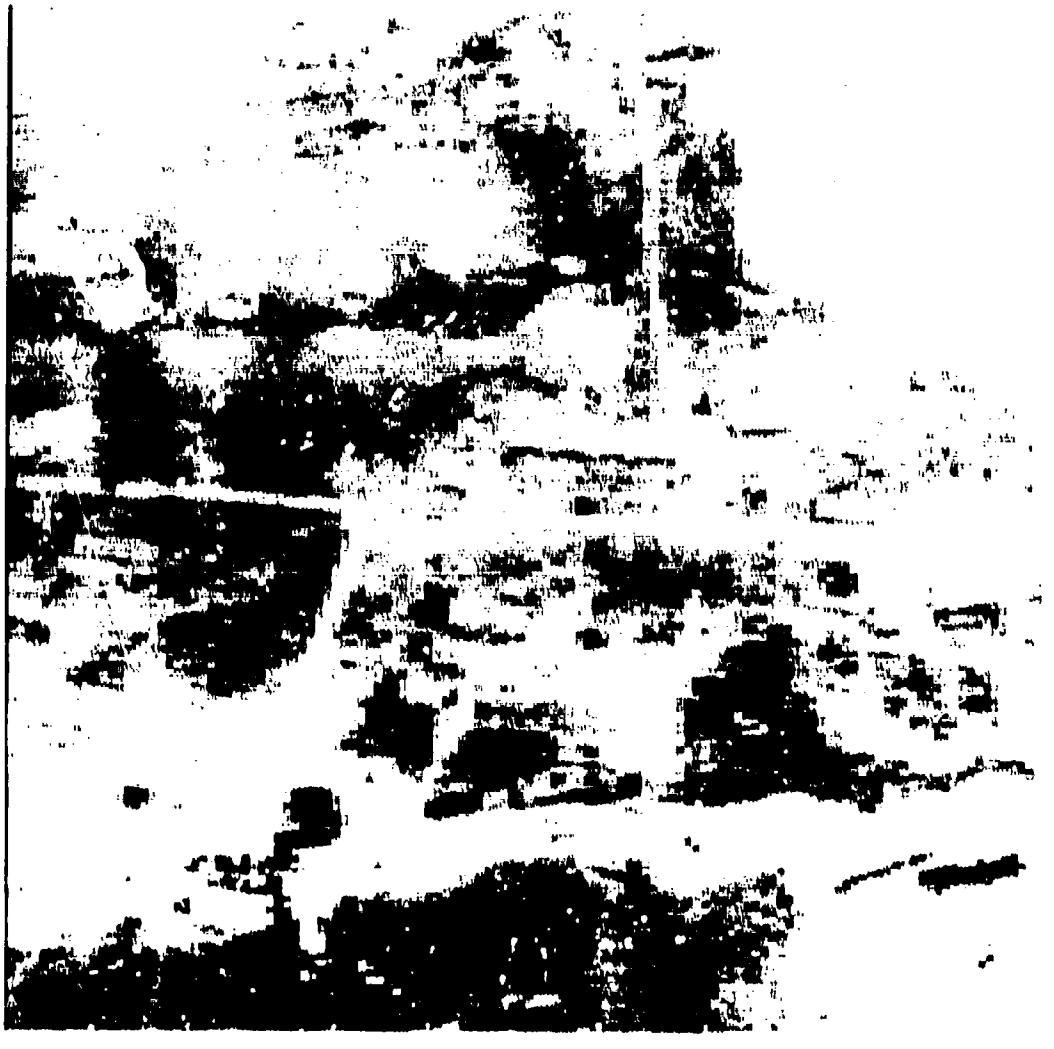

4.4.9b Hybrid Coding (Transform-DPCM) of the Scene of the Coast; 0.5 bits/pel.

4.4.9c Hybrid Coding (Transform-DPCM) of the Scene of the Coast; 1.0 bits/pel.

4.4.9d Hybrid Coding (Transform-DPCM) of the Scene of the Coast; 1.5 bits/pel.

It has been noted previously that the MSE measure does not at times correlate with subjective evaluations. This is particularly true when one compares results of different techniques or different pictures. The MSE measure does seem to give useful results when comparisons are restricted to the same picture and the same technique. One main disadvantage of the MSE measure, which has been pointed out before, is its inability to indicate degradations in small regions of high resolution within a picture. In order to determine the usefulness of a particular scheme several local area mean-squared-error calculations were made for the areas containing the tank and truck. These results are given in Table 4.4.8 for both the Hybrid technique and the two-dimensional transform techniques. It is noted that local MSE for both the scenes of the "Truck" and the "Tank" are essentially the same, which was not true for the total MSE calculations given before. The threshold effects between 0.5 and 1.0 bits/pel are very evident in these results.

Table 4.4.9 compares the results obtained using NDSE. These results correlate very well with those obtained using the local MSE. This indicates that the NDSE criterion would be a better measure of "goodness" of the picture in terms of resolution in regions of high activity within the picture.

Similar results are given in Figs. 4.4.3a and 4.4.3b and Table 4.4.10 for all six pictures. Using these results one can definitely see the threshold effect between 0.5 and 1.0 bits/pel. Below this threshold the pictures are severely degraded while above this threshold the pictures are acceptable.

The results of this section are summarized below:

(1) At 0.5 bits/pel and below the pictures are severely degraded in terms of resolution.

(2) Using 1.0 bits/pel or higher results in pictures which are essentially [illegible] original (no noticeable degradation).

		0.25	0.50	1.0	1.5
Truck	2-D Hadamard	0.137605	0.104656	0.080081	0.063042
	2-D Cosine		0.088049	0.062126	0.055018
	Hybrid Coding (n=1)		0.121776	0.112092	0.057497
	Hybrid Coding ($R = \sigma_y = 0.04434$)		0.087657	0.056282	0.042219
Tank	2-D Hadamard	0.117502	0.090413	0.051869	0.044056
	2-D Cosine		0.073780	0.045163	0.035128
	Hybrid Coding ($R = \sigma_y = 0.05531$)		0.082747	0.050158	0.035788

Table 4.4.8. Local Mean-Squared Error

Truck	2-D Hadamard	1.12487	1.03855	0.78083	0.50033
	2-D Cosine		0.98963	0.69503	0.51607
	Hybrid Coding (n=1)		1.05223	0.77999	0.58759
	Hybrid Coding ($R = \sigma_y = 0.04434$)		1.08443	0.85876	0.76431
Tank	2-D Hadamard	1.20331	1.13586	0.86538	0.60979
	2-D Cosine		1.02675	0.80725	0.56446
	Hybrid Coding ($R = \sigma_y = 0.05531$)		1.11037	0.97795	0.81101

Table 4.4.9. Normalized Derivative Squared Error.

(3) The Hybrid coding scheme performs superior to the two-dimensional transform techniques.

(4) The local MSE or LDSE is a better measure of a particular scheme's performance in terms of resolution and can be useful in interpreting results for different pictures and different processes.

		0.25 b/p	0.50 b/p	1.0	1.5
MSE	#1	0.045915	0.034021	0.023545	0.015122
	2	0.089508	0.062092	0.038979	0.028699
	3	0.062845	0.038762	0.022145	0.016898
	4	0.123720	0.085477	0.051024	0.034726
	5	0.078673	0.046188	0.024358	0.016891
	6	0.106611	0.076020	0.043468	0.031492
LDSE	#1		1.11637	0.97795	0.81101
	2	1.13152	1.08445	0.86836	0.73431
	3	1.32364	1.21553	0.91040	0.78864
	4	1.19758	0.15007	0.15427	0.79489
	5	1.35000	1.22964	0.91931	0.78992
	6	1.11507	1.10444	0.87655	0.75997
MAE	#1	0.089595	0.078931	0.065048	0.051427
	2	0.103021	0.083785	0.069038	0.054252
	3	0.165310	0.128457	0.098814	0.079510
	4	0.160493	0.133553	0.105389	0.084037
	5	0.177666	0.134015	0.101718	0.080041
	6	0.132010	0.111128	0.086711	0.070271

Table 4.4.10. Comparison of Six Pictures (Hybrid Coding)

4.5 The Effects of Channel Noise on the Two-Dimensional Hadamard Transform and Hybrid Coding Techniques

In this section the effects of channel noise on both the two-dimensional Hadamard Transform and Hybrid Coding schemes are investigated. The probabilities of bit error used in these investigations are .001 and .01. The relatively high noise channel was assumed so that the effects of channel noise on the two techniques would be readily apparent, so that comparison between the two techniques in a noisy environment could easily be made. The effects of noise were simulated by calling a random number from the random number generator on the digital computer and if this number exceeded a predetermined level a bit error was assumed.

Table 4.5.1 shows the effects of channel errors on the MSE for various bit rates using two-dimensional Hadamard transform. Figs. 4.5.1a, b and c show the effects on the scene of the "Tank" using a probability of bit error of .001. Noticeable errors are apparent as black or white squares within the picture, which result when the first coefficients have errors in them. If one observes the pictures closely a number of other errors, in form of square blocks, of less subjective degradation are also apparent. Figs. 4.5.2a, b and c show the effects of a very high probability of bit error equal to .01. Even at this relatively high probability of bit error the 1.0 bit/pel picture still has a large amount of information intact. Subjectively the

Bits Per Pel	MSE	Bits in Error	Pels in Error	Blocks in Error	Prob. of Bit Error
0.25	0.06494	67	67	66	10^{-3}
0.5	0.049154	134	134	134	10^{-3}
1.0	0.029275	274	274	270	10^{-3}
0.25	0.1420	778	724	674	10^{-2}
0.5	0.1153	1321	1315	1160	10^{-2}
1.0	0.0906	2623	2606	1943	10^{-2}

Table 4.5.1 Mean-Squared-Error for the Scene of the Tank Using Two-Dimensional Hadamard Transform.

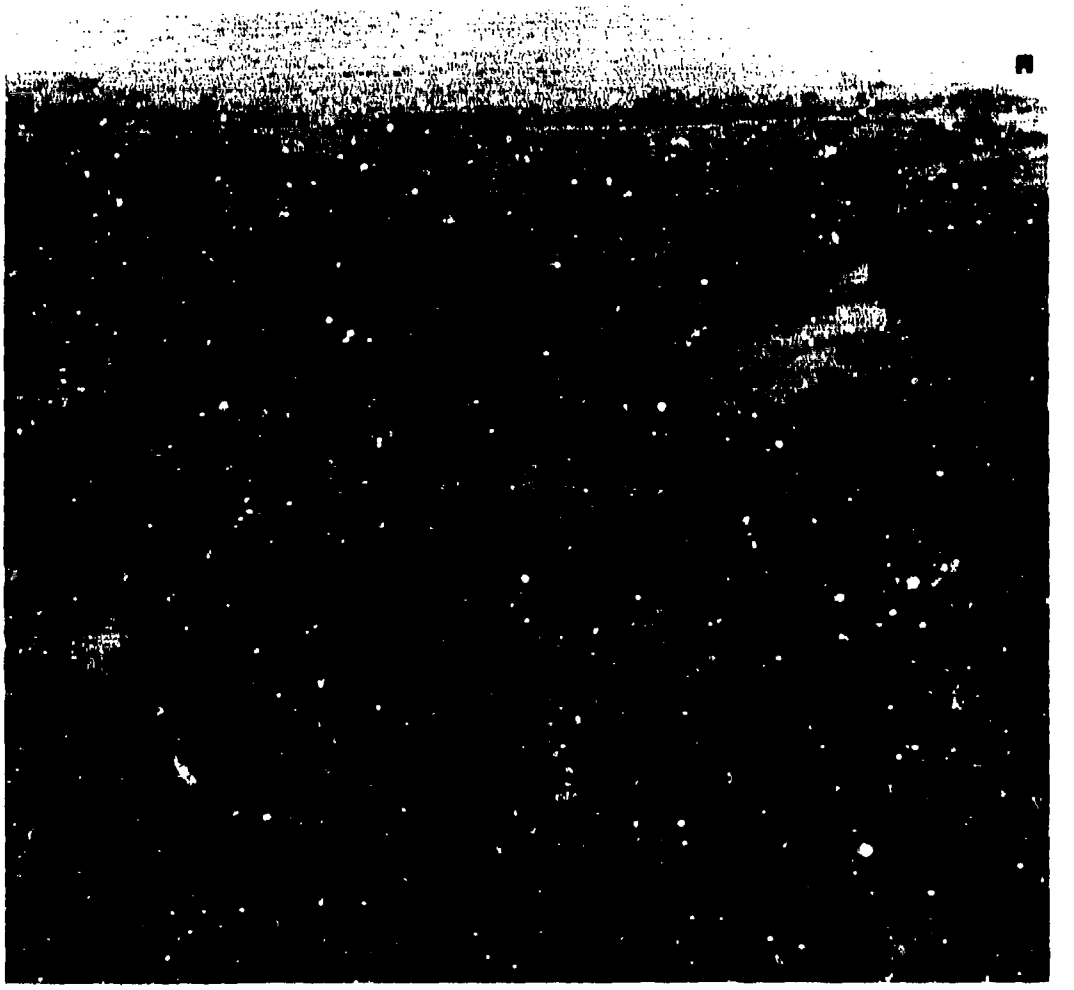

4.5.1a Two-Dimensional Hadamard Transform Technique of the Scene of the Tank; Probability of Bit Error = .001; 0.25 bits/pel.

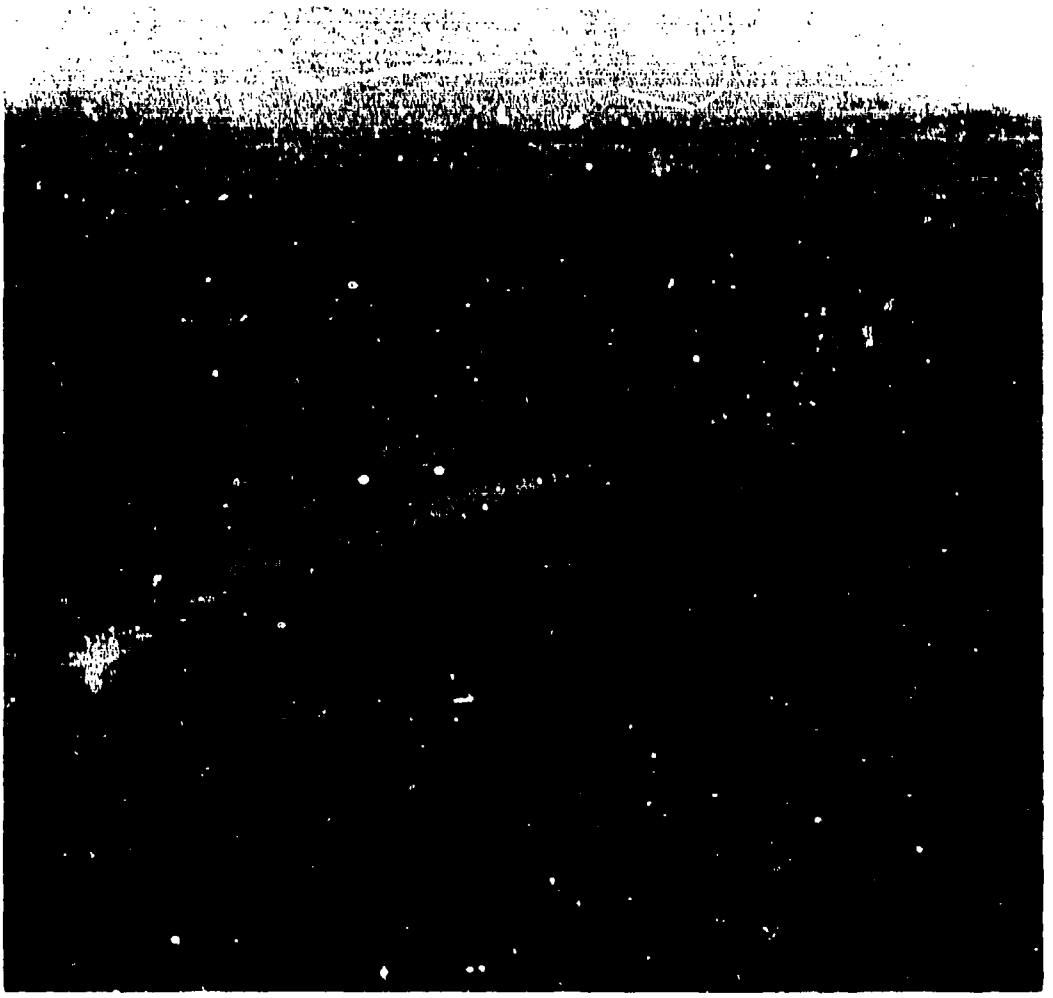

4.5.1b Two-Dimensional Hadamard Transform Technique of the Scene of the Tank; Probability of Bit Error = .001; 0.5 bits/pel.

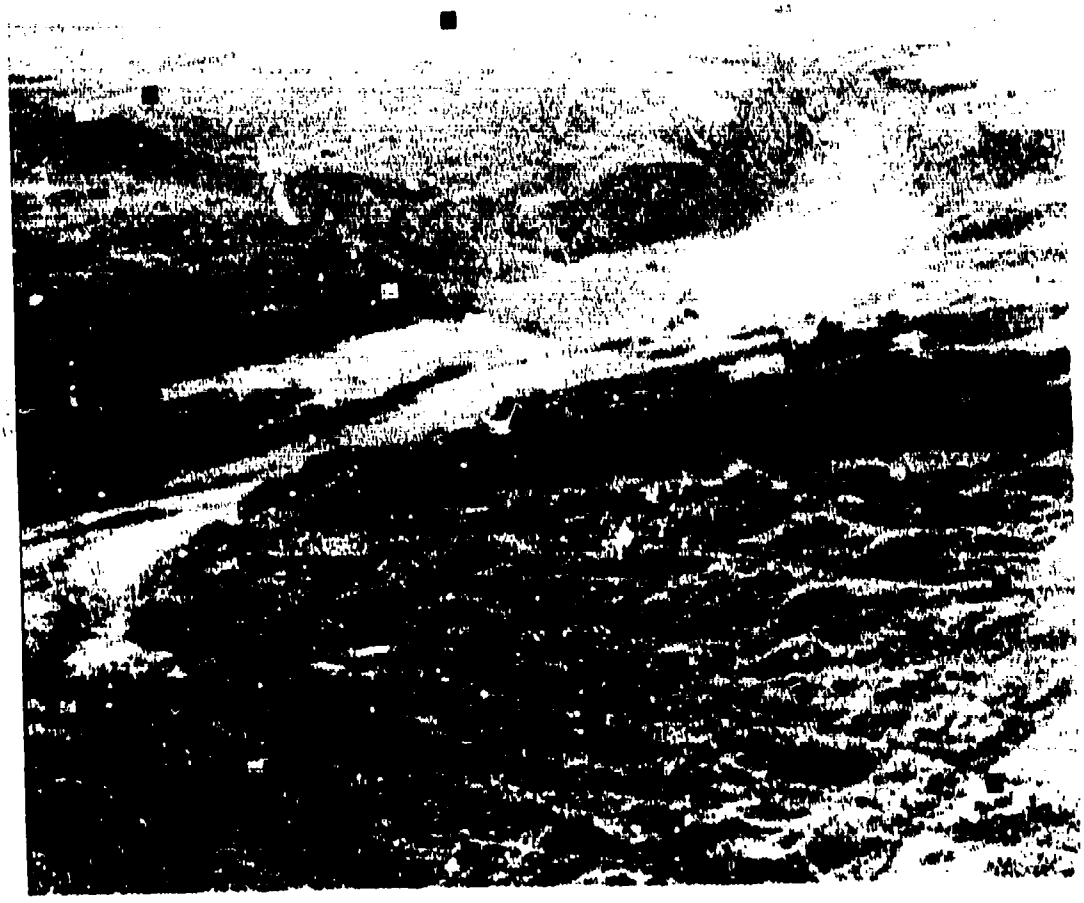

4.5.1c Two-Dimensional Hadamard Transform Technique of the Scene of the Tank; Probability of Bit Error = .001; 1.0 bits/pel.

4.5.2a Two-Dimensional Hadamard Transform Technique of the Scene of the Tank; Probability of Bit Error = .01; 0.25 bits/pel.

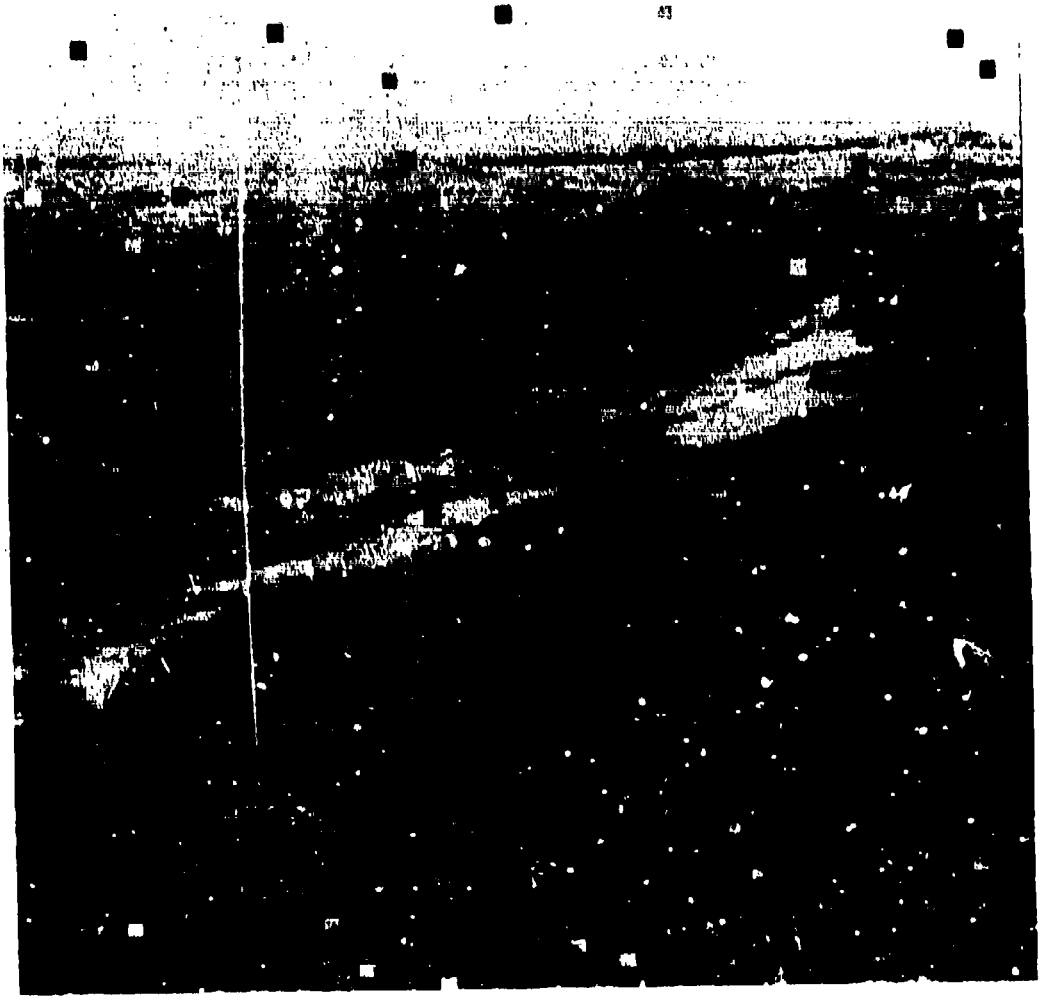

4.5.2b Two-Dimensional Hadamard Transform Technique of the Scene of the Tank; Probability of Bit Error = .01; 0.5 bits/pel.

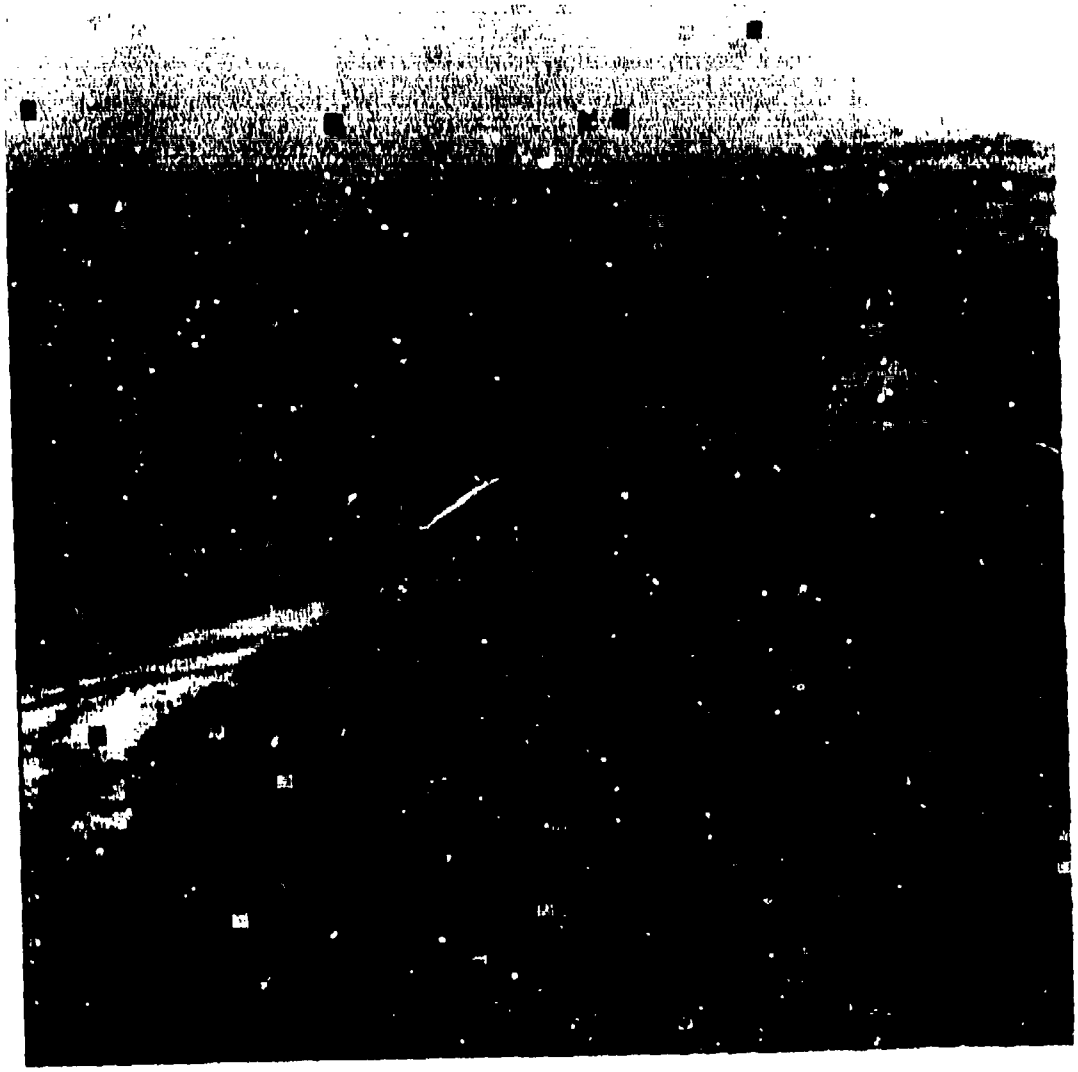

4.5.2c Two-Dimensional Hadamard Transform Technique of the Scene of the Tank; Probability of Bit Error = .01; 1.0 bits/pel.

Bits Per Pel	MSE	Bits in Error	Pels in Error	Blocks in Error	Prob. of Bit Error
0.25	0.0486	59	59	59	10^{-3}
0.5	0.0383	134	134	134	10^{-3}
1.0	0.0277	273	273	273	10^{-3}
0.25	0.0742	645	642	635	10^{-2}
0.50	0.0717	1319	1308	1274	10^{-2}
1.0	0.0736	2618	2593	215	10^{-2}

Table 4.5.2. Mean-Squared-Error for the Scene of the Tank Using Hybrid Coding. The Same Prediction Coefficient is Used for Each Coefficient.

effects of channel noise on the two-dimensional Hadamard transform technique seem to be rather minimal

The effects of channel errors on the MSE measure for the Hybrid coding schemes are given in Table 4.5.2. It is noted that the MSE for the Hybrid coding technique is substantially less than those for the two-dimensional transform technique; however, the qualities of the pictures obtained are considerably poorer than those obtained using two-dimensional Hadamard transform.

Figs. 4.5.3a,b,c and 4.5.4a,b,c show these results. In these pictures a considerable amount of streaking in the vertical direction is noted. This is due to the fact that DPCM coding is used on the coefficients in the vertical direction and differential coding is very sensitive to noise. For these results the prediction coefficients for DPCM coders are the same and they are equal to the vertical correlation coefficient.

Table 4.5.3 shows the results obtained using different prediction coefficients for the DPCM encoder. These coefficients are equal to the calculated correlations of individual transform coefficients when Transform-DPCM coding is used. Since no significant improvements are seen pictures were not reproduced for these cases.

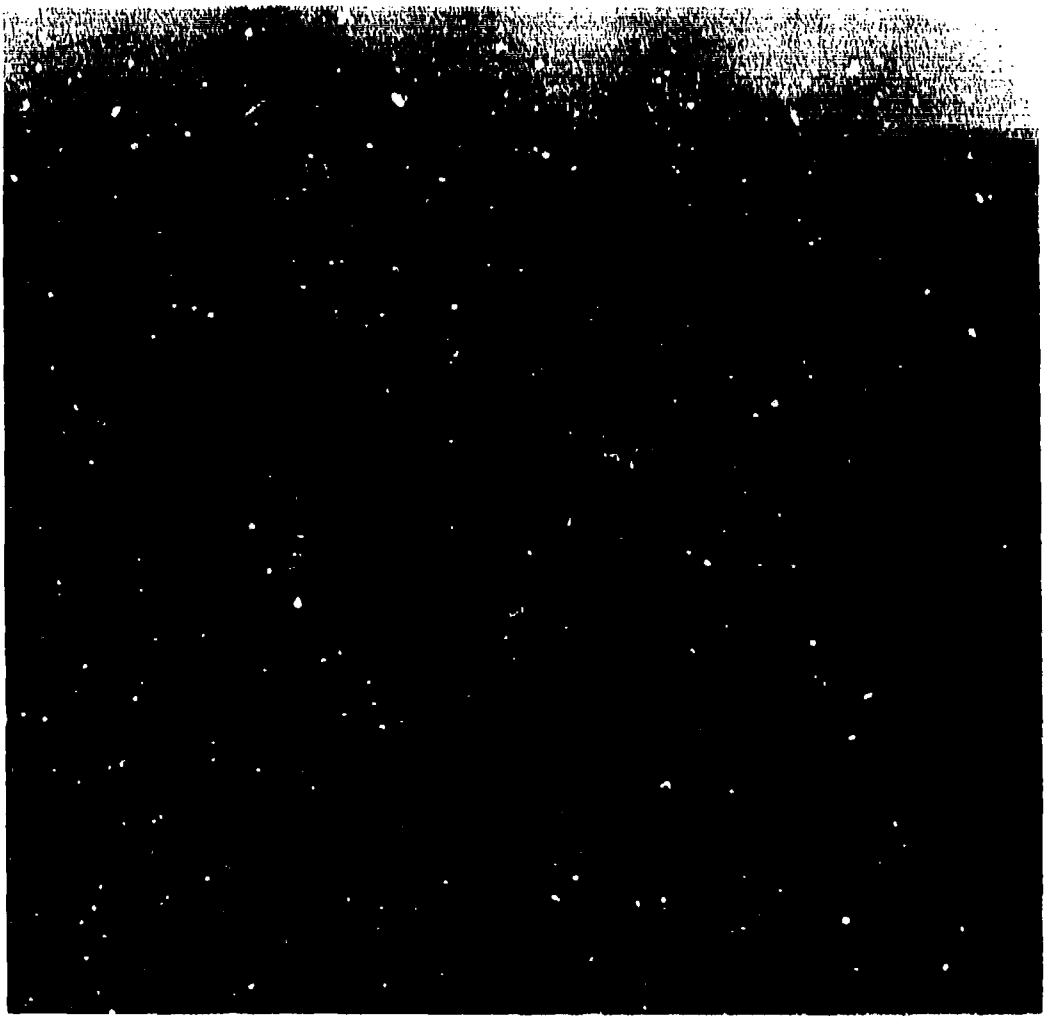

4.5.3a Hybrid Coding (Transform-DPCM) of the Scene of the Tank; Probability of Bit Error = .001; 0.25 bits/pel.

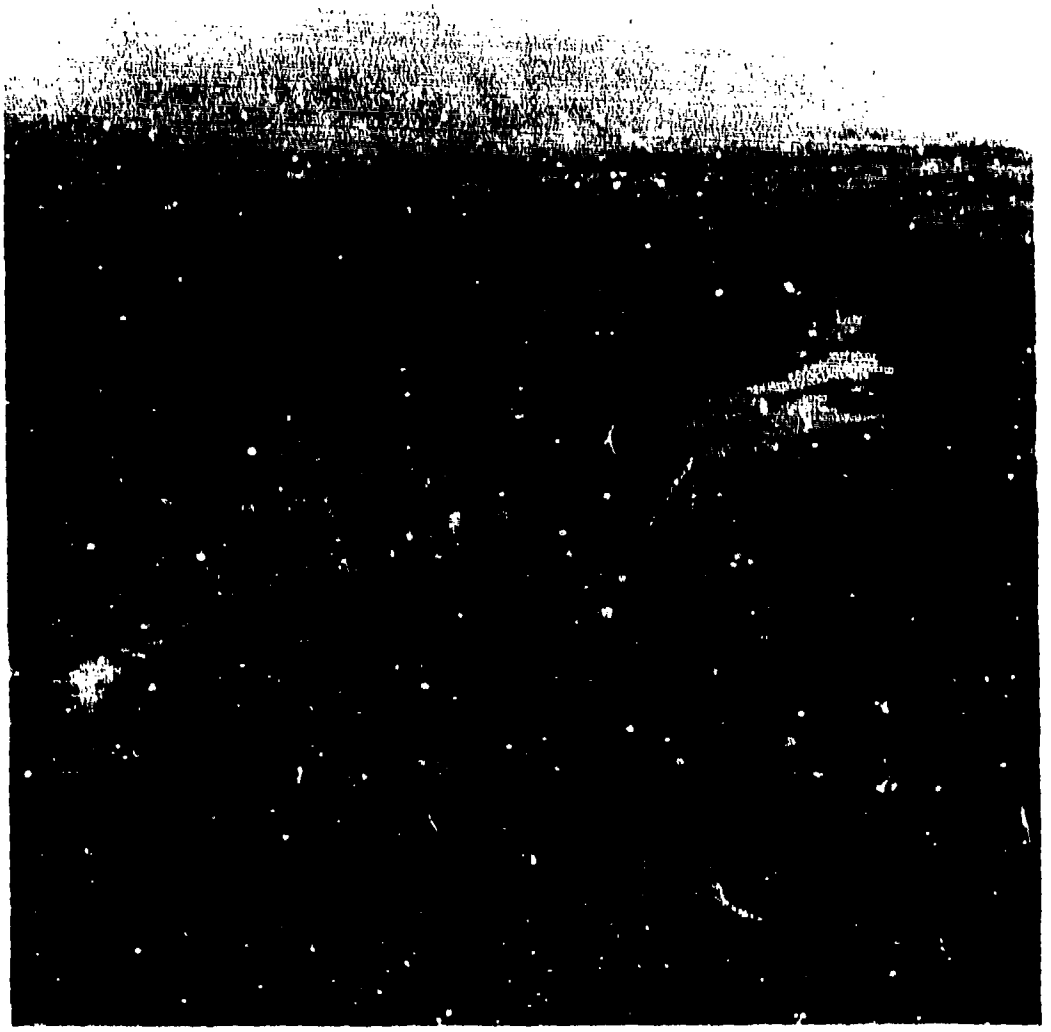

4.5.3b Hybrid Coding (Transform-DPCM)
of the Scene of the Tank;
Probability of Bit Error = .001;
0.5 bits/pel.

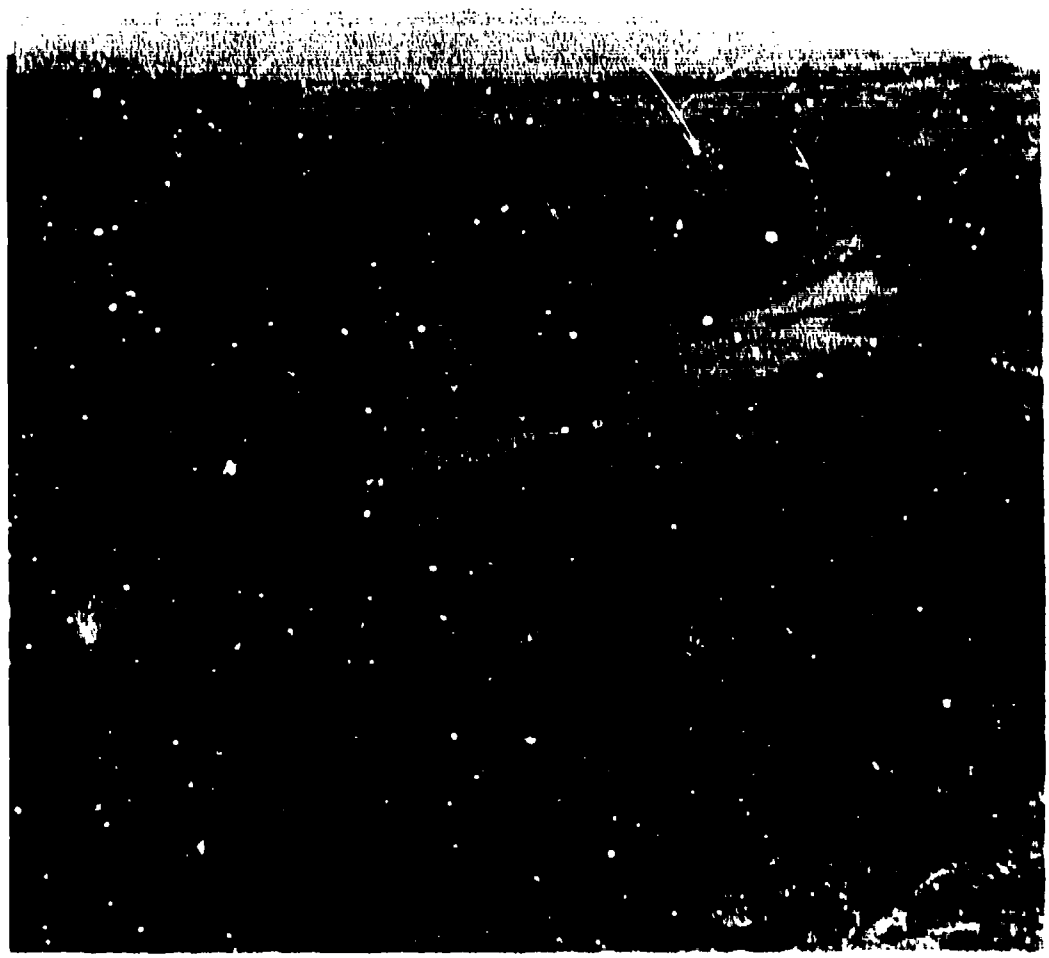

4.5.3c Hybrid Coding (Transform-DPCM) of the Scene of the Tank; Probability of Bit Error = .001; 1.0 bits/pel.

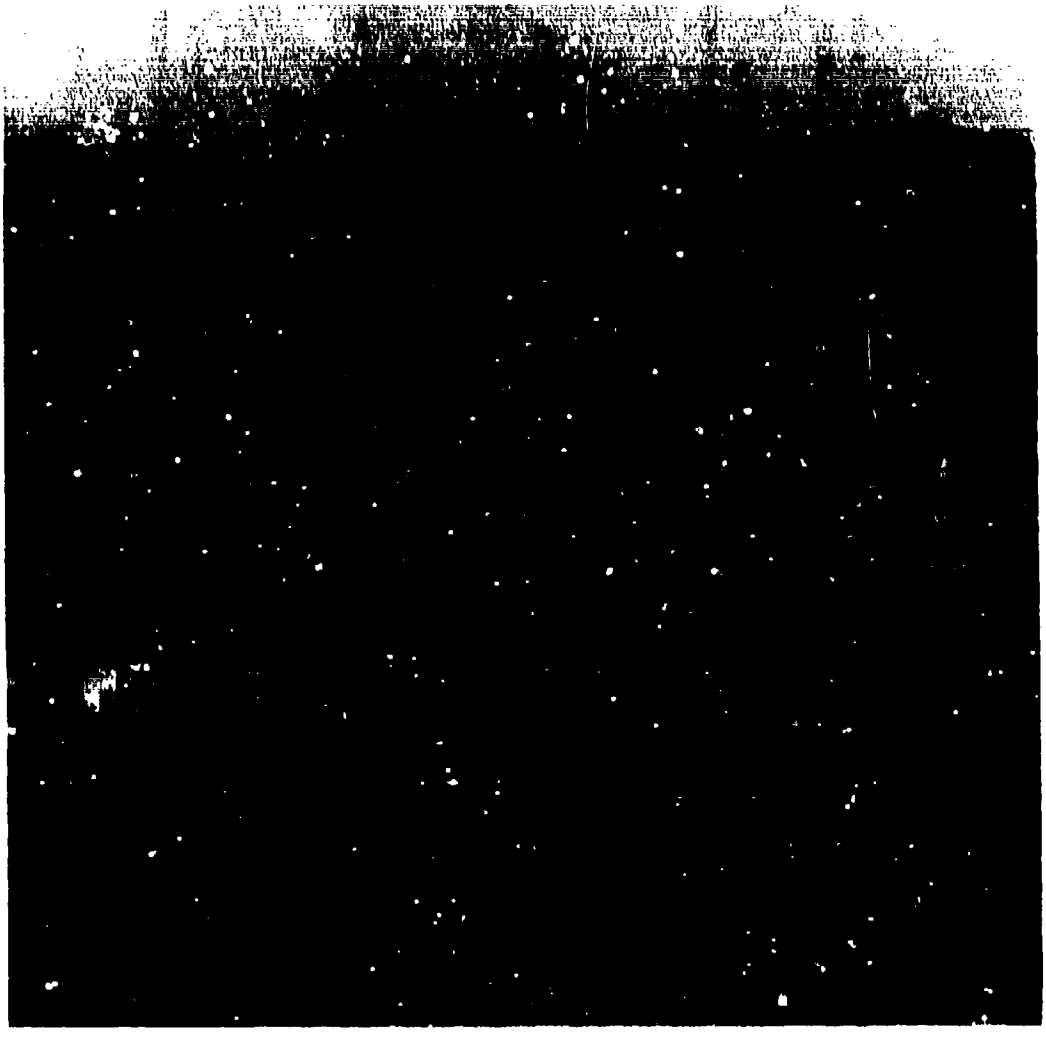

4.5.4a Hybrid Coding (Transform-DPCM) of the Scene of the Tank; Probability of Bit Error = .01; 0.25 bits/pel.

4.5.4b Hybrid Coding (Transform-DPCM) of the Scene of the Tank; Probability of Bit Error = .01; 0.5 bits/pel.

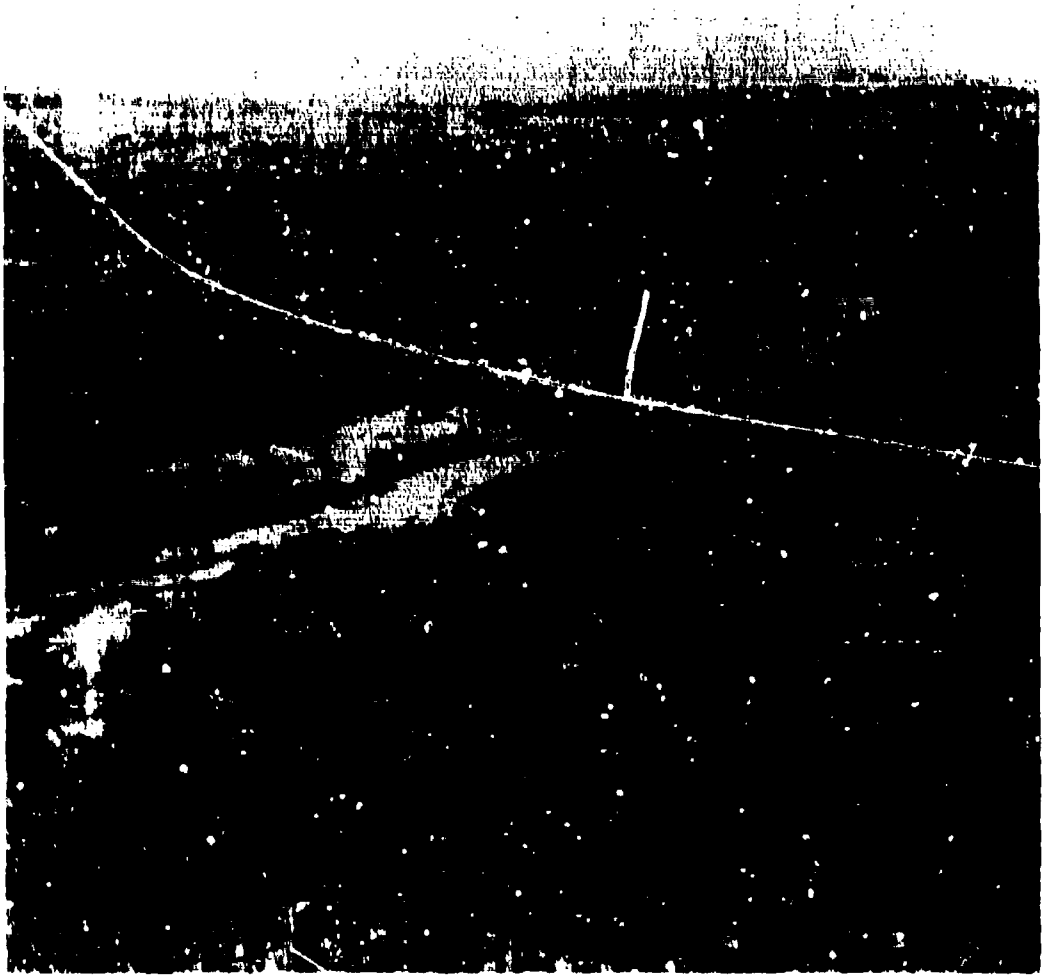

4.5.4c Hybrid Coding (Transform-DPCM)
of the Scene of the Tank;
Probability of Bit Error = .01;
1.0 bits/pel.

Bits Per Pel	MSE	Bits in Error	Pels in Error	Blocks in Error	Prob. of Bit Error
0.25	0.0531	59	59	59	10^{-3}
0.50	0.0416	134	134	134	10^{-3}
1.0	0.0280	273	273	273	10^{-3}
0.25	0.1062	645	642	635	10^{-2}
0.50	0.0966	1319	1306	1274	10^{-2}
1.0	0.0846	2618	2593	2415	10^{-2}

Table 4.5.3. Mean-Squared-Error for the Scene of the Tank Using Hybrid Coding. A Different Prediction Coefficient is Used for Each Coefficient.

In the next section optimization of the Hybrid coding schemes in order to reduce the disastrous effects of channel noise is considered.

4.6 Optimization of The Hybrid Coding Scheme

Results of the previous section have indicated the sensitivity of the Hybrid coding schemes to noisy channel. This was expected using differential encoding. In this section results are given using an optimized system.

The prediction coefficients were optimized taking into account the channel noise as described theoretically in Chapter III. Fig. 4.6.1 shows plots of the optimum prediction coefficient as a function of the number of bits/pel. These curves show that as the channel noise increases the prediction coefficient decreases. This is to be expected since a lower value for the prediction coefficient will allow any error to die out. Similar results have been obtained previously for one-dimensional DPCM by Esman and Wintz [158]. Table 4.6.1 and Fig. 4.6.2 show the MSE obtained using the optimum prediction coefficients. Comparing these results with those given in the previous section, it appears (using the MSE measure) that there is little improvement. Subjectively, the improvements

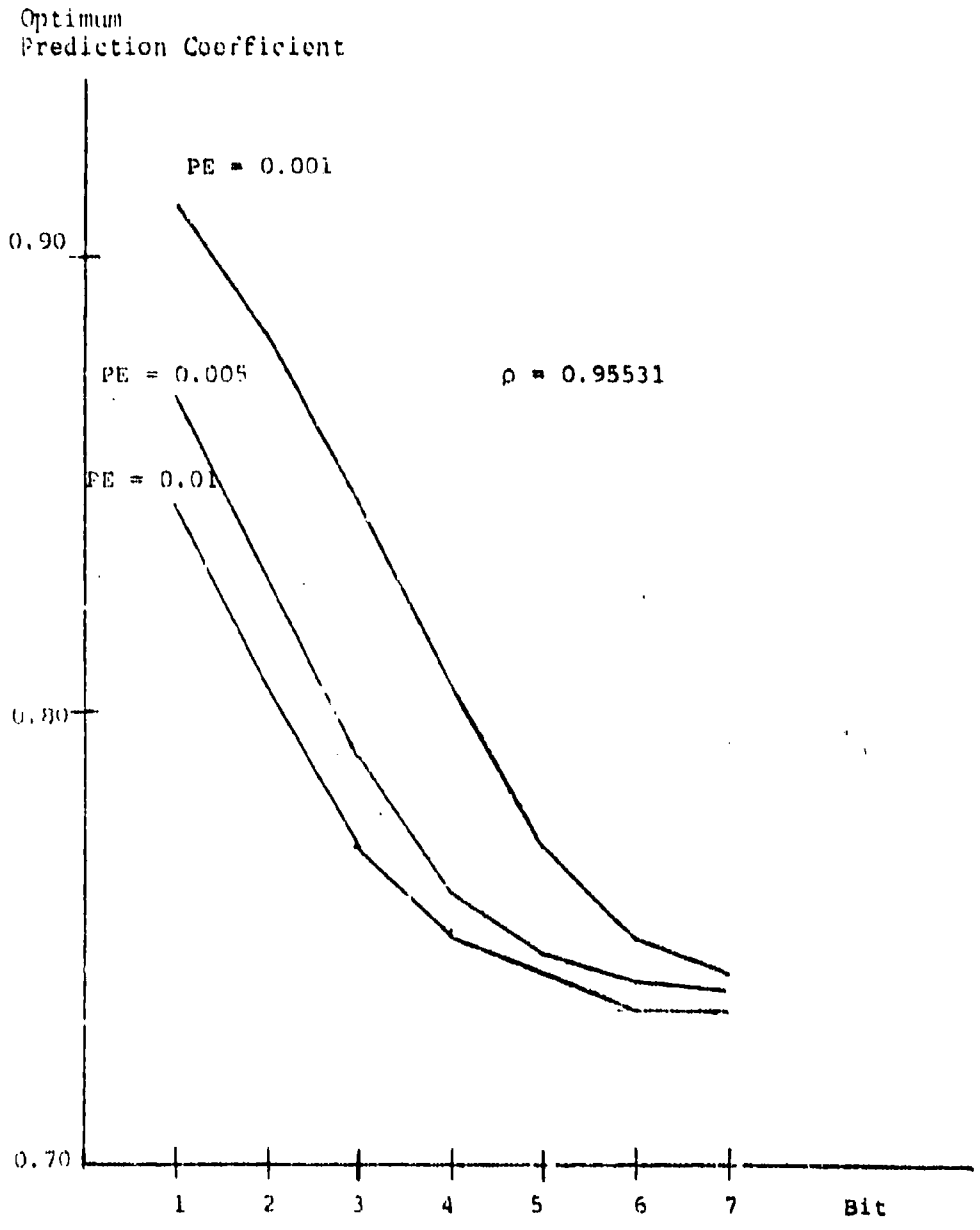

Fig. 4.6.1. Optimum Prediction Coefficient

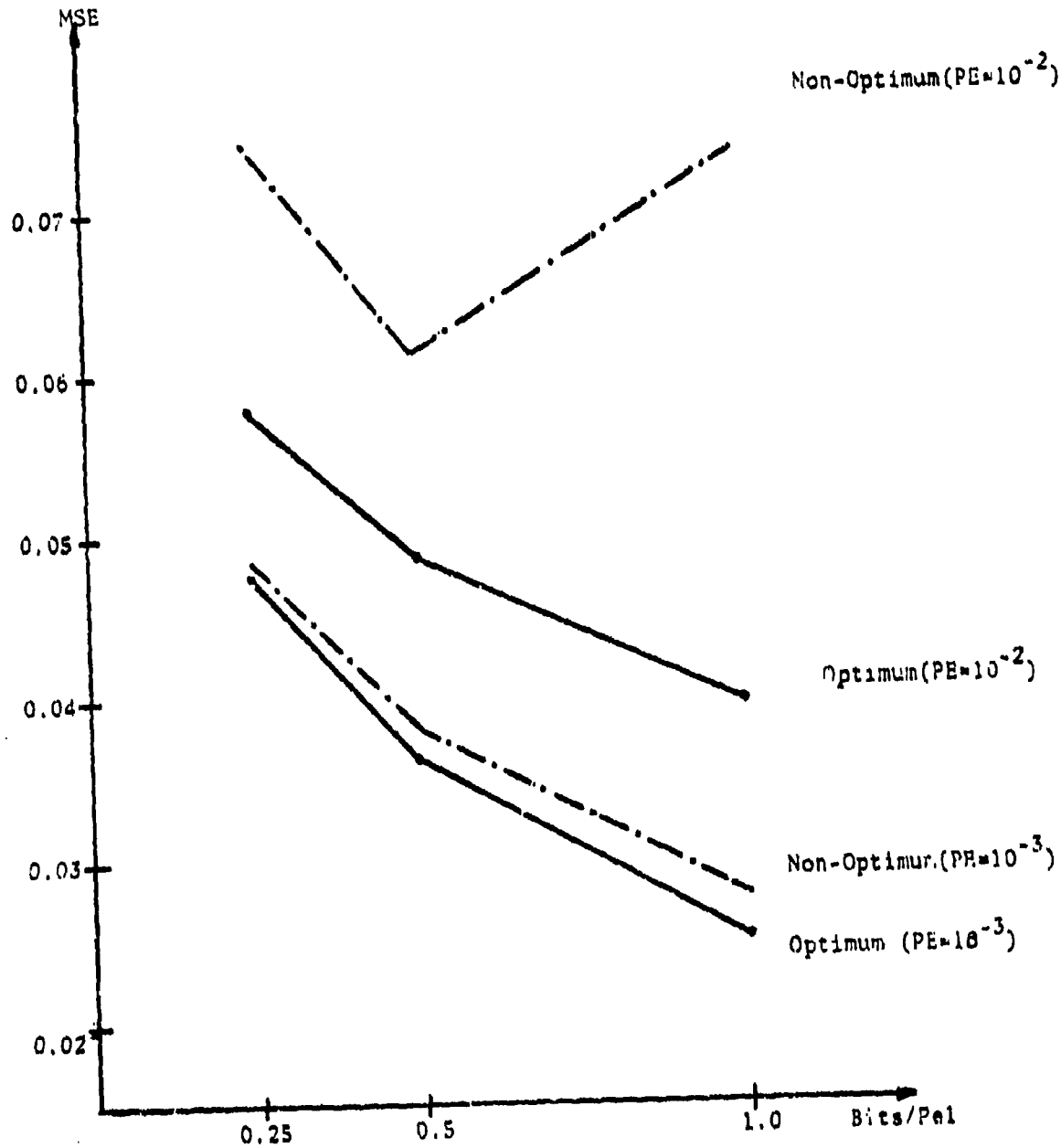

Fig. 4.6.2. Mean-Squared-Error Using Optimum Prediction Coefficient.

	Average Bit/Pel	A = 0.95531	Optimum A's
$PE=10^{-3}$	0.25	0.048595	0.047725
	0.50	0.038294	0.036299
	1.0	0.027681	0.025138
$PE=10^{-2}$	0.25	0.074222	0.057805
	0.50	0.061200	0.048775
	1.0	0.073664	0.039698

Table 4.6.1. The Effects of Using Optimum Prediction Coefficients in the Transform-DPCM System for the Scene of the "Tank".

at high noise levels are substantial. These improvements can be seen by comparing Figs. 4.5.4a,b,c with Figs. 4.6.4a,b,c. It is observed that at high bit-error rates (.01) the streaking is significantly reduced (see Figs. 4.5.4c and 4.6.4c). The improvements at lower error rates are not as apparent. Since it has been shown that the picture quality is insensitive to the prediction coefficients for a noiseless channel, the use of the optimum prediction coefficients would not substantially degrade the picture quality even for noiseless channels.

Comparing Figs. 4.5.2a,b,c, which are pictures obtained using the two-dimensional Hadamard transform, with the results given in Figs. 4.6.4a,b,c for the Hybrid coding scheme, it is seen that using the optimized prediction coefficients, subjectively, gives essentially equivalent results as the transform method; although the MSE using the Hybrid coding schemes is considerably less.

One of the mean disadvantages of the Hybrid coding techniques is its sensitivity to noise. Using the optimum prediction coefficients in the DPCM coders alleviates this to a certain extent. This optimization scheme basically reduces the prediction coefficients so that the errors can damp out more rapidly.

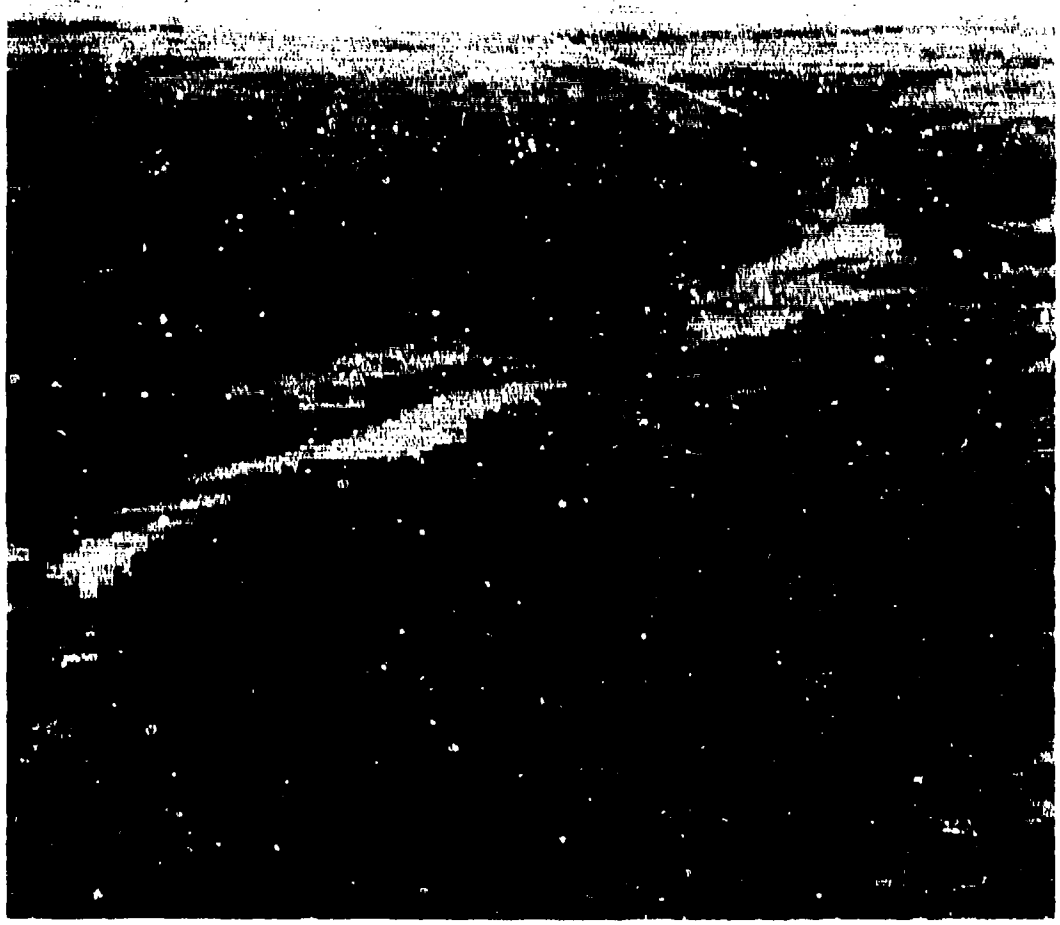

4.6.3c. Hybrid Coding (Transform-DPCM) of the Scene of the Tank Using Optimum Prediction Coefficient; Probability of Error = .001; 0.25 bits/pel.

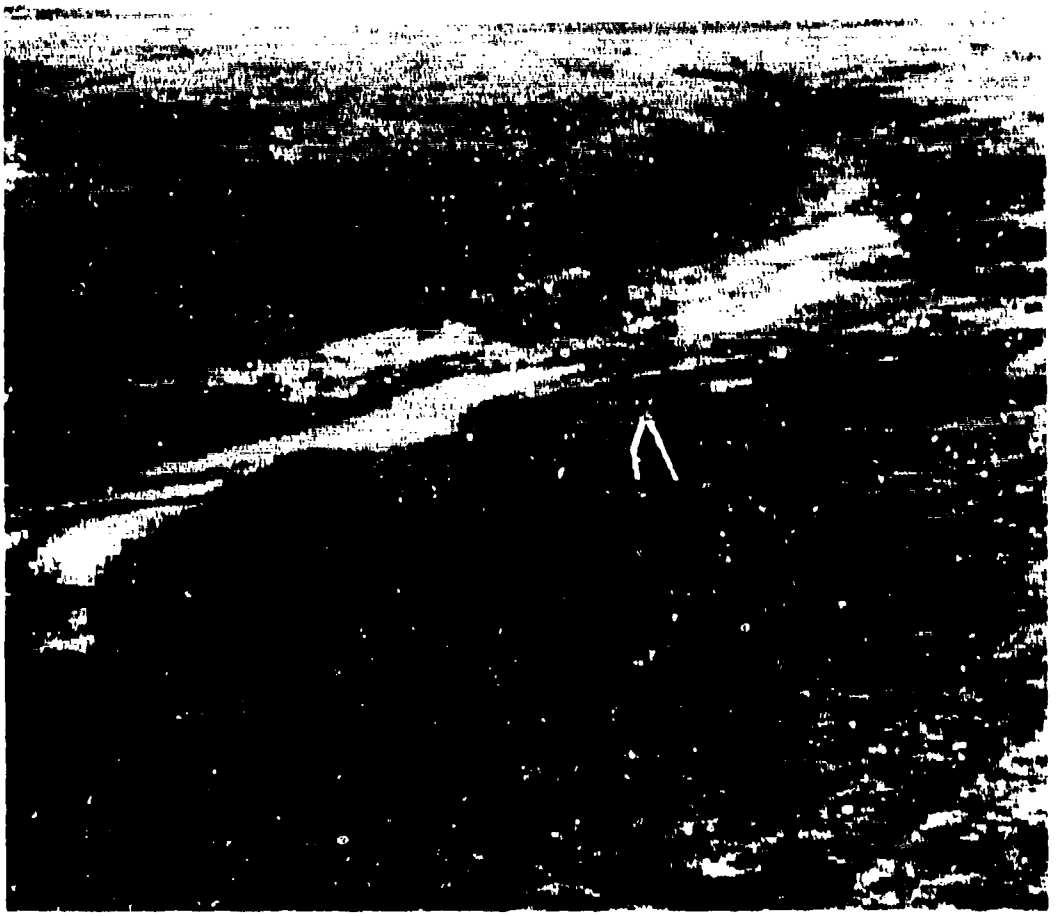

4.6.3b Hybrid Coding (Transform-DPCM) of the Scene of the Tank Using Optimum Prediction Coefficient; Probability of Error = .001; 0.5 bits/pel.

4.6.3c Hybrid Coding (Transform-DPCM) of the Scene of the Tank Using Optimum Prediction Coefficient; Probability of Error = .001; 1.0 bits/pel.

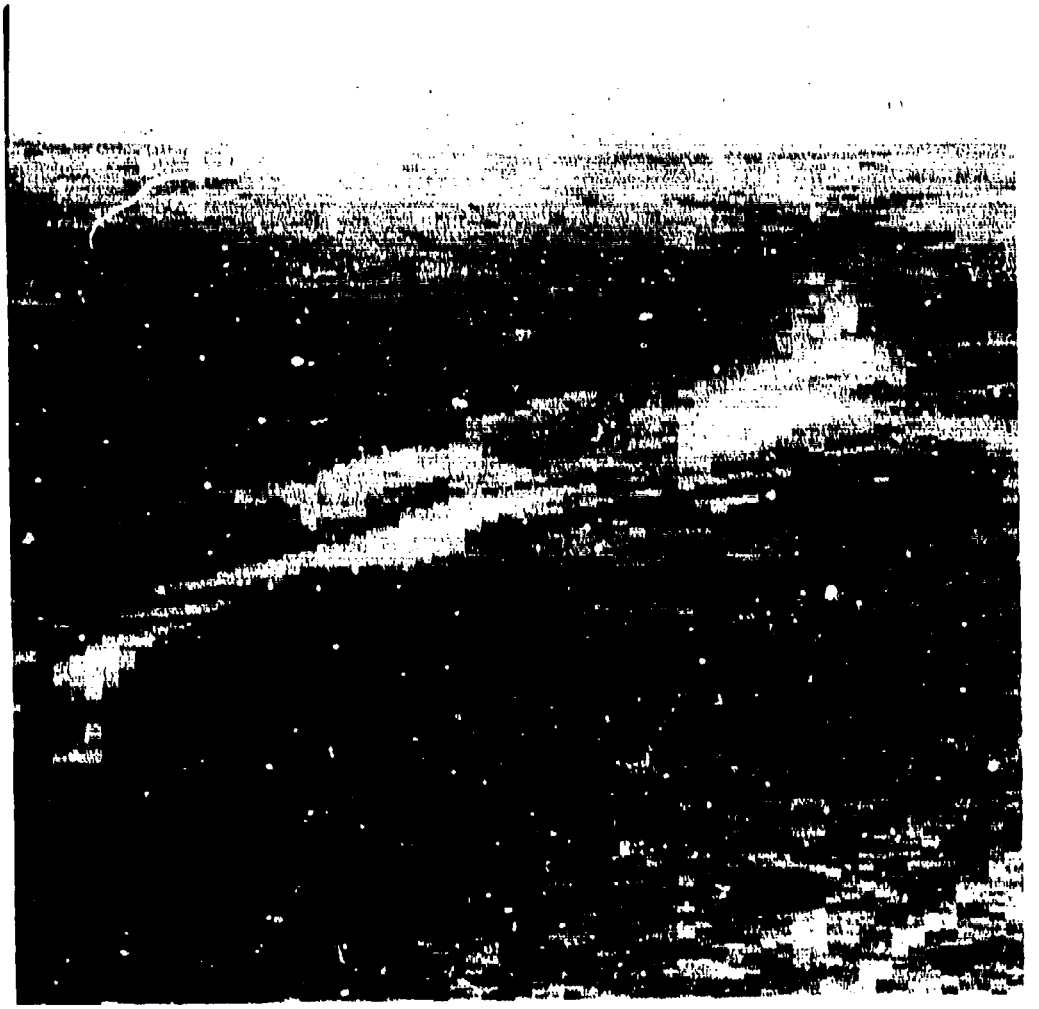

4.6.4a Hybrid Coding (Transform-DPCM) of the Scene of the Tank Using Optimum Prediction Coefficient; Probability of Error = .01; 0.25 bits/pel.

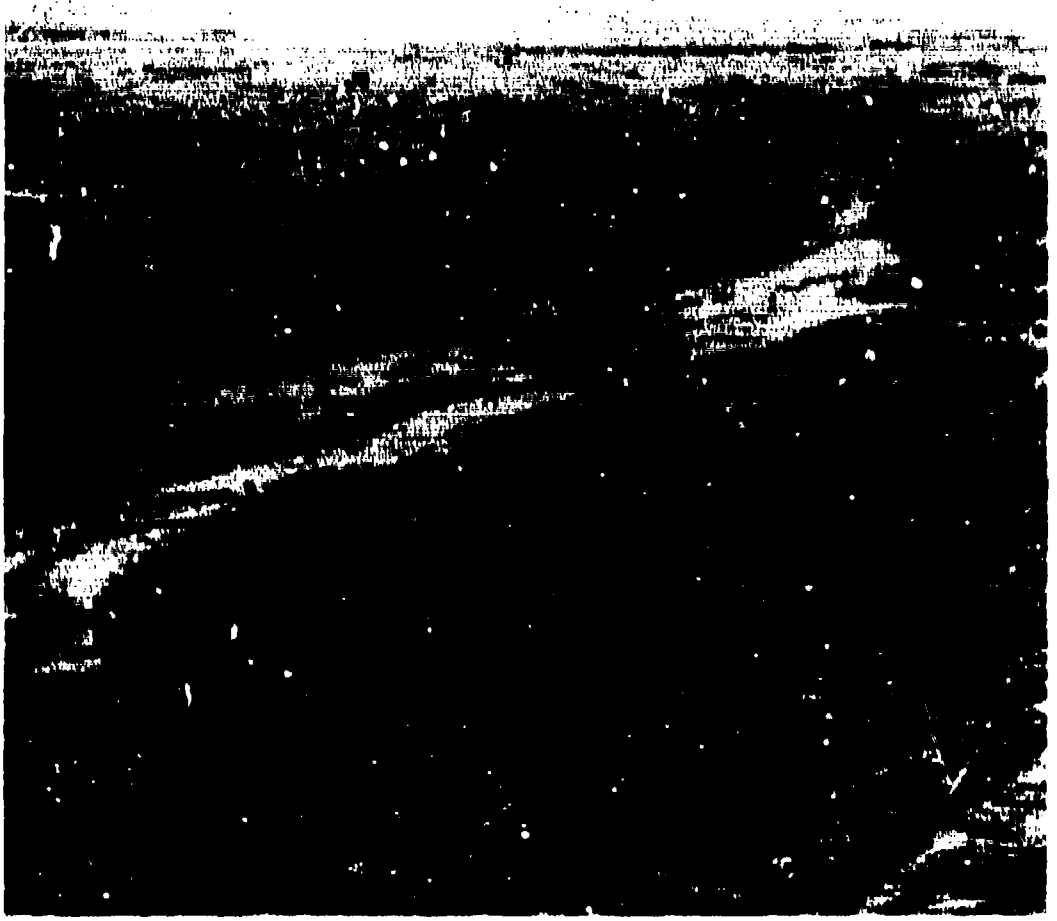

4.6.4b Hybrid Coding (Transform-DPCM) of the Scene of the Tank Using Optimum Prediction Coefficient; Probability of Error = .01; 0.5 bits/pel.

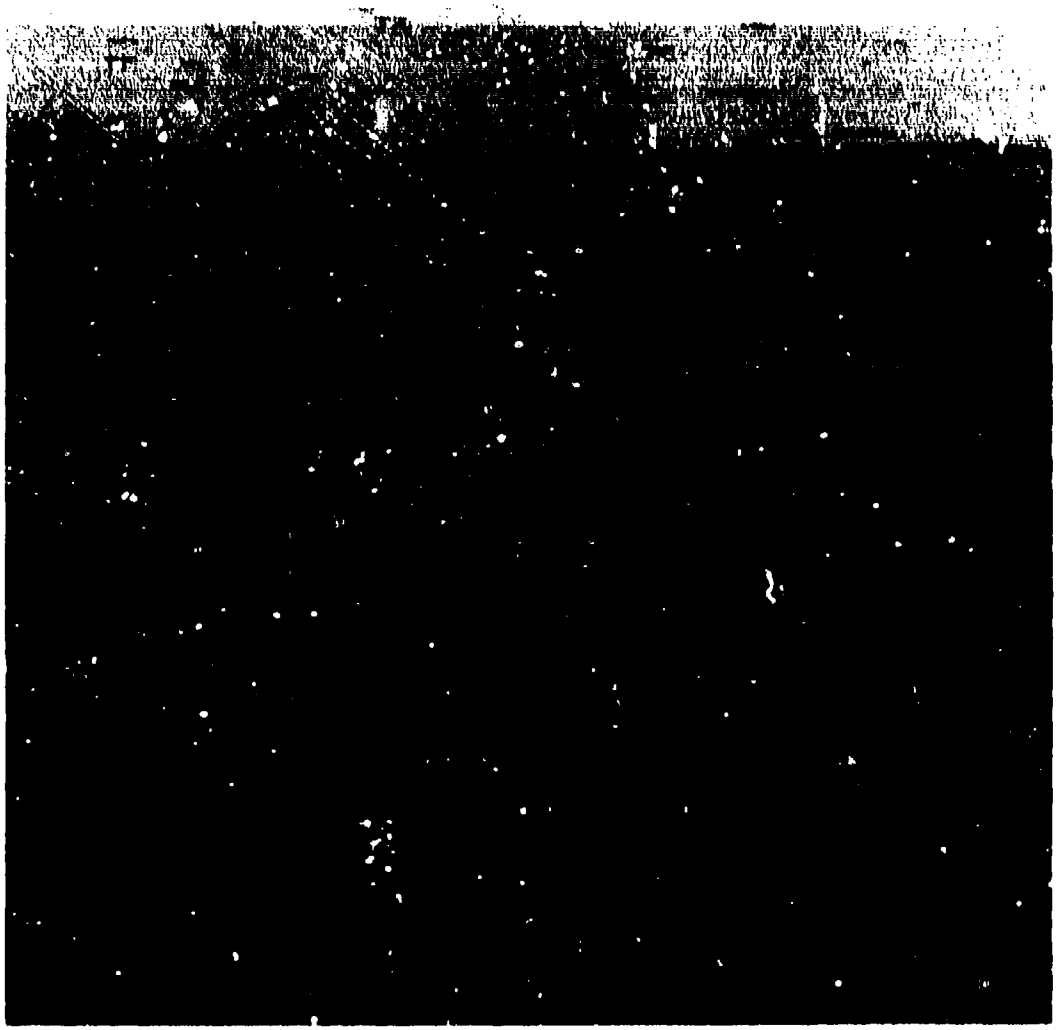

4.6.4c Hybrid Coding (Transform-DPCM) of the Scene of the Tank Using Optimum Prediction Coefficient; Probability of Error = .01; 1.0 bits/pel.

It is the propagation of errors in the differential encoding scheme which causes the severe streaking in the pictures. Periodic resetting or initialization can be used effectively to remedy the propagation of errors in DPCM.

Figs. 4.6.6a,b,c and 4.6.7a,b,c show the effects of resetting the DPCM process after every 16 lines for probability of errors of .001 and 0.01 respectively. Figs. 4.6.8a,b and 4.6.9a,b,c show the result obtained if the periodic resettings are done every 32 lines. In all cases the optimum prediction coefficients were used. Considerable improvements in picture qualities when channel noise is present are obtained using the periodic resetting technique. The results of these pictures are superior to those using the transform techniques in the presence of channel noise.

Since most of the information is contained in the first coefficient, errors in this coefficient would have significant effect on picture quality. The use of error correcting coding on the important coefficients would be advantageous. Figs 4.6.10a,b,c and 4.6.11a,b show results assuming error correcting coding on the first coefficient for probability of bit errors of 0.001 and 0.01 respectively. The bits/pel specified on these pictures do not include the bits required for the error correction; however, since only the first coefficient is assumed to be coded in this manner the average bits/pel will not change significantly. For the results shown in these figures no periodic resetting was done; however, the optimum prediction coefficients were used in the DPCM coders. The results are seen to be significantly better than those obtained using only the optimum prediction coefficients; however, they are poorer than those obtained using periodic resetting.

Figs. 4.6.12a,b,c and 4.6.13a,b,c show the effects of using a prediction coefficient of 0.5. This was an arbitrary choice to see the effects on picture quality. Using such a low value for the prediction coefficient eliminates a considerable amount of the streaking which occurs when either optimum non-noise or optimum-noise

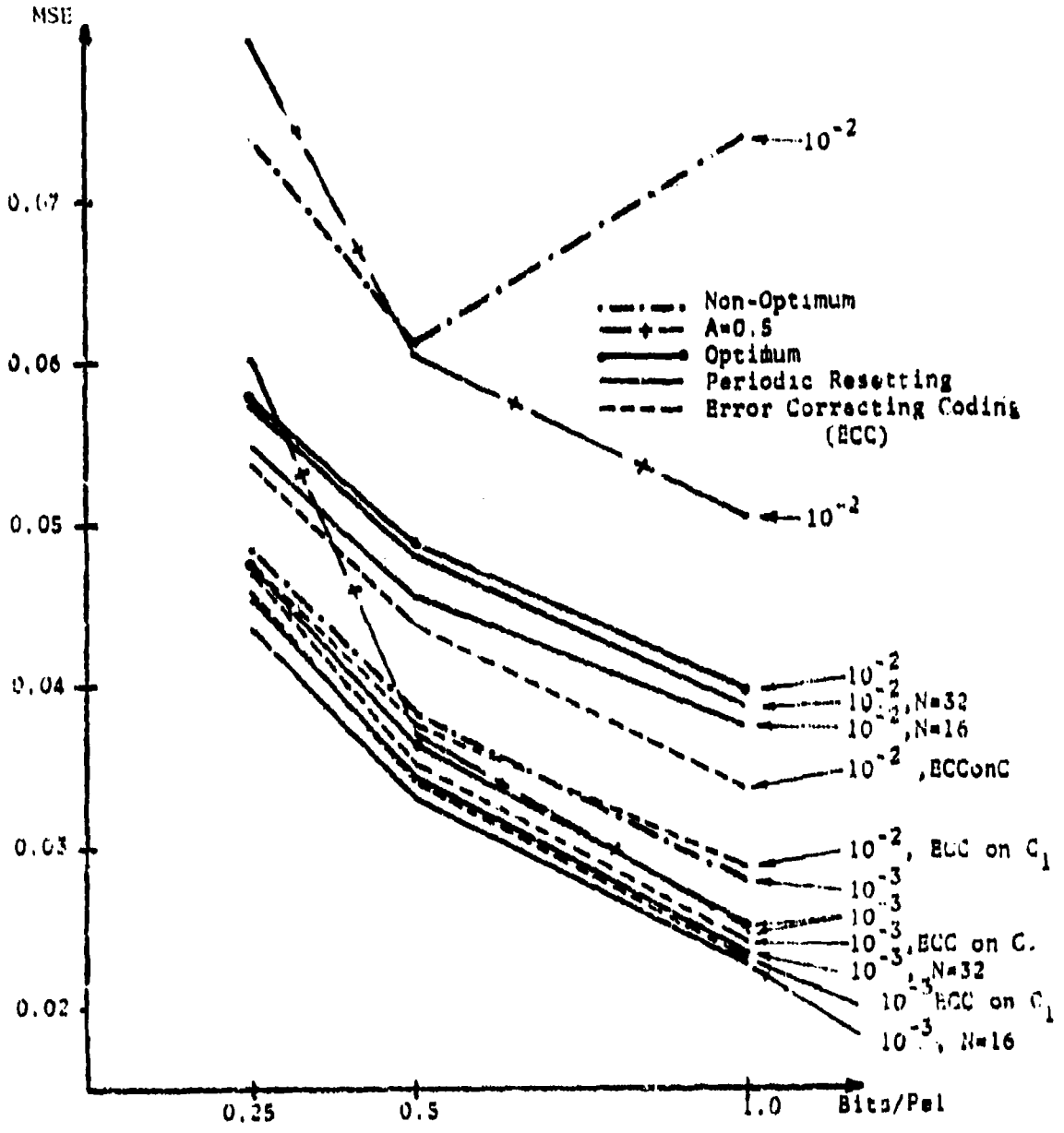

Fig.4.6.5. Hybrid Coding(Noisy Channel) , Mean-Squared-Error.

Reproduced from
best available copy.

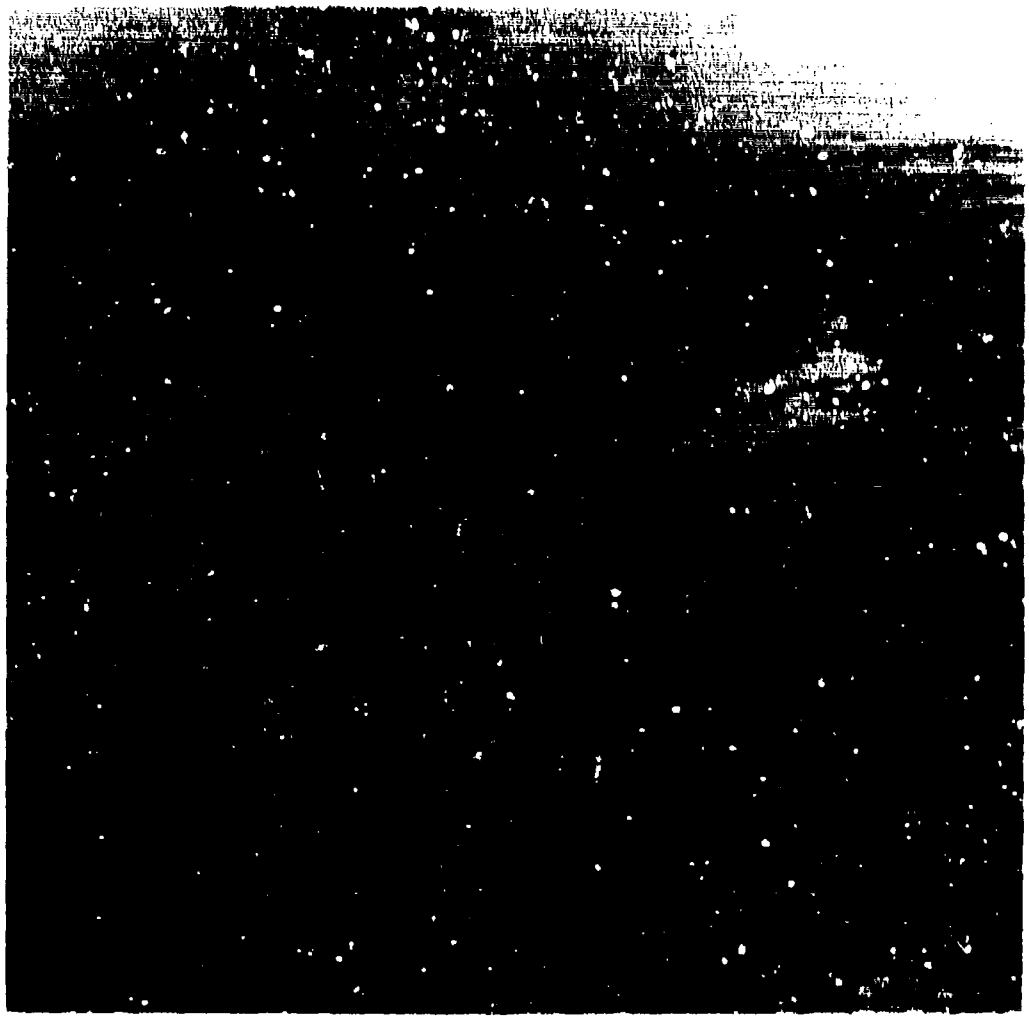

4.6.6a Hybrid Coding Scheme Using Periodic Resetting; N = 16; Probability of Error = .001; 0.25 bits/pel.

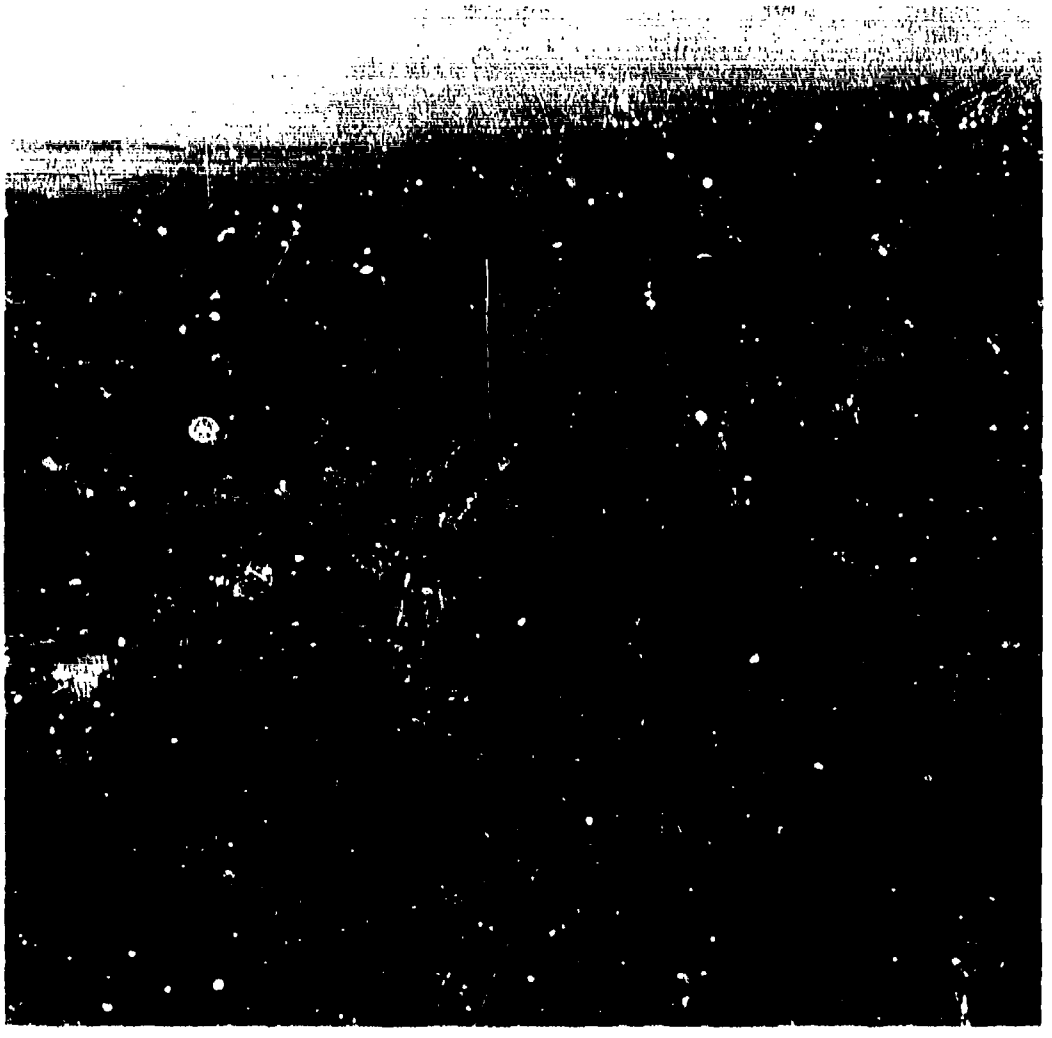

4.6.6r Hybrid Coding Scheme Using Periodic Resetting; N = 16; Probability of Error = .001; 0.5 bits/pel.

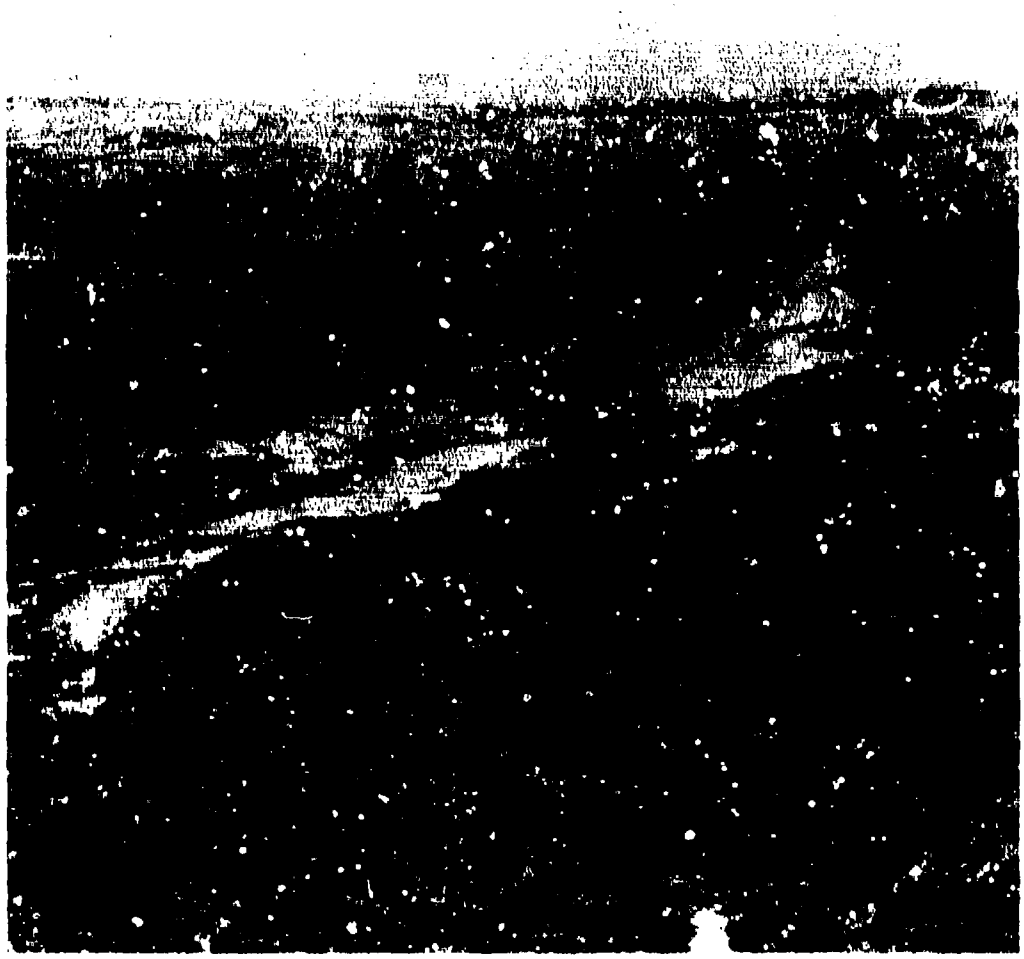

4.6.6c Hybrid Coding Scheme Using Periodic Resetting; N = 16; Probability of Error = .001; 1.0 bits/pel.

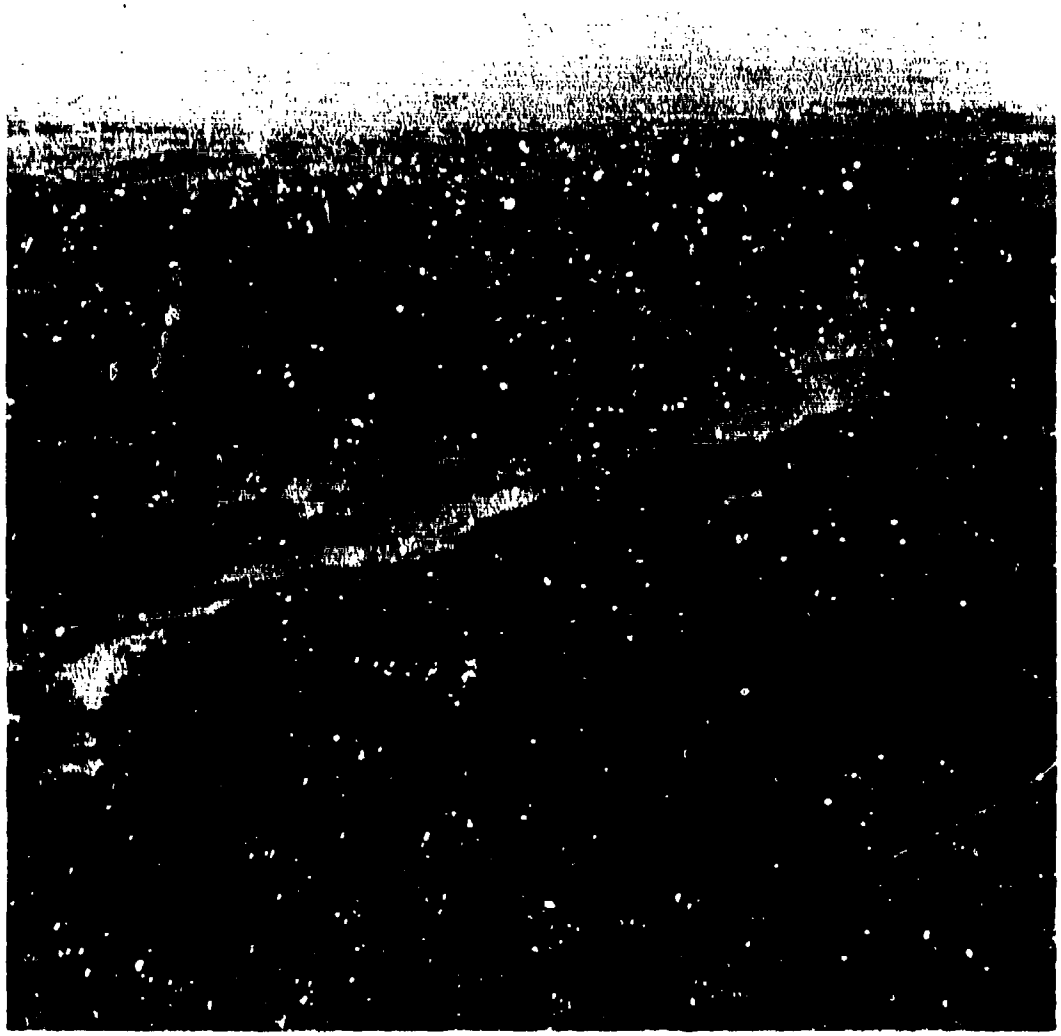

4.6.5c Hybrid Coding Scheme Using Periodic Resetting; N = 16; Probability of Error = .001; 1.0 bits/pel.

4.6.7a Hybrid Coding Scheme Using Periodic Resetting; N = 16; Probability of Error = .01; 0.25 bits/pel.

4.6.7b Hybrid Coding Scheme Using Periodic Resetting; N = 16; Probability of Error = .01; 0.5 bits/pel.

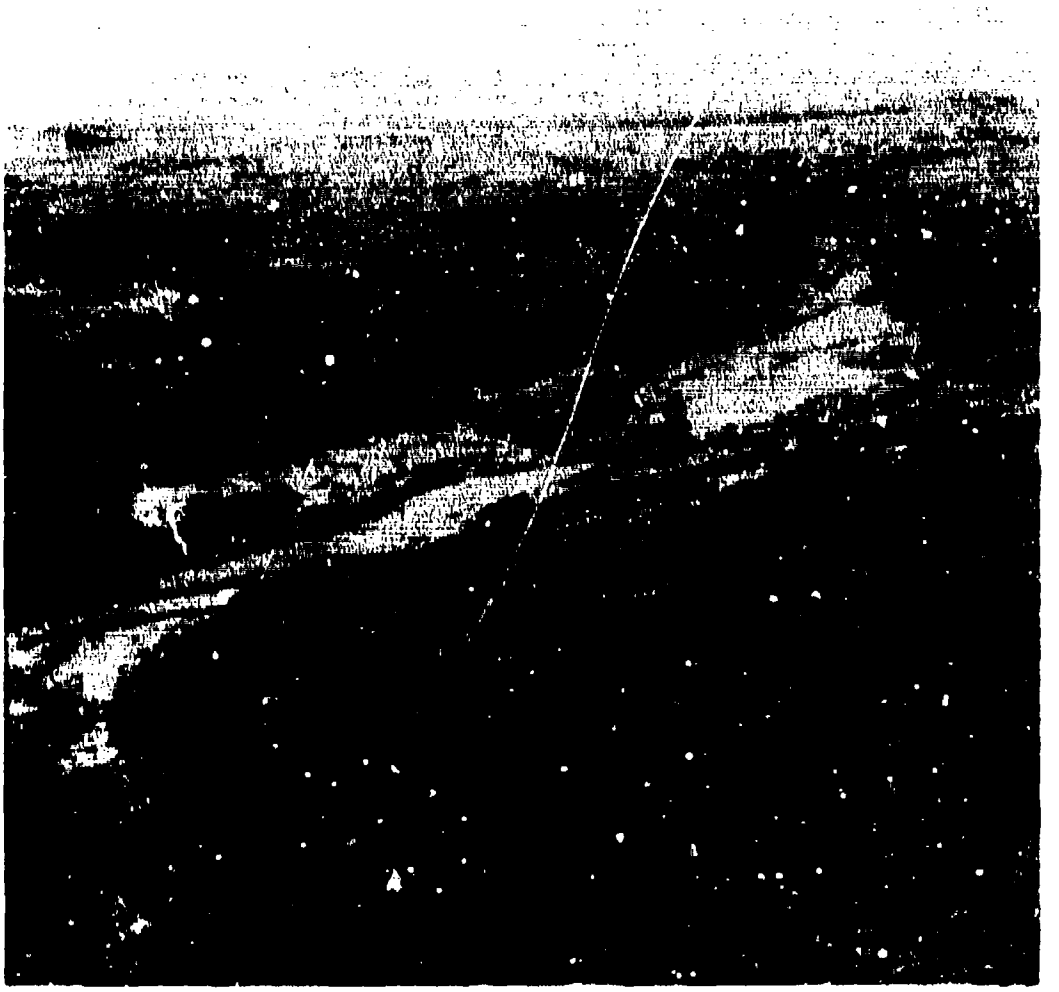

4.6.7c Hybrid Coding Scheme Using Periodic Resetting; N = 16; Probability of Error = .01; 1.0 bits/pel.

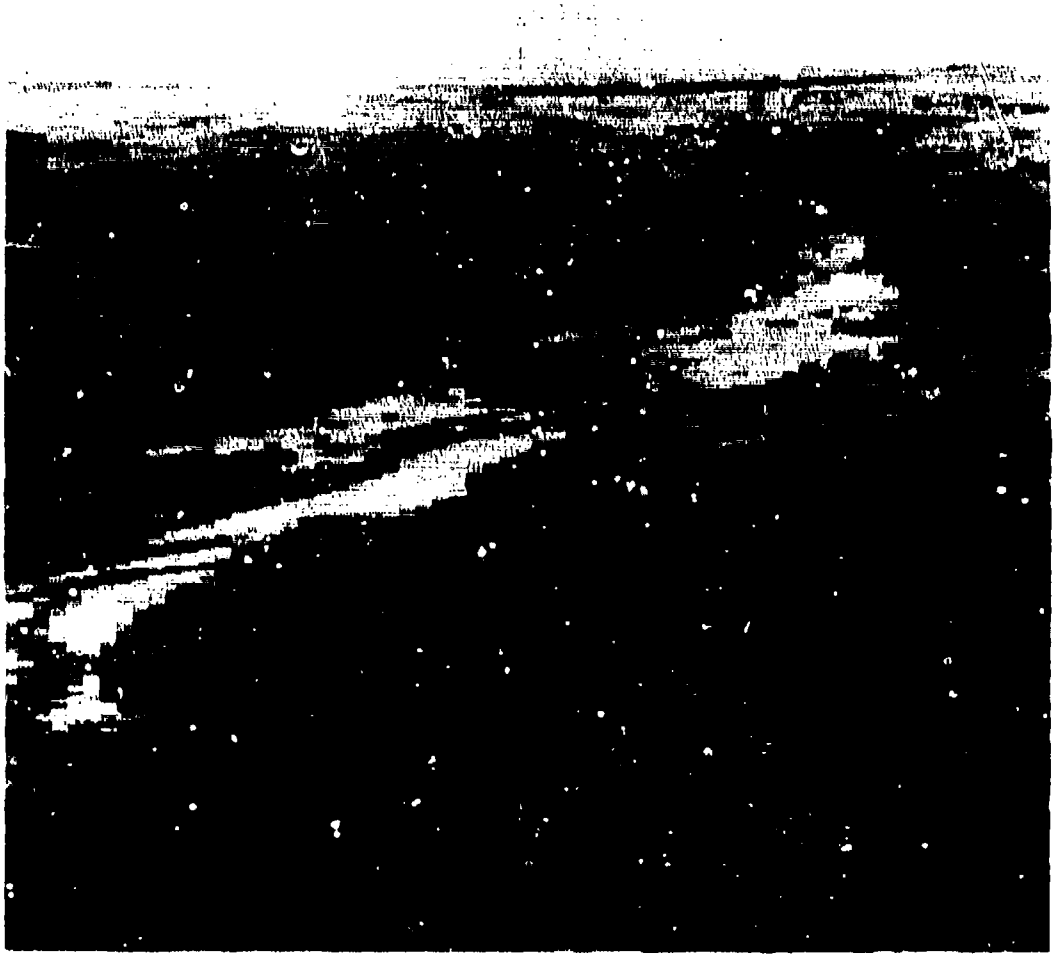

4.6.8a Hybrid Coding Scheme Using Periodic Resetting; N = 32; Probability of Error = .001; 0.25 bits/pel.

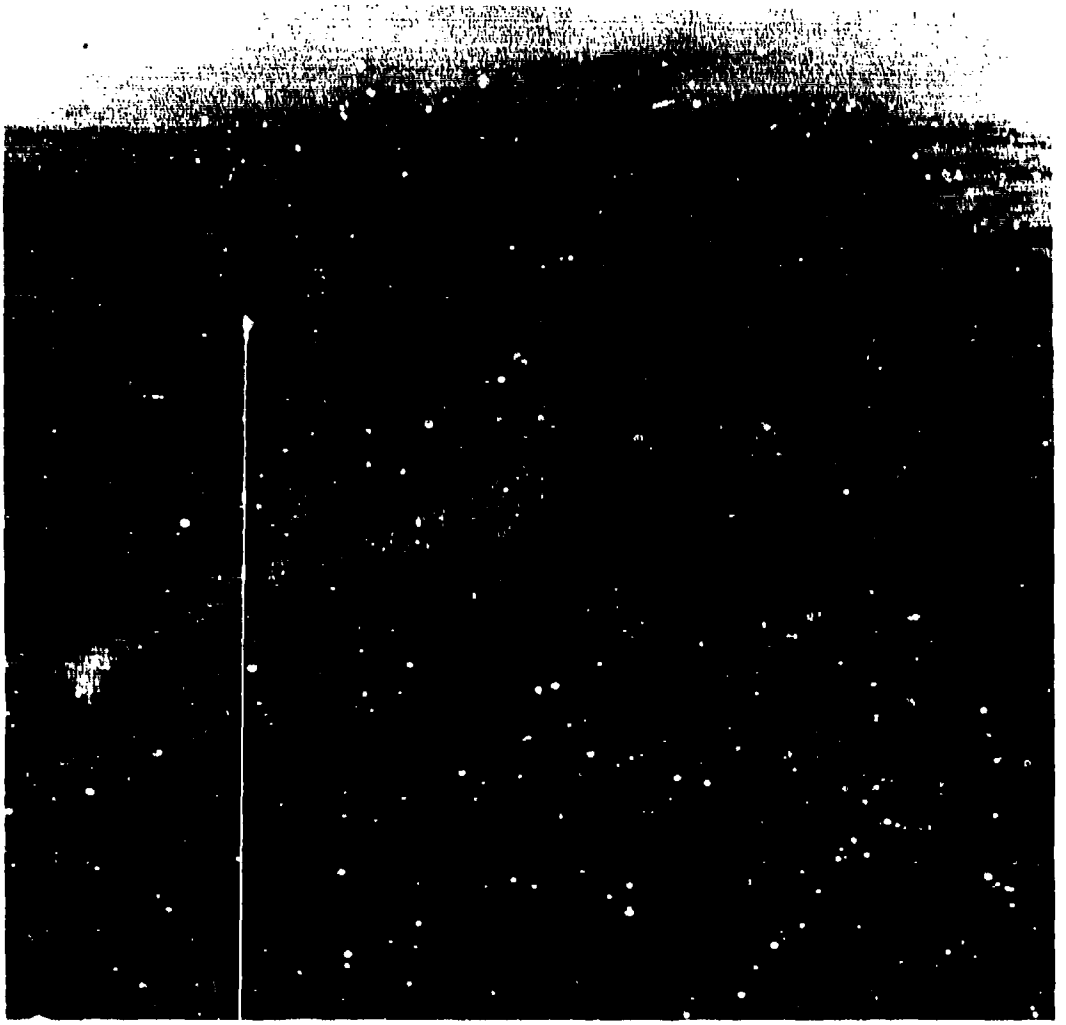

4.6.8b Hybrid Coding Scheme Using Periodic Resetting; N = 32; Probability of Error = .001; 0.5 bits/pel.

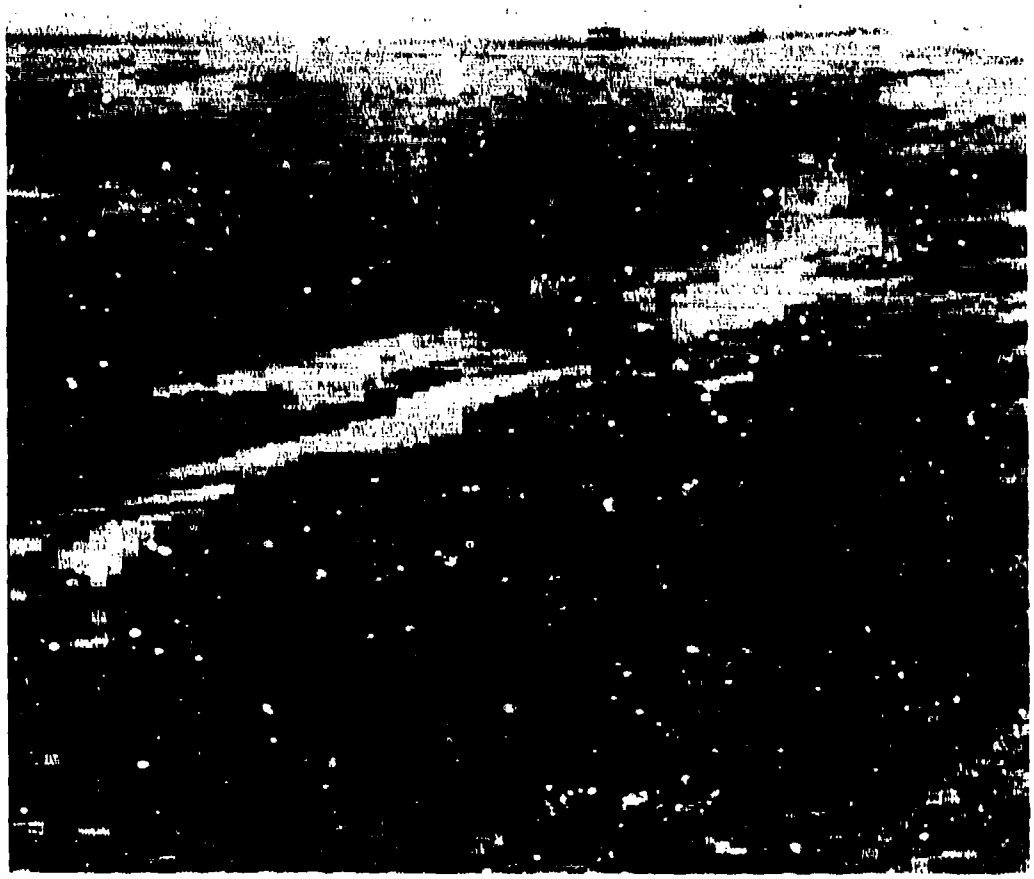

4.6 9a Hybrid Coding Scheme Using Periodic Resetting; N = 32; Probability of Error = .01; 0.25 bits/pel.

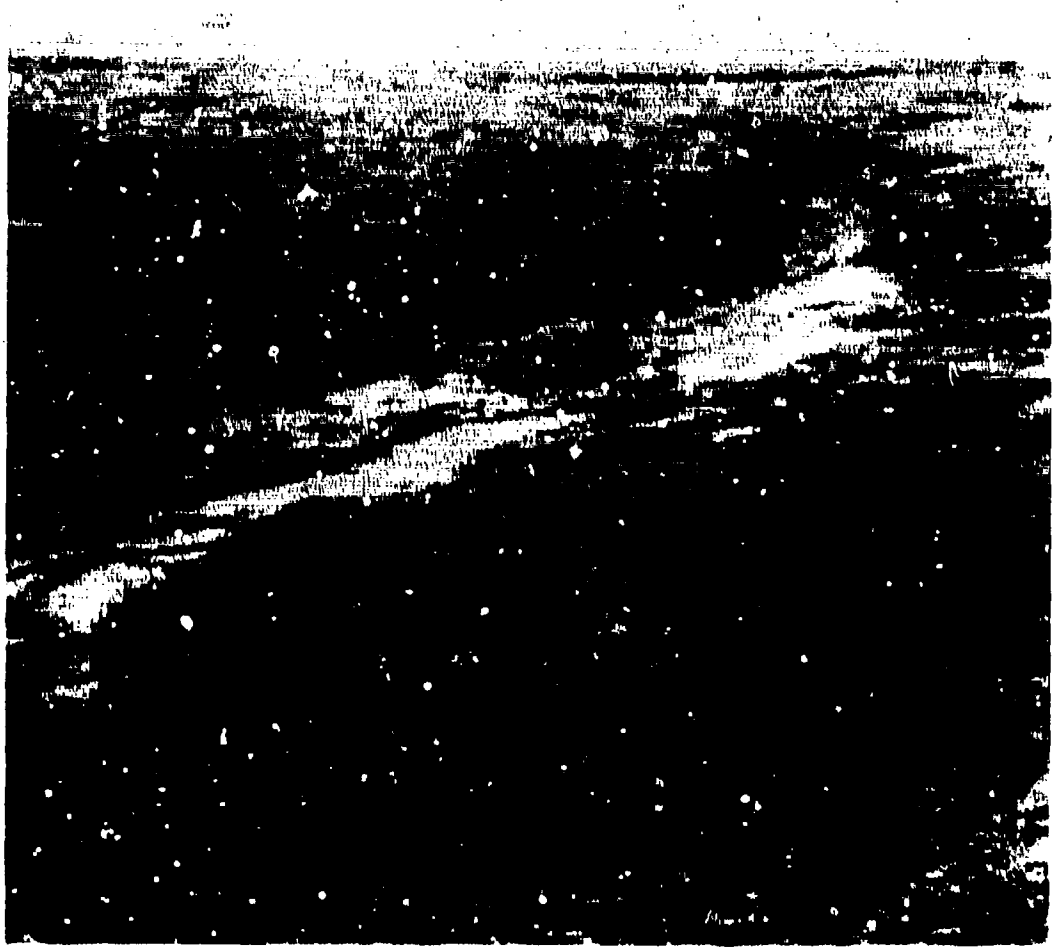

4.6.9b Hybrid Coding Scheme Using Periodic Resetting; N = 32; Probability of Error = .01; 0.5 bits/pel.

4.6.9c Hybrid Coding Scheme Using Periodic Resetting; N = 32; Probability of Error = .01; 1.0 bits/pel.

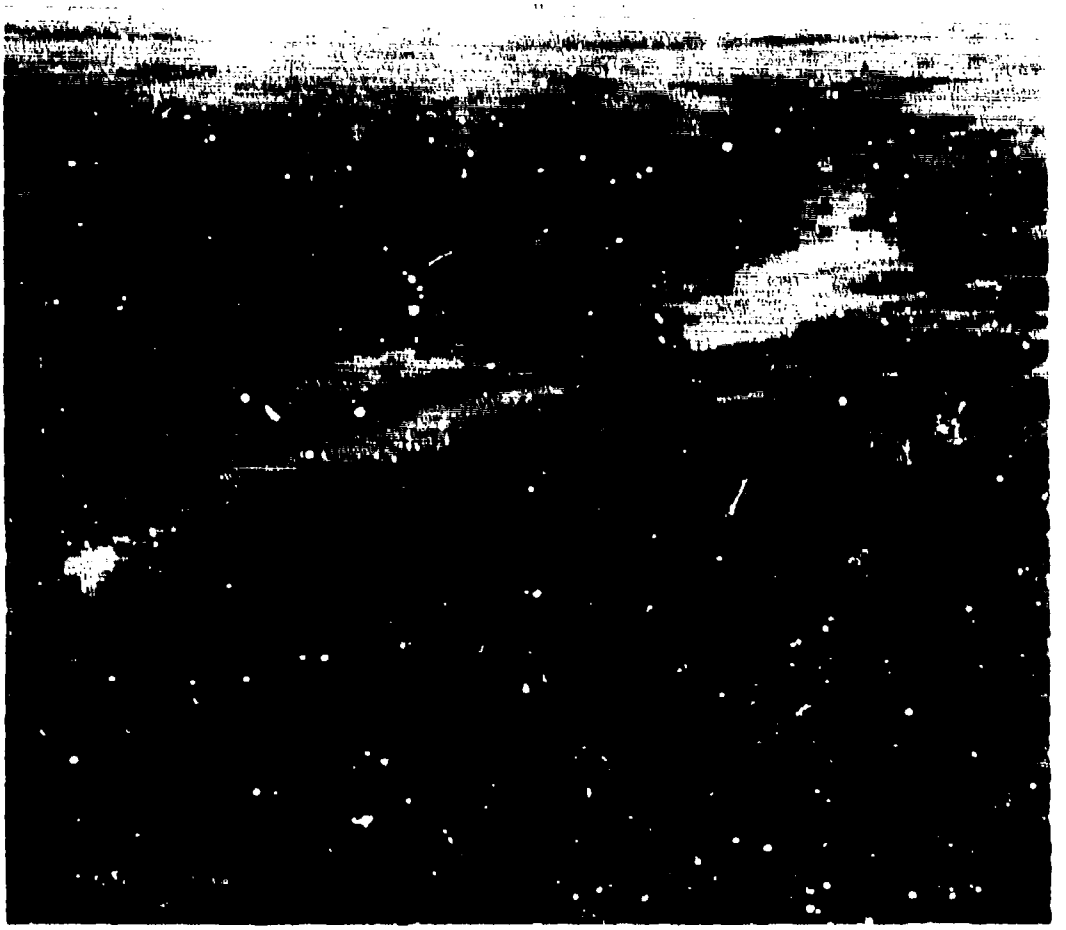

4.6.10a Hybrid Coding Scheme Using Error Correcting Code on First Coefficient; Probability of Error = .001; 0.25 bits/pel.

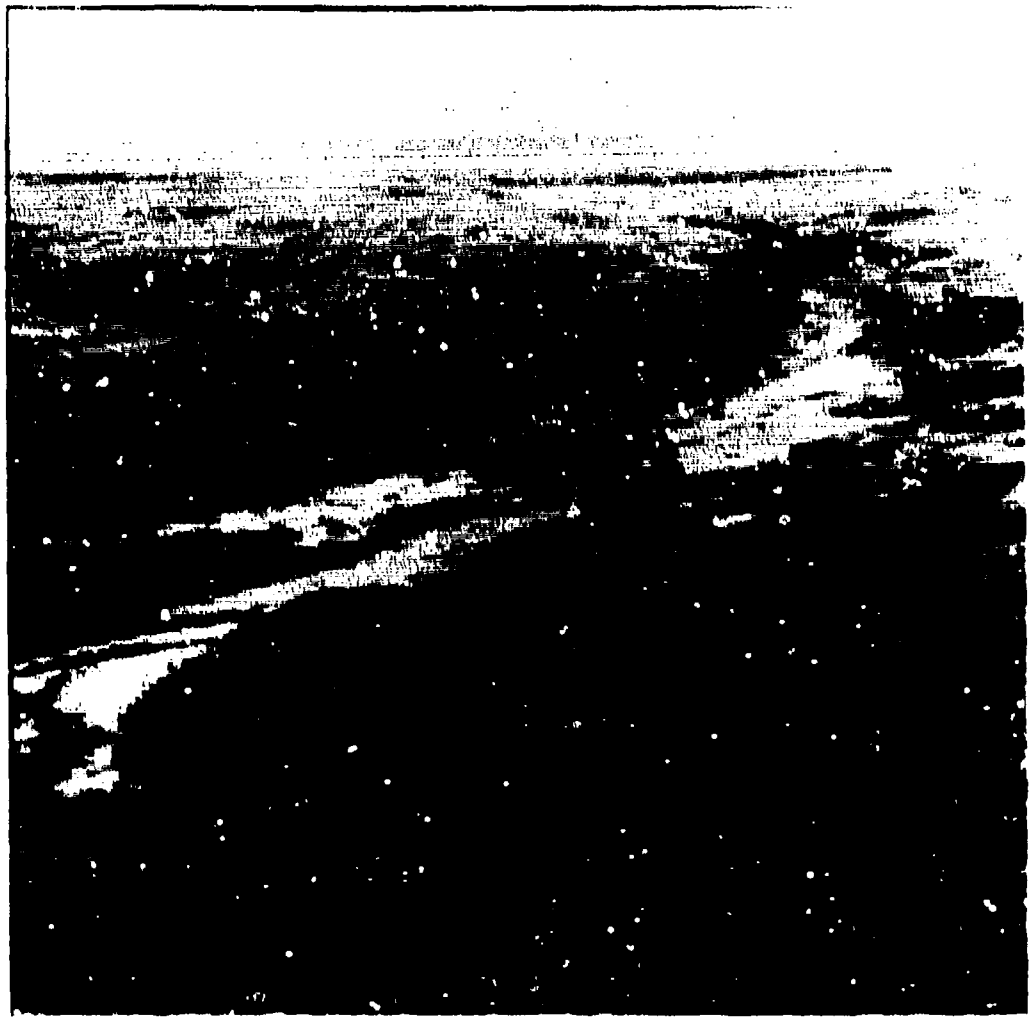

4.6.10b Hybrid Coding Scheme Using Error Correcting Code on First Coefficient; Probability of Error = .001; 0.5 bits/pel.

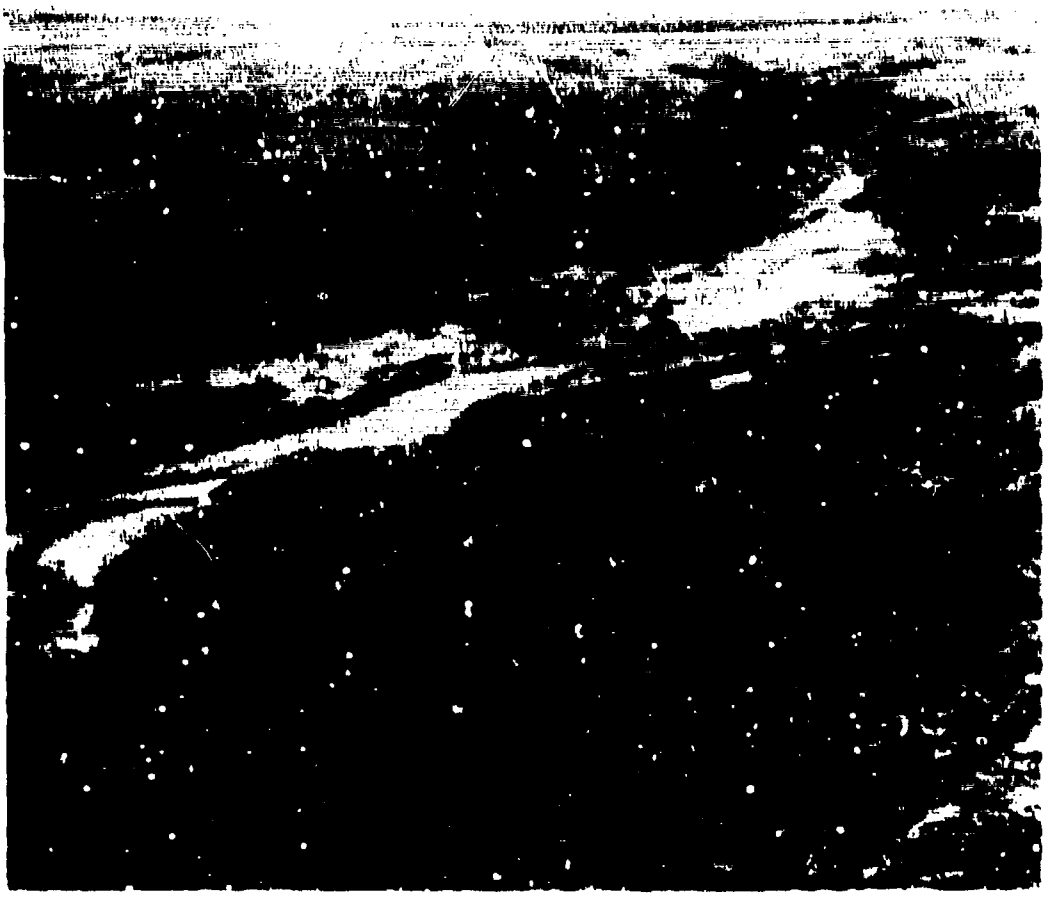

4.6.10c Hybrid Coding Scheme Using Error Correcting Code on First Coefficient; Probability of Error = .001; 1.0 bits/pel.

4.6.11a Hybrid Coding Scheme Using Error Correcting Code on First Coefficient; Probability of Error = .01; 0.25 bits/pel.

4.6.11b Hybrid Coding Scheme Using Error Correcting Code on First Coefficient; Probability of Error = .01; 1.0 bits/pel.

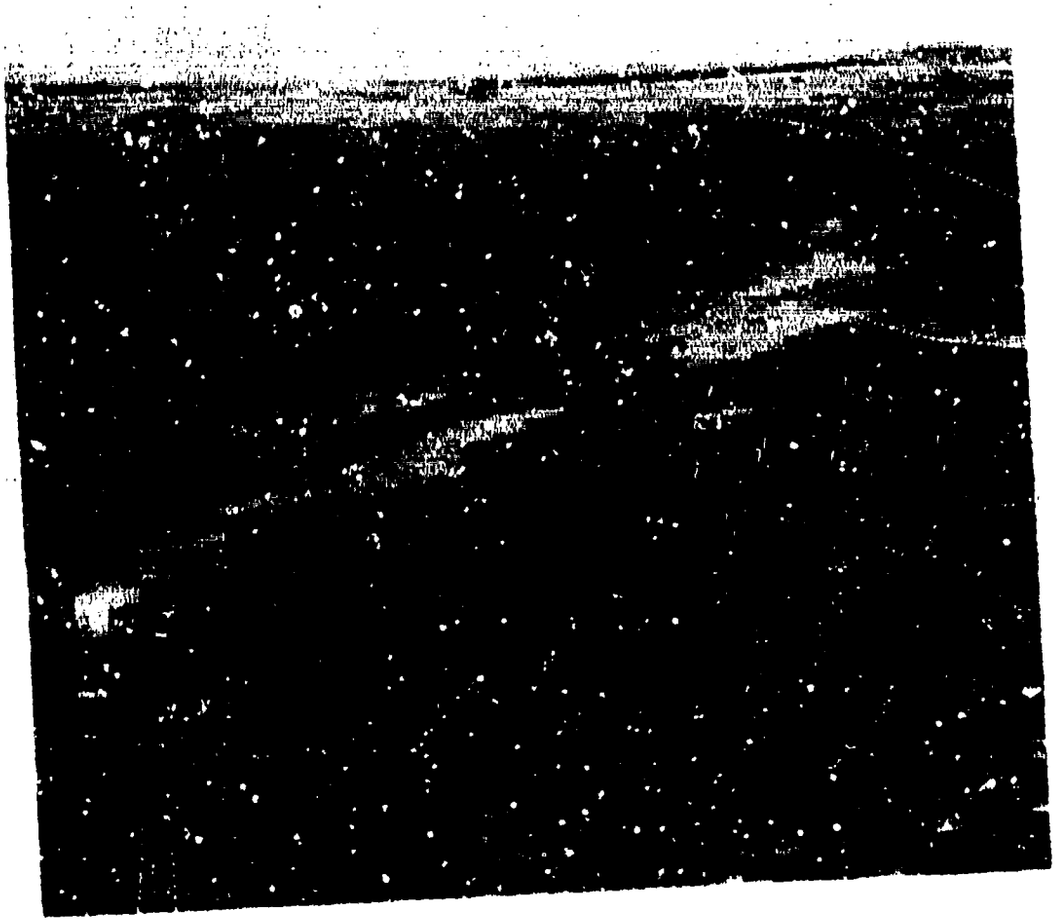

4.6.12a Hybrid Coding Scheme Using Prediction Coefficient of 0.5 (Non-Optimum); Probability of Error = .001; 0.25 bits/pel.

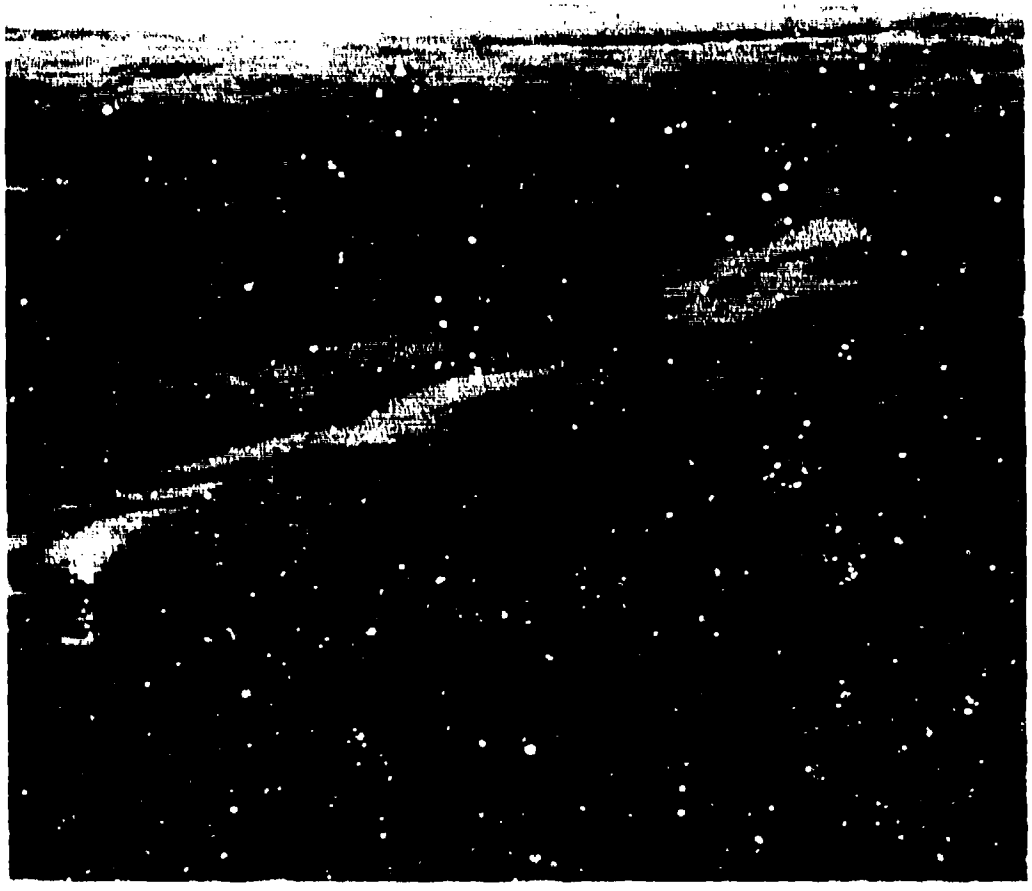

4.6.12b Hybrid Coding Scheme Using Prediction Coefficient of 0.5 (Non-Optimum); Probability of Error = .001; 0.5 bits/pel.

4.6.12c Hybrid Coding Scheme Using Prediction Coefficient of 0.5 (Non-Optimum); Probability of Error = .001; 1.0 bits/pel.

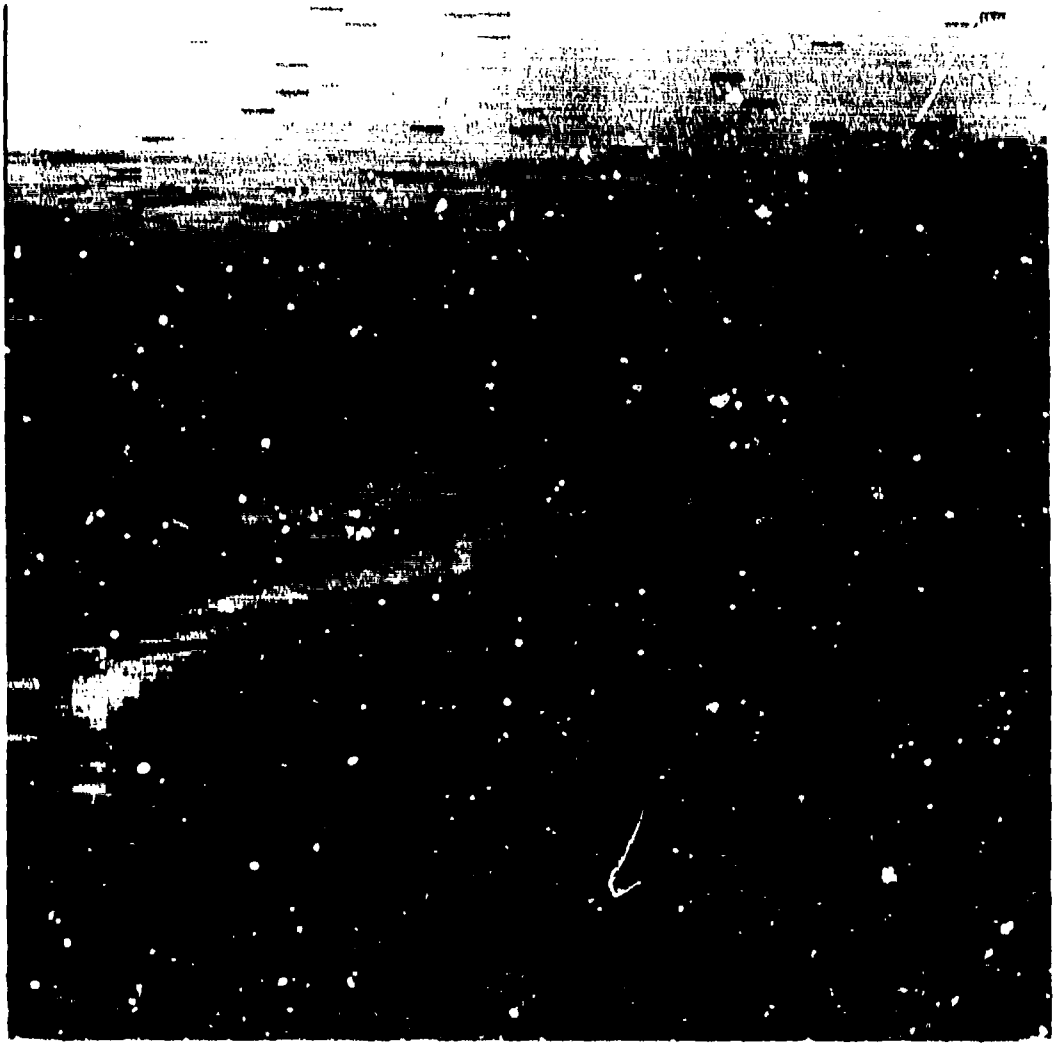

4.6.13a Hybrid Coding Scheme Using Prediction Coefficient of 0.5 (Non-Optimum) Probability of Error = .01; 0.25 bits/pel.

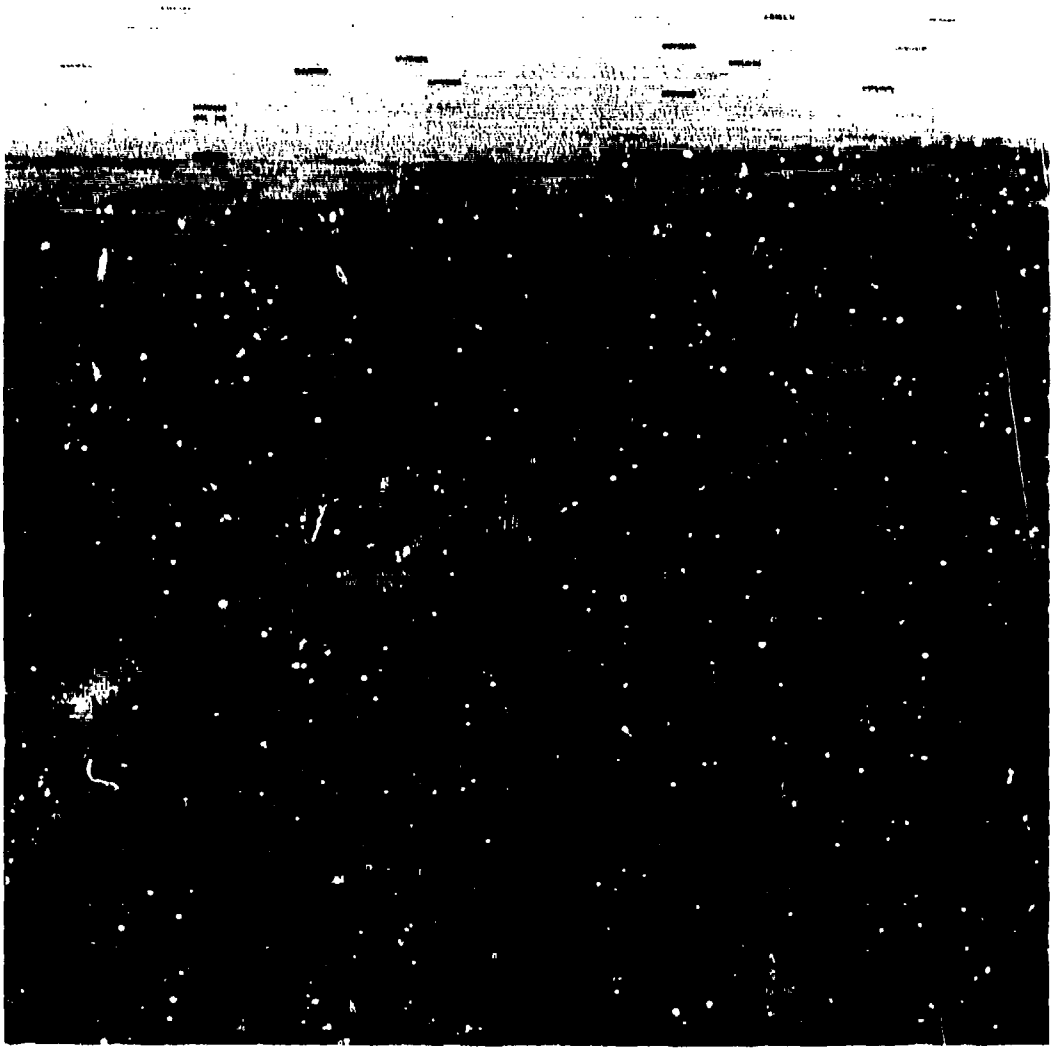

4.6.13b Hybrid Coding Scheme Using Prediction Coefficient of 0.5 (Non-Optimum) Probability of Error = .01; 0.5 bits/pel.

4.6.13c Hybrid Coding Scheme Using Prediction Coefficient of 0.5 (Non-Optimum) Probability of Error = .01; 1.0 bits/pel.

prediction coefficients are used (see Figs. 4.5.3a,b,c and 4.6.3a,b,c). The picture quality is not substantially reduced.

Figs 4.6.14a,b,c and 4.6.15a,b,c show the effects of using a value for all prediction coefficients equal to the vertical correlation of the picture and assuming error correcting coding on the first coefficient.

Table 4.6.2 compares the MSE for the various techniques used in these investigations. The results and conclusions about Hybrid Coding Schemes are summarized below:

(1) The picture quality is very insensitive to the prediction coefficient except for the case of noisy channel. In these cases a low value for the prediction coefficient should be used.

(2) The MSE does depend on the prediction coefficients and indicates at times the opposite conclusions than subjective evaluations.

(3) The Hybrid coding schemes can be designed to out perform two-dimensional transform techniques even when channel noise is considered.

(4) Periodic resetting using the optimum prediction coefficient gives superior results than all other techniques.

(5) Error correcting coding on the first coefficient is effective in improving the results in the noisy channel case.

	Bits/Pel	Periodic * Resetting(N=32)	Periodic* Resetting(N=16)	Error Correction First Coeff.*	Error Correction First Coeff.(1)
P = 0.001	0.25	0.045436	0.043703	0.045872	0.047285
	0.50	0.034348	0.033075	0.034104	0.035176
	1.00	0.023364	0.022703	0.023050	0.024040
P=0.01	0.25	0.057559	0.054928	0.047641	0.053684
	0.50	0.047993	0.045628	0.037491	0.043838
	1.00	0.033844	0.037630	0.028607	0.033426

* Using optimum prediction coefficients.

1) Prediction coefficients = 0.955

Table 4.6.2. Optimization of the Hybrid Coding Technique.

4.6.14a Hybrid Coding Scheme Using Error Correcting Code on First Coefficient; All A = ρ_y; Probability of Error = .001; 0.25 bits/pel.

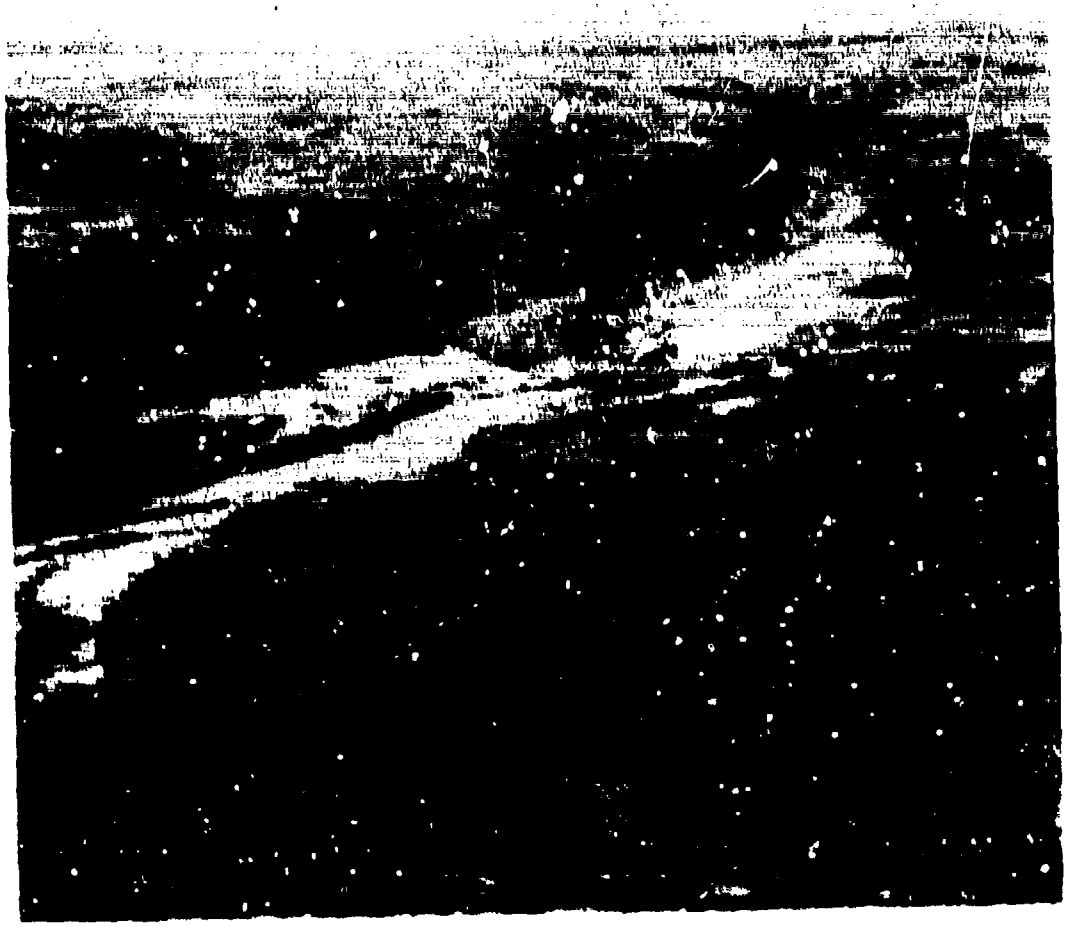

4.6.14b Hybrid Coding Scheme Using Error Correcting Code on First Coefficient; All A = ρ_v; Probability of Error = .001; 0.5 bits/pel.

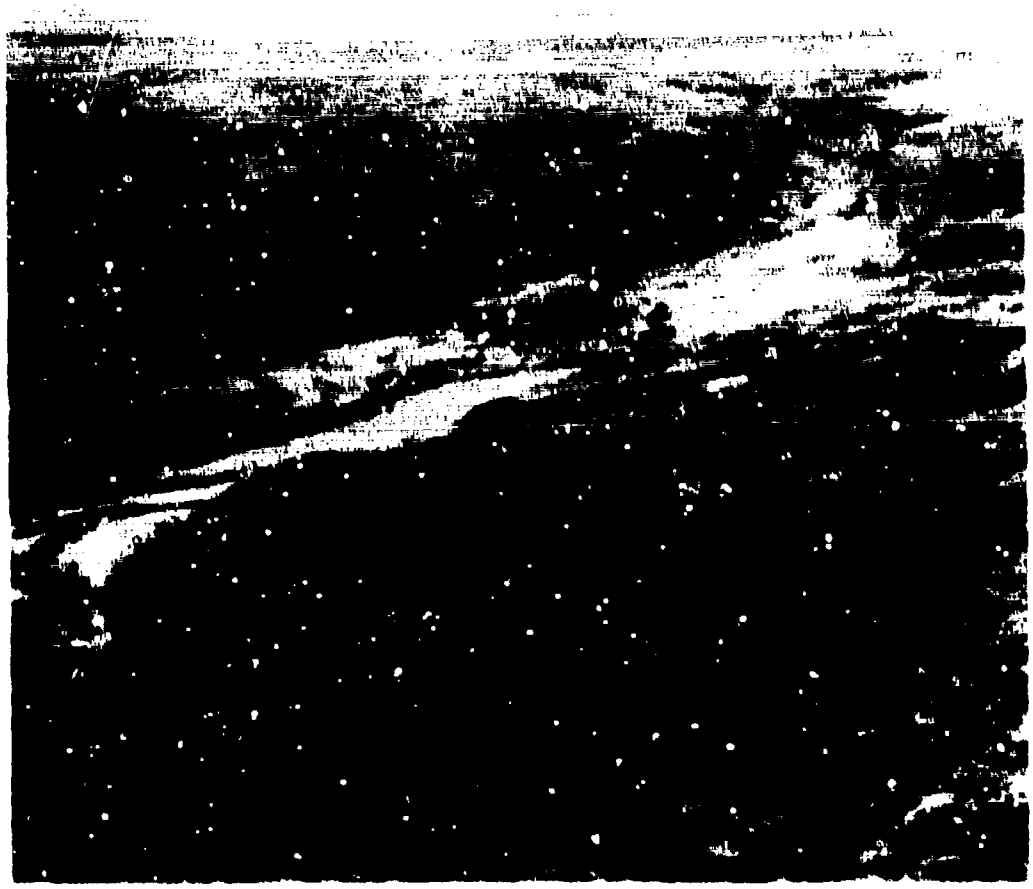

4.6.14c Hybrid Coding Scheme Using Error Correcting Code on First Coefficient; All A = ρ_y; Probability of Error = .001; 1.0 bits/pel.

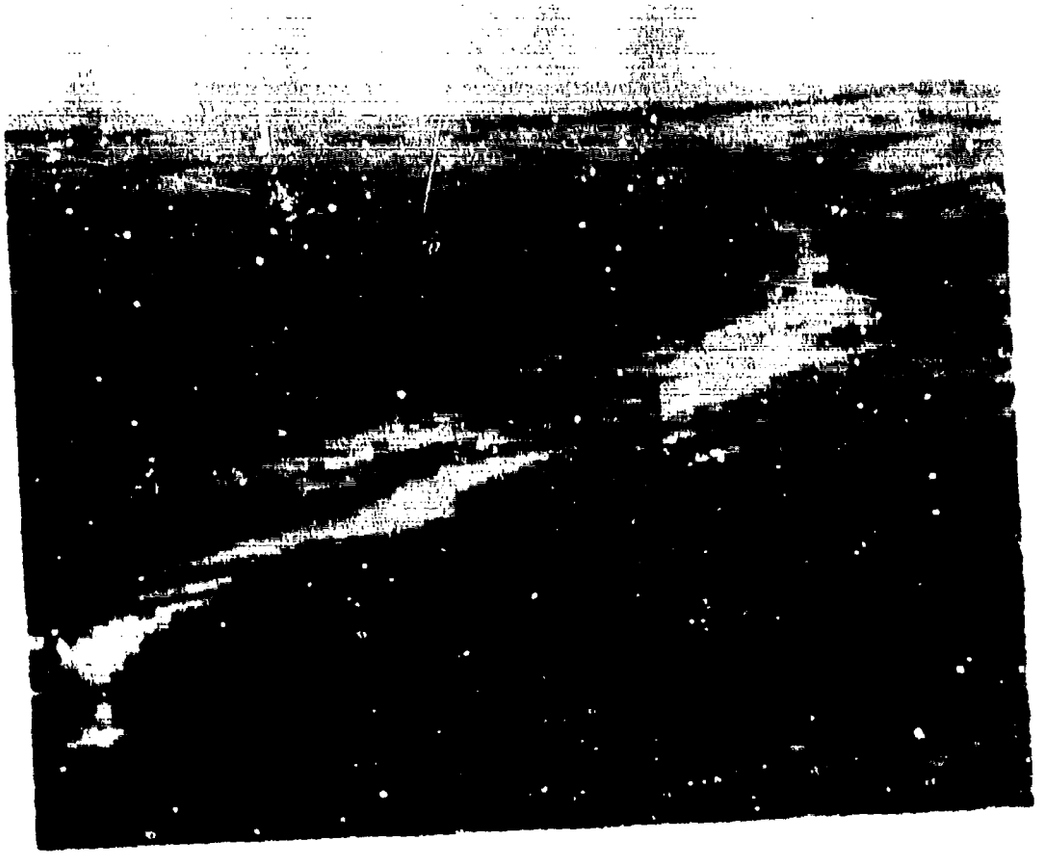

4.6.15a Hybrid Coding Scheme Using Error Correcting Code on First Coefficient; All $\Lambda = \rho_y$; Probability of Error = .01; 0.25 bits/pel.

4.6.15b Hybrid Coding Scheme Using Error Correcting Code on First Coefficient; All A = ρ_y; Probability of Error = .01; 0.5 bits/pel.

4.6.15c Hybrid Coding Scheme Using Error Correcting Code on First Coefficient; All A = ρ_y; Probability of Error = .01; 1.0 bits/pel.

CHAPTER V

2-D TRANSFORM WITH ADAPTIVE QUANTIZATION

5.1 Introduction

In this section we describe and evaluate the performance of the two-dimensional transform technique using adaptive quantization. In a typical two-dimensional transform system the process is to compute the transform of a sub-image of size n x n, resulting in n^2 coefficients. Redundancy reduction is achieved by eliminating all but the M most important coefficients. These coefficients are quantized and coded by some type of "optimum" coders which are matched to the statistics of the coefficients. For sequency type transformations the variances of the coefficients decrease thus packing most of the information in the low-sequency coefficients and the number of quantization levels used to quantize each coefficient decreases with decreasing variance. For this type of operation the number of quantizers required will be the same as the number of coefficients retained. In general, the quantizers are assumed fixed and the design of each quantizer is based on the average statistics over a large number of pictures. This type of procedure performs satisfactorily on the average; however, the quantization error can be relatively large in regions of high activity, resulting in a considerable loss of resolution. On the other hand if one designs fixed quantizers based on regions of high activity within the image, then coefficients in regions of low activity (constant intensity levels) are quantized with more accuracy than is required, thus reducing the overall reduction ratio. The adaptive system shown in Fig. 5.1.1 is proposed as a relatively simple scheme for improving resolution in regions of high activity within the image.

In operation, the block transformation and truncation procedures are the same as a conventional two-dimensional scheme resulting in M coefficients which are

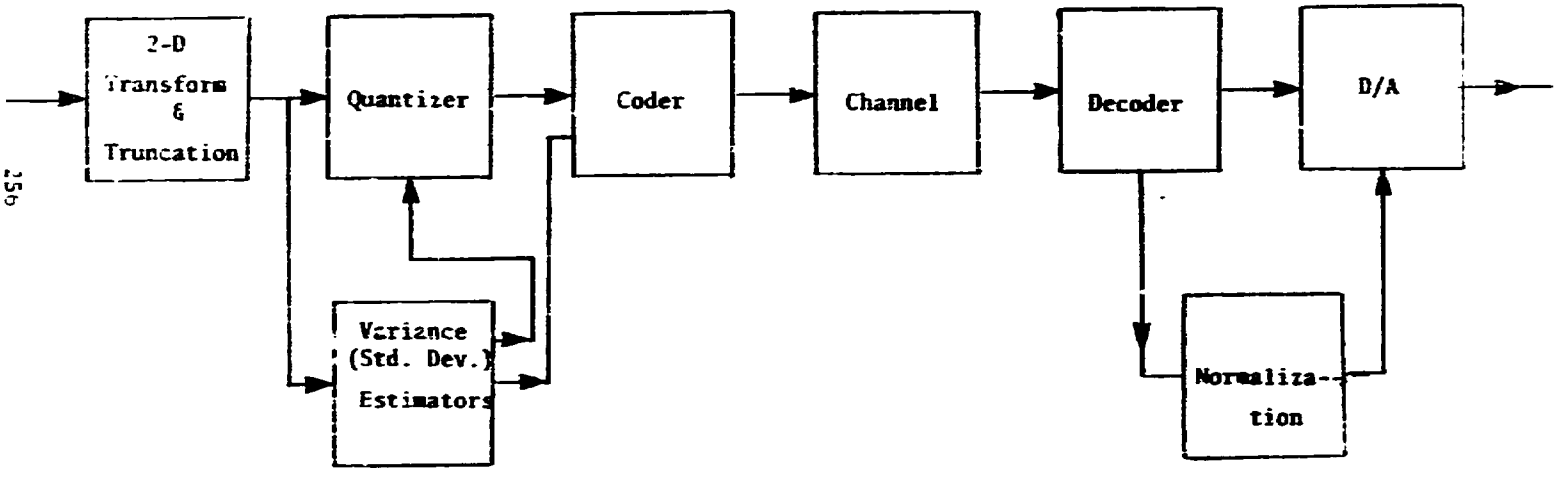

Fig. 5.1.1. Block Diagram of Adaptive Scheme.

deemed sufficient for the quality of picture desired. In a conventional non-adaptive system, these coefficients would be quantized using different number of quantization levels for each coefficient depending on the variances. Using fixed quantizers this procedure results in only an average approximation to the "optimum" quantizer as indicated before. In the proposed system shown in Fig. 5.1.1 the variances of each coefficient are continuously estimated using K previous samples i.e.

$$\hat{\sigma}_i^2 = \frac{1}{K} \sum_{p=1}^{K} i_p^2 \qquad (5.1.1)$$

where i denotes the coefficient. These estimates of the variances of the coefficients are used to normalize the coefficients before quantization, thus resulting in a better "match" of the signal to the quantizer. The rapidity of the adaptation algorithm depends on the number of samples (K) used in estimating the variances. For active regions in the image a small value of K may be desirable; however, too small of K will result in considerable error in estimation of the variance, thus resulting in degradation of the compressed picture. Using such a technique as described above requires, of course, transmission of information to the receiver of the variances or standard deviations of the coefficients.

It is the purpose of this chapter to investigate the performance of the adaptive system along with various tradeoffs in terms of system complexity, bit reduction ratio, etc.

5.2 Two-Dimensional Hadamard Using 32-Coefficients

Normalization of the transform coefficients and using the same quantizer for all coefficients would result in a considerable reduction of hardware required; however, the resulting picture would be considerably degraded using fixed quantizers.

It is of interest to investigate the possibility of using the adaptive scheme using only one quantizer for all the coefficients and to compare this system with different bit assignments for each coefficient. For this investigation we keep the 32-coefficients with the highest energy content rather than letting the bit assignment algorithm truncate the coefficients as was done in Cahpter IV.

This normalization procedure was simulated for the picture of the "Truck" using a 4-bic exponential quantizer and the Max's [137] 4-bit quantizer. The results of these simulations are given in Table 5.2.1.

	Max Quantizer	Exponential Quantizer
MSE	.0046177	.004753
MDSE	.0061003	.0059698

Table 5.2.1. Mean-Squared-Error and Mean-Derivative-Squared-Error for the Scene of the Truck.

For comparison purposes the bit assignment procedure used in Chapter IV was used assuming the total number of coefficients to be 32 instead of 64

As pointed out in Chapter IV using the total number of coefficients as 32 and applying the bit assignment rule described in Chapter IV results in a reduction the MSE by an order of magnitude. This is to be expected since by arbitrarily truncating the number of coefficients to 32 results in more bits being assigned to the most important coefficients. Using the bit assignment algorithm on 64 coefficients as was done in Chapter IV results in several high order coefficients being assigned 1 or 2 bits which does not contribute significantly to the picture quality.

Table 5.2.2 (which has been presented in Chapter IV) shows the bit assignments used for effective bit rates of 0.5, 1.0 and 1.5 bits/pel. Table 5.2.3 shows the

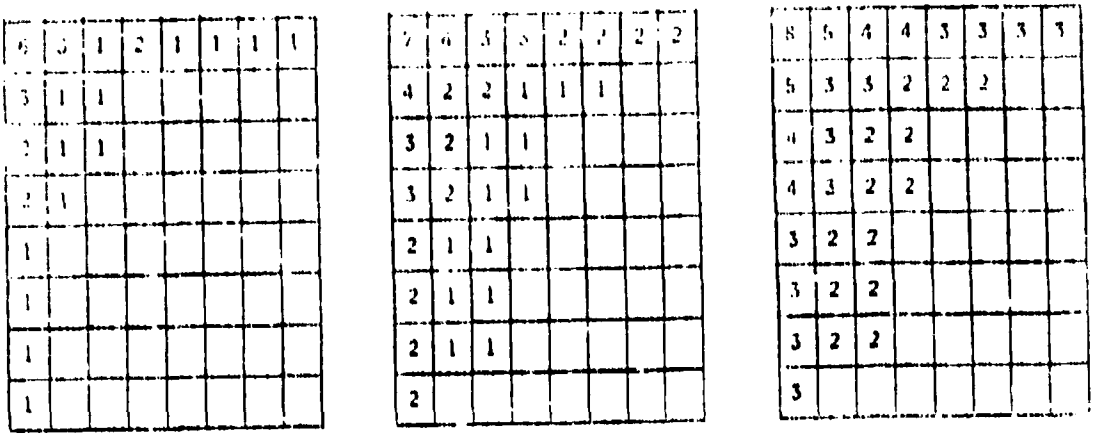

0.5 bits/pel | 1.0 bits/pel | 1.5 bits/pel

Table 5.2.2. Bit Assignments Using 32 Total Coefficients.

errors obtained using this procedure along with the error obtained using 64 coefficients and letting the bit assignment algorithm truncate the number of coefficients as was done in Chapter IV. A considerable decrease in the total MSE is noted.

5.3 Adaptive Algorithm Using One Quantizer

In this section we evaluate the performance using one quantizer which is adjusted by the adaptation algorithm described earlier. As was mentioned before the variances or the standard deviation of each coefficient are estimated from the K previous coefficients and these estimates are used to normalize the coefficients. Table 5.3.1 shows the results obtained using various number of coefficients for estimating the variance. For these simulations a 1 bit exponential quantizer was used.

Bits/Pel	MQE	MMQE	MSE	MDSE	Coeff. Retained	MSE from Chapter IV
0.5	0.0089657	0.23507	0.011993	0.017753	20	0.1
1.0	0.0043256	0.10716	0.0057216	0.0085961	32	0.08
1.5	0.0016579	0.037865	0.0032147	0.0048386	32	0.04

Table 5.2.3. Error Measures for the Scene of the Truck.

Sample Size	MSE	MDSE
8	0.015969	0.57513
16	0.0084124	0.57259
32	0.0059297	0.54978
64	0.0060447	0.55245
128	0.0060791	0.55104
256	0.0060519	0.54845

Table 5.3.1. The Effects of Sample-Size in Estimating the Variance of the Coefficients.

A problem exists using small sample sizes when the intensity level is essentially constant. In this case the estimated variance will be zero which would cause a normalization problem. This situation was encountered using sample sizes of 8 and 16 in the simulations. This situation could be remedied by several techniques, such as using a different "activity" measure or using some predetermined algorithm used in these cases were to initialize the standard deviation to one and then to increase it by one until the coefficient fell within the quantizers range.

Using too large of a sample size in estimating the variance will result in little or no adaptation characteristics. The results of Table 5.3.1 indicate that a sample size of 32 would give the best results.

Results using a sample size of 32 for estimating the variance and a common 4-bit exponential quantizer for each coefficient and bit assignments according to the Winz Kurtenbach algorithm [51] for the 32 estimates of the standard deviations are given in Table 5.3.2. The bit assignments used are shown in Table 5.3.3

Effective Bit Rate	Effective Bits Assigned to Estimate	MSE	MDSE
3	1.0	0.0062644	0.57226
4	2.0	0.0060391	0.55693
5	3.0	0.0060274	0.54915

Table 5.3.2. Error Measures Using a Common Quantizer for The Coefficients and Different Quantizers for The Estimates of The Standard Deviations.

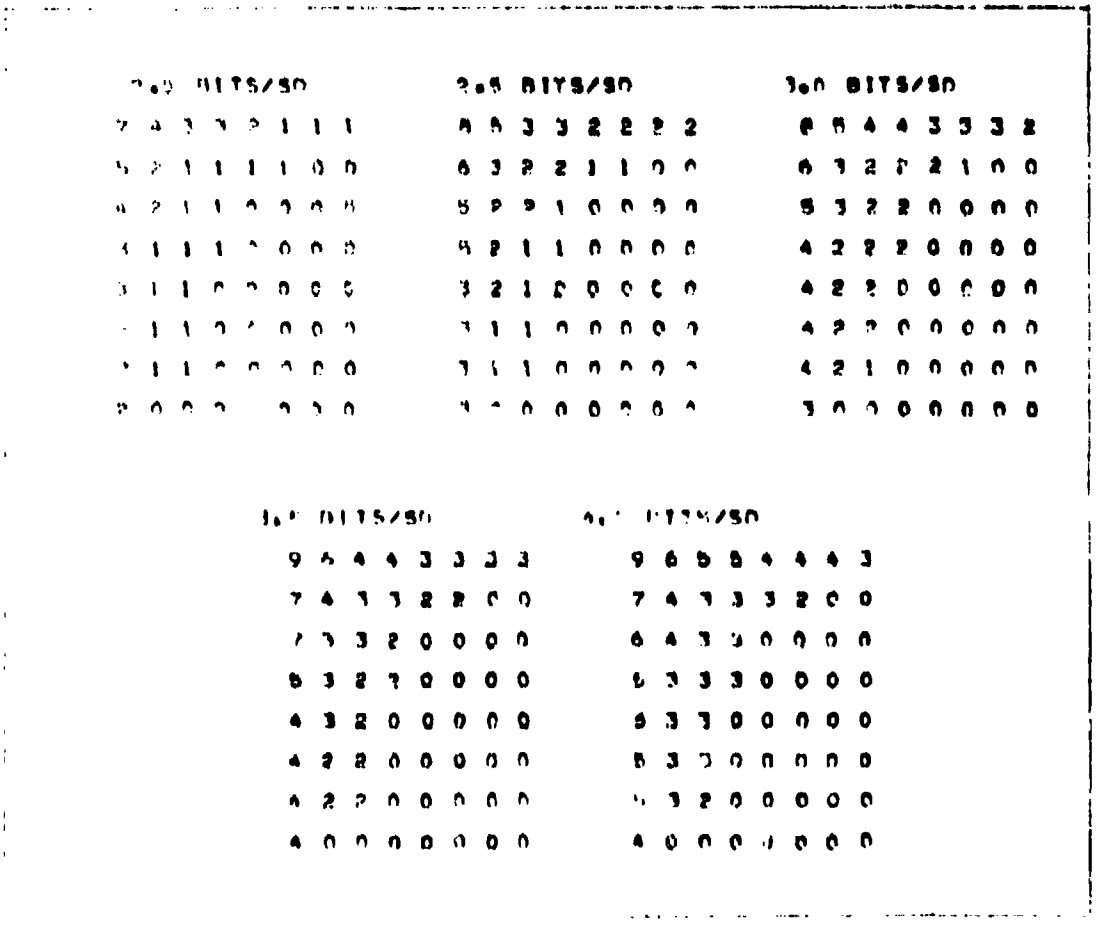

Table 5.3.3. Bit Assignments

These results indicate that this structure would be of little use for data compression and are only included for completeness.

5.4 DPCM Encoding of The Estimates of The Variances

In this section we investigate the results obtained using differential encoding of the estimates of the variance and using different quantizers for each of the coefficients.

Fig. 5.4.1 shows the autocorrelation of the variance estimates for coefficient one using different sample sizes for estimating the variances of the coefficients. Similar results have been obtained for the other coefficients and are essentially the same as those shown for coefficient one. Figs. 5.4.2 through 5.4.6 show plots of the estimated variances for the first coefficient. It is noted for a sample size of 32, which gives minimum MSE, the estimates have considerable variations. It is these variations which provide the adaptive feature. As the sample size for estimating the variances is increased there is very little change in the variance estimate from sample to sample. A sample size too large will negate the adaptive feature. Figs. 5.4.7 through 5.4.10 show representative plots using a sample size of 32 for the second through the fifth coefficient estimates of the variance. Similar results have been obtained for the remaining coefficients, up through the thirty-second.

The effects of using too large or too small of a sample size are evident from these correlation curves given in Fig. 5.4.1. Too large of a sample size will not allow the estimate of the variance to change in regions of high activity within the picture.

Using a sample size of 32 for the estimates of the variances, histograms of the difference between the estimated variances are shown in Figs. 5.4.11 through 5.4.14

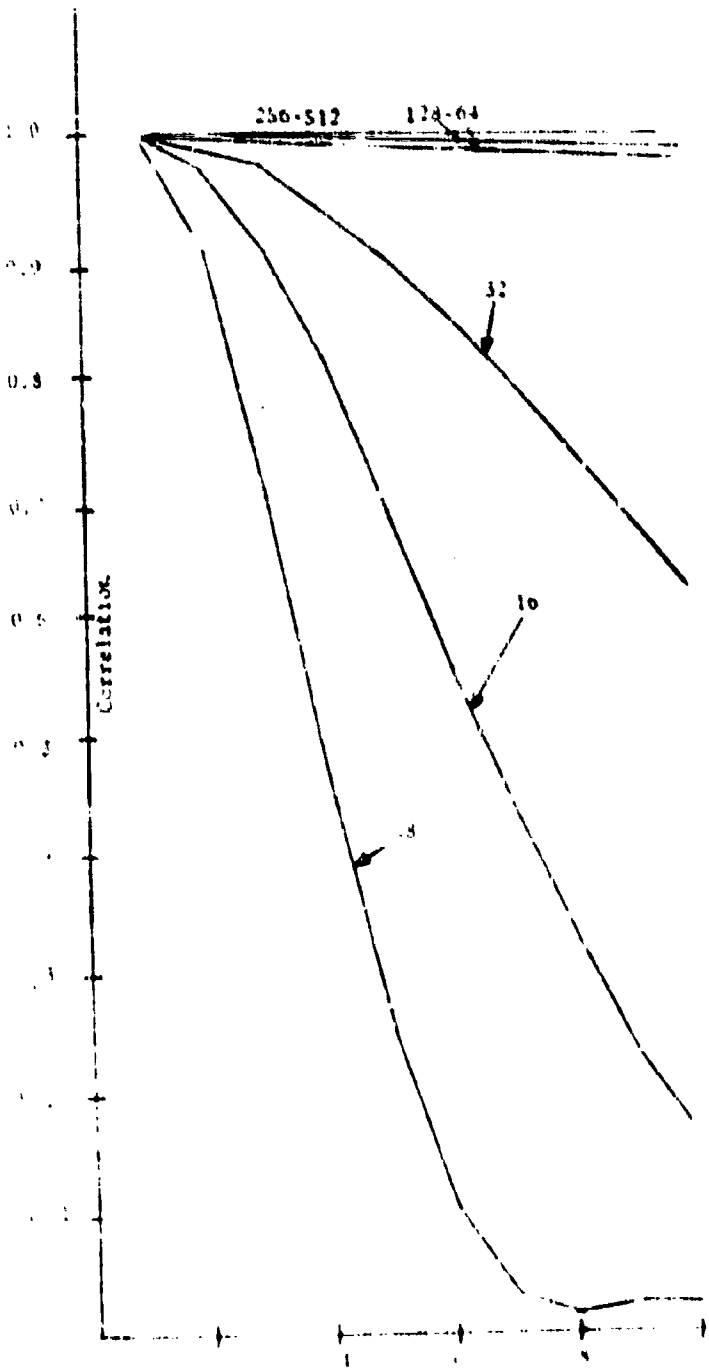
256-512
128-64
32
16
8
Correlation
Samples

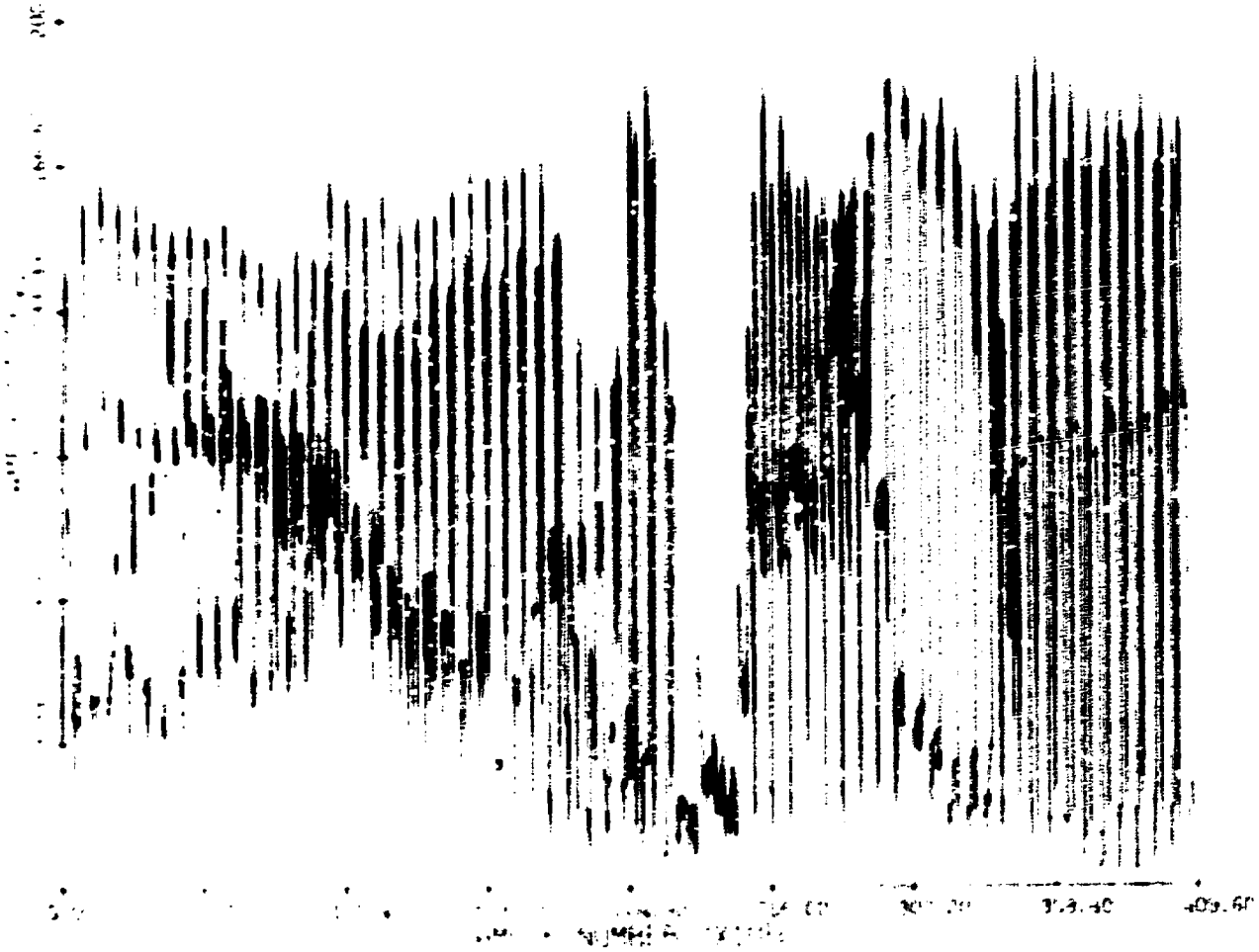

Fig 5.4.2 Estimated Variance for C_1(N=16).

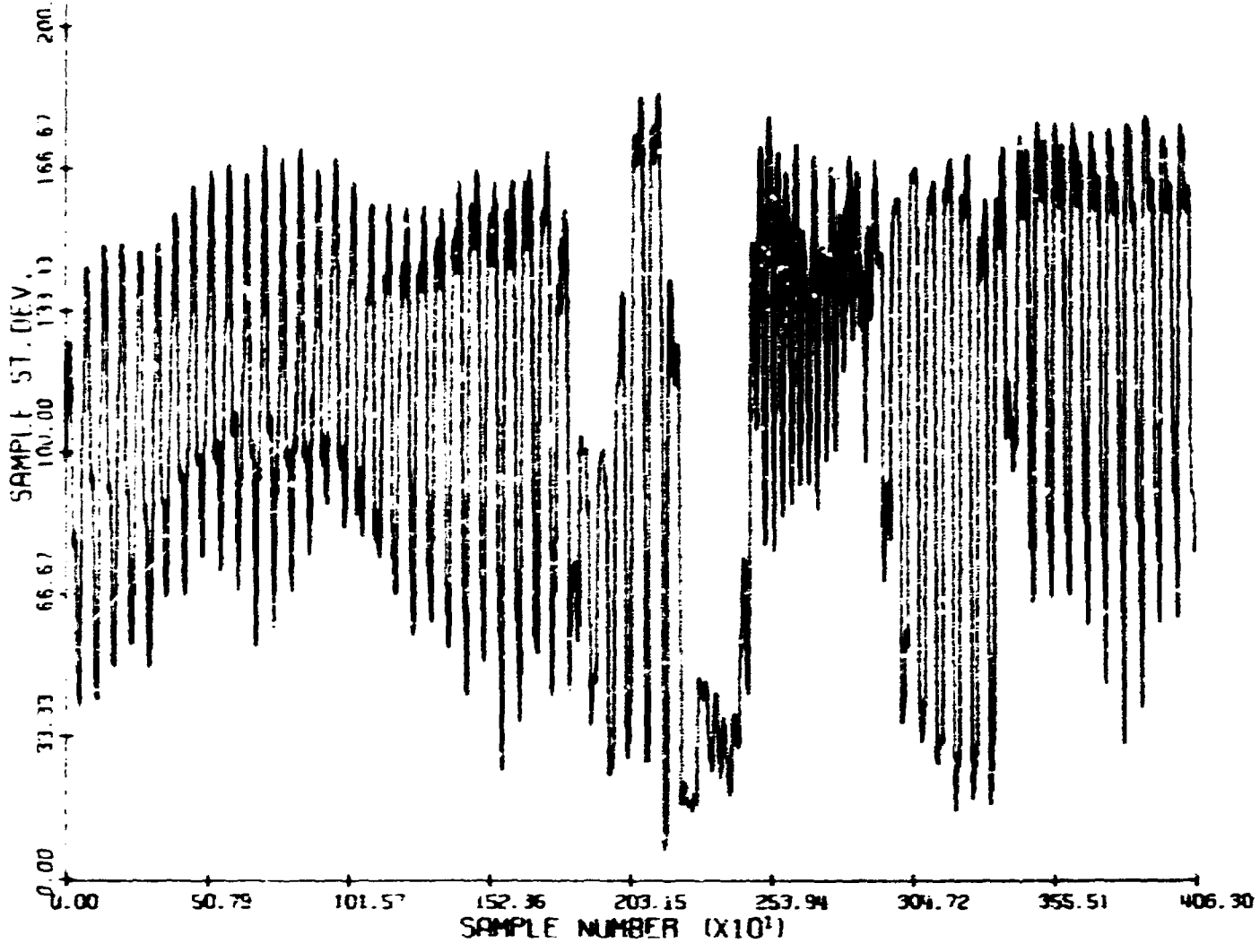

Fig. 5.4.3. Estimated Variance for C_1(N=32).

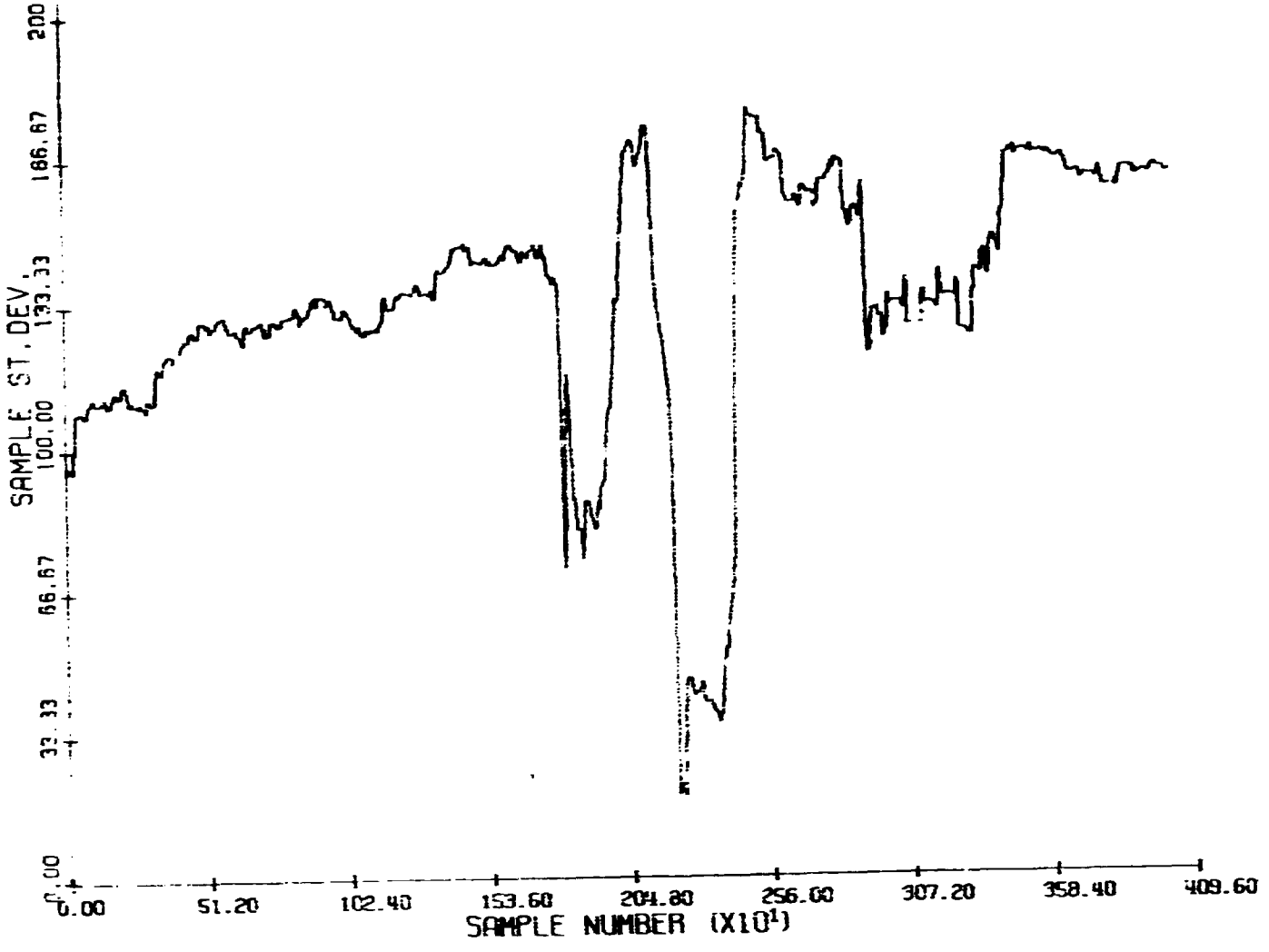

Fig. 5.4.4. Estimated Variance for C_1(N=64).

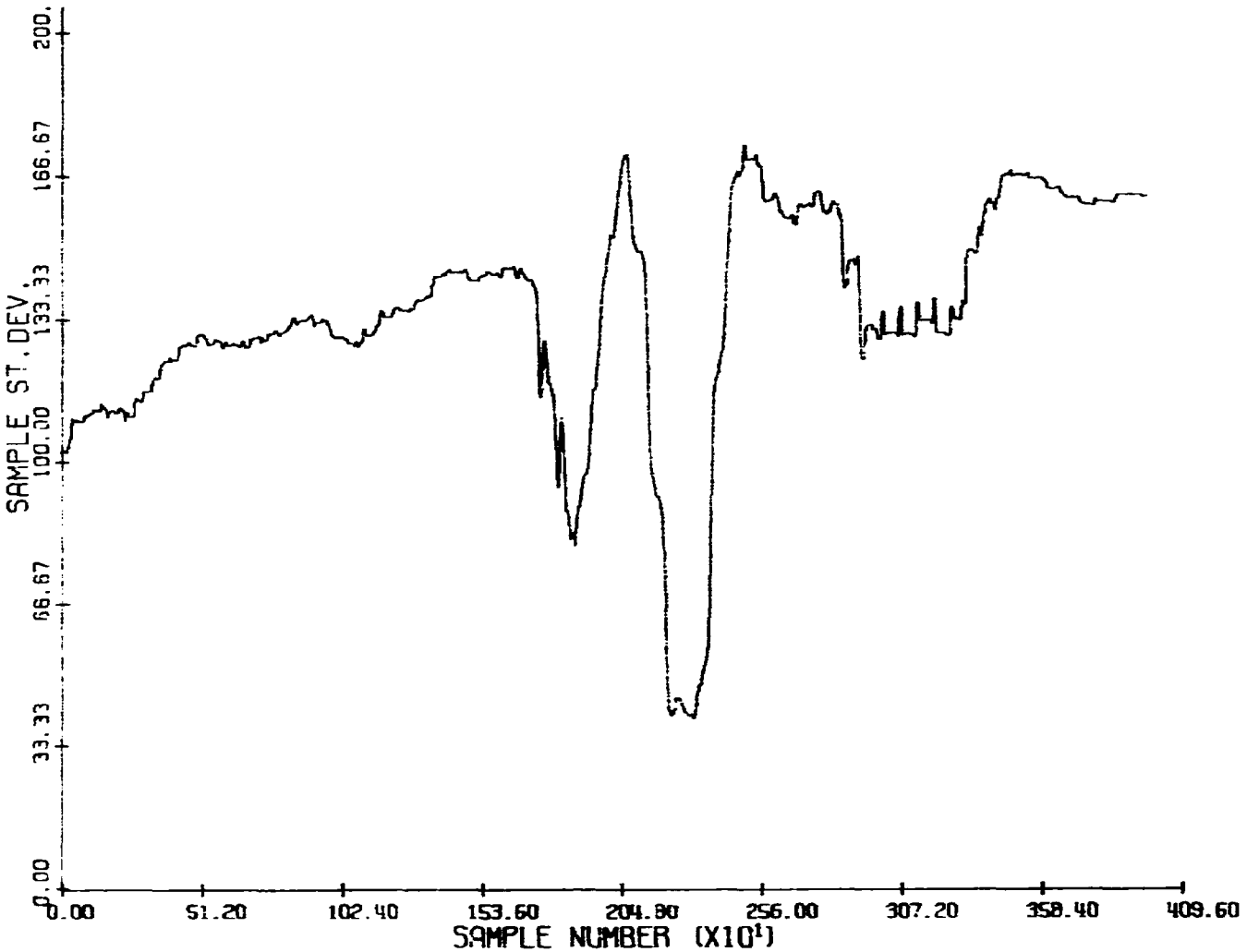

Fig. 5.4.5. Estimated Variance for C_1(N=128).

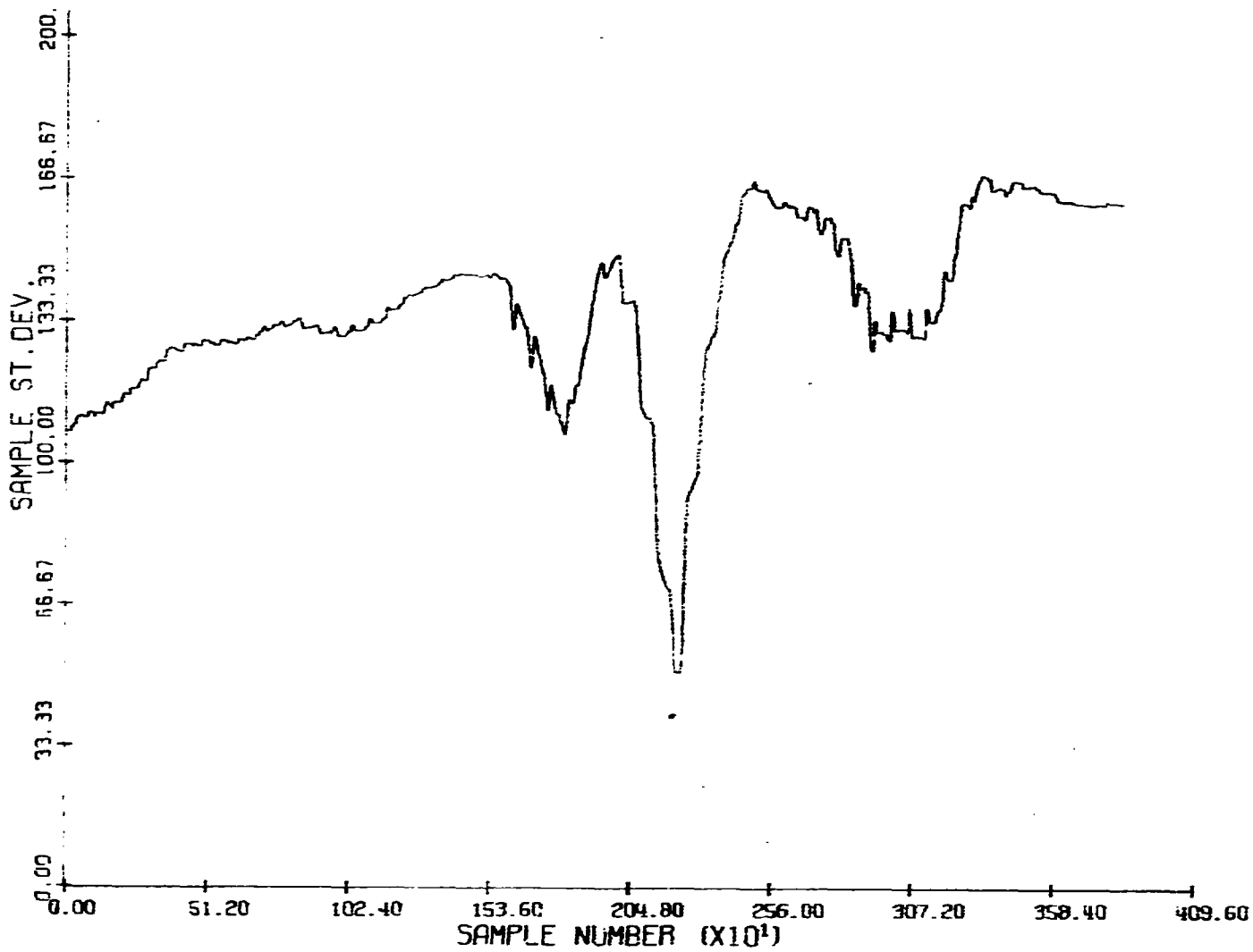

Fig. 5.4.6. Estimated Variance for C_I (N=256)

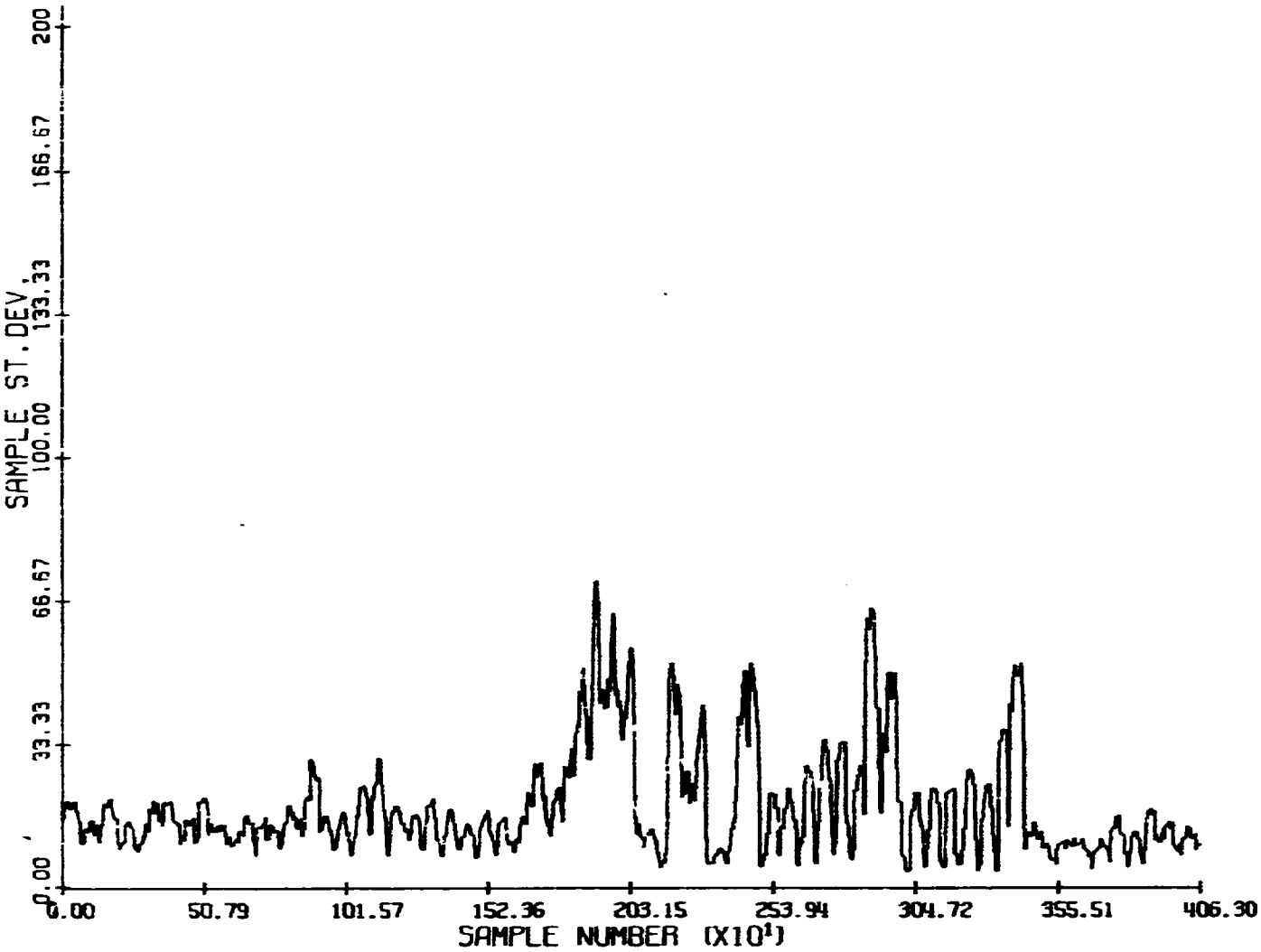

Fig. 5.4.7. Estimated Variance for C_2(N=32).

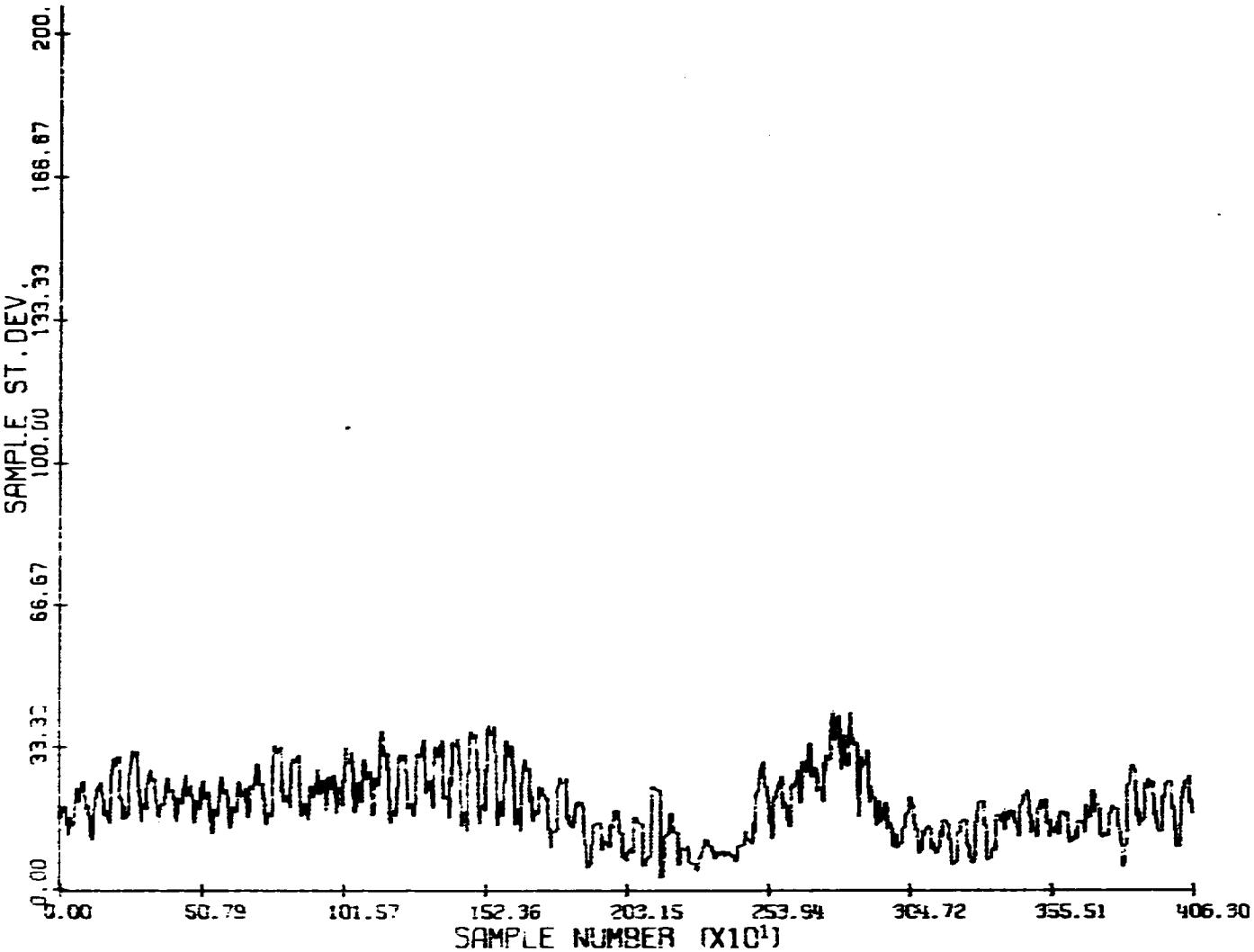

Fig. 5.4.6. Estimated Variance for C_3(N=32).

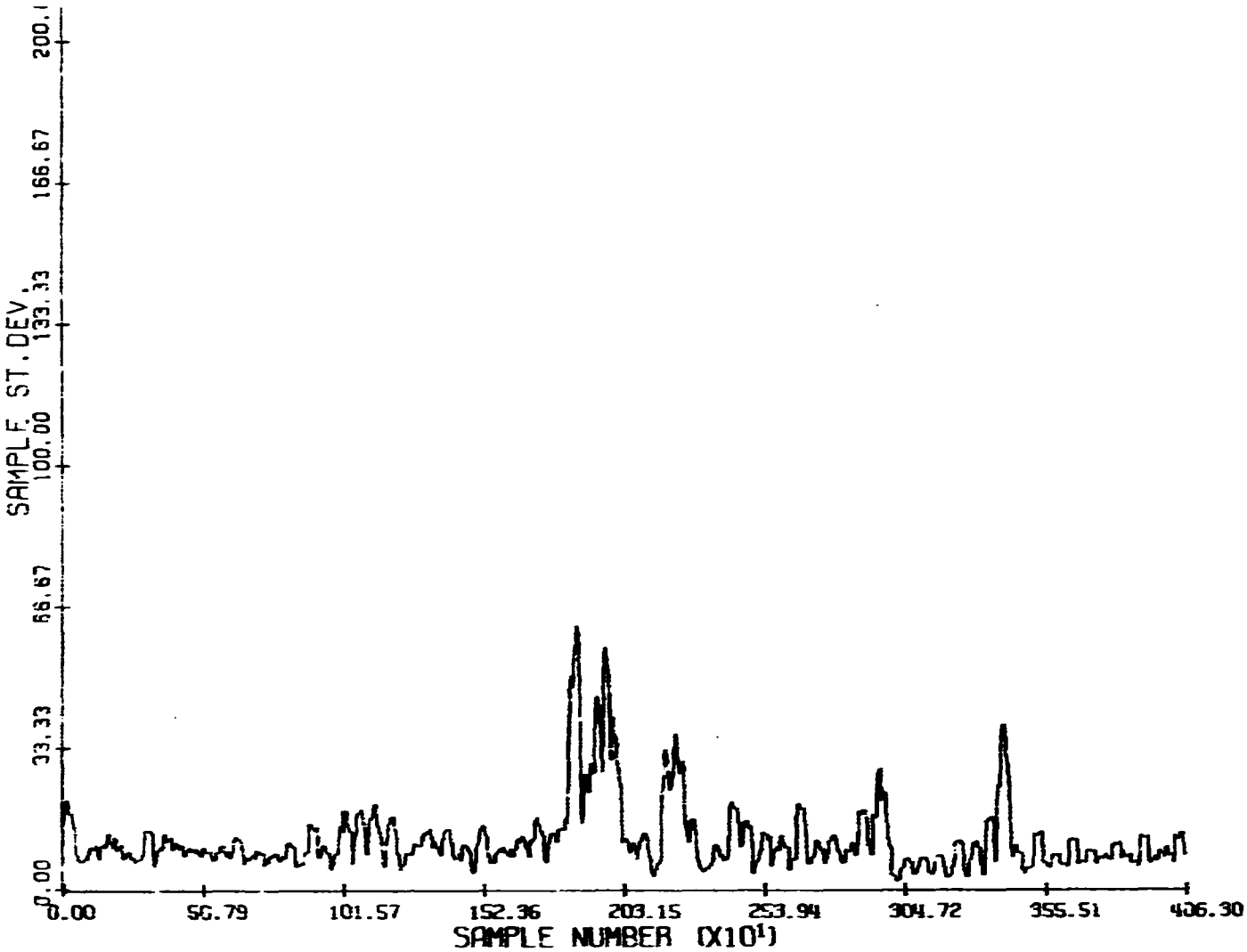

Fig. 5.4.9. Estimated Variance for C_4(N=32).

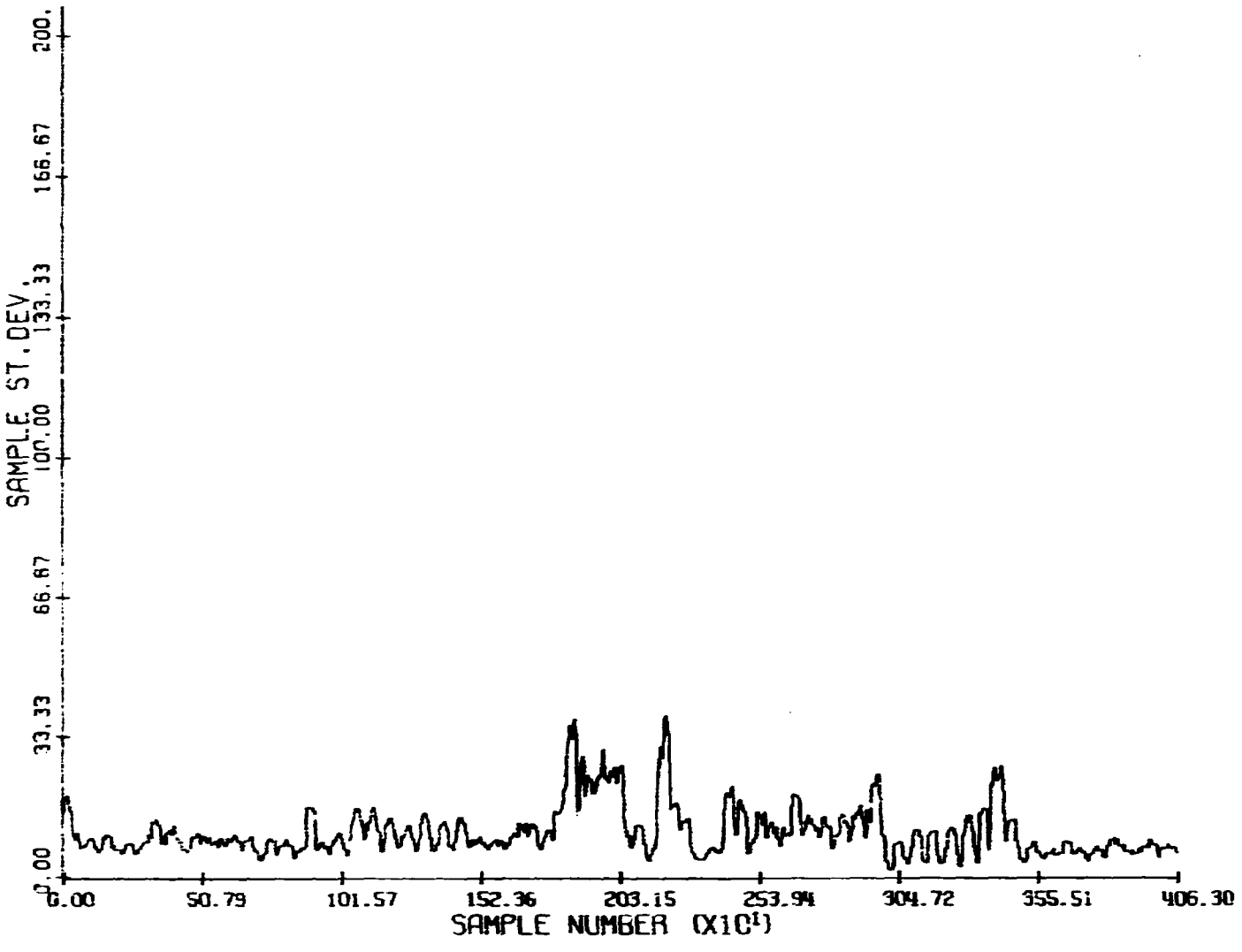

Fig. 5.4.10. Estimated Variance for C_5(N=32).

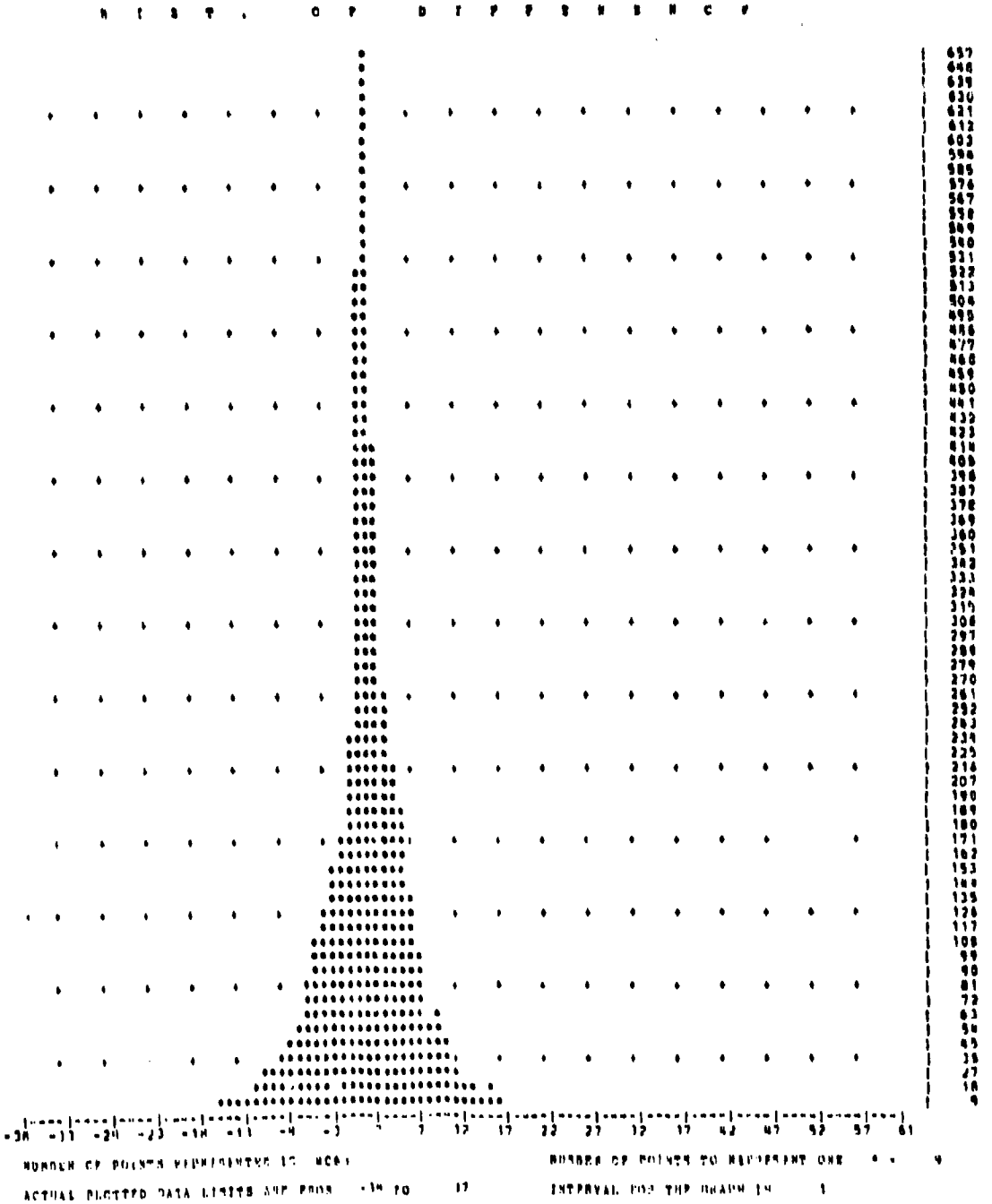

Fig. 5.4.11. Histogram of the Differences in the Estimated Variances for Coefficient #1.

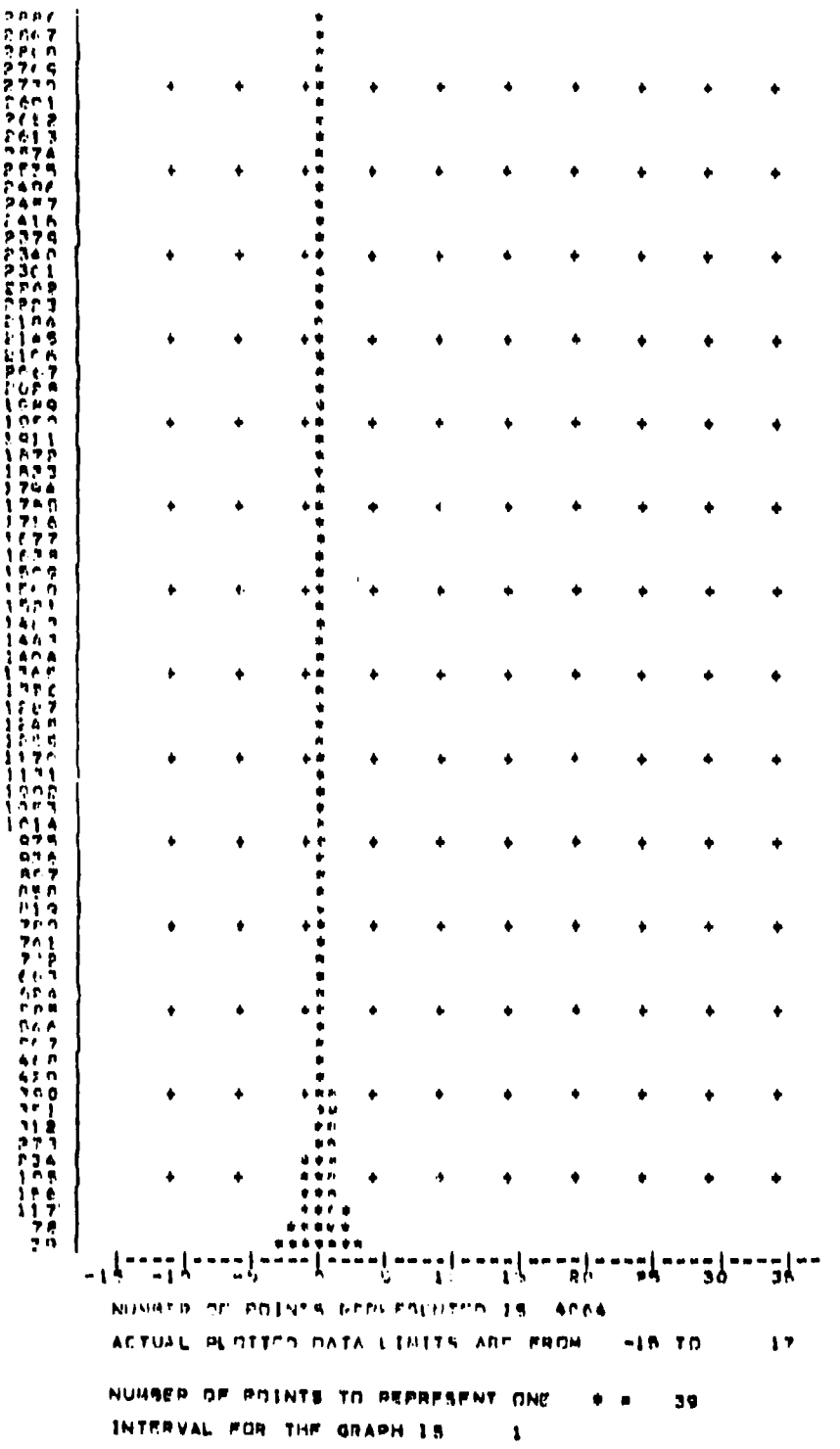

Fig. 5.4.12. Histogram of the Differences in the Estimated Variances for Coefficient #2.

Reproduced from
best available copy.

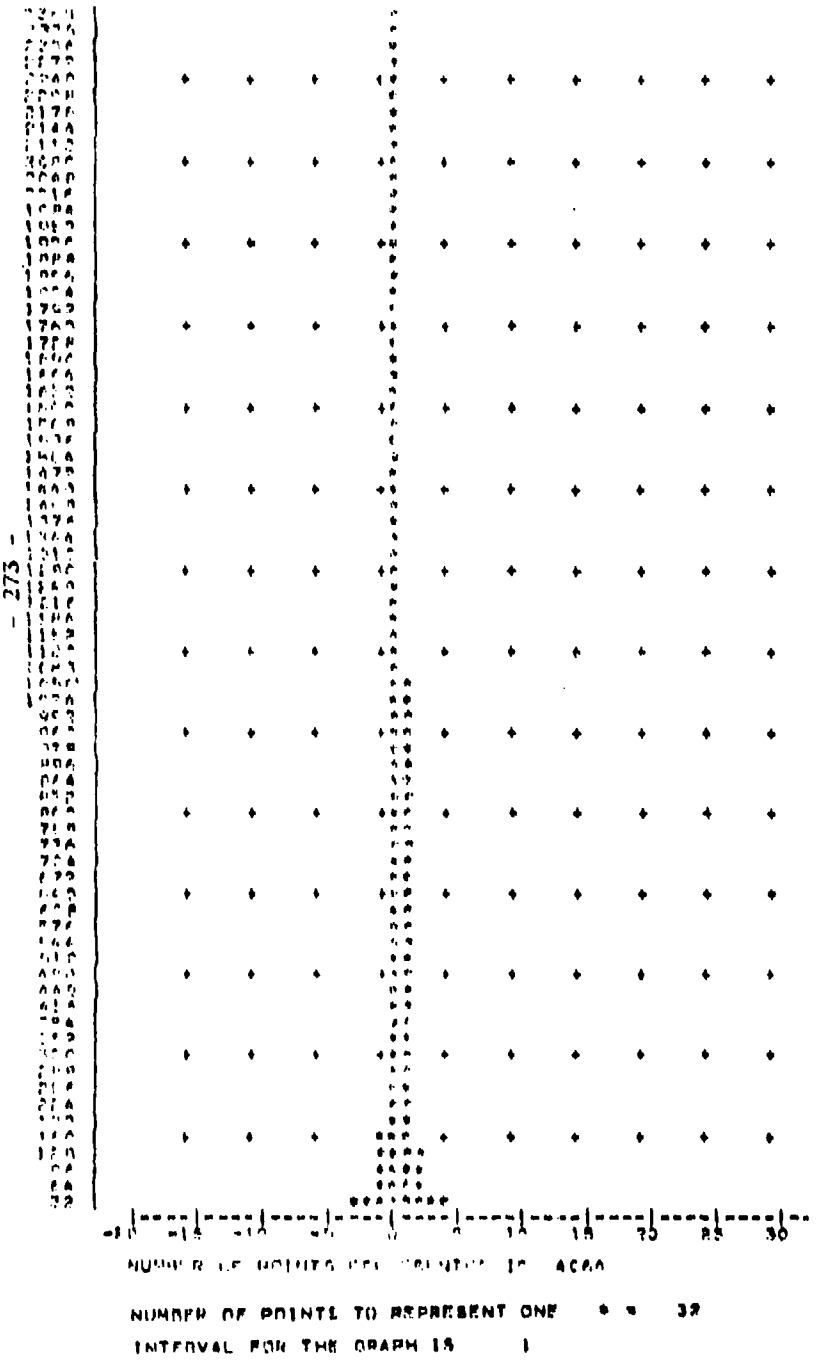

Fig. 5.4.13. Histogram of the Differences in the Estimated Variances for Coefficient #4.

Reproduced from
best available copy.

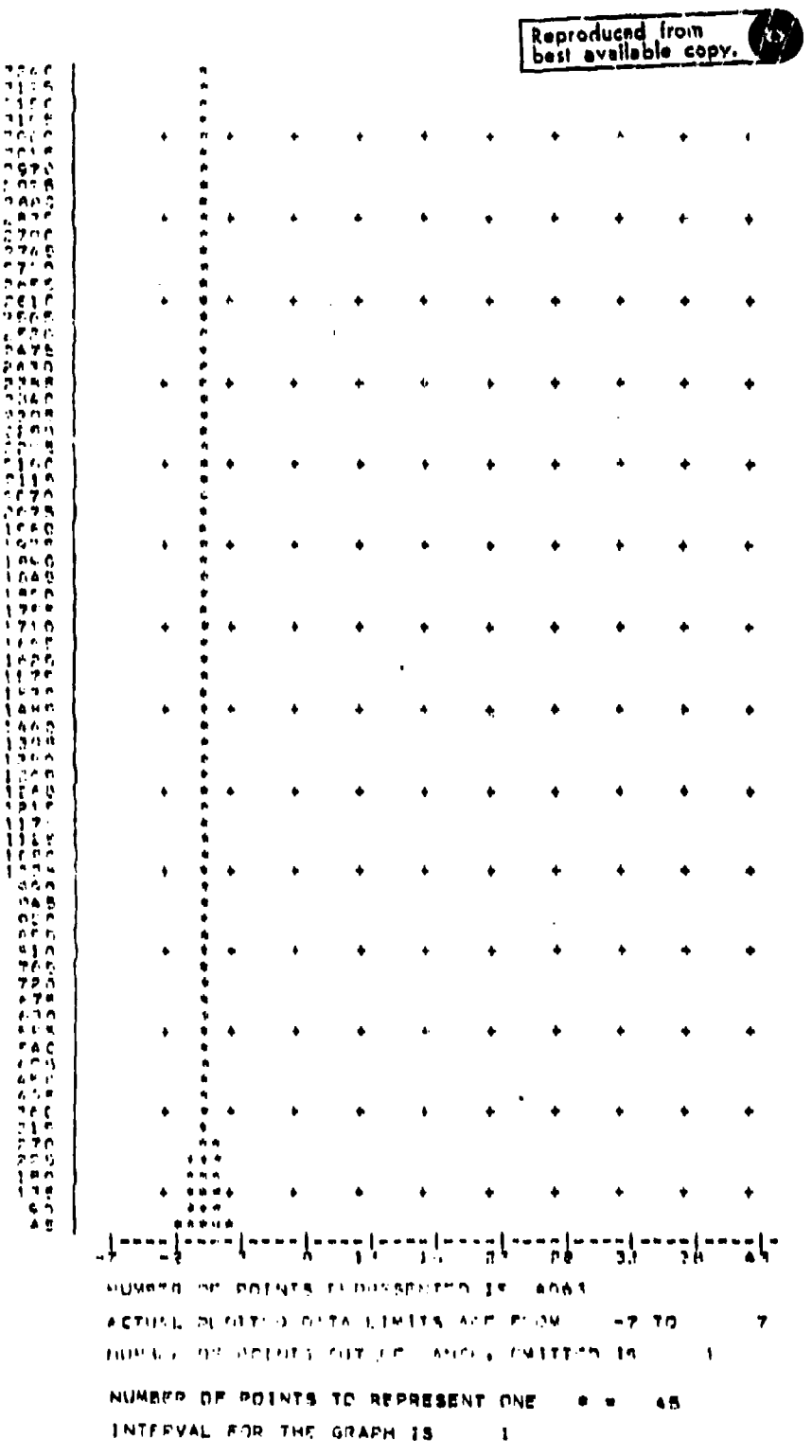

Fig. 5.4 14. Histogram of the Differences in the Estimated Variances for Coefficient #5.

for coefficients 1 through 4 respectively. These are to be compared with the histograms of the estimates of variances shown in Fig. 5.4.15 (shown for coefficient 1 only).

Simulation results were obtained for the scene of the "Truck" using a sample size of 32 for estimating the variances. A two-dimensional Hadamard Transformation was performed on a block size of 8 x 8, resulting in 64 coefficients. The transform coefficients were arbitrarily truncated to the 32 containing the most information and then the Wintz-Kurrenbach bit assignment algorithm applied to these remaining 32 coefficients. DPCM encoding was used on the estimates of the standard deviations. Only one DPCM encoder was used to encode the estimates of the standard deviations; however, in this simple system it is necessary to transmit 32 additional pieces of information regarding the estimates of the standard deviations.

Table 5.4.1 shows these results in tabulated form. Also shown in this Table are the results obtained using the non-adaptive two-dimensional Hadamard transform scheme.

Bits/pel for Intensity	Bits for Differential Encoding of S.D. Estimates	Effective Bit Rate	MSE	NDSE
0.5	1	1.5	0.016279 (0.033530)	0.90194 (0.50030)
0.5	2	2.5	0.015188	0.83545
0.5	3	3.5	0.014833	0.31605
1.0	1	2.0	0.008986	0.7520
1.0	2	3.0	0.0083825	0.71167
1.0	3	4.0	0.007802	0.69896
1.5	1	2.5	0.0050283	0.56272
1.5	2	3.5	0.0047879	0.55775
1.5	3	4.5	0.004204	0.54165

Table 5.4.1. Simulation Results Using Adaptive Scheme For The Scene of The "Truck"

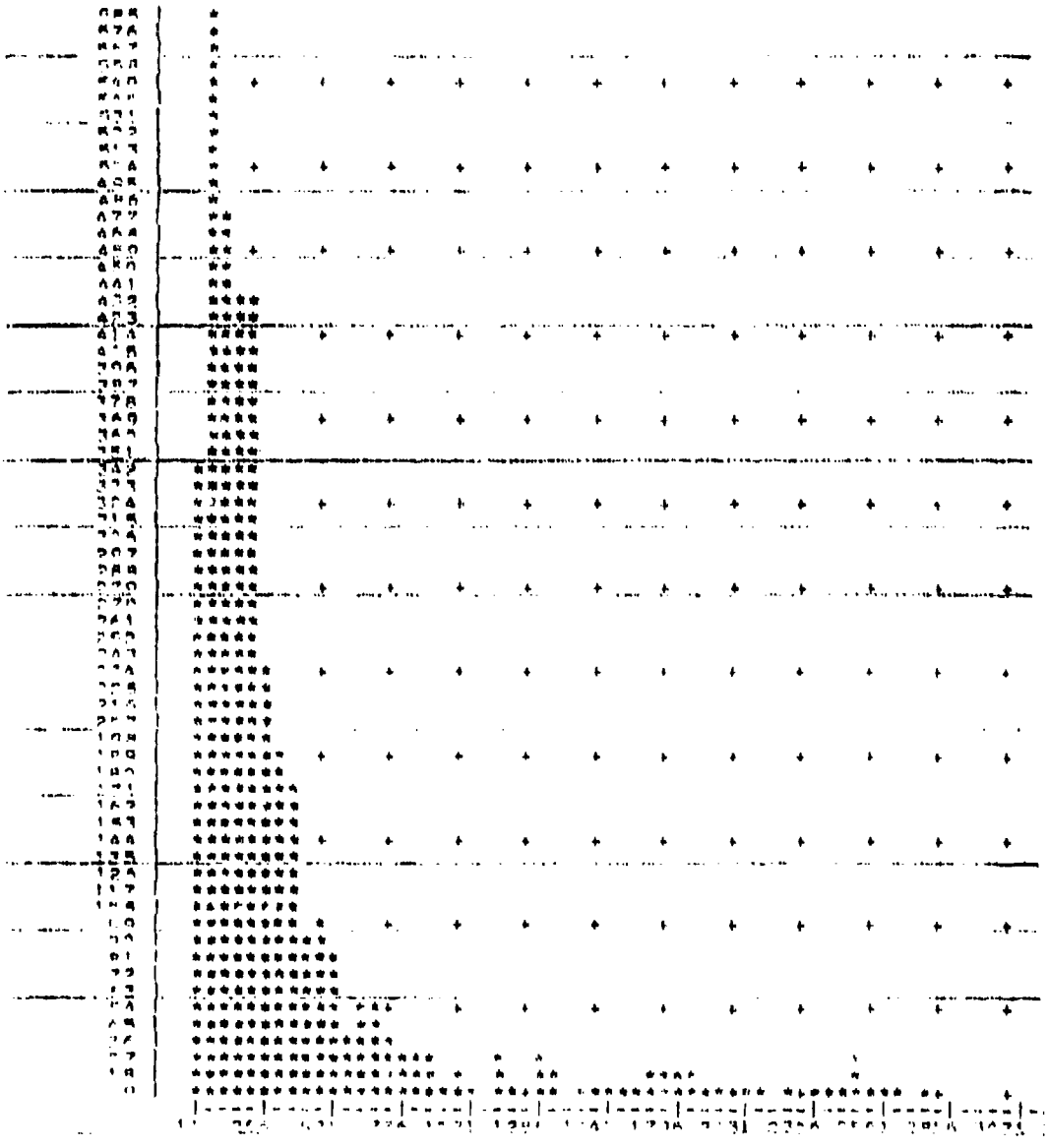

Fig. 5.4.15. Histogram of the Estimates of the Variance for Coefficient #1.

Figs. 5.4.16 through 5.4.27 show photographs of truck using the adaptive scheme. Those pictures are to be compared with the non-adaptive results given in Chapter IV. Significant improvements are noted using the adaptive scheme. For example if we compare the cases of approximately 0.5 bits per picture element using the adaptive technique shown in Fig. 5.4.24 with the non-adaptive case in Fig. 4.3.4b, we see that the adaptive case is superior. Similar results are observed for the 1. bit/pel case.

The preliminary investigations given here for the adaptive scheme seem to indicate that it has merit and probably should be investigated more thoroughly.

Reproduced from
best available copy.

5.4.16 Two-dimensional Hadamard transform with zonal filtering using the exponential quantizer. 4 bits/pel. 32 retained coefficients.

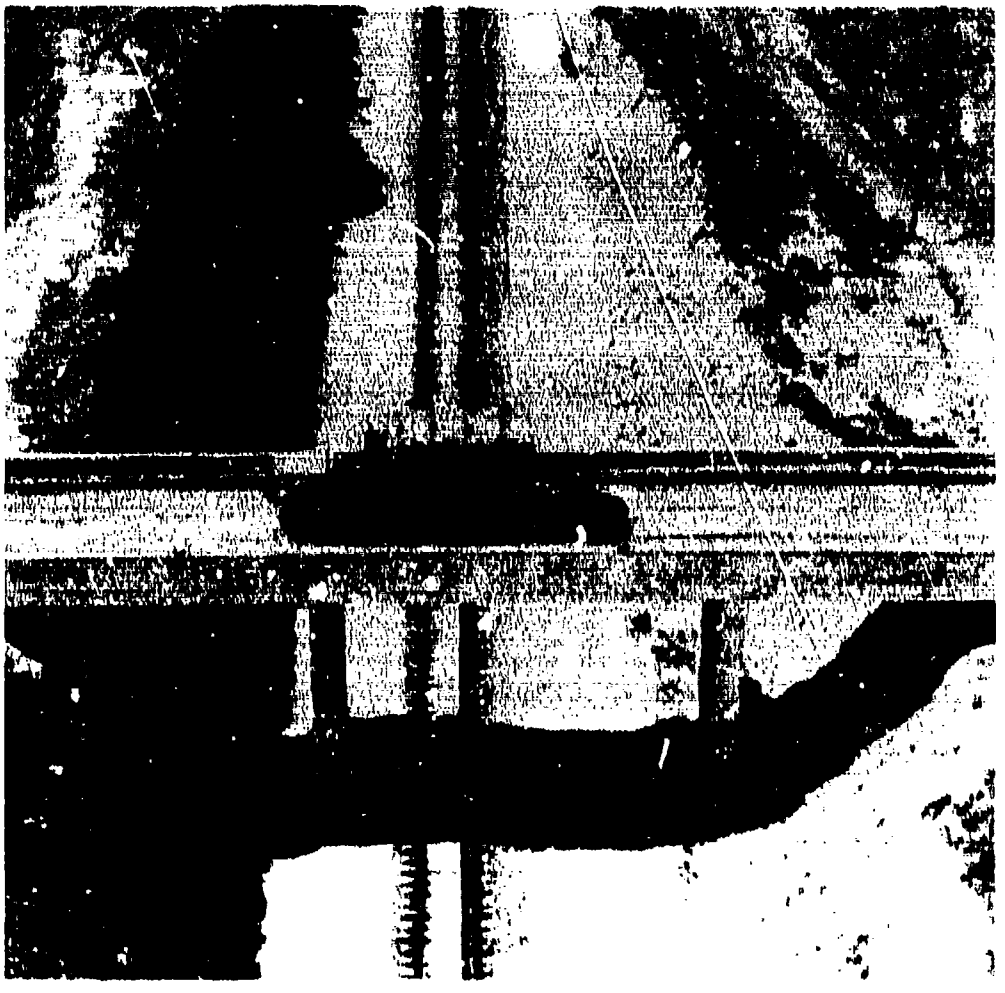

5.4.17 Two-dimensional Hadamard transform with zonal filtering and PCM encoding. Different bit assignments from chapter 4. 32 retained coefficients. 1.5 bits/pel.

5.4.18 Two-dimensional Hadamard transform with zonal filtering and PCM encoding. Different bit assignments from chapter 4. 32 retained coefficients. 1.0 bits/pel.

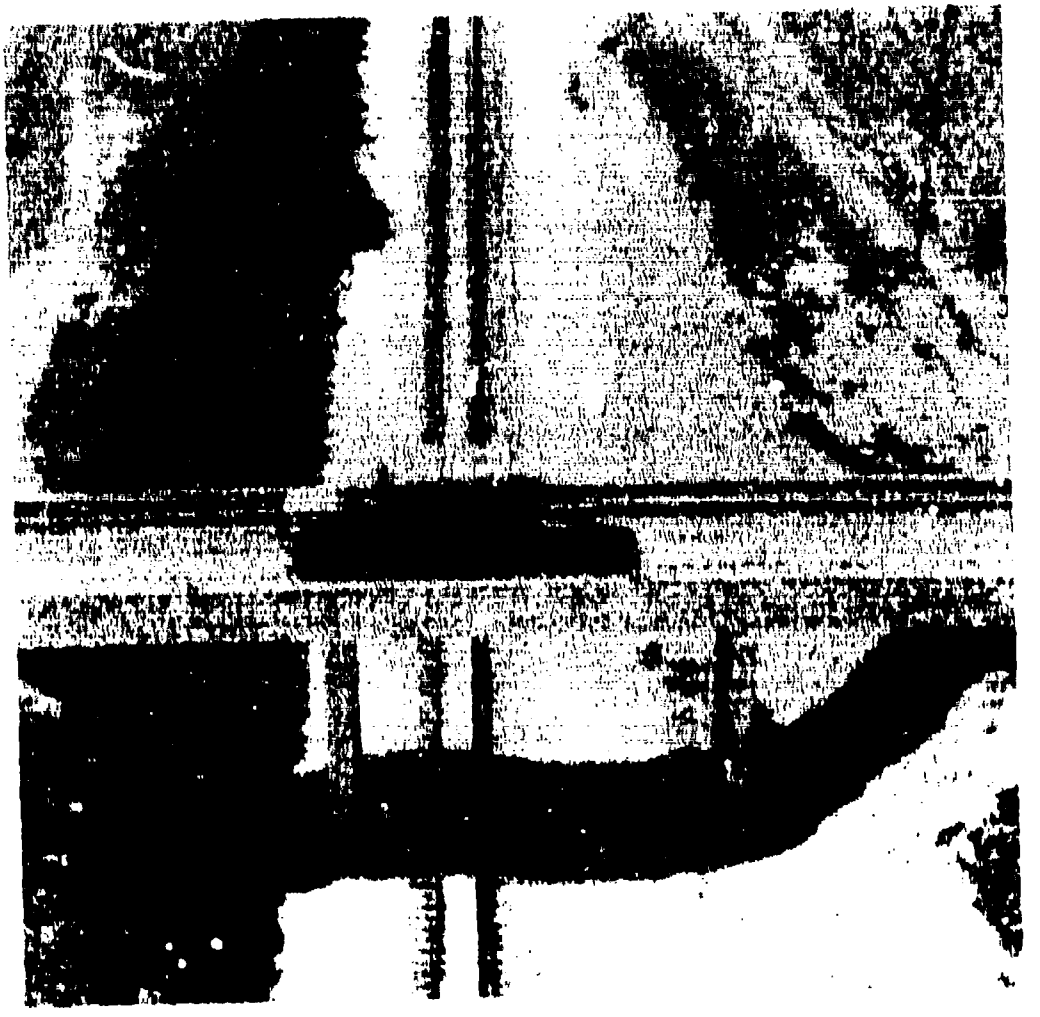

5.4.19 Two-dimensional Hadamard transform with zonal filtering and PCM encoding. Different bit assignments from chapter 4. 20 retained coefficients. 0.5 bits/pel.

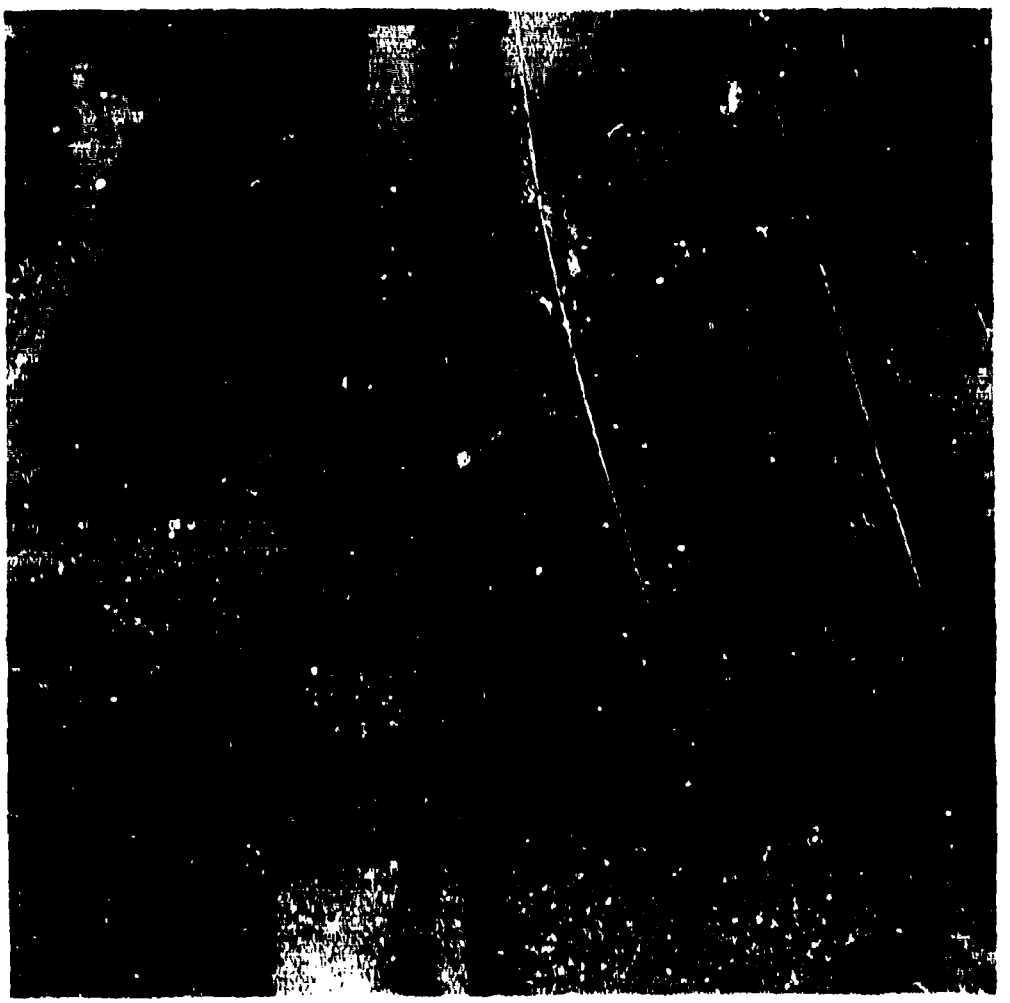

5.4.20 Two-dimensional Hadamard transform with zonal filtering and differential encoding. 2.0 bits/pel. Adaptive algorithm on 32 retained coefficients.

5.4.21 Two-dimensional Hadamard transform with zonal filtering and differential encoding. 1.5 bits/pel. Adaptive algorithm on 32 retained coefficients.

Reproduced from
best available copy.

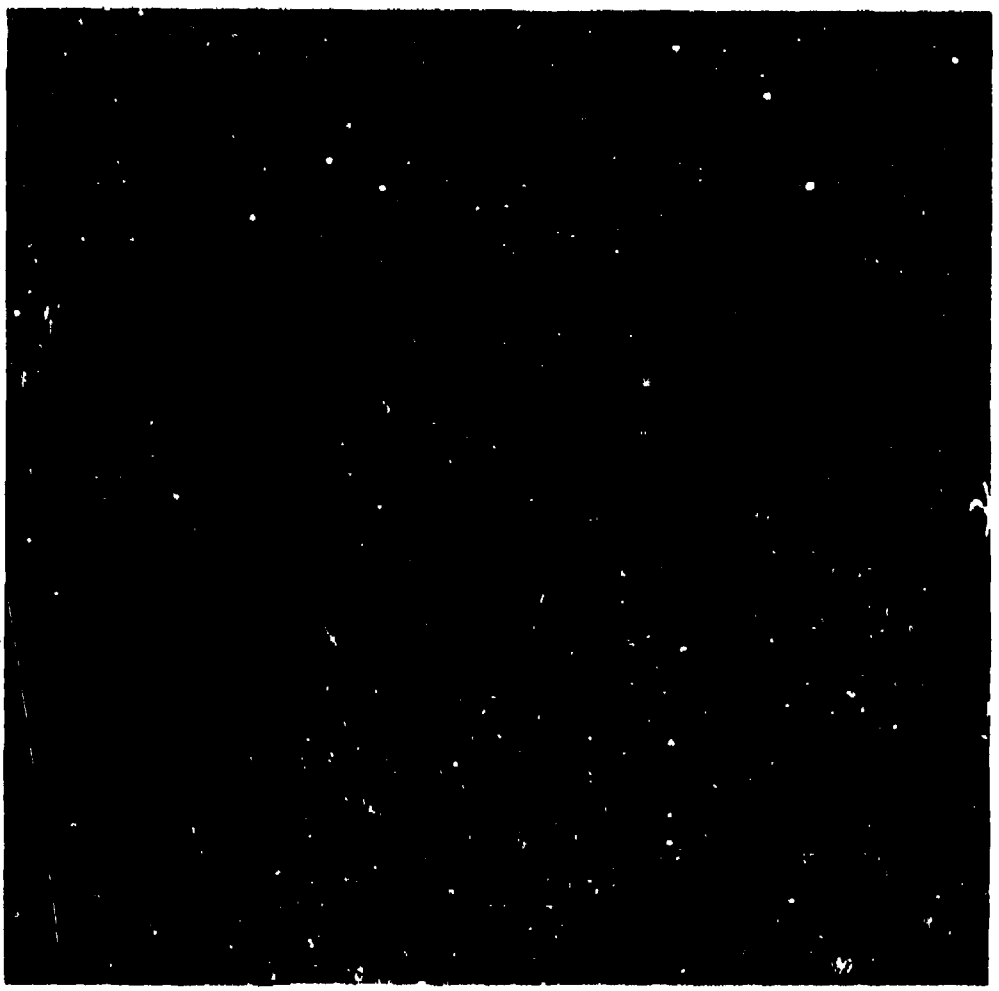

5.4.22 Two-dimensional Hadamard transform with zonal filtering and DPCM encoding. 1.0 bits/pel. Adaptive algorithm on 20 retained coefficients.

5.4.23 Two-dimensional Hadamard transform with zonal filtering and adaptive differential encoding on c_1 only. 20 coefficients retained. 0.5156 bits/pel.

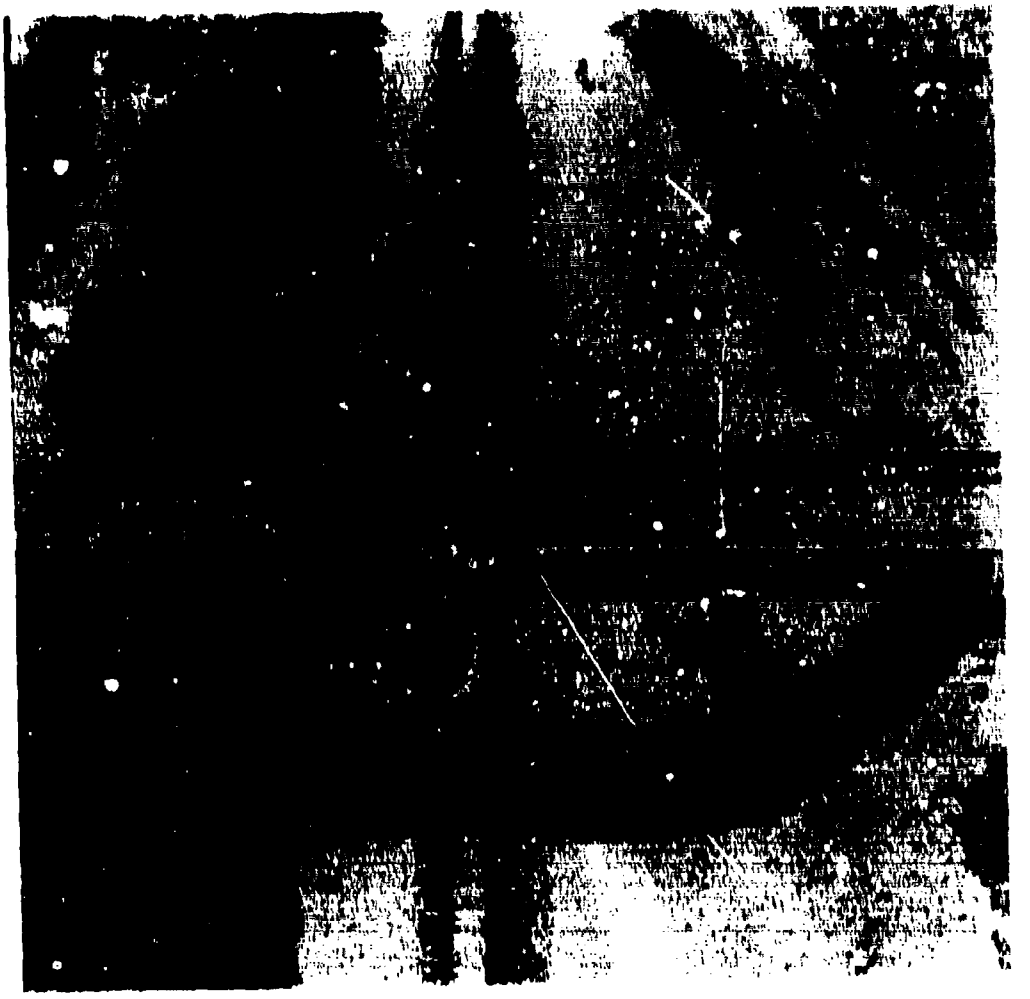

5.4.24 Two-dimensional Hadamard transform with zonal filtering and adaptive differential encoding on c_1. and c_2 only. 20 coefficients retained. 0.53125 bits/pel.

5.4.25 Two-dimensional Hadamard transform with zonal filtering and adaptive differential encoding on c_1, c_2 and c_3 only. 20 coefficients retained. 0.55469 bits/pel.

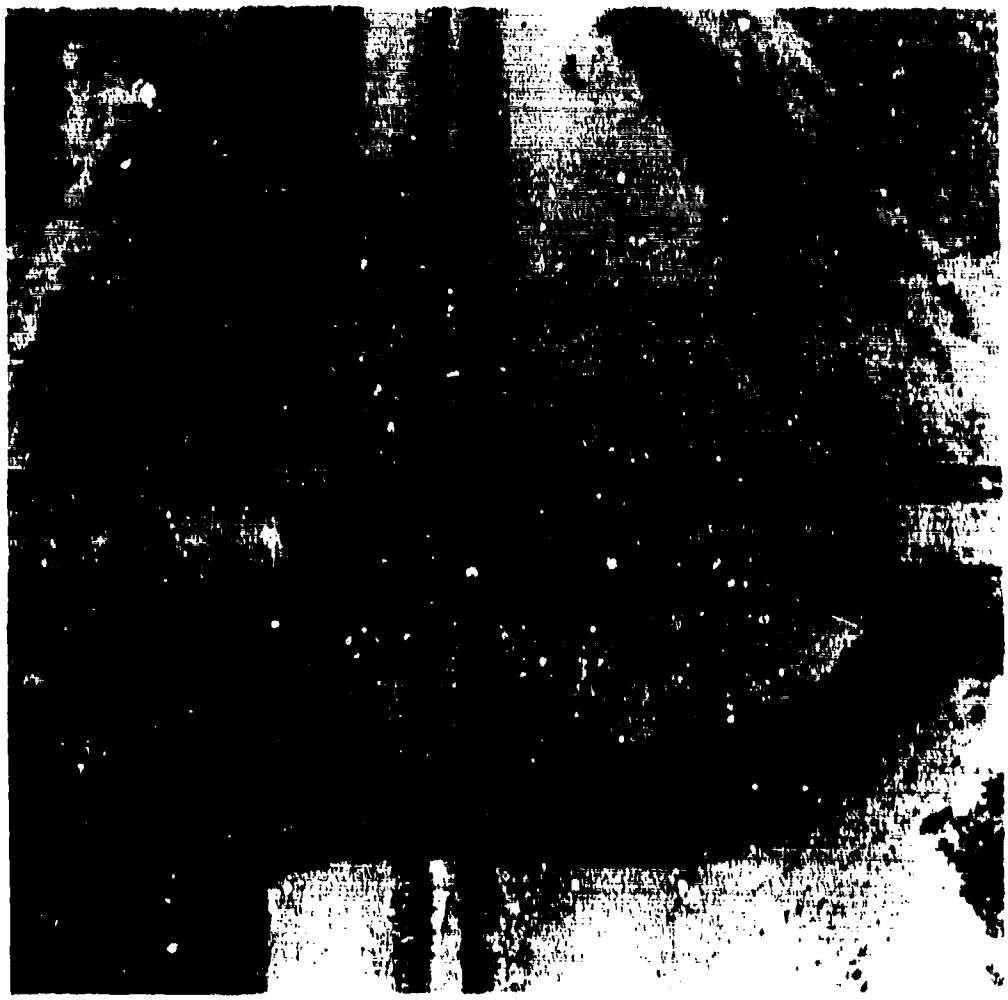

5.4.26 Two-dimensional Hadamard transform with zonal filtering and adaptive differential encoding on 8 coefficients. 12 retained coefficients. 0.5 bits/pel.

5.4.27 Two-dimensional transform with
zonal filtering and adaptive DPCM.
24 retained coefficients.
8 adaptive coefficients.
1.0 bits/pel.

Reproduced from
best available copy.

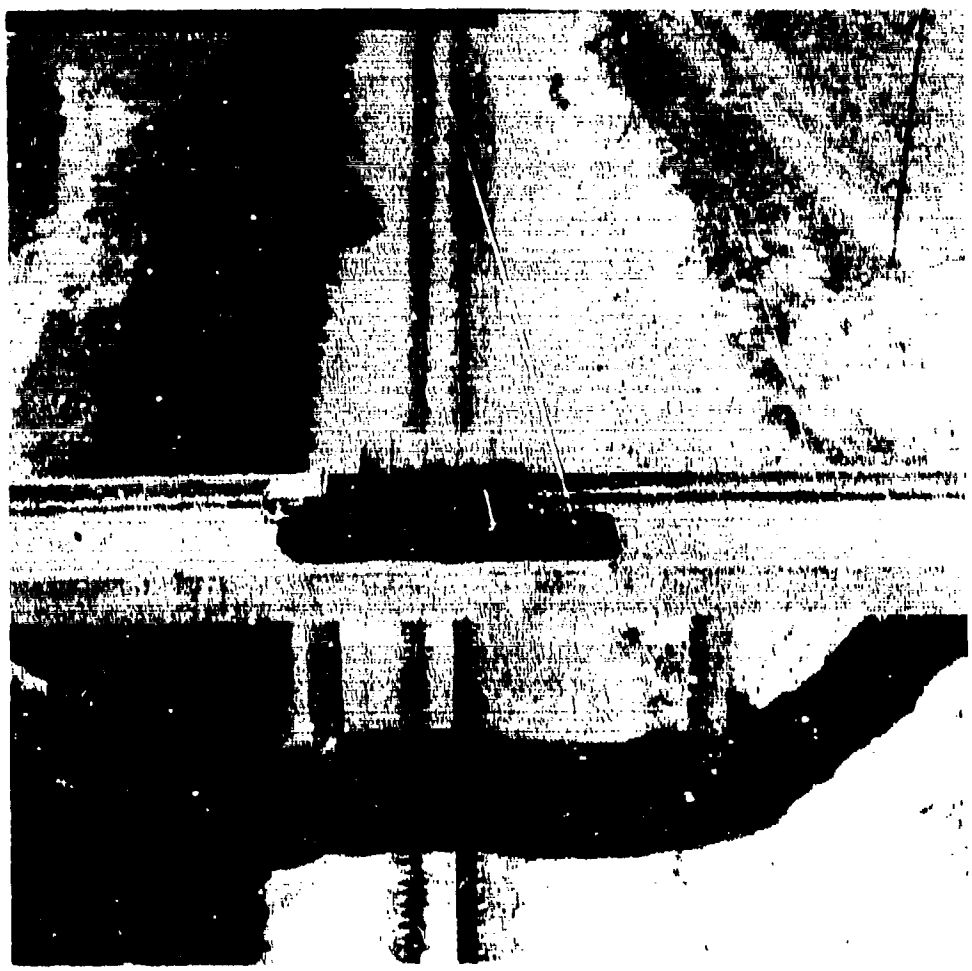

5.4.28 Two-dimensional Hadamard transform with zonal filtering and differential encoding. 11 retained coefficients 11 adaptive coefficients. 2 bits/diff. Average bit assignment: 1.0625 bits/pel.

5.5 Variations in Adaptive Scheme and Recommendations for Further Investigations.

The results given in Section 5.4 relied on assigning at least one bit for encoding the difference in the estimates of the standard deviations. Using this scheme and an average of 0.5 bits to encode the coefficients results in an average of 1.5 bits/pel for the effective bit rate. Several variations in the scheme could be tried such as using a bit assignment procedure to encode the differences in the standard deviations. This would result in truncating some of the estimates and transmitting only the important ones.

In order to see what effects such a procedure would have on the error, several simulations were performed using adaptation on only the first few coefficients. These results are shown in Table 5.5.1.

Number of Coefficients Using the Adaptive Scheme	Average Bits Assigned to Transform Coefficient	Bits Assigned to the Difference of the Estimate	Effective Bit Rate	MSE	NDSE
1	.5	1.0	0.5156	0.011866	0.515625
1 and 2	.5	1.0	0.53125	0.011967	0.83463
1, 2 and 3	.5	1.0	0.54875	0.0119	0.8.601

Table 5.5.1. Results Using the Adaptive Scheme on Only The First Few Coefficients.

It is seen from these results that using the adaptive feature on only the first few most important terms give equivalent and as a matter of fact slightly better results than those obtained in the previous section (see Table 5.4.1). This is due to the fact that using only 32 samples to estimate the standard deviations can result in error as explained before and thus it is entirely possible that using the adaptive feature on the lower and more information carrying coefficients could result in less error.

The results given in this chapter are far from conclusive. The study of the adaptive scheme was initialized during the last month of the contract which did not leave sufficient time for complete theoretical and experimental investigations Even with the preliminary results obtained thus far it is seen that this adaptive scheme performs considerably better than the non-adaptive scheme. The hardware involved in implementing this scheme is rather minimal e.g.

(1) For estimating the variance, a divide by a multiple of two can be implemented by a shift register.

(2) Normalization of Coefficient.

(3) DPCM encoders for the estimates.

In view of the results obtained to present, it is recommended that additional effort be expended to optimize the systems described above. One other improvement which should be investigated is the elimination of the necessity of transmitting the estimates of the variances. This could be accomplished by having a predetermined algorithm which by looking at the bit stream for each of the coefficients we could adjust the quantizer in some predetermined manner. The receiver could then use the same rules to adjust its quantizers thus eliminating the need for transmitting information about the estimates of the variance. Such companding rules (for example the 7-7-4-3 rule) have been used successfully in designing adaptive systems for speech signals. In addition the adaptive procedures described here could be used on the Hybrid coding techniques.

An investigation of this type can readily be performed by computer search techniques.

CHAPTER VI

CONCLUSIONS AND RECOMMENDATIONS

The frame-to-frame reduction techniques described in Chapter II do not seem at the present time to be applicable to the RPV mission due to the complexity of implementation and the large amount of storage required. In order to obtain large bit reduction ratios, it is necessary to be able to predict the movement of picture elements from one frame to another. This requires that relative accurate knowledge about such parameters as:

(1) Vertical and horizontal fields of vision

(2) The velocity vector

(3) The altitude

(4) Optical parameters such as focal length, etc.

(5) Depression angles

(6) Frame rate

(7) Dimensions of the frame

If the parameters noted above are known, large bit reductions are possible, even though it is required that synchronization information be transmitted along with each sample. The system was analyzed in Chapter II using simulated pictures and the results are presented there. Sensitivity to the accuracy of the parameters given above are included. Real pictures could not be used in the simulation due to the lack of consistent data from frame-to-frame.

The frame-to-frame techniques described in Chapter II would be useful and practical for synthetic frame generation at the remote ground station. This would enable the use of relatively slow frame rates and using the algorithms given, one could easily generate synthetic frames for insertion at the ground

station. This would eliminate some of the psychophysical effects of using slow frame rates.

Chapter III gives theoretical results using two-dimensional transform techniques and Hybrid coding techniques. For the Hybrid coding schemes both the Transform-DPCM and DPCM-Transform techniques are considered. It is shown that both systems have exactly equivalent performances; hence, due to the simplicity of the Transform-DPCM it is preferred.

The order of implementation complexities of the two-dimensional transform techniques and also their order of performances are:

(1) Karhunen Loève

(2) Discrete Cosine

(3) Fourier

(4) Hadamard

(5) Haar

Due to implementation simplicities the Hadamard or the Haar transforms are generally preferred for practical systems. These two-dimensional schemes are generally performed using two one-dimensional transforms. One in the horizontal direction to remove the correlation in that spatial direction and then one in the vertical direction to remove the correlation in that spatial direction. Although theoretically the removal of the correlation in one spatial direction does not affect the correlation in the other, for real data, such as the pictures used in this investigation, this is shown not be the case.

It is shown that the Hybrid coding schemes perform better than most two-dimensional transform techniques, being almost equal in performance to the two-dimensional Karhunen Loève transform techniques. The sensitivity to the prediction coefficients in the DPCM encoders are shown to be minimal.

The effects of channel noise on the Hybrid coding schemes are shown to be considerably more degrading using these schemes than on the two-dimensional transform schemes. However, by optimization of the Hybrid coding schemes and by periodic initialization the sensitivity to noise can be greatly reduced.

Several different error criteria were investigated to see if some type of quantitative measures could be obtained which would correlate well with subjective evaluations. Those investigated were:

(1) Normalized-mean-squared-error (MSE)

(2) Normalized-derivative-squared-error (NDSE)

(3) Normalized-mean-absolute error (MAE)

Results indicate that the MSE measure gives good correlation when one restricts the evaluations to the same picture and to the same processing techniques. This measure can be used effectively for determining the effects of lowering the bit rate, noise, etc. when comparing the same processing techniques. The NDSE measure appears to be more correlated with subjective evaluations, as far as the resolution obtained is concerned.

An adaptive scheme for the two-dimensional Hadamard transform technique was proposed and investigated which gives considerably better results than fixed two-dimensional transforms. This technique is slightly more complex; however, the improvements may well be worth this increased complexity.

Numerous pictures using the techniques described above are given in Chapters IV and V.

Table 6 summarizes the important average characteristics of the techniques studied in this investigation along with several results taken from the literature. These methods are thought to be the most applicable to the RPV.

It is recommended that further study be performed on the adaptive algorithm

presented in Chapter V. In particular an adaptation algorithm should be determined which requires the transmission of no additional information. Such a system should not be much more complex than the conventional two-dimensional transformations or Hybrid coding techniques. The use of error correcting coding for both types of systems (Transform and Hybrid) should be investigated along with channel characteristics and transmission modems. The effects of finite word lengths used on a practical system should be considered with regards to the sensitivity of the processing techniques.

	DPCM[1]			Time Predictive[1]	
	1-D	2-D	2-D Adaptive DPCM	Zero Order Predictor	Fan
MSE	.025	.016		.009	.0098
MOSE					
Sensitivity to Picture Statistics	Large	Large	Moderate	Small	Small
Sensitivity to Noise	Large (See Comment)	Large (See Comment)	Large	Moderate	Moderate
Computational Complexity	Very Small	Very Small	Moderate	Large	Large
Implementation Cost	Very Small	Very Small	Moderate	Large	Large
Reduction[2] Ratio	2.6	2.6	3.5	8.9-2	8.9-2
Bits/pel	3.0	3.0	2.3	0.9-4	.9-4
Subject in Quality of Pictures	Good	Good	Good	Moderate	Moderate
Comments	Can be made less sensitive to noise by optimization			Synchronization Information and Buffer storage required	

(1) Taken from Literature (2) Experimental Results

Table 6. Summary of Data Compression Techniques (continued on next 2 pages)

	2-D Transform						
	Karhunen-Loève	Discrete Cosine[2]	Slant[1]	Discrete Linear[1]	Fourier	Hadamard[2]	Haar
MSE	.001-.02	.015-.02	<.01 (See Comment)	<.03	.012-.005 (See Comment)	.01-.04	.02-.05
NMSE		.5-.8				.5-.87	
Sensitivity to Picture Statistics	Large	Small	Small	Small	Small	Small	Small
Sensitivity to Noise	Small	Small	Small	Small	Small	Small	Small
Computational Complexity	Very Large (N^4 Computations)	Large [$4N^2$ ($1+\log_2 N$ Computations]	Moderate [$2N^2 \log_2 N$ $+N^2-4N$]	Moderate	Moderate [$2N^2 \log_2 N$ Complex Computations]	Very Moderate [$2N^2 \log_2 N$ Additions and Subtractions]	Small [$4N(N-1)$ Add. and Subtract.]
Implementation Cost	Very Large	Large	Moderate	Moderate	Large	Very Moderate	Small
Reduction[2] Ratio	4.0	8-5.3	8-2.6	7.5-3.4 (See Comment)	8-4	8-5.3	8-5.3
Bits/pel	2.0	1.0-1.5	.-3	.8-1.75	1-2	1-1.5	1-1.5
Subject in Quality of Pictures	Very Good	Acceptable to Good	Good	Good	Good	Acceptable to Good	Acceptable to Good
Comments			Using a 4-1 reduction	Based on 6-Bit Picture	Using 2 bits/pel		

(1) Taken from Literature

(2) Experimental Results

Table 6. (continued)

			Hybrid Coding			Interframe	
	Adaptive[2] Coding (2-D Hadamard)	Adaptive[1] Block Quantization	Transform-DPCM (Hadamard)[2]	DPCM-Transform[2] (Hadamard)	Contour Coding[1]	Frame-to[2] Frame DPCM	Conditional Replenishment[1]
MSE	.001-.004	.002-.06	.02-.035	Same as Transform-DPCM		See Comment	See Comment
MDSE	.5-.9		.6-1.0	Same as Transform-DPCM		See Comment	See Comment
Sensitivity to Picture Statistics	Very Small	Large	Moderate	Same as Transform-DPCM	Large	Large	Moderate
Sensitivity to Noise	Small	Small	Large (See Comment)	Same as Transform-DPCM	Large	Large	Large
Computational Complexity	Moderate	Very Large	Very Small	Same as Transform-DPCM	Very Large	Very Large	Very Large
Implementation Cost	Moderate	Very Large	Very Small	Same as Transform-DPCM	Very Large	Very Large	Very Large
Reduction[2] Ratio	8-4	13-6	8-5.3	Same as Transform-DPCM	23-4	13-2.6	3-2
Bits/pel	1-1.5	1.3-0.6	1-1.5	Same as Transform-DPCM	0.25-1.5	.6-3	1-4
Subject in Quality of Pictures	Good	Good-Acceptable	Good	Same as Transform-DPCM	Poor-Good		Poor-Good
Comments			Can be made less sensitive to noise by optimization	Same as Transform-DPCM		Results given for simulated pictures in Chapter II	Results for picture data

(1) Taken from Literature (2) Experimental Results

Table 6. (continued)

APPENDIX

Typical Histograms for the Transform Coefficients

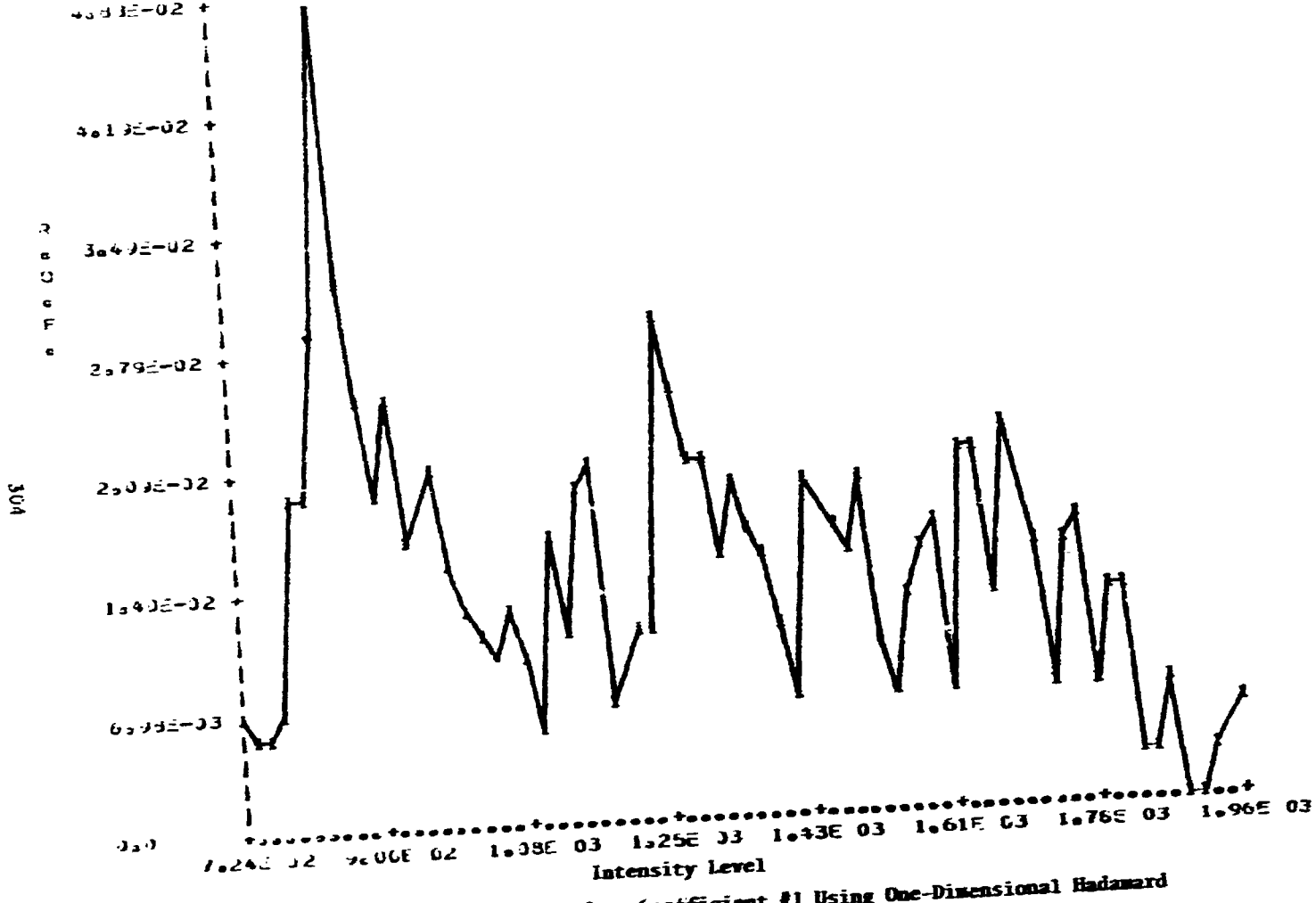

Fig. A-1 Histogram of Transform Coefficient #1 Using One-Dimensional Hadamard Transform (Block Size 1x32), Variance = 3473.328.

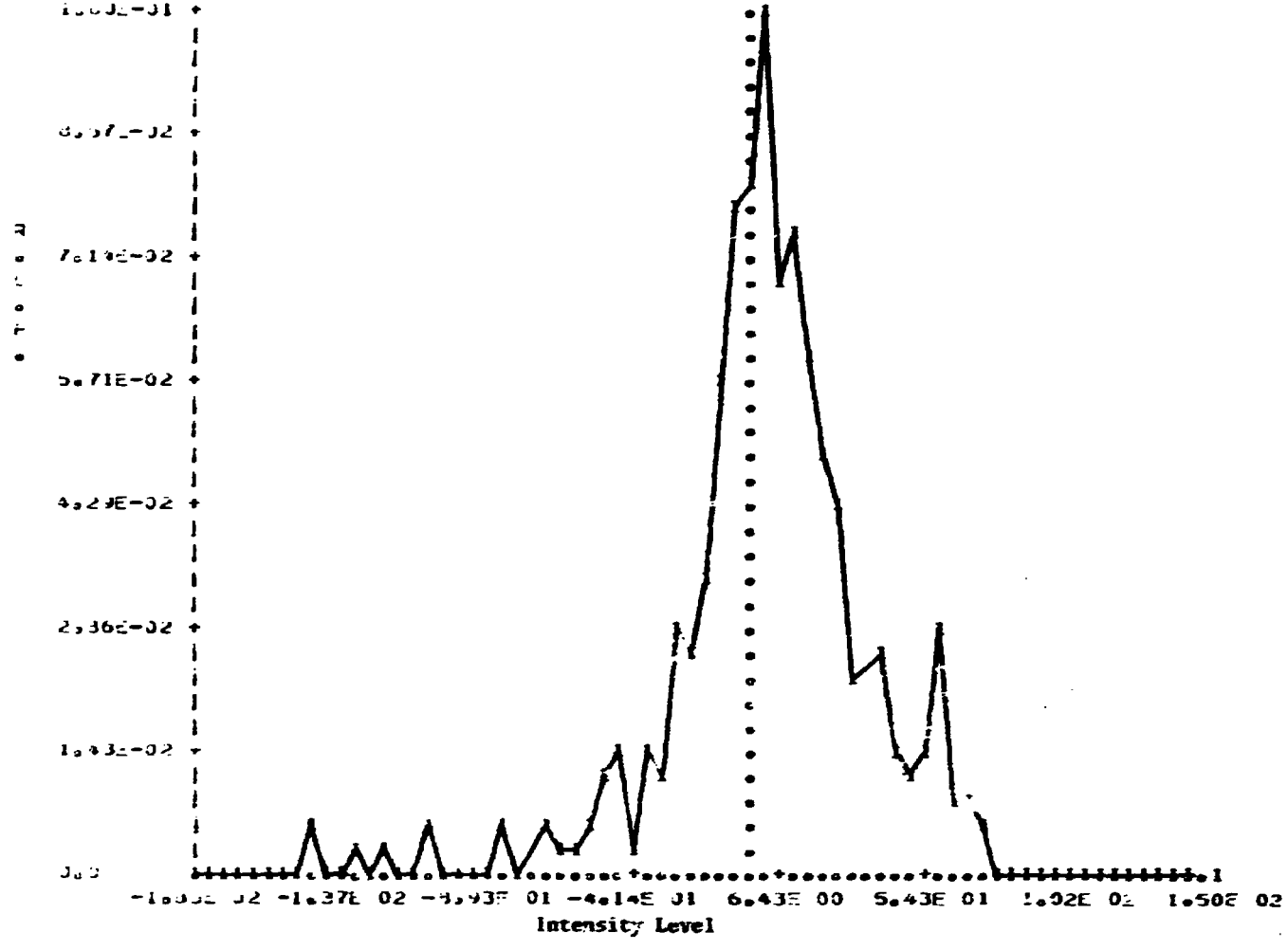

Fig. A-2. Histogram of Transform Coefficient #4 Using One-Dimensional Hadamard Transform (Block Size 1x32), Variance = 47.0241.

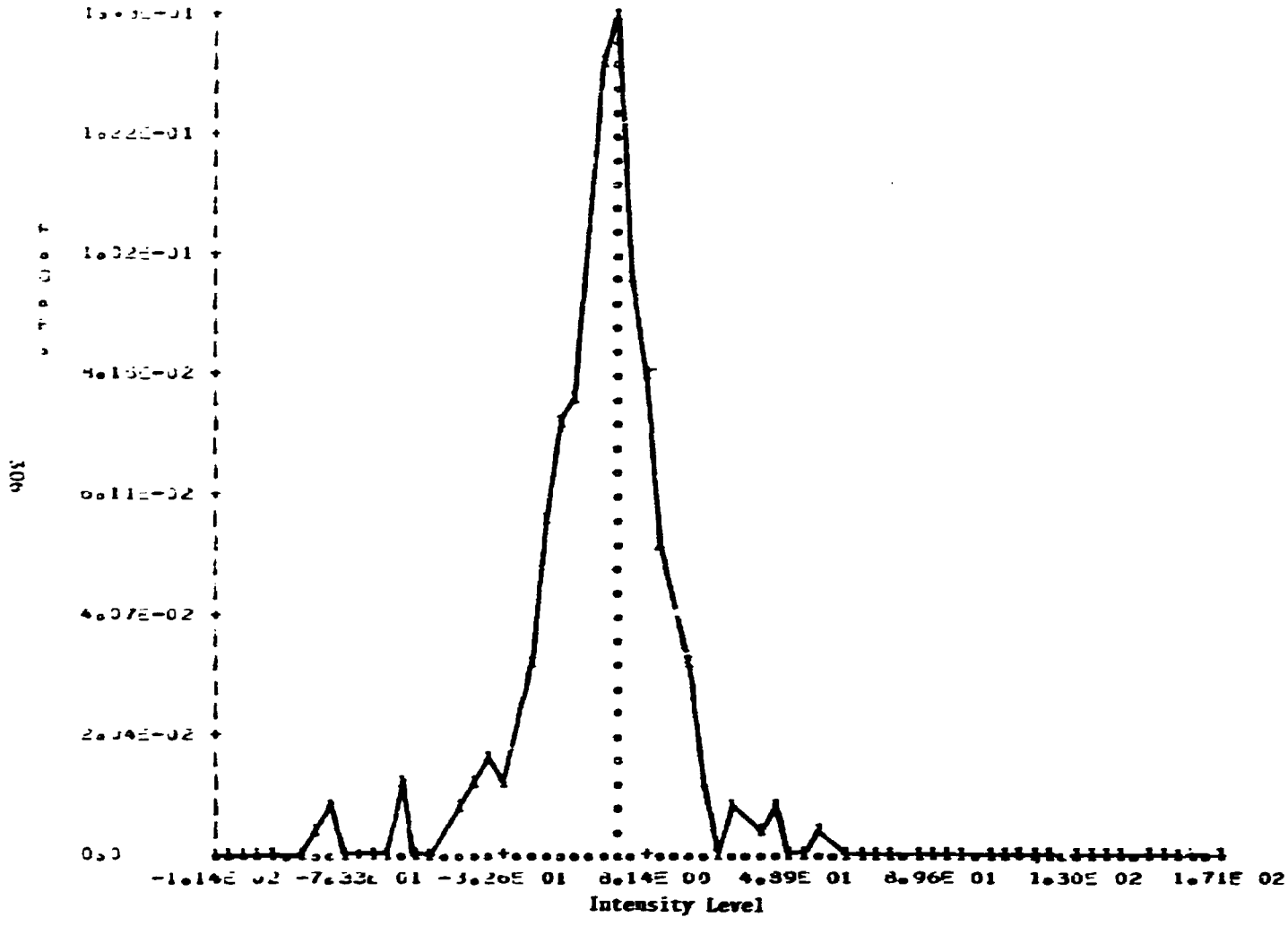

Fig. A-3. Histogram of Transform Coefficient #7 Using One-Dimensional Hadamard Transform (Block Size 1x32), Variance = 31.8469.

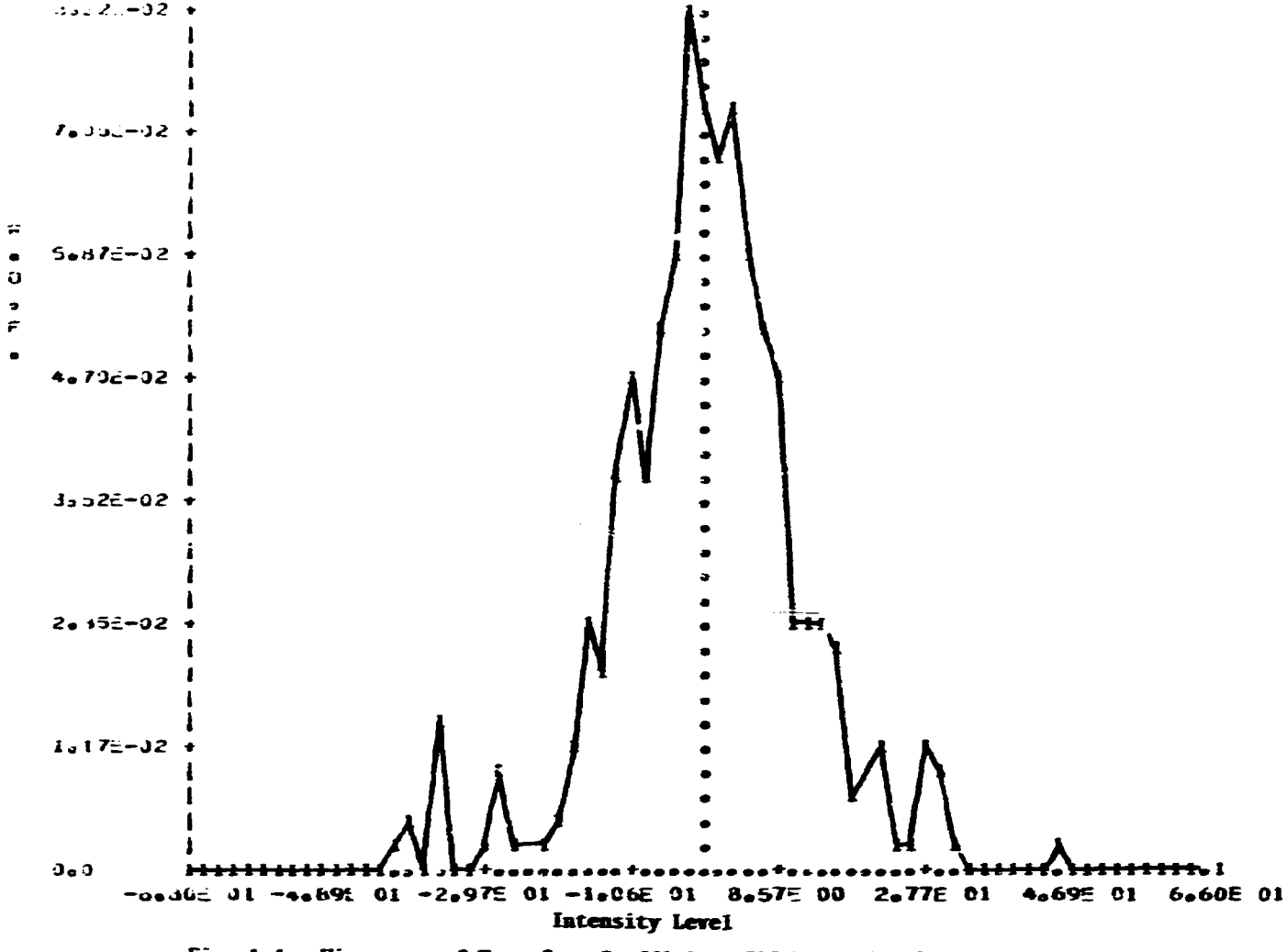

Fig. A-4. Histogram of Transform Coefficient #10 Using One-Dimensional Hadamard Transform (Block Size 1x32), Variance = 7.775C.

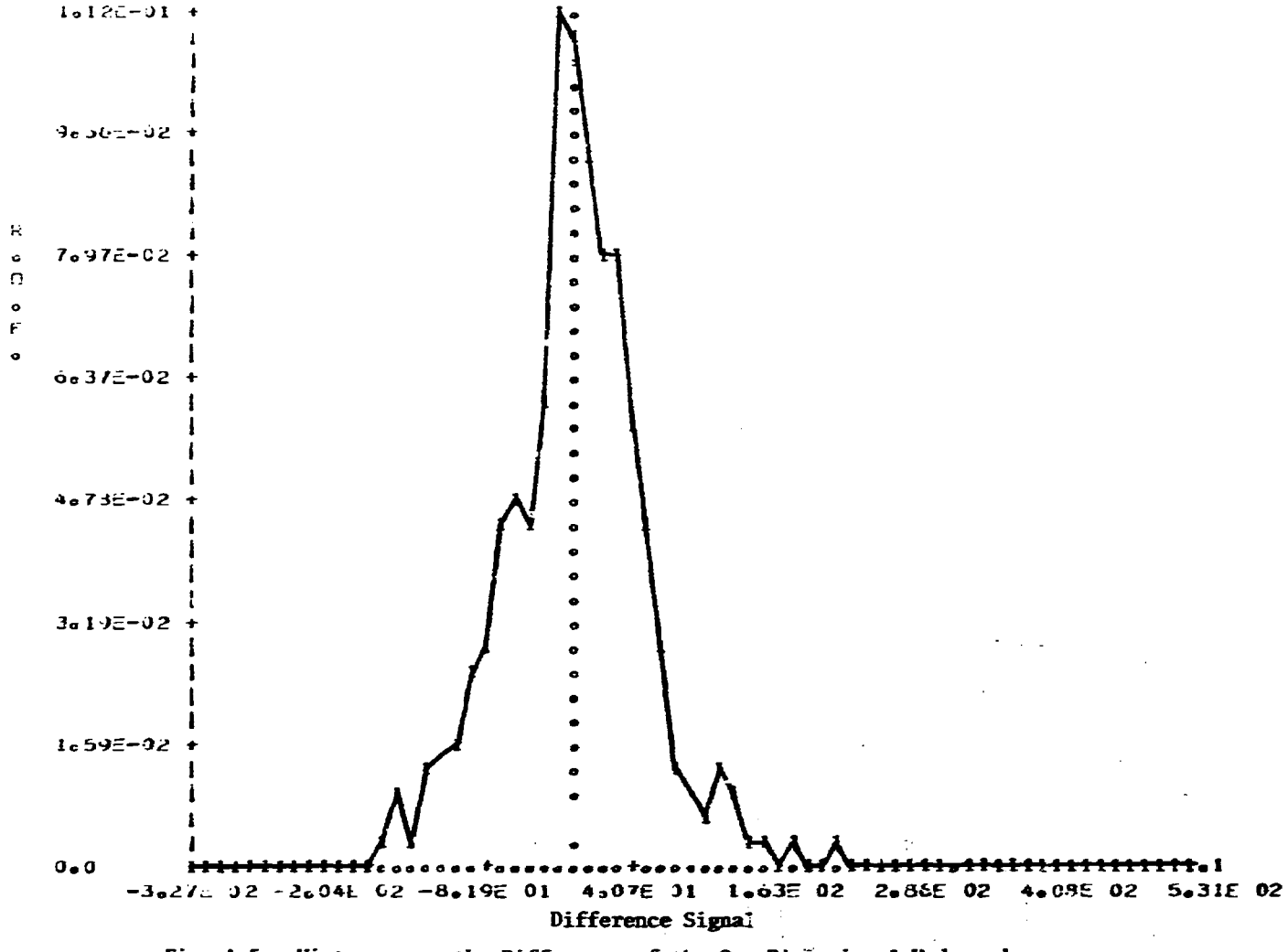

Fig. A-5. Histogram of the Difference of the One-Dimensional Hadamard Transform Coefficient #1 (Block Size 1x32), Variance = 127.214.

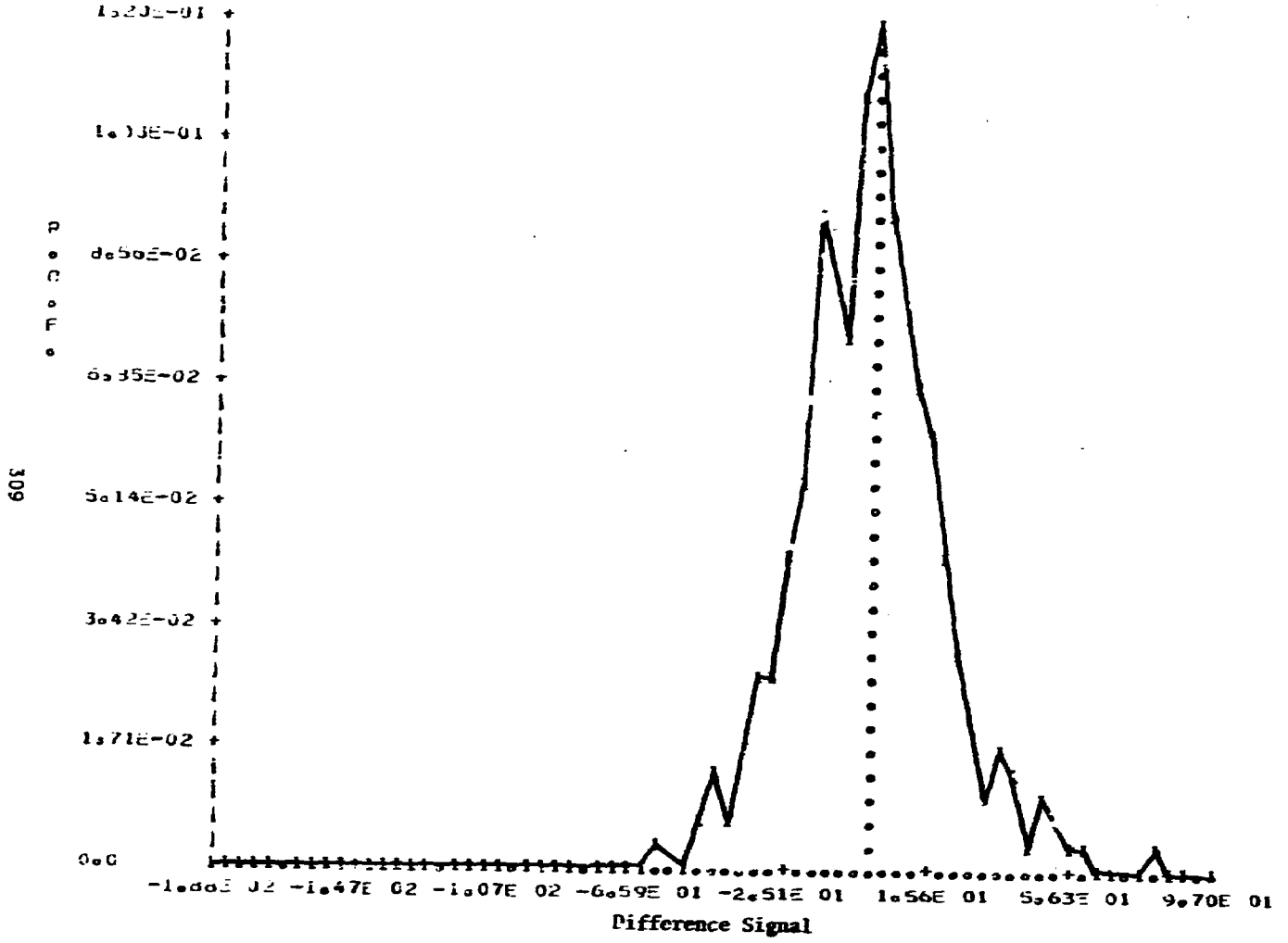

Fig. A-6. Histogram of the Difference of the One-Dimensional Hadamard Transform Coefficient #4 (Block Size 1x32), Variance = 17.612.

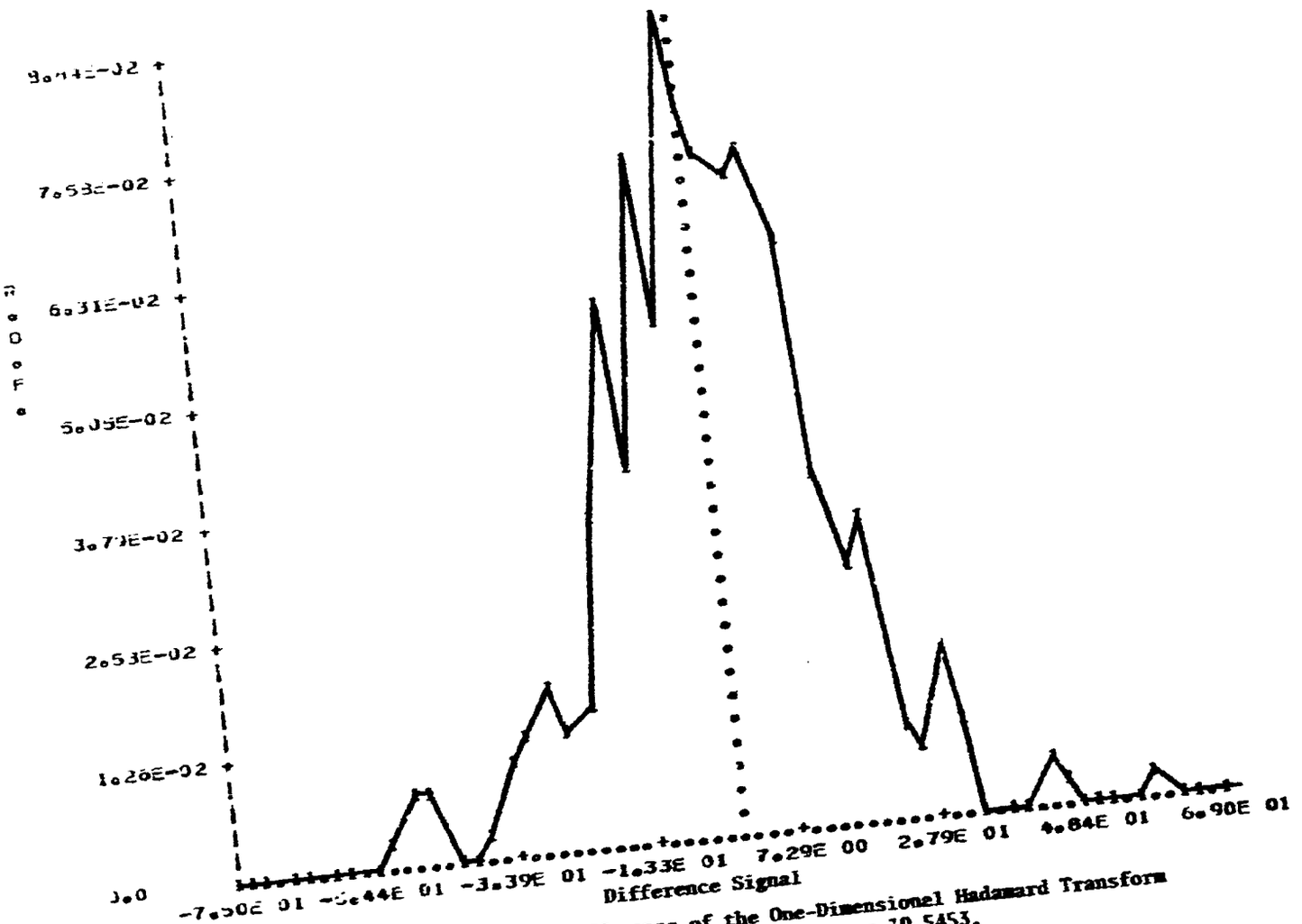

Fig. A-7. Histogram of the Difference of the One-Dimensional Hadamard Transform Coefficient #7 (Block Size 1x32), Variance = 10.5453.

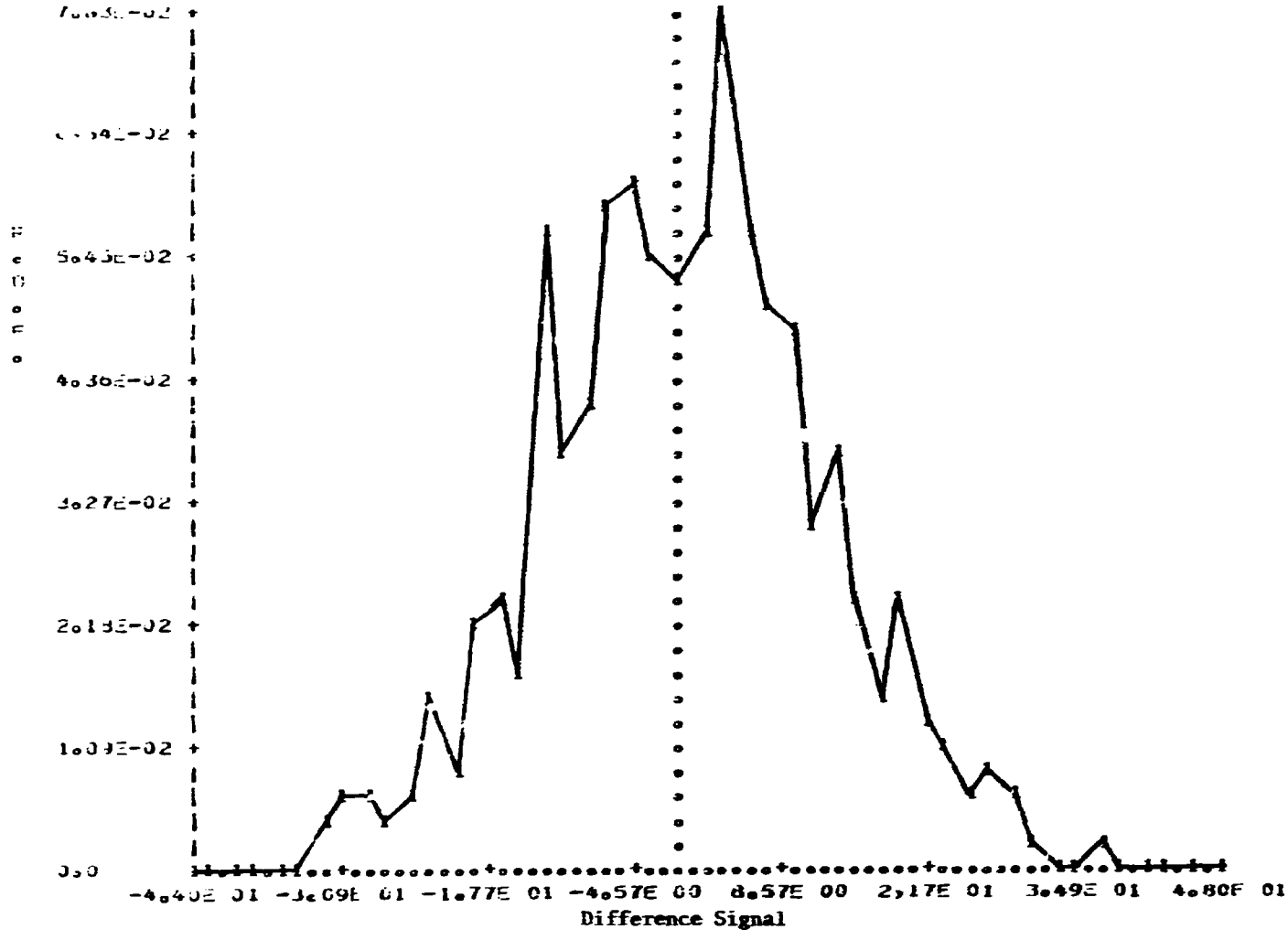

Fig. A-8. Histogram of the Difference of the One-Dimensional Hadamard Transform Coefficient #10 (Block Size 1x32), Variance = 5.8997.

REFERENCES

I. TRANSFORM-THEORY AND APPLICATION

[1] T. S. Huang, "PCM Picture Transmission," IEEE Spectrum, Vol. 2, pp. 57-63, December, 1965.

[2] T. S. Huang, W. F. Schreiber and O. J. Tretiak, "Image Processing," Proc. IEEE, Vol. 59, No. 11, pp. 1586-1609, November, 1971.

[3] H. Hotelling, "Analysis of a Complex of Statistical Variables into Principle Components," J. Educ. Psychol., Vol. 24, pp. 417-441 and pp. 498-520, 1933.

[4] V. R. Algazi and D. J. Sakrison, "On the Optimality of the Karhunen-Loeve Expansion," IEEE Trans. Info. Theory, Vol. IT-15, No. 2, pp. 319-321, March, 1969.

[5] K. Shanmugam and R. M. Haralick, "A Computationally Simple Procedure for Imagery Data Compression by the Kahunen-Loéve Method," IEEE Trans. Syst., Man, Cybern., (Corresp.) Vol. SMC-3, pp. 202-204, March, 1973.

[6] W. D. Ray and R. M. Driver, "Further Decomposition of the Karhunen-Loeve Series Representation of a Stationary Random Process," IEEE Trans. Info. Theory, Vol. IT-16, No. 6, November, 1970.

[7] W. K. Pratt, "Karhunen-Loéve Transform Coding of Images," presented at the 1970 IEEE Int. Symp. Infor. Theory, June, 1970.

[8] J. L. Brown, Jr., "Representation of Random Processes by Complete Orthonormal Sequences," Proc. IEEE, Vol. 58, No. 1, pp. 172-173, January, 1970.

[9] J. Pearl, "Karhunen-Loéve Transforms Processing of Stationary Data Comparison with Discrete Fourier Transform," IEEE Trans. Inform. Theory, pp. 229-232, May, 1973.

[10] J. Pearl, H. C. Andrews and W. K. Pratt, "Performance Measures for Transform Data Coding," IEEE Trans. Comm. Tech., Vol. COM-20, pp. 411-415, June, 1972.

[11] J. J. Y. Huang and P. M. Schultheiss, "Block Quantization of Correlated Gaussian Random Variables," IEEE Trans. Comm. Systems, Vol. CS-11, pp. 289-296, September, 1963.

[12] H. P. Kramer and M. V. Matthews, "A Linear Coding for Transmitting a Set of Correlated Signals," IRE Trans. Inform. Theory, Vol. IT-2, pp. 41-46, September, 1956.

[13] A. Habibi and P. A. Wintz, "Optimum Linear Transformations for Encoding Two-Dimensional Data," School of Elect. Engr., Purdue Univ., Lafayette, Indiana, Tech. Rep. TR-EE69-15, May, 1969.

[14] W. B. Davenport, Jr., and W. L. Root, An Introduction to the Theory of Random Signals and Noise, McGraw-Hill, New York, New York, 1958.

[15] J. Pearl, "On Coding and Filtering Stationary Signals by Discrete Fourier Transforms," IEEE Trans. Info. Theory, Vol. IT-19, No. 2, pp. 229-232. March, 1973.

[16] C. L. Rino, "The Inversion of Covariance Matrices by Finite Fourier Transforms," IEEE Trans. Info. Theory, Vol. IT-16, No. 2, pp. 230-232, February, 1970.

[17] K. Brayer, "Euclidian Orthogonal Data Transmission," Proc. IEEE. Vol. 49, No. 1, pp. 79-80, January, 1971.

[18] R. M. Gray, "Toiplitz and Circular Matrices: A Review," Stanford Univ., Stanford, Calif., Rep. SU-SEL-71-032, June, 1971.

[19] J. L. Brown, "Mean Square Truncation Error in Series Expansions of Random Functions," J. SIAM, Vol. 8, pp. 18-32, March, 1960.

[20] J. H. McClellan and T. W. Parks, "Eigenvalue and Eigenvector Decomposition of the Discrete Fourier Transform," IEEE Trans. Audio and Electroacoustics, Vol. AU-20, No. 1, pp. 66-75, March, 1972.

[21] M. Hamidi and J. Pearl, "On the Residual Correlation of Finite-Dimensional Discrete Fourier Transforms of Stationary Signals," IEEE Trans. on Inform. Theory, Vol. IT-25, No. 4, pp. 480-482, July, 1975.

[22] L. M. Goodman, "A Binary Linear Transformation for Redundancy Reduction," Proc. IEEE (letters) (Special Issue on Redundancy Reduction), Vol. 55, pp. 467-468, March, 1967.

[23] W. K. Pratt and H. C. Andrews, "Application of Fourier-Hadamard Transformation to Bandwidth Compression," presented at the 1969 Symp. on Picture Bandwidth Compression, M.I.T., Cambridge, Mass.

[24] T. S. Huang and J. W. Woods, "Picture Bandwidth Compression by Block Quantization," presented at the 1969 Int. Symp. Information Theory, Ellenville, N. Y., January 28-31.

[25] T. S. Huang and J. W. Woods, "Picture Bandwidth Compression by Linear Transformation and Block Quantization," presented at the 9th Symp Picture Bandwidth Compression, M.I.T., Cambridge, Mass.

[26] G. B. Anderson and T. S. Huang, "Piecewise Fourier Transformation for Picture Bandwidth Compression," IEEE Trans. Comm. Tech., Vol. COM-19, No. 2, pp. 133-140, April, 1971.

[27] H. C. Andrews and W. K. Pratt, "Digital Image Transform Processing," Proc. 1970 Walsh Functions Symp., pp. 183-194.

[28] A. Habibi and P. [illegible], "Image Coding by Linear Transformations and Block Quantization;" IEEE Trans. Comm. Tech., Vol. COM-19, pp. 50-62, February, 1971.

[29] A. Habibi, "Comparison of nth Order DPCM Encoder With Linear Transformations and Block Quantization Techniques," IEEE Trans. Comm. Tech., Vol. COM-19, No. 6, pp. 948-956, December, 1971.

[30] M. Tasto and P. A. Wintz, "Image Coding by Adaptive Block Quantization," IEEE Trans. Comm. Tech., Vol. COM-19, pp. 50-62, February, 1971.

[31] W. K. Pratt, H. C. Andrews, "Transform Image Coding," Univ. of Southern Calif., Los Angeles, Calif., Final Rep. USCEE287, March, 1970.

[32] P. A. Wintz, "Transform Picture Coding," Proc. IEEE, Vol. 60, No. 7, pp. 809-820, July, 1972.

[33] J. L. Walsh, "A Closed Set of Orthogonal Functions," American Journal Mathematics, Vol. 55, pp. 5-24, 1923.

[34] H. Rademacher, "Eininge Satze von Allgemeinen Orthogonal-Funktiones," Mathematics Annals, Vol. 87, pp. 122-138, 1922.

[35] A. Haar, "Zur Theorie des Orthogonalen Funktiones-Systems," Inaugural Dissertation, Math. Annals, Vol. 69, pp. 331-371, 1910 and Vol. 71, pp 33-53, 1912.

[36] H. F. Harmuth, "A Generalized Concept of Frequency and Some Applications," IEEE Trans. Info. Theory, Vol. IT-14, No. 3, pp. 375-382, May, 1968.

[37] D. E. Bowyer, "Walsh Functions, Hadamard Matrices and Data Compression," in Appl. Walsh Functions Symp., pp. 33-37, April, 1971.

[38] S. C. Kak, "A Note on the Information Transmission with Continuous Signals," Proc. IEEE, Vol 57, No. 1, pp. 111-112, January, 1969.

[39] G. S. Robinson, "Quantization Noise Consideration in Walsh Transform Image Processing," Proc Appl. of Walsh Functions Symp. Washington, D.C. pp. 240-247, March, 1972.

[40] S. C. Kak, "On Matrices with Walsh Functions as the Eigenvectors," in Proc. Appl. of Walsh Functions Symp., pp. 384-387, March, 1972.

[41] L. R. Welch, "Walsh Functions and Hadamard Matrices," in Proc. Appl. of Walsh Functions Symp., pp. 163-165, 1970.

[42] C. W. Yuen, "Remarks on the Ordering of Walsh Functions", IEEE Trans. Computers, pp. 1452, December, 1972.

[43] G. G. Murray, "Modified Transforms in Imagery Analysis," in Proc. Appl. of Walsh Functions Symp., pp. 235-239, March, 1972.

[44] W. A. Parkyn, Jr., "Digital Image Processing Aspects of the Walsh Transform," in Proc. Appl. of Walsh Functions Symp., pp. 152-156, April, 1970.

[45] R. B. Lacky and D. Meltzer, "A Simplified Definition of Walsh Functions," IEEE Trans. Computers, Vol. C-20, No. 2, pp. 211-213, February,1971.

[46] J. W. Carl, "Comments on A Simplified Definition of Walsh Functions," IEEE Trans. Computers, Vol. C-20, No. 12, pp1617, December,1971.

[47] A. C. Davies, "Onthe Definition and Generation of Walsh Functions," IEEE Trans. Computers, Vol. C21, No. 2,pp187-189, February,1972.

[48] G. R. Redinko, "Transform of Generalized Walsh Functions," Proc. IEEE, Vol.59, No. 9, pp 1352-1353, December,1971.

[49] N. Ahmed, K. R. Rao and R. B. Schultz, "A Generalized Discrete Transform," Proc. IEEE, Vol. 59, No. 9, pp 1352-1353, December, 1971.

[50] K. R. Rao, L. C. Mrig and N. Ahmed, "A Modified Generalized Discrete Transform," Proc. IEEE, Vol. 61, No. 5, pp 668-669, March, 1973.

[51] P. A. Wintz and A. J. Kurtenbach, "Analysis and Minimization of Message Error in PCM Telemetry Systems," School of Elect. Engr., Purdue University, Lafayette ,Indiana, Technical Report, TR-EE67-19, December, 1967.

[52] P. A. Wintz and A.J. Kurtenbach, " Waveform Error Control in PCM Telemetry," IEEE Trans. Inform. Theory, Vol. IT-14, pp 650-661, September,1968.

[53] J. F. Hayes and R. Bobilin, "Efficient Waveform Encoding," School of Elect. Engr., Purdue University, Lafayette, Indiana, TR EE69-4, February, 1969.

[54] H. F. Harmuth, Transmission of Information by Orthogonal Functions, Springer-Verlog, Berlin-Heidenberg, 1972.

[55] N. Ahmed, H. H. Schreiber and P. V. Lopresti, "On Notation and Definition of Terms Related to a Class of Complete Orthogonal Functions," IEEE Trans. Electromagnetic Compatibility, Vol. EMC-15, No. 2, pp. 75-77, May, 1973.

[56] W. K. Pratt, J. Kane and H. C. Andrews, "Hadamard Transform Image Coding," Proc. IEEE, Vol. 57, No. 1 pp. 58-68, January,1969.

[57] E. J. Clair, S. M. Farber and R. R. Green, "Practical Techniques for Transform Data Compression/Image Coding," Proc. 1971 Applications of Walsh Functions Symp., pp. 2-6, Washington, D.C., April, 1971.

[58] J. Poncin, "Utilization de la Transformation de Hadamard pour le Codage et la Compression de Signaux d'Images," Ann. Telecommun, July-August, 1971.

[59] H. J. Landau and D. Slepian, "Some Computer Experiments in Picture Processing for Bandwidth Reduction," B.S.T.J., Vol. 50, No. 5, pp. 1525-1540, May-June, 1971.

[60] P. J. Ready and P. A. Wintz, "Multispectral Data Compression Through Transform Coding and Block Quantization," School of Elect. Engr., Purdue University, Lafayette, Indiana, Tech. Rep. TR_EE72-29, May, 1972.

[61] J. W. Woods, "Video Bandwidth Compression by Linear Transformation," Quartly Report, NO. 91, M.I.T. Research Lab. of Electronics, pp. 219-224, October 15 ,1968.

[62] J. D. Kennedy, "Walsh Function Imagery Analysis," Proc. Appl. of Walsh Functions Symp., Washington, D.C. 1971.

[63] H. C. Andrews, "Walsh Functions in Image Processing, Feature Selection and Pattern Recognition," Proc. Appl. of Walsh Functions, Washington, D.C., April, 1971.

[64] H. Enomoto and K. Shibata, "Orthogonal Transformation Coding System for Television Signals," Proc. 1971 Walsh Function Symp., pp. 11-17

[65] T. Fukinukki and M. Miyata, "Intraframe Image Coding by Cascaded Hadamard Transforms," IEEE Trans. Communications, Vol. COM-21, No. 3, pp. 175-180, March, 1973.

[66] L. F. Judd, C. J. Levy and I. D. McWaters, "Transform Data Compression Based on Various Transmission Schemes," Proc. Appl. of Walsh Functions Symp.,pp. 132-136, 1973.

[67] A. Habibi, W. K. Pratt, G Robinson, R. Means, H. Whitehouse and J. Speiser, "Real Time Image Redundancy Reduction Using Transform Coding Techniques," Intern'l Commmunications Conference, January, 1974.

[68] H.C. Andrews, "Entropy Considerations in the Frequency Domain," Proc. IEEE, Vol. 58, No. , pp. 113-144, Jan. 1968.

[69] J. Pearl, "Basis-Restricted Transformations and Performance Measures for Spectral Representations," IEEE Trans. Inform. Theory, Vol. IT-17, No. 6, pp. 751-752, Nov. 1971.

[70] H. H. Schreiber, "Weighted Quantization Error for Basis-Restricted Transformation," Proc. Appl. of Walsh Functions Symp., Wash. D.C., pp. 259-267, Apr. 1973.

[71] C. Reader, "Spatial Subsampling for the Transform Coding of Images," Proc. Appl of Walsh Functions Symp., pp. 248-252, March 1972.

[72] J. E. Shore, "On the Application of Haar Functions," IEEE Trans. Comm., Vol. COM-21, No.3, pp. 209-216, March 1973.

[73] B. J. Fino,"Relations Between Haar and Walsh/Hadamard Transforms," Proc. IEEE, Vol. 60, No. 5, pp. 647-648, May 1972.

[74] N. Ahmed, T. Natarajan and K. R. Rao, "Some Considerations of the HAAR and Modified Walsh-Hadamard Transforms," Proc. Appl. of Walsh Functions Symp., pp. 91-95, Apr. 1973.

[75] W. K. Pratt, L. R. Welch and W. Chen, "Slant TRansforms for Image Coding," Proc. Appl. of Walsh Functions Symp., Apr. 1972.

[76] W. H. Chen and W. K. Pratt, "Color Image Coding with the Slant Transform," Proc. Appl. of Walsh Functions Symp., pp. 153-161, Apr. 1973.

[77] K. Shibata, "Block Waveform Coding of Image Signals by Orthogonal Transformation," Proc. Appl. of Walsh Functions Symp., pp. 137-143, Apr. 1973.

[78] W. K. Pratt, W. H. Chen and L.R. Welch. "Slant Transform Image Coding," IEEE Trans. Comm., Vol COM-22, No. 8, pp. 1075-1093, August 1974.

[79] N. Ahmed, D. H. Lenhert and T. Natarajan, "On the Orthogonal Transform Processing of Image Data," Proc. 29th Natl' Electronics Conf., Chicago, Ill., Vol. 28, pp. 274-279, Oct. 1973.

[80] N. Ahmed, T. Natarajan and K. R. Rao, "Discrete Cosine Transform," IEEE Trans. Computers, Vol. C-23, No. 1, pp.90-93, Jan. 1974.

[81] W. K. Pratt, "Linear and Nonlonear Filtering in the Walsh Domain," Proc. Appl. of Walsh Functions Symp., pp. 38-42, Apr. 1971.

[82] J. I. Gimlett, "Use of "Activity" Classes in Adaptive Transform Image Coding," IEEE Trans. Comm., Vol. COM-23, No. 7, pp. 785-786, July 1975.

II. HYBRID CODING

[83] R. M. Haralick, K. Shanmugam, J. Young and D. Goel, "A Comparative Study of Transform Data Compression Techniques for Digital Imagery," Proc. Natl' Electronics Conf., Vol. 27, pp. 89-94, 1972.

[84] M. Arisawa, F. Kanaya and H. Noguchi, "Image Coding by the Differential Hadamard Transform," Proc. Appl. of Walsh Functions Symp., 1973.

[85] A. Habibi, "Unitary Transformations and DPCM Coding of Pictorial Data," Proc. Appl. of Walsh Functions Symp., 1973.

[86] A. Habibi, "Unitary Tramsformations and DPCM Coding of Pictorial Data," Proc. Image Coding Symp., 1973.

[87] A. Habibi, "Hybrid Coding of Pictorial Data," IEEE Trans. Comm., Vol. COM-22, No. 5, pp. 614-624, May 1974.

[88] R. M. Haralick and K. Shanmugam, "Comparative Study of a Discrete Linear Basis For Image Data Compression," IEEE Trans. Syst., Man and Cybern., Vol. SMC-4, No. 1, pp. 16-27, Jan. 1974.

[89] A. Habibi and R. S. Hershel, "A Unified Representation of Differential Pulse Code Modulation (DPCM) and Transform Coding Systems," IEEE Trans. Comm., Vol. COM-22, No. 5, pp. 692-696, May 1974.

[90] E. Angel and A. K. Jain, "A Nearest Neighbors Approach to Multidimensional Filtering," presented at the Conf. Decision and Control, New Orleans, La., Dec. 1972.

[91] A. K. Jain, "Image Modelling for Unification of Transform and DPCM Coding of Two-Dimensional Images," Proc. 29th Natl' Electronics Conf., Vol. 28, pp. 280-285, Oct. 1973.

[92] A. K. Jain and E. Angle, "Image Restoration, Modelling and Reduction of Dimensionality," IEEE Trans. Computers, Vol. C-23, No. 5, pp. 470-476, May 1974.

[93] B. G. Haskell, "Frame-to-Frame Coding of Television Pictures Using Two-Dimensional Fourier Transforms," IEEE Trans. Inform. Theory, Vol. IT-20, No. 1, pp. 119-120, Jan. 1974.

III. FAST TRANSFORM

[94] J. W. Cooley and J. W. Turkey, "An Algorithm for the Machine Calculation of Complex Fourier Series," Mathematics of Computation, Vol. 19, No. 90, Apr. 1965.

[95] W. T. Cochran, J. W. Cooley, D.L. Favin, H. D. Helms, R. A. Kaenel, W. W. Lang, G. C. Maling, Jr., D. E. Nelson, C. M. Rader and P.D. Welch, "What is the Fast Fourier Transform ?," Proc. IEEE, Vol. 55, pp. 1664-1674, Oct. 1967.

[96] J. W. Cooley, P. A. W. Lewis and P. D. Welch, "Historical Notes on the Fast Fourier Transform," Proc. IEEE, Vol. 55, pp. 1675-1677, Oct. 1967.

[97] J. W. Cooley, P. A. W. Lewis and P. D. Welch, "The Finite Fourier Transform," IEEE Trans. Audio Electroacoustics, Vol. AU-17, pp.77-85, June 1969.

[98] R. C. Singleton, "A Short Bibliography on the Fast Fourier Transform," IEEE Trans. Audio Electroacoustics, Vol. AU-17, pp. 166-169, June 1969.

[99] W. M. Gentlemen, "Matrix Multiplication and Fast Fourier Transform," BSTJ, Vol. 47, No. 6, pp. 1099-1104, July-August 1968.

[100] G. Rams, "Analog Computation of the FAst Fourier Transform," Proc. IEEE, Vol. 58 No. 11, pp. 1861-1863, Nov. 1970.

[101] H. L. Croginsky, "An FFT Chart," Proc. IEEE, Vol. 58, No.10, pp. 1782-1783, Oct. 1970.

[102] J. L. Vernet, "Real Signals Fast Fourier Transform : Storage Capacity and Step Number Reduction by Means of an Odd Discrete Fourier Transform," Proc. IEEE, Vol. 58, No. 10, pp.1782-1783, Oct. 1970.

[103] N. Ahmed, K. R. Rao and R. B. Schultz, "Fast Complex BIFORE Transform by Matrix Partitioning," IEEE Trans. Computers, Vol. C-20, No. 6, pp.707-710, June 1971.

[104] L. J. Ulman, "Computation of the Hadamard Transform and the R-Transform in Ordered Form," IEEE Trans. Computers, Vol C-19, pp. 359-360, Apr. 1970.

[105] V. J. Rejchrt, "Signal Flow Graph and a FORTRAN Program for Haar-Fourier Transform," IEEE Trans. Computers, Vol. C-21, No. 9, pp.1026-1027, Sept. 1972.

[106] Y. Y. Shum and A. R. Elliot, "Computation of the Fast Hadamard Transform," Proc. Appl. of Walsh Functions Symp., pp. 177-180, March 1972.

[107] J. W. Manz, "A Sequency-Ordered Fast Walsh Transform," IEEE Trans. Audio, Vol AU-20, pp. 204-205, August 1972.

[108] A. B. Fontaine, "Simple Dyadic and Sequency FORTRAN Mechanizations of the Fast Walsh Transform," Proc. 29th Natl' Electronics Conf., Vol. 28, pp. 271-273, Oct. 1973.

[109] H. Y. L. Mar and C. L. Sheng, "Fast Hadamard Transform Using the H Diagram," IEEE Trans. Computers, Vol. C-22, No. 10, pp. 957-960, Oct. 1973.

[110] J. W. Carl and R. V. Swartwood, "A Hybrid Walsh Transform Computer," IEEE Trans. Computers, Vol. C-22, No. 7, pp. 669-672, July 1973.

IV. FRAME-TO-FRAME TECHNIQUE

[111] F. K. Manasse, "Directional Correlation - A Technique to Reduce Bandwidth in PCM Television Transmissions," IEEE Trans. Comm. Tech., Vol. COM-15, No. 2, pp. 204-208, Apr. 1967.

[112] F. Rocca, "Television Bandwidth Compression Utilizing Frame-to-Frame Correlation and Movement Compensation," in Symp. Picture Bandwidth Compression, M.I.T., Cambridge, Massachusetts, Apr. 1969.

[113] F. Rocca and S. Zanoletti, "Bandwidth Reduction Via Movement Compensation on a Model of the Random Video Process," IEEE Trans. Comm., Vol. COM-20, No. 6, pp. 907-912, Dec. 1971.

[114] F. W. Mounts, "Low Resolution TV : An Experimental Digital System for Evaluating Bandwidth Reduction Techniques," BSTJ, Vol. 46, Jan. 1967.

[115] R. C. Brainard, F. W. Mounts and B. Prasada, "Low Resolution TV : Subjective Effects of Frame Repetition and Picture Replenishment," BSTJ, Vol. 46, No. 1, pp. 261-271, Jan. 1967.

[116] F. W. Mounts, "Frame-to-Frame Digital Processing of TV Pictures to Remove Redundancy," presented at the 1969 Symp. Picture Bandwidth Compression, M.I.T., Cambridge, Massachusetts, Apr. 1969.

[117] F. W. Mounts and D. E. Pearson, "Apparent Increase in Noise Level when Television Pictures are Frame-Repeated," BSTJ, Vol. 48, pp.527-539, 1969.

[118] J. E. Cunningham, "Frame-Correction Coding," presented at the 1969 Symp. Picture Bandwidth Compression, M.I.T., Cambridge, Massachusetts, Apr. 1969.

[119] R. F. W. Pease and J. O. Limb, "Exchange of Spatial and Temporal Resolution in Television Coding," BSTJ, Vol. 50, No. 1, pp. 191-200, Jan. 1971.

[120] J. C. Candy, Mrs. M. A. Franks B. G. Haskell and F. W. Mounts, "Transmitting Television as Clusters of Frame-to-Frame Differences," BSTJ, Vol. 50, No. 6, pp. 1889-1918, July-August 1971.

[121] J. O. Limb and R. F. W. Pease, "A Simple Interframe Coder for Videotelephony," BSTJ, Vol. 52, No. 1, pp. 35-51, Jan. 1973.

[122] B. G. Haskell, F. W. Mounts and J. C. Candy, "Interframe Coding of Videotelephone Pictures," Proc. IEEE, Vol. 60, No. 7, pp. 792-800, July 1972.

[123] D. J. Connor, B. G. Haskell and F. W. Mounts, "A Frame-to-Frame Picturephone Coders for Signals Containing Differential Quantizing Noise," BSTJ Vol. 52, pp. 35-51, Jan. 1973.

[124] H. D Quyen, "Transmission of Video Data by Frame-to-Frame Differential Pulse-Code-Modulation," M.S. Thesis, Ohio University, Athens, Ohio, March 1974.

[125] R. T. Bobilin, "Interframe Picturephone Coding Using Unconditional Vertical and Temporal Subsampling Techniques," BSTJ, Vol. 53, No. 2, pp. 395-400, Feb. 1974.

[126] J. O. Limb, R. F. W. Pease and K. A. Walsh, "Combining Intraframe and Frame-to-Frame Coding for Television," BSTJ, Vol. 53, No. 6, pp. 1137-1173, July-August 1974.

[127] D. J. Connor and J. O. Limb, "Properties of Frame-Difference Signals Generated by Moving Images," IEEE Trans. Comm., Vol. COM-22, No. 10, pp. 1564-1575, Oct. 1974.

[128] B. G. Haskell, "Frame-to-Frame Coding of Television Pictures Using Two-Dimensional Fourier Transforms," IEEE Trans. Inform. Theory, Vol. IT-20, No. 1., pp. 119-120, Jan. 1974.

V. DATA THEORY

[129] E. R. Kretzmer, "Statistics of Television Signals," BSTJ, pp. 751-763, July 1952.

[130] L. E. Franks, "A Model for the Random Video Process," BSTJ, Apr. 1966.

[131] B. M. Kurkjian, "Digital Generation of Band-Limited Gaussian Noise," Harry Diamond Labs., Proj. 39800, Oct. 1965.

[132] A. Habibi, "Two-Dimensional Bayesian Estimate of Images," Proc. IEEE, Vol. 60, No. 7, pp. 878-883, July 1972.

[133] J. W. Woods, "Two-Dimensional Discrete Markovian Fields," IEEE Trans. Inform. Theory, Vol. IT-18, No. 2, pp. 232-240, March 1972.

[134] T. S. Huang, "The Subjective Effect of Two-Dimensional Pictorial Noise," IEEE Trans. Inform. Theory, Vol. IT-11, pp. 43-53, Jan. 1965.

VI. QUANTIZATION AND CODING

[135] P. F. Panter and W. Dite, "Quantization Distortion in Pulse-Count-Modulation with Nonuniform Spacing of Levels," Proc. IRE, pp. 44-48, Jan. 1951.

[136] B. Smith, "Instantaneous Companding of Quantized Signals," BSTJ, Vol. 36, pp. 248-252, 1957.

[137] J. Max, "Quantizing for Minimum Distortion," IRE Trans. Inform. Theory, Vol. IT-6, pp. 7-12, March 1960.

[138] R. E. Totty and G. C. Clark, "PCM Transmission with Minimum Mean-Square Error," Proc. Intern'l Telemetry Conf., Vol. 2, 1966.

[139] R. E. Totty and G. C. Clark, "Reconstruction Error in Waveform Transmission," IEEE Trans. Inform. Theory, Vol. IT-13, pp. 336-338, Apr. 1967.

[140] B. M. Oliver, "Efficient Coding," BSTJ, pp. 724-750, July 1952.

[141] R. C. Wood, "On Optimum Quantization," IEEE Trans. Inform. Theory, Vol. IT-15, pp. 248-252, March 1969.

[142] A. J. Kurtenbach and P. A. Wintz, "Optimum Quantization," IEEE Trans. Aerospace and Electronics Syst. (suppl.), Vol. AES-3, pp. 563-570, Nov. 1967.

[143] A. J. Kurtenbach and P. A. Wintz, "Quantizing for Noisy Channels," IEEE Trans. Comm. Tech., Vol. COM-17, pp. 291-302, Apr. 1969.

[144] B. R. N. Murphy and P. A. Wintz, "Uniform Quantizers for Noisy Channels," IEEE Trans. Comm., Vol. COM-22, No. 3, pp. 323-326, March 1974.

[145] H. Gish and J. N. Pierce, "Asymptotically Efficient Quantizing," IEEE Trans. Inform. Theory, Vol. IT-14, pp. 676-683, Sept. 1968.

[146] J. B. O'Neal, Jr., "Entropy Coding in Speech and Television Differential PCM Systems," IEEE Trans. Inform. Theory, Vol. IT-17, No. 6, pp. 758-761, Nov. 1971.

[147] M. D. Paez and T. H. Glisson, "Minimum Mean Squared Error Quantization in Speech PCM and DPCM Systems," IEEE Trans. Comm., Vol. COM-20, No. 2, pp. 225-229, Apr. 1972.

[148] D. A. Huffman, "A Method for the Construction of Minimum Redundancy Codes," Proc. IRE, Vol. 40, pp. 1098-1101, Sept. 1952.

[149] H. Meyer, H. G. Rosdolsky and T. S. Huang, "OPtimum Run Length Code, " IEEE Trans. Comm., Vol. COM-22, No. 6. pp. 826-835, June 1974.

[150] J. O. Limb, "Picture Coding : The Use of a Viewer Model in Source Encoding," BSTJ, Vol. 52, No. 8, pp. 1271-1302, Oct. 1973.

VII. DPCM TECHNIQUE

[151] C. W. Harrison, "Experiments with the Linear Prediction in Television," BSTJ, pp. 764-783, July 1952.

[152] B. M. Oliver, "Efficient Coding," BSTJ, pp. 724-750, July 1952.

[153] J. B. O'Neal, Jr., "Predictive Quantizing Systems (Differential Pulse Code Modulation) for the Transmission of Television Signals," BSTJ, pp. 689-721, May-June 1966.

[154] W. Kaminski and E. F. Brown, "An Edge-Adaptive Three-Bit Ten-Level Differential PCM Coder for Television," IEEE Trans. Comm. Tech., Vol. COM-19, No. 6, pp. 944-947, Dec. 1971.

[155] R. P. Abbott, "A Differential Pulse-Code-Modulation Codec for Video-telephony Using Four Bits per Sample," IEEE Trans. Comm. Tech., Vol. COM-19, pp. 907-912, Dec. 1971.

[156] D. J. Connor, R. F. W. Pease and W. G. Scholes, "Television Coding Using Two-Dimensional Spatial Prediction," BSTJ, Vol. 50, pp. 1049-1061, March 1971.

[157] D. J. Connor, R. C. Brainard and J. O. Limb, "Intraframe Coding for Picture Transmission," Proc. IEEE, Vol. 60, No. 7, pp. 779-791, July 1972.

[158] J. B. Ssman and P. A. Wintz, "Theory and Application of DPCM and Comparison of DPCM with other Time Predictive Techniques," School of Elect. Engr., Purdue Univ., Lafayette, Indiana, Tech. Rep. TREE-72, July 1972.

[159] J. B. O'Neal, Jr., and R. W. Stroh, "Differential PCM for Speech and Data signals," IEEE Trans. Comm., Vol. COM-20, No. 5, pp. 900-911, Oct. 1972.

[160] P. Cummiskey, N. S. Jayant and J. L. Flanagan, "Adaptive Quantization in Differential PCM Coding of Speech," BSTJ, Vol.52, No. 7, pp. 1105-1118, Sept. 1973.

[161] N. S. Jayant, "Adaptive Quantization with a One-Word Memory," BSTJ, Vol. 52, pp. 1119-1143, Sept. 1973.

[162] J. O. Limb, C. B. Rubinstein and K. A. Walsh, "Digital Coding of Color Picturephone Signals by Element-Differential Quantization," IEEE Trans. Comm. Tech., Vol. COM-19, pp. 992-1006, Dec. 1971.

[163] J. Agrawal and J. B. O'Neal, Jr., "Low Bit Rate Differential PCM for Monochrome Television Signals," IEEE Trans. Comm., Vol. COM-21, No. 6, pp. 706-714, June 1973.

[164] J. W. Mark, "An Innovations Approach to Adaptive Data Compression in Data Transmission," IEEE Trans. Comm., Vol. COM-22, No. 10, pp. 1618-1929, Oct. 1974.

[165] J. B. O'Neal, Jr., "A Bound on Signal-to-Quantizing Noise Ratios for Digital Encoding Systems," Proc. IEEE, Vol. 55, pp. 287-292, March 1967.

[166] T. P. Stanly and B. Liu, "Data Compression for Discrete Markov Signals," Proc. Natl' Electronics Conf., Vol. 23, pp. 534-539, Oct. 1967.

[167] K. Virupaksha and J. B. O'Neal, Jr., "Entropy-Coded Adaptive Differential Pulse-Code-Modulation (DPCM) for Speech," IEEE Trans. Comm., Vol. COM-22, No. 6, pp. 777-787, June 1974.

[168] T. Fukinuki, "Optimization of D-PCM for TV Signals with Consideration of Visual Property," IEEE Trans. Comm., Vol. COM-22, No. 6, pp. 821-826, June 1974.

[169] N. S. Jayant, "Digital Coding for Speech Waveforms : PCM, DPCM and DM Quantizers," Proc. IEEE, Vol. 62, No. 5, pp. 611-632, May 1974.

[170] A. K. Jain, "Linear and Non-Linear Interpolation for 2-Dimenaional Image Enhancement," presented at the Conf. Decision and Control, New Orleans, La., Dec. 1972.

[171] R. Angle and A. K. Jain, "A Dimensionality Reducing Model for Distributed Filtering," IEEE Trans. Automatic Control, Vol. AC-18, pp. 59-62, Feb. 1973.

[172] R. J. Argullo, H. R. Sellner and J. A. Stuller, "The Effect of Channel Error in the Differential-Pulse-Code-Modulation of Sampled Imagery," IEEE Trans. Comm. Tech., Vol. COM-19, pp. 926-933, Dec. 1971.

[173] K. Y. Chang and R. W. Donalson, "Analysis, Optimization and Sensitivity Study of Differential PCM Systems Operating on Noisy Communication Channels," IEEE Trans. Comm., Vol. COM-20, No. 3, pp. 338-350, June 1972.

[174] K. Y. Chang and R. W. Donalson, "Non-Adaptive DPCM Transmission of Monochrome Pictures Over Noisy Communication Channels," (to be published).

[175] J. E. Eaaman and P. A. Wintz, "The Effects of Channel Errors in DPCM Systems and Comparison with PCM Systems," IEEE Trans. Comm., Vol. COM 21, No. 8, pp. 867-877, August 1973.

[176] A. K. Jain, "Image Coding Via A Nearest Neighbors Image Model," (to be published).

[177] J. B. O'Neal, Jr., "Differential PCM with Entropy Coding," (to be Published).

[178] J. C. Candy, "Limiting the Propagation of Errors in One-Bit Differential CODECS," BSTJ, Vol. 53, No. 3, pp. 1667-1676, Oct. 1974.

[179] J. B. O'Neal, Jr., "Delta Modulation Quantizing Noise Analytical and Computer Simulation Results for Gaussian and Television Input Signal," BSTJ, pp. 117-141, Jan. 1966.

[180] J. E. Abate, "Linear and Adaptive Delta Modulation," Proc. IEEE, Vol. 55, No. 3, pp. 298-307, March 1967.

[181] Atsushi Tomozawa and Hisashi Kaneko, "Companded Delta Modulation for Telephone Transmission", IEEE Transactions on Communication Technology, Vol. Com-16, No. 1, pp. 149-157, February, 1968.

[182] P. A. Deschênes and M. Villeret, "A Continuous Delta Modulator and a Numerical Converter for an Integrated Telecommunication Network", 70-CP-234-COM, 7-27-7-32, Electrical Engr. Dept., Université de Sherbrooke, Sherbrooke, Canada.

[183] J. A. Greefkes, "A Digitally Controlled Delta Codec for Speech Transmission", 70-CP-235-COM, 7-33-7-48, Philips Research Laboratories, N. V. Philips' Gloeilampenfabrieken, Eindhover-Netherlands.

[184] Tatsuo Ishiguro and Hisashi Kaneko, "A Nonlinear DPCM Codec Based on ΔM/DPCM Code Conversion with Digital Filter", pp. 1-27-1-32, Central Research Laboratories Nippon Electric Co., Ltd., Kawasaki, Japan.

[185] John A. Betts, "Adaptive Delta Modulator for Telephony and Its Application to the Aduptifon System-An Alternative Implementation of the Lincompex Concept", IEEE Transactions on Communication Technology, August, 1971, pp. 547-551.

[186] Hiroshi Inose and Yasuhiko Yasuda, "A Unity Bit Coding Method by Negative Feedback", Proceedings of the IEEE, pp. 1524-1533, November, 1963.

[187] Roger M. Wilkinson, "An Adaptive Pulse Code Modulator for Speech", pp. 1-11 1-15, Ministry of Aviation Supply, Signals Research and Development Establishment, Christchurch, Hampshire BH23 4JB England.

[188] David J. Goodman and James L. Flanagan, "Direct Digital Conversion Between Linear and Adaptive Delta Modulation Formats", pp. 1-33-1-36, Bell Telephone Laboratories, Incorporated, Murray Hill, New Jersey.

[189] N. S. Jayant, "Adaptive Delta Modulation with a One-Bit Memory", The Bell System Technical Journal, Vol. 49, No. 3, March, 1970, pp. 321-342.

[190] C. J. Kikkert, "Digital Techniques in Delta Modulation", IEEE Transactions on Communication Technology, August, 1971, pp. 570-573.

[191] R. H. Bosworth and J. C. Candy, "A Companded One-Bit Coder for Television Transmission", The Bell System Technical Journal, Vol. 48, No. 5, May-June, 1969, pp. 1459-1479.

[192] N. S. Jayant, "Further Results on Adaptive Delta Modulation with a One-Bit Memory", pp. 1-16 1-21, Bell Telephone Laboratories, Murray Hill, New Jersey.

[193] Stephen J. Brolin and James M. Brown, "Companded Delta Modulation for Telephony", IEEE Transactions on Communication Technology, Vol. Com-16, No. 1, February, 1968, pp. 157-162.

[194] David J. Goodman, "A Digital Approach to Adaptive Delta Modulation", The Bell System Technical Journal, Vol. 50, No. 4, April, 1971, pp. 1421-1426.

[195] Earl F. Brown, "A Sliding-Scale Direct-Feedback PCM Coder for Television", The Bell System Technical Journal, Vol. 48, No. 5, May-June, 1969, pp. 1537-1553.

[196] Michael Oliver, "An Adaptive Delta Modulator with Overshoot Suppression for Video Signals", IEEE Transactions on Communications, March, 1973, pp. 243-247.

[197] Protonotarios, E. N., "Slope Overload Noise in Differential Pulse Code Modulation Systems", B.S.T.J., pp. 2119-2161, November, 1967.

[198] Aaron, M. R., et.al., "Response of Delta Modulation to Gaussian Signals", B.S.T.J., pp. 1167-1195, May-June, 1969.

[199] McDonald, R. A., "Signal-to-Noise and Idle Channel Performance of Differential Pulse Code Modulation Systems-Particular Applications to Voice Signals", B.S.T.J., pp. 1123-1155, September, 1966.

[200] Goodman, D. J., "The Application of Delta Modulation to Analog-to-PCM Encoding", B.S.T.J., pp. 321-343, February, 1969.

[201] Goodman, D. J., "Delta Modulation Granular Quantizing Noise", B.S.T.J., pp. 1197-1217, May-June, 1969.

[202] Bosworth, R. H. and Candy, J. C., "A Companded One-Bit Coder for Television Transmission", B.S.T.J., pp. 1459-1479, May-June, 1969.

[203] Smith, B., "Instantaneous Companding of Quantized Signals", B.S.T.J., pp. 653-709, May, 1957.

[204] Brown, E. F., "A Sliding-Scale Direct-Feedback PCM Coder for Television", B.S.T.J., pp. 1537-1553, May-June, 1969.

[205] Donaldson, R. W. and Douville, R. J., "Analysis Subjective Evaluation Optimization, and Comparison of the Performance Capabilities of PCM, DPCM, AM, AM, and PM Voice Communication Systems", IEEE Transactions on Communication Technology, Vol. COM-17, No. 4, August, 1969.

[206] Donaldson, R. W., and Chan, D., "Analysis and Subjective Evaluation of Differential Pulse-Code Modulation Voice Communications Systems", IEEE Transactions on Communication Technology, Vol. COM-17, No. 1, February, 1969.

[207] Schindler, H. R., "Delta Modulation", IEEE Spectrum, pp. 69-78, October, 1970.

[208] English, M. J., "Dual IC's Simplify Delta Modulation Systems", pp. 41-43, Electronic Products, March, 1970.

[209] Laane, R. R., "Measured Quantizing Noise Spectrum for Single-Integration Delta-Modulation Coders", B.S.T.J., pp. 191-195, February, 1970.

[210] Brainard, R. C. and Candy, J. C., "Direct-Feedback Coders: Design and Performance with Television Signals", Proceedings of the IEEE, Vol. 57, No. 5, May, 1969.

[211] Wang, P. F., "Idle Channel Noise of Delta Modulation", IEEE Transactions on Communication Technology, Vol. Com-16, No. 5, October, 1968.

[212] Scroh, R. W. and Boorstyn, R. R., "Optimum and Adaptive Differential Pulse Code Modulation", Technical Report, Department of Electrical Engineering, Polytechnic Institute of Brooklyn, 1970.